

Robotic Automation of Turning Machines in Fenceless Production:
A Planning Toolset for Economic-based Selection Optimization between
Collaborative and Classical Industrial Robots

Von der Fakultät für Maschinenbau der
Technischen Universität Chemnitz

Genehmigte

Dissertation

Zur Erlangung des akademischen Grades
Doktoringenieur
Dr.-Ing.

vorgelegt

von M.Sc. Christopher Schneider
geboren am 14.11.1992 in Chemnitz
eingereicht am 09.11.2021

Gutachter: Prof. Dr.-Ing. Matthias Putz
Prof. Dr.-Ing. Martin Dix
Prof. Dr. Prof. h.c. Uwe Götze

Chemnitz, den 01.11.2022

<https://nbn-resolving.org/urn:nbn:de:bsz:ch1-qucosa2-819296>

This work is licensed under Creative Commons Licence. 4.0 International (CC BY 4.0) <https://creativecommons.org/licenses/by/4.0/> The images or other third party material are included in the Creative Commons license, unless indicated otherwise in a credit line to the material. If material is not included in the Creative Commons license and your intended use is not permitted by statutory regulation or exceeds the permitted use, you will need to obtain permission directly from the copyright holder.



Bibliographische Beschreibung

Schneider, Christopher

Thema

Robotic Automation of Turning Machines in Fenceless Production: A Planning Toolset for Economic-based Selection Optimization between Collaborative and Classical Industrial Robots

Dissertation an der Fakultät für Maschinenbau der Technischen Universität Chemnitz, Institut für Werkzeugmaschinen und Produktionsprozesse, Chemnitz, 2021

253 Seiten

70 Abbildungen

18 Tabellen

256 Literaturquellen

39 Anhänge

Schlagworte

Maschinenbeladung, Kollaborative Roboter, Industrieroboter, Mensch-Roboter-Kollaboration, Schutzzaunlose Fertigung, Anlagenplanung, Layoutplanung, Wirtschaftliche Optimierung, Biomechanische Grenzwerte, Kraft- und Druckmessungen, Quasi-statischer Kontakt, Transienter Kontakt, Sicherheitstechnik

Kurzreferat

Ursprünglich wurden Industrieroboter hauptsächlich hinter Schutzzäunen betrieben, um den Sicherheitsanforderungen gerecht zu werden. Mit der Flexibilisierung der Produktion wurden diese scharfen Trennbereiche zunehmend aufgeweicht und externe Sicherheitstechnik, wie Abstandssensoren, genutzt, um Industrieroboter schutzzaunlos zu betreiben. Ausgehend vom Gedanken dieser Koexistenz bzw. Kooperation wurde die Sicherheitssensorik in den Roboter integriert, um eine wirkliche Kollaboration zu ermöglichen. Diese sogenannten kollaborierenden Roboter, oder Cobots, eröffnen neue Applikationsfelder und füllen somit die bestehenden Automatisierungslücken. Doch welche Automatisierungsvariante ist aus wirtschaftlichen Gesichtspunkten die geeignetste? Bisherige Forschung untersucht zum Großteil isoliert eine der beiden Technologien, ohne

dabei einen Systemvergleich hinsichtlich technologischer Spezifika und Wirtschaftlichkeit anzustellen. Daher widmet sich diese Dissertation einer Methodik zum wirtschaftlichen Vergleich von kollaborierenden Robotern und Industrierobotern in schutzzaunlosen Maschinenbeladungssystemen. Besonderer Fokus liegt dabei auf dem Herausarbeiten der technischen Faktoren, die die Wirtschaftlichkeit maßgeblich beeinflussen, um ein Systemverständnis der wirtschaftlichen Struktur beider Robotertechnologievarianten zu erhalten. Zur Untersuchung werden die Inhalte eines solchen Planungsvorhabens beschrieben, kategorisiert, systematisiert und modularisiert. Auf wirtschaftlicher Seite wird ein geeignetes Optimierungsmodell vorgestellt, während auf technischer Seite vor allem die Machbarkeit hinsichtlich Greifbarkeit, Layoutplanung, Robotergeschwindigkeiten und Zykluszeitbestimmung untersucht wird. Mit deduktiven, simulativen, empirischen und statistischen Methoden wird das Systemverhalten für die einzelnen Planungsinhalte analysiert, um die Gesamtwirtschaftlichkeit mit einem Minimum an Investment,- Produktions,- und Zykluszeitinformationen a priori vorhersagen zu können. Es wird gezeigt, dass durch einen Reverse Engineering Ansatz die notwendigen Planungsdaten, im Sinne von Layoutkomposition, Robotergeschwindigkeiten und Taktzeiten, mithilfe von Frontloading zu Planungsbeginn zur Verfügung gestellt werden können. Dabei dient der Kapitalwert als wirtschaftliche Bewertungsgrundlage, dessen Abhängigkeit vom Mensch-Roboter-Interaktionsgrad in einem Vorteilhaftigkeitsdiagramm für die einzelnen Technologiealternativen dargestellt werden kann. Wirtschaftlich fundierte Entscheidungen können somit auf quantitativer Basis getroffen werden.

Bibliographic Description

Schneider, Christopher

Topic

Robotic Automation of Turning Machines in Fenceless Production: A Planning Toolset for Economic-based Selection Optimization between Collaborative and Classical Industrial Robots

Doctoral Thesis at the Faculty of Mechanical Engineering at Chemnitz University of Technology, Institute for Machine Tools and Production Processes, Chemnitz, 2021

253 Pages

70 Figures

18 Tables

256 References

39 Appendices

Keywords

Machine Tending, Collaborative Robots, Industrial Robots, Human-Robot-Collaboration, Fenceless Production, System Engineering, Layout Planning, Economic Optimization, Biomechanical Thresholds, Force and Pressure Measurements, Quasi-static Contact, Transient Contact, Safety Engineering

Abstract

Initially, industrial robots were mainly operated behind safety fences to account for the safety requirements. With production flexibilization, these sharp separation areas have been increasingly softened by utilizing external safety devices, such as distance sensors, to operate industrial robots fenceless. Based on this idea of coexistence or cooperation, safety technology has been integrated into the robot to enable true collaboration. These collaborative robots, or cobots, open up new application fields and fill the existing automation gap. But which automation variant is most suitable from an economic perspective? Present research dealt primarily isolated with one technology without comparing these systems regarding technological and economic specifics. Therefore, this doctoral thesis pursues a methodology to economically compare collaborative and industrial

robots in fenceless machine tending systems. A particular focus lies on distilling the technical factors that mainly influence the profitability to receive a system understanding of the economic structure of both robot technology variants. For examination, the contents of such a planning scheme are described, categorized, systematized, and modularized. A suitable optimization model is presented on the economic side, while the feasibility regarding gripping, layout planning, robot velocities, and cycle time determination is assessed on the technical side. With deductive, simulative, empirical, and statistical methods, the system behavior of the single planning entities is analyzed to predict the overall profitability a priori with a minimum of investment,- production,- and cycle time information. It is demonstrated that the necessary planning data, in terms of layout composition, robot velocities, and cycle times, can be frontloaded to the project's beginning with a reverse engineering approach. The net present value serves as the target figure, whose dependency on the human-robot interaction grade can be illustrated in an advantageousness diagram for the individual technical alternatives. Consequently, sound economic decisions can be made on a quantitative basis.

Table of Contents

Bibliographische Beschreibung	- 2 -
Bibliographic Description.....	- 1 -
Table of Contents.....	7
List of Figures	11
List of Tables	15
List of Abbreviations	17
List of Short Symbols	21
1. Introduction.....	25
1.1 Research Domain	25
1.2 Research Niche.....	26
1.3 Research Structure.....	28
2. State of the Art and Research.....	31
2.1 Turning Machines and Machine Tending	31
2.1.1 Tooling Machine Market Trends and Machine Tending Systems.....	31
2.1.2 Workpiece System	34
2.1.3 Machine System.....	36
2.1.4 Logistics System	39
2.1.5 Handling System.....	41
2.2 Robotics.....	43
2.2.1 Robot Installation Development and Application Fields.....	43
2.2.2 Fenceless Industrial and Collaborative Robots.....	48
2.2.3 Robot Grippers.....	55
2.3 Planning and Evaluation Methods.....	56
2.3.1 Planning of General and Manual Workstations	56
2.3.2 Cell Planning for Fully Automated and Hybrid Robot Systems.....	59
2.3.3 Robot Safety Planning	61
2.3.4 Economic Evaluation Methods	70
2.4 Synthesis - State of the Art and Research	71
3. Solution Approach	77
3.1 Need for Research and General Solution Approach	77
3.2 Use Case Delineation and Planning Focus.....	80

3.3	Economic Module – Solution Approach.....	86
3.4	Gripper Feasibility Module – Solution Approach.....	89
3.5	Rough Layout Discretization Model – Solution Approach.....	94
3.6	Cycle Time Estimation Module – Solution Approach.....	97
3.7	Collaborative Speed Estimation Module – Solution Approach	103
3.7.1	General Approach	103
3.7.2	Case 1: Quasi-static Contact with Hand	107
3.7.3	Case 2: Transient Contact with Hand	109
3.7.4	Case 3: Transient Contact with Shoulder.....	111
3.8	Synthesis – Solution Approach	114
4.	Module Development.....	117
4.1	Economic Module – Module Development	117
4.1.1	General Approach	117
4.1.2	Calculation Scheme for Manual Operation.....	117
4.1.3	Calculation Scheme for Collaborative Robots.....	118
4.1.4	Calculation Scheme for Industrial Robots	120
4.2	Gripper Feasibility Module – Module Development	121
4.3	Rough Layout Discretization Module – Module Development	122
4.3.1	General Approach	122
4.3.2	Two-Dimensional Layout Pattern.....	123
4.3.3	Three-Dimensional Layout Pattern.....	125
4.4	Cycle Time Estimation Module – Module Development	126
4.4.1	General Approach	126
4.4.2	Reachability Study	127
4.4.3	Simulation Results	128
4.5	Collaborative Speed Estimation Module – Module Development.....	135
4.5.1	General Approach	135
4.5.2	Case 1: Quasi-static Contact with Hand	135
4.5.3	Case 2: Transient Contact with Hand	143
4.5.4	Case 3: Transient Contact with Shoulder.....	145
4.6	Synthesis – Module Development.....	149
5.	Practical Verification	155
5.1	Use Case Overview	155

5.2	Gripper Feasibility.....	155
5.3	Layout Discretization	156
5.4	Collaborative Speed Estimation	157
5.5	Cycle Time Estimation.....	158
5.6	Economic Evaluation	160
5.7	Synthesis – Practical Verification	161
6.	Results and Conclusions	165
6.1	Scientific Findings and Results	165
6.2	Critical Appraisal and Outlook	173
	References.....	177
	List of Appendices	201
	Appendix.....	203
	Curriculum Vitae	253

List of Figures

Figure 1.1: Structure of the Present Doctoral Thesis	28
Figure 2.1: Machine Tending Cell System Composition.....	34
Figure 2.2: Tooling Machine Subsystem	37
Figure 2.3: Clamping Device Subsystem Alternatives	38
Figure 2.4: Door Subsystem Alternatives	39
Figure 2.5: Robot Subsystem - Single Machine Tending Installation Possibilities.....	42
Figure 2.6: Robot Subsystem - Multi-Machine Tending Installation Possibilities.....	43
Figure 2.7: Industry Segment Robot Installations in 2018	44
Figure 2.8: Robot Installations by Industry in 2018	45
Figure 2.9: Robot Installations by Application in 2018.....	45
Figure 2.10: Robot Applications in Handling Operations/ Machine Tending in 2018.....	46
Figure 2.11: Robot Installation Development from 2017 to 2018.....	46
Figure 2.12: Payload-Reach Distribution of Collaborative Robots	48
Figure 2.13: Robot Subsystem - Kinematic Possibilities.....	48
Figure 2.14: Four Modes of Human-robot-interaction	51
Figure 2.15: Cobot Representatives with different active Safety Technologies.....	53
Figure 2.16: Human-Robot Interaction Classification.....	54
Figure 2.17: Gripper Subsystem Possibilities.....	56
Figure 2.18: Layout Structure of a Machine Station.....	58
Figure 2.19: Human Anatomy with considered Body Regions	63
Figure 2.20: Force and Pressure Measurement Setup.....	64
Figure 2.21: Considered Lathe Machine Tending Elements	72
Figure 3.1: Solution Approach.....	77
Figure 3.2: Process Pipeline for CNC Lathe Machine Tending	81
Figure 3.3: Technical Options for Fenceless Lathe Machine Tending.....	82
Figure 3.4: Payload-Reach Distribution of Yaskawa Robot Installations	85
Figure 3.5: Ishikawa Diagram for Economic Module	87
Figure 3.6: Deduction Procedure for Economic Module.....	88
Figure 3.7: Allowable Wrist Load Diagram and Gripper Force Diagram.....	89
Figure 3.8: Ishikawa Diagram for Robot-based Gripping Feasibility Module.....	91
Figure 3.9: Simulation Procedure for Gripper Feasibility Module.....	94

Figure 3.10: Ishikawa Diagram for Layout Discretization Module.....	95
Figure 3.11: Modeling Procedure for Rough Layout Discretization Module.....	96
Figure 3.12: Ishikawa Diagram for Cycle Time Estimation Module	98
Figure 3.13: General Workflow of Lathe Machine Tending	100
Figure 3.14: Top and Stretched Gripping	101
Figure 3.15: Simulation Procedure for Cycle Time Estimation Module	102
Figure 3.16: Identified Risk Scenarios.....	104
Figure 3.17: Ishikawa Diagram for the Collaborative Speed Estimation Module.....	105
Figure 3.18: Measurement Procedure for Collaborative Speed Estimation Module	107
Figure 3.19: Measurement Setup for Case 1	108
Figure 3.20: Measurement Setup for Case 2	110
Figure 3.21: Measurement Setup for Case 3.....	112
Figure 3.22: Overall Presented Approach and Interrelations of the Single Modules	115
Figure 4.1: Feasible Workpiece Diameter-Length Combinations	122
Figure 4.2: 3-dimensional Representation of Relevant Machine Coordinates	123
Figure 4.3: Discretized 2D General Layout Pattern.....	125
Figure 4.4: 3D Representation of the Layout Pattern and Application Example	126
Figure 4.5: Reachability Differences between Collaborative and Industrial Robot	127
Figure 4.6: Door-Spindle Feed Simulation Results	128
Figure 4.7: Behavior Analysis of all Door-Spindle Feed Movement Simulations	130
Figure 4.8: Nonlinear Regression Progression Door-Spindle Feed Movement	131
Figure 4.9: Spindle Feed-Spindle Simulation Results	132
Figure 4.10: Turning Simulation Results.....	133
Figure 4.11: Material Feed-Material Simulation Results	134
Figure 4.12: Selected Tested Gripper and Workpiece Setups	136
Figure 4.13: Test on Gripper and Material for 110 mm	137
Figure 4.14: Force measurements to identify the MRCS	138
Figure 4.15: Force Development Behavior over Time for Quasi-static Contact Cases.....	139
Figure 4.16: Exemplary Pressure Foil Results.....	141
Figure 4.17: Maximum Allowed Collaborative Speed	142
Figure 4.18: Setup for Transient Contact with the Elbow Big Cap	147
Figure 4.19: Setup for Transient Contact with Elbow Small Cap	147
Figure 4.20: Setup for Transient Contact with Forearm	148

Figure 4.21: Experiment on Transient Contact with Wrist Cap	148
Figure 4.22: Maximum Allowed Collaborative Speed by Protective Measure	149
Figure 5.1: Discretized Use Case Layout	156
Figure 5.2: Dimensional Relations to Calculate the Position Value.....	157
Figure 5.3: Deviation Analysis between Approximated and Simulated Cycle Times	159
Figure 5.4: Economic Evaluation of the Three Technical Variants.....	161

List of Tables

Table 2.1: General Workpiece Criteria	35
Table 2.2: Tooling Machine Automation Degrees	37
Table 2.3: Methodological Economic Coverage of HRI in Present Literature.....	74
Table 3.1: Handling Execution-based Working Systems	83
Table 3.2: General Experiment Specifications for Collaborative Speed Estimation.....	106
Table 3.3: Experiment Specifications for Case 1 – Quasi-static Contact with Hand	109
Table 3.4: Experiment Specifications for Case 2 – Transient Contact with Hand	111
Table 3.5: Experiment Specifications for Case 3 – Transient Contact with Hand	114
Table 4.1: Feasible Reachable Door Positions based on Robot Position	127
Table 4.2: Axis Speed Differences between Collaborative and Industrial Robot	129
Table 4.3: Nonlinear Regression Coefficients for Door-Spindle Feed Movement	130
Table 4.4: Weights of the Tested Workpieces for D110 mm	136
Table 4.5: Weights of the Tested Workpieces for D80 mm to D20 mm	137
Table 4.6: Determined Standard Time Values for Different Motions	152
Table 5.1: Use Case Input Data for Process, Production, and Investment	155
Table 5.2: Calculated Main Times for all Robots and Operating Modes	158
Table 5.3: Calculated Cycle Times for Material Feed-Material and Turning	158
Table 5.4: Calculated Side Times and Process Times P5 and P7	159

List of Abbreviations

Abbreviation	Designation
ABC	Activity-based Costing
AET	Annual Execution Time
AGV	Automated Guided Vehicle
AND	And Logical Operator
BGHM	Berufsgenossenschaft Holz und Metall – Trade Association Wood and Metal
BMBF	Bundesministerium für Bildung und Forschung – Federal Ministry of Education and Research
BMWi	Bundesministerium für Wirtschaft und Energie – Federal Ministry for Economic Affairs and Energy
C	Collaborative
CAD	Computer-aided Design
CAGR	Continuous Average Growth Rate
Cap	Elbow Small Cap & Wrist Cap Robot Contact Geometry
Cat.	Category
CIF	Cash-In Flow
CNC	Computer Numerical Control
COF	Cash-Out Flow
CPS	Cyber-physical System
CR	Collaborative Robot
CS	Collaborative Speed
CW	Closing Width
DAX	Deutscher Aktienindex – German Stock Index
DGUV	Deutsche Gesetzliche Unfallversicherung – German Statutory Accident Insurance
DIN	Deutsches Institut für Normung – German Institute for Standardization
DIS	Draft International Standard
DSF	Door – Spindle Feed
DT	Direct Teach

DTS	Driverless Transport System
EC	European Commission
Elb	Elbow Big Cap Robot Contact Geometry
EN	Europäische Norm – European Standard
EPC	Event-based Process Chain
EPE	Expanded Polyethylene
ESPE	Electro-sensitive protective equipment
ET	Execution Times
F	Research Focus
FS	Full-Speed
GP	General Purpose
HC	Human-Collaborative
HG	Hand Guiding
HM	Hybrid Mode
HRC	Human-Robot-Collaboration
HRI	Human-Robot-Interaction
I	Industrial
IAO	Institut für Arbeitswirtschaft und Organisation – Institute for Industrial Engineering
IEC	International Electrotechnical Commission
IFF	Institut für Fabrikbetrieb und -automatisierung – Institute for Factory Operation and Automation
IFR	International Federation of Robotics
INIT	Initialization Phase
I/O	Input/Output
IOR	Inclusive Or Logical Operator
IP	Ingress Protection
IR	Industrial Robot
ISO	International Organization for Standardization
IT	Information Technology
L	Lathe Machine
LBR	Leichtbauroboter – Lightweight Robot
LLW	Pressure sensitive foils with a resolution of 50 - 300 N/cm ²

LW	Pressure sensitive foils with a resolution of 250 - 1200 N/cm ²
LOOP	Loop Phase
LRG	Labor Release Grade
LUL	Loading and Unloading
M	Manual Operation
MACS	Maximum Allowed Collaborative Speed
MFD	Material Feed - Door
MFM	Material Feed - Material
MH	Material Handling
MI	Moment of Inertia
MICLASS	Metal Institute Classification System
MOVJ	Joint Movement
MOVL	Linear Movement
MRK	Mensch-Roboter Kollaboration – Human-Robot-Collaboration
MRCS	Minimum Required Collaborative Speed
MT	Machine Tending
MTM	Methods-time Measurement
NC	Numerical Control
ND	Non-dominant
NPV	Net Present Value
O.E.E.	Overall Equipment Effectiveness
OW	Opening Width
PFL	Power and Force Limiting
PFMD	Pressure and/ or Force Measurement Device
P	Process
PL	Performance Level, Position Level
PLA	Polylactid Acid
POM	Polyoxymethylene
PREP	Preparation Phase
PRMS	Pilz Robot Measurement System
PwC	PricewaterhouseCoopers
R&D	Research & Development

REFA	Reichsausschuss für Arbeitsstudien – Association for Work Design, Business Organization and Business Development
RIA	Robotics Industries Association
ROI	Return on Investment
RQ	Research Question
RTM	Robot Time and Motion
S	Side Gripping
SCARA	Selective Compliance Articulated Robot Arm
SF	Scientific Finding
SFS	Spindle Feed - Spindle
SI	Système internationales (d'unités) – International System of Units
SLS	Safely-Limited Stop
SLT	Safely-Limited Torque
SME	Small- and Medium-sized Enterprises
SRMS	Safety-rated Monitored Stop
SSM	Speed and Separation Monitoring
STO	Safe Torque Off
T	Turning, Top Gripping
TC	Technical Committee
TCO	Total Cost of Ownership
TCP	Tool Center Point
TMU	Time Measurement Unit
TR	Technical Report
TS	Technical Specification
UR	Universal Robots
VC	Value Creation
VDE	Verband Deutscher Elektrotechniker – Association for Electrical, Electronic & Information Technologies
VDMA	Verband Deutscher Maschine- und Anlagenbau – Mechanical Engineering Industry Association
WD	Workpiece Diameter
XOR	Exclusive Or Logical Operator
XP	Increased Body Protection

List of Short Symbols

Short Symbol	Unit	Designation
A	mm^2	Contact Area
AET	h	Annual Execution Time
B_M	m	Machine Width
B_{MA}	m	Total Width
B_n	-	Batch with batch number n
C	€	Annual Operator Cost
CIF	€	Periodical Cash-In Flow
COF	€	Periodical Cash-Out Flow
CT	s	Cycle Time
CW	mm	Minimal Closing Width
d	mm	Diameter
E	J	Transfer Energy
ET	h	Execution Time
F_F	m^2	Manufacturing Area
F_{MA}	m^2	Machine Station Area
F, F_{max}	N	Maximum Permissible Force
F_T	m^2	Transport Area
F_W	m^2	Workshop Space
F_Z	m^2	Additional Area
F_{ZL}	m^2	Intermediate Storage Area
I	$\text{kg} * \text{m}^2$	Moment of Inertia
I_0	€	Initial Net Investment in $t = 0$
k	N/mm	Effective Spring Constant
l	mm	Length
L	m	Mass Center from Flange
LRG	%	Labor Release Grade
m	kg	Mass
m_H	kg	Effective Body Region Mass
m_L	kg	Effective Robot System Payload

m_R	kg	Effective Robot Mass
M	kg	Total Mass of Moving Robot Parts
$MACS$	mm/s	Maximum Allowed Collaborative Speed
$MRCS$	mm/s	Minimum Required Collaborative Speed
$M_{\%Max}$	%	Moment Utilization of Maximum Load
$MI_{\%Max}$	%	Moment of Inertia Utilization of Maximum Load
N	-	Total Number of Produced Batches
N_+	-	Batch Share
NPV	€	Net Present Value
O_A	workpieces	Total Annual Output
O_R	workpieces	Rest Output in Batch Share
OW	mm	Opening Width
p	%	Percental Reach Utilization of Position
p_{max}	N/mm ²	Maximum Permissible Pressure
P_p	h	Process Time of the Process p
q	%	Discount Factor
R	h	Rest Capacity
R_G	mm	Gripper Repeatability
R_R	mm	Robot Repeatability
s	N	Sensor Sensitivity/ Force Limit
t	year	Time Index
T	years	Observed Time Period
T_M	m	Machine Depth
T_{MA}	m	Total Depth
v	m/s	Operating Speed
$v_{rel}, v_{rel,max}$	m/s	Maximum Relative Speed between Collision Bodies
VC	€	Value Creation per Workpiece
W	h	Annual Working Time
WD_{min}	mm	Minimal Workpiece Diameter
WD_{max}	mm	Maximal Workpiece Diameter
Z_1	m	Clearance for Operation and Safety
Z_2	m	Clearance for Maintenance

α	%	Interaction Grade
ΔO	workpieces	Annual Output Deviation
μ	kg	Reduced Mass of Collision Bodies
ρ	kg/m ²	Density

1. Introduction

1.1 Research Domain

The traditional automation field of machine tending (MT) has utilized industrial robots for decades, usually focusing on high volumes of mainly automotive companies in partially or fully fenced-in operating areas [1, 2]. Within the last years, collaborative robot (cobot) machine tending installations increased rapidly with growing potential to become one of the main cobot applications [3]. Especially small-and-medium-sized companies (SMEs) face the challenge of recruiting CNC professionals due to demographic change while managing the needs for flexibility, automation, and digitalization [4, 5]. Cobots address low in-house experience in automation planning and implementation of those SMEs with easy programming, plug & play, and online-based training and configuration.

Over the last years, the perception of cobots as a technology enabler for providing flexibility and usability subsided increasingly due to lacking truly collaborative use cases. Promises such as easy integration and fast return on investment (ROI) have been too idealistic when the first projects faced safety requirements. The standard-compliant operating speeds and the correspondent cycle times were often insufficient, and many cobots ended up as a cooperative, coexistent, or fenced-in automation solution to ensure the required profitability [6]. In such cases, industrial robots equipped with additional safety devices would have been likewise suitable for fenceless operation at a lower cost level.

This contradiction reveals a methodological gap in selecting the optimal human-robot-interaction (HRI) technology. The problem of many cobot flagship projects lies in the paradigm to take a collaborative robot as the prerequisite, followed by planning steps for the task, the tool, and the work cell [7]. Despite the potential of cobots to guarantee easy implementation and commissioning, it turns out that planning such a system includes even more parameters of uncertain data than a fenceless or fenced-in industrial robot system. Obstacles can be traced back to the requirements that have been defined in ISO/TS 15066, especially regarding application-specific force and pressure measurements and the respective allowed operating speed. When adding external safety devices to enable the robot to switch between full- and collaborative speed, according to the operator's proximity, the planning complexity is enlarged even more [6]. In contrast, classical planning methods rather focus on the work cell by already incorporating the system concept, workflow, cycle time,

and profitability. Safety engineering, as a core element in HRI, is already conceptualized in the

early planning stages. Based on this initial concept, appropriate tooling is designed for the specific task to meet the technical requirements. After designing system alternatives with collaborative and industrial robots, the preferred option is determined, and the optimal robot technology is selected respectively in a very late stage of the planning process [7].

Hence, a clash of planning philosophies between traditional industrial robotics and the new cobot world can be observed: while the cobot world claims that this technology is the easiest and most profitable solution, the industrial world prefers, in many cases, fenceless industrial robots. Higher operation speeds, increasing usability, and decreasing prices of industrial robots challenge the stated cobot benefits. After the first cobot flagship projects were completed, more pragmatism arrived in the world of fenceless robotics, which puts the advantageousness of cobots for discussion.

1.2 Research Niche

This doctoral thesis focuses on a holistic system consideration to compare the profitability of both industrial and collaborative robot installations in fenceless machine tending cells. This should assist the planner in making well-founded investment decisions already in the rough planning phase. A calculation scheme should serve as a basis that covers all economically relevant factors for both automation alternatives. To minimize planning efforts in the early project stages, such as time-consuming design and simulation studies or feasibility tests, estimation models should frontload all relevant information by approximating the required parameters. This approach targets a simplification of the planning procedure to derive a high-abstract rough cell concept with particular emphasis on the sufficient accuracy level. The respective scientific tension field lies in the provision of significant information while streamlining the procedure simultaneously. By focusing on the planning parameter description on the robot side, the scope of observation needs to be narrowed down on the machine side. Therefore, a restriction to lathe machines is suitable for predefined positions in the main spindle and the limitation to rotary workpieces. Based on this problem consideration, the following research questions (RQ) has been derived:

- RQ 1: By which technical systems and subsystems can lathe machine tending cells be classified in general and in particular regarding fenceless robotic systems?

- RQ 2: Which technical alternatives are available to implement human-robot collaboration, and how do they affect the economic feasibility? What are the main technical influencing factors on the economic feasibility of an automation project?
- RQ 3: Which methods are currently suitable to determine these influencing factors, and how can they be transferred to a frontloading planning approach?
- RQ 4: How can an integrated rough planning methodology be derived that provides all required economic information at the beginning of the project?
- RQ 5: Under which circumstances is a collaborative robot economically superior to an industrial one in lathe machine tending applications?

An interdisciplinary approach is required to answer these research questions that utilize the research fields of factory planning, robotics, and economics. Essential are methods in layout design, industrial engineering, robot offline simulation, and investment decision theory. Due to the interdisciplinarity of the planning problem, the comprehensive topic coverage of the research questions, and the normative directives, especially regarding the ISO/TS 15066, the overall system complexity can be assumed as very high. Therefore, this doctoral thesis will focus on the most relevant factors to build a fundamental system categorization and description that is extendable by additional relevant parameters in further research. Due to the large variety of available methods (e.g., simulation and design software) and technologies (e.g., robot or gripper models), it is impossible to use various kinds of software or robot technology to describe the system behavior. For this reason, and to ensure the transferability to industry and the ability to validate the results in practice, a selected set of software and technology representatives is used. To guarantee scientific validity, the essential premise is to develop a general methodological procedure that can be transferred to other simulation and measurement methods and other technology models. Despite the mentioned complexity, the developed methods should be easy-to-use to enable inexperienced planners (e.g., SMEs) to design robotic work cells and build up internal know-how. For future extensions, it should be formulated in a computable way to transfer it to a software system later.

Therefore, the methods of this doctoral thesis should provide a factual basis for future knowledge-based expert systems, whose databases can be extended with the provided general methods. In this way, the comparability of different robot technologies regarding

their profitability within a clearly defined application area is enabled. In the validation phase of this work, it needs to be proven that the developed modules apply to practical use cases and that the proposed method set supplements itself to provide realistic investment decision assistance.

1.3 Research Structure

In Figure 1.1, an overview of the structure of this doctoral thesis is given.

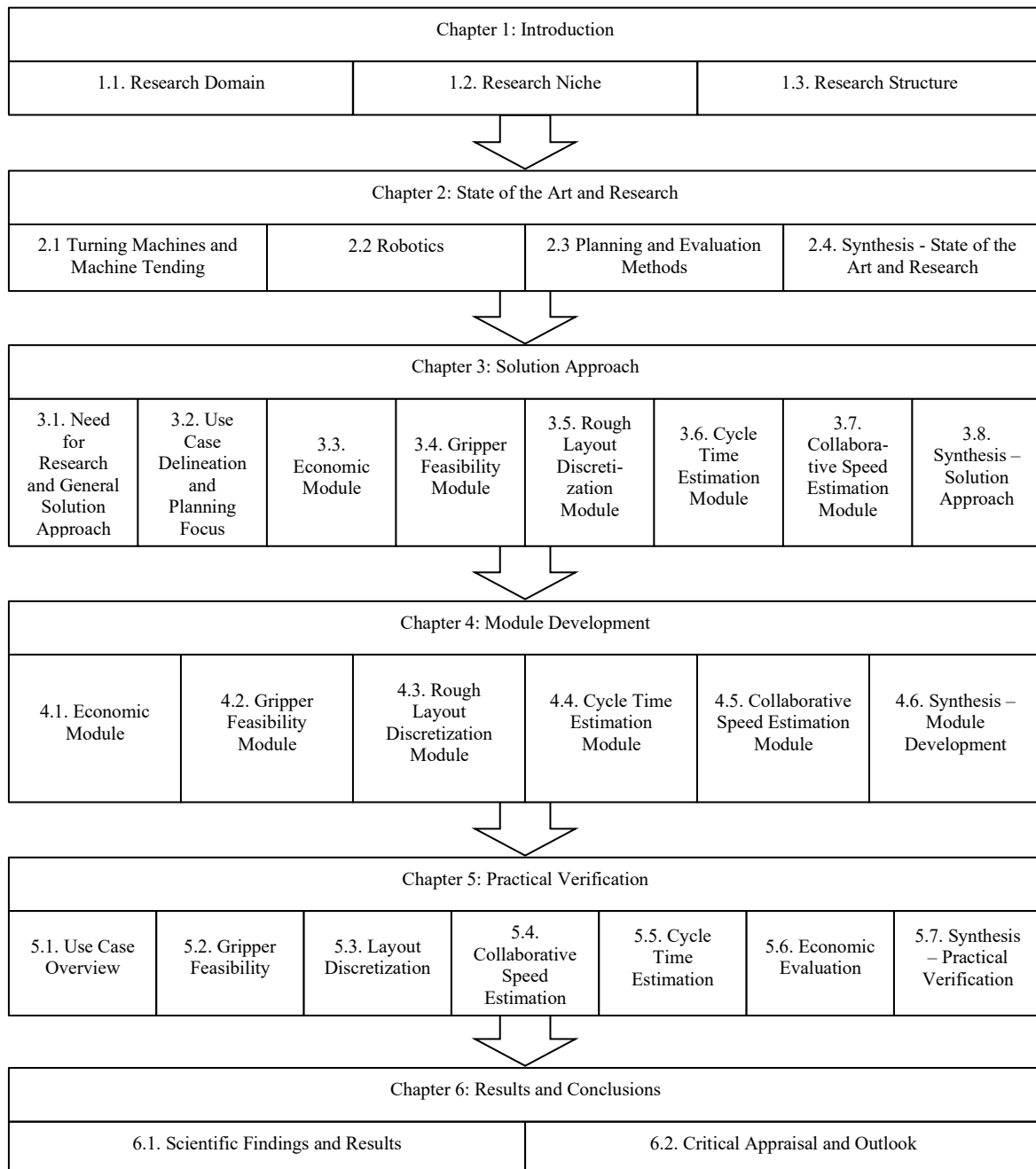


Figure 1.1: Structure of the Present Doctoral Thesis

As a solid discussion base, chapter 2 summarizes the state of the art and research in three fundamental fields of knowledge for this thesis. First, turning machines are described in general as well as regarding the automation possibilities. Due to the focus on robotized machine tending, this automation option is detailed further. To better understand robotic aspects of the system, a solid robotics fundamental is given with a strong emphasis on collaborative robots and fenceless operations. To understand the underlying planning aspects, respective engineering and economical methods from different research directions are presented. In chapter 3, research gaps are revealed to conclude the need for action in terms of turning machine tending planning. To define the scope of observation of this doctoral thesis, focus fields are defined, and the use case is delineated. As a solution approach, an economic calculation scheme and various engineering methods are developed in this work, which is defined in this chapter. Based on the method description, chapter 4 deals with their development under the use of conductive, simulative, empirical and statistical methods. For practical verification, the overall economic model and the single methods are verified with a use case application in chapter 5. The last chapter 6 summarizes the results and discusses the answering to the previously defined research questions. Furthermore, optimization potentials, as well as further research entry points, are discussed.

2. State of the Art and Research

2.1 Turning Machines and Machine Tending

2.1.1 Tooling Machine Market Trends and Machine Tending Systems

With over 1 million employees and 218 billion Euro revenue, machine and systems engineering builds an important pillar in the German economic structure. The German machine tool industry obtained with 71,600 employees in over 500 companies, the revenue of 15.8 billion euros in 2015, and constituted, therefore, the backbone of the German economy. It serves as the basis for innovation in new products as well as manufacturing procedures. Around 75 % of the production volume is achieved by chipping machines, mainly delivered to the automotive industry [8].

In order to meet the market requirements regarding the need for higher product individualization, production strategies shift from mass production to mass customization [9]. Challenges arise in the field of flexible production due to the following characteristics [8, 10–13]:

- 1) reacting to demand variations with short product iterations,
- 2) fulfilling the customer demands of high quality and short delivery times,
- 3) managing product personalization resulting in small lot sizes with high workpiece complexity and variety,
- 4) install flexible and agile production processes,
- 5) provide production rentability and optimization, e.g., machine utilization or material flow and
- 6) combine different procedures.

A survey conducted by Autodesk [13] analyzed the Mass Customization readiness level of about 50 companies, revealing that this activity field is still insufficiently dealt with. While typical mass-production factories use specialized machines with high productivity for high quantities, plants with a high-variant production need several universal machines with high flexibility [14]. Besides higher investments for more flexible machines, variant-oriented productions have smaller repetition rates of work steps [15]. As a result, learning effects and working productivity are decreased [16].

The rising need for flexibility demands higher-skilled labor, increasing production and work costs [4]. Especially SMEs face the challenge of recruiting operating specialists [5].

The effects of the skilled labor shortage and growing staff turnover reinforce this problem [17]. PwC [18] forecasted a competency mismatch in 2030 within the production environment of 8 % in professionals, 15 % in higher professionals, and 9 % in academic professions. Meanwhile, a surplus of 8 % is predicted for unskilled labor [18]. For this problem statement, three possible future scenarios occur [8]:

- 1) Upgrading
- 2) the Automated Factory, and
- 3) Polarization.

While upgrading promises stability in employment with an increasing qualification level, workers will be substituted by automation in the automated factory, mainly focusing on employees with lower qualifications and standardized work contents. In the most probable, the polarization scenario, digitalization, will increase the gap between those employees who benefit from Industry 4.0 from those who become disadvantaged by this development [8].

The future vision Industry 4.0, which was started in 2011 by the Ministry of Education and Research (BMBF) and the Ministry for Economic Affairs and Energy (BMWi) of Germany, implies different technical activity fields, among others, digitalization, automation, assistance systems, and human-system-interaction [19, 20]. It can be designated as *“a way of making any manufacturing environment more market and demand appropriate by employing technology to seamlessly and automatically improve cycle time, batch-magnitude, process characteristics, quality or manifestly change output according to – or even anticipating – demand.”* [21]. Important innovation fields constitute mobile and collaborative robots, machine learning, and reconfigurable production [21]. This fourth industrial revolution impacts machine tools regarding the fusion of physical machines with information technology to so-called “cyber-physical systems” (CPS) as well as interconnected production and automation solutions. As a result, reconfigurable production systems with high machine runtimes in terms of unmanned night shifts or continuous weekend operations are pursued. To keep the required variety on a low-cost level, the characteristics of adaptability, flexibility, standardization, and modularization are essential enablers for this vision [8]. Especially SMEs, which have no or low experience and inhouse knowledge about implementing such technologies, feel under growing pressure [22].

To tackle this complex issue, robotized machine tending solutions have been used for years [1, 2]. High system cost, the workpiece variety, and retrofitting difficulties constitute the main investment obstacles so far. Today, more than 50 % of all new FANUC tooling

machines are installed with an automation solution with increasing demand, while robots are used for about 7 % [23]. Overall, only 5 % of the production is automated, with a 2 % rate in robotics [24]. While pallet handling has been the predominant solution for machine tending so far, current developments in flexible jaw and gripper changing systems increase the deployment of product handling systems [23]. Furthermore, collaborative robots offer new possibilities of machine automation, either as a stand-alone system or for direct interaction with the operator [25]. Recent innovations in mobile robots enable simple interlinking by transporting workpieces between single machines and storages, leading to high-flexible processing [25, 26].

According to ISO 21919-1 [27], a machine tending system is “*a functional unit transporting parts without changing their physical properties.*”. An automated machine tending can be defined as the “*process of transporting parts into or out of a machine by a machine tending system*” [27]. Besides this standard, further underlying ones are ISO/TC 184 [28] and ISO 11161 [29], while ISO/DIS 21919-2 [30] is currently under development. A machine tending cell consists of single subsystems, which can be further distinguished into even smaller ones. Additionally, to the general equipment classification into manufacturing, assembling-, and logistic equipment, robotic workstations, and especially machine tending cells can be classified in more detail.

Firstly, general robotic workstation classifications are presented. [31] differentiate between logistics equipment, safety devices, the robot, the correspondent grippers, and machine vision. [32] divide resources into human-based, robot-based, and mechatronic-based ones. [33] mention besides robots, also part feeders and fixtures. [34] only discuss the robot by subdividing it into the arm, the hand, and the sensors. [35] consider the two entities robot (arm, gripper, and tool) and the operator.

Secondly, machine tending-specific equipment classifications are summed up as follows. [36] describes the fundamental elements of a machine tending cell, which are, besides the basic entities CNC machine (including the machine door), operator and robot, also the vice, the controller, the teach pendant, parts, and the gripper. [37] classify such a cell into the machine tool (including chucks and the door), the robot, the gripper, the sensor system, the workpiece, and the respective workpiece depot. A very comprehensive subdivision was done by [38] into the robot system, the human, the machine tool, fixtures, structures, stations for tool change, inspection, loading and operator, the workpiece, and safeguards. [39] consider the whole cell with a very detailed subdivision into the following elements: product buffer,

handling, operator, operation, maintenance, operating equipment, information- and organization, design, machine installation, and disposal.

Based on the presented differentiations, appropriate sub-systems have been summed up and concluded in Figure 2.1, at least from a hardware perspective. Possible specifications for each subsystem, illustrated as a morphological case, are enclosed in Appendix 1 and will be explained in the following subchapters. Communication systems between machines and robots have been summed up by [40].

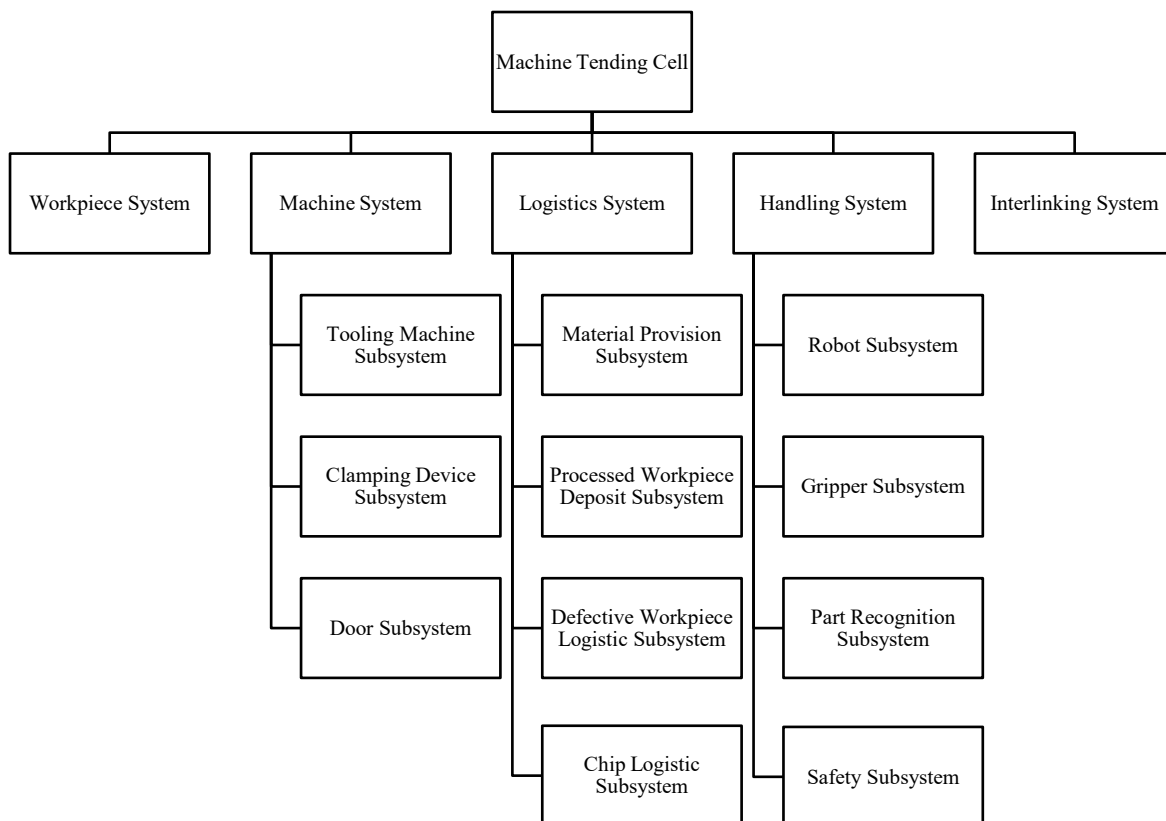


Figure 2.1: Machine Tending Cell System Composition

2.1.2 Workpiece System

Due to the diverse range of rotary workpieces, various classification criteria can be used. In 1966, [41] described workpieces according to geometry, material, features, and functionality. Opitz [42] introduced a coding system, which subdivides between rotational parts with and without deviations. Further classification criteria are the principal shape, rotational machining, external and internal shape elements, surface machining, auxiliary holes, drilling patterns, and gear teeth. Another coding system, called MICLASS, was developed in 1975 [43]. In the same year, [44] described workpieces according to different

technical features, such as threads, holes, or gears. [45] used the shape, length/ diameter ratio, material, functionality, dimensions, tolerances, and surface as differentiation criteria.

The CLASS and the FORCOD systems have been published in the following years by [46] and [47]. [48] analyzed the issue from a robotic gripping perspective and classified workpieces according to their geometry, form elements, physical characteristics, and static and dynamic behavior. [49] builds a classification system based on the shape, several form features, and the raw material. [50] describe workpiece shapes, sizes, dimensions, and further characteristics. Based on the Opitz and the MICLASS system, [51] developed a new coding system for cylindrical parts, which classifies, among others, the shape and various other features. For this doctoral thesis, the Opitz classification system is used as a basic framework for the following reasons: the classification system is formulated in a general way, easy to apply, and widely represented in literature. Since this research focuses on human-robot collaboration in lathe machine tending, which implies potential collisions between the gripped workpiece and an operator, only the outer contours of the rotary workpieces are further considered.

The most relevant criteria with the respective specifications and characteristics are presented in Table 2.1, clustered in general and specific criteria. While general criteria serve only the nominal description of a workpiece, specific criteria characterize the workpiece in a metric way by introducing measurable factors (extended version see Appendix 2). The comprehensive workpiece classification has been published in [52] within the EU-funded COVR research project.

Table 2.1: General Workpiece Criteria

Category	General Criteria	Criteria	Specifications
Material (Workpiece)	General criteria	Geometry	Spherical, cylindrical, cubical, flat, hollow, cone
		Form	Straight, bent, c-line, dome, cone, torus/ ring
		Diameter consistency	Uniform diameter along the entire length, changing diameter along the entire length
		Centre of gravity	Central, decentral
		Material	Steel, aluminum, synthetic
		Form stability	Stable, unstable
		Stepped/ tapers	None, stepped to one end, stepped to both ends

2.1.3 Machine System

Usually, cutting movements on the workpiece are fulfilled by its movement, making lathe machines primarily suitable for rotationally symmetric parts. It is also possible that the workpiece itself is fixed and the tool is rotating [53]. The addition of functions enables turning machines to execute drilling and milling operations in different operation angles. Machine classifications are based on technical main and side criteria as well as their structure and integrated modules. Typical machine components imply the base form, the relative position between workpiece and tool, compound slides, tool carrier, auxiliary systems, and feeding possibilities [54]. Firstly, the bedform and relative tool-workpiece positioning determine the primary processing direction and, therefore, limit the robot's workpiece tending possibilities. Possible loading and unloading directions are front loading, rear loading, and top-loading [53]. Secondly, the presence of a counter spindle defines the extraction point of the workpiece. Chuck parts are usually fed and taken out from the main spindle, while longer shafts are clamped first between the main and counter spindle during processing, then handed over to the counter spindle, and finally cut off in order to take the workpiece out of the counter spindle. Consequently, these elements determine the loading and unloading positions for the robot. Lastly, the workpiece clamping is a crucial variable, which gives information about the strategy and direction of gripping [53, 54]. From an automation engineering perspective, especially the maximum workpiece mounting- and turning diameter, the maximum workpiece length, and the type and amount of workpiece holders are to consider. That information determines the available workpiece possibilities, which are relevant to the manipulability of the robot [53]. To conclude the automation degrees of the tooling machine, the essential equipment components must be analyzed, such as the machine itself and tool and workpiece flow systems [54]. Based on the automation degrees, tooling machines can be classified into conventional tooling machines, CNC machines, machining centers, manufacturing cells, and manufacturing systems (see Figure 2.2) [53].

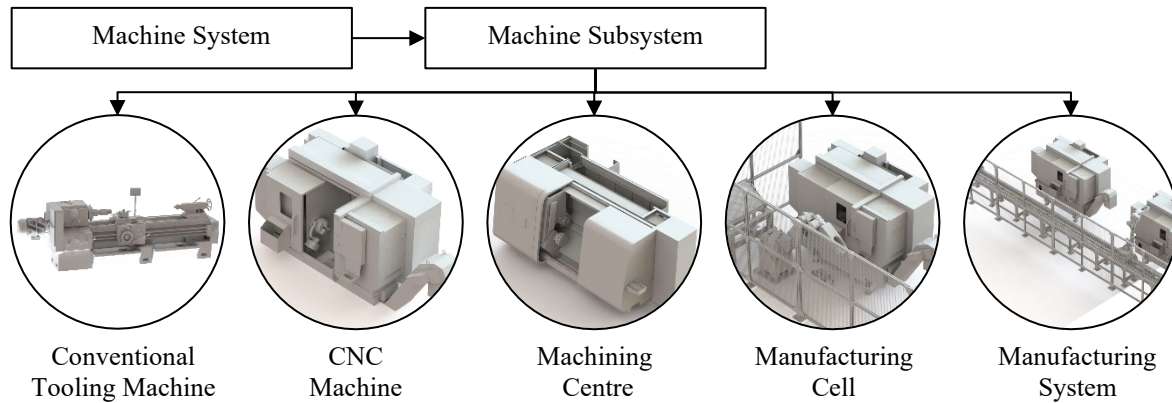


Figure 2.2: Tooling Machine Subsystem

Each automation stage implies different devices and features in terms of processing, tool, workpiece, control, and component (see Table 2.2) [53].

Table 2.2: Tooling Machine Automation Degrees based on [53]

Category	Functionality	Conventional Tooling Machine	CNC Machine	Machining Centre	Manufacturing Cell	Manufacturing System
Processing	Generating cutting- and feed movement and processing forces	•	•	•	•	•
	Multi-sided machining (4 th and 5 th axis)	○	○	•	•	•
Tool	Tool revolver	○	•	•	•	•
	Automated tool change from own tool magazine	○	○	•	•	•
Workpiece	Automated work cycle for equal workpieces	○	•	•	•	•
	Automated workpiece pallet changer and workpiece monitoring	○	○	•	•	•
	Automation workpiece loading/unloading device from own workpiece magazine	○	○	○	•	•
	Flexible workpiece sequence	○	○	○	•	•
	Automated workpiece flow	○	○	○	○	•
Control	Sequence control of machine functions	○	•	•	•	•
	Automated program fetch	○	○	•	•	•
	Automated process control	○	○	○	•	•
	Automated transport monitoring and process control via master computer	○	○	○	○	•
Components	Integrated monitoring and measurement devices	○	○	○	•	•
	Additional devices for measuring and cleaning	○	○	○	○	•
	Multiple complementary machines	○	○	○	○	•

While the automation of levels 1 to 3 is machine-related, levels 3 to 5 are process-related. Furthermore, levels 1 to 3 are always single machines, while level 5 is always a multi-machine system. Level 4 can occur in both shapes [53]. For this research, only CNC lathe machines and turning-milling machining centers are further considered.

Different clamping devices are required to fix the workpiece during processing, synchronizing the workpiece axis with the spindle rotation axis and enabling the power transmission on the workpiece [54]. Based on the technique itself, clamping equipment can be classified according to its automation grade, clamping type, and accuracy. While traditional machines use manual clamping techniques, higher-automated variants offer mechanical, hydraulic, pneumatic, and electromechanical actuation. The clamping type can be divided into inside and outside clamping, while the accuracy is either low or high [53, 54]. Fundamentally, (clamping) chucks are used for the process-stable clamping of chuck parts. For rotation-symmetric parts, centric three-jaw chucks are used ($3 \times 120^\circ$), and for prismatic parts multiple-jaw chucks. Chucks are available for both inside and outside clamping and in different surface shapes: soft surfaces for finishing and hard surfaces for rough processing. Typical manual devices are the plane spiral chuck and the wedge bar chuck; automated ones are the hollow and partially hollow clamping devices. Shafts are usually clamped with face drivers, which can be fixed with a center tip on the tailstock on the opposite workpiece side. For the automated handling of bar material, collets are used, which have multiple jaws and allow clamping with high forces and accuracy. Very long parts must be additionally supported with steady rests during processing. Further clamping devices are mechanically or hydraulically actuated mandrels, membrane clamping devices, or horizontal tables for big and irregular parts [53, 54]. Figure 2.3 illustrates both main options. For this research, only clamping chucks are further considered.

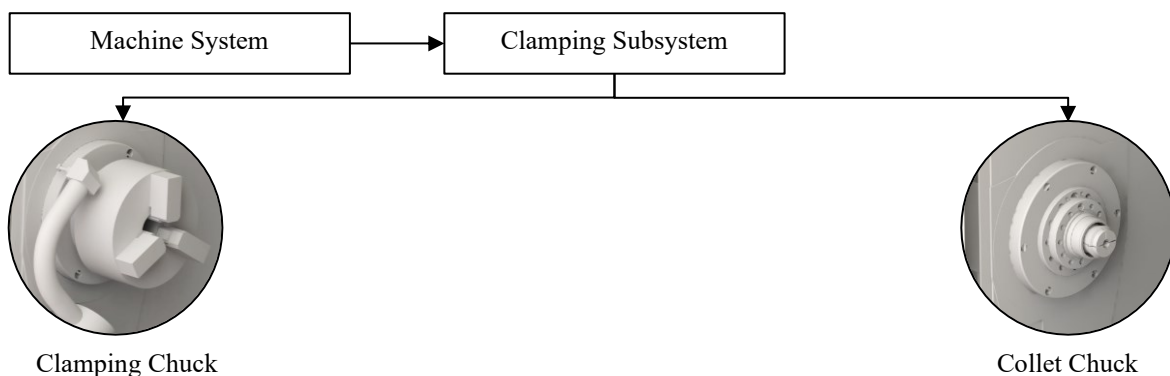


Figure 2.3: Clamping Device Subsystem Alternatives

To enter the machine's workspace, doors are either manually or automatically opened and closed. For automation, three fundamental options are to choose from. According to [55], an internal door actuation system can be added as a machine extension, such as pneumatic or hydraulic cylinders. Another option is utilizing the robot, either by gripping the door handle for mechanic actuation or by initializing a signal to actuate the beforementioned cylinder [36, 56–58]. According to machinery directive 2006/42/EC [59], DIN EN 61800-5-2 [60], DIN EN ISO 13849-1 [61], the door must be closed and monitored safely during processing due to hazards of machining. Therefore, internal door actuation systems require performance level category 3 (PL d, Cat. 3) to provide a safe two-channel signal about the door status (open or close). Such a control system monitors the two machine door contacts (contact open and contact close) and the two actuators (actuator for opening and closing) with PL d, Cat. 3 for safe operation [62]. Furthermore, the functions STO (Safe Torque Off), SLS (Safely Limited Stop), and SLT (Safely Limited Torque) are required [63]. In Figure 2.4, both options are outlined. For this research, only door actuation systems are further considered.

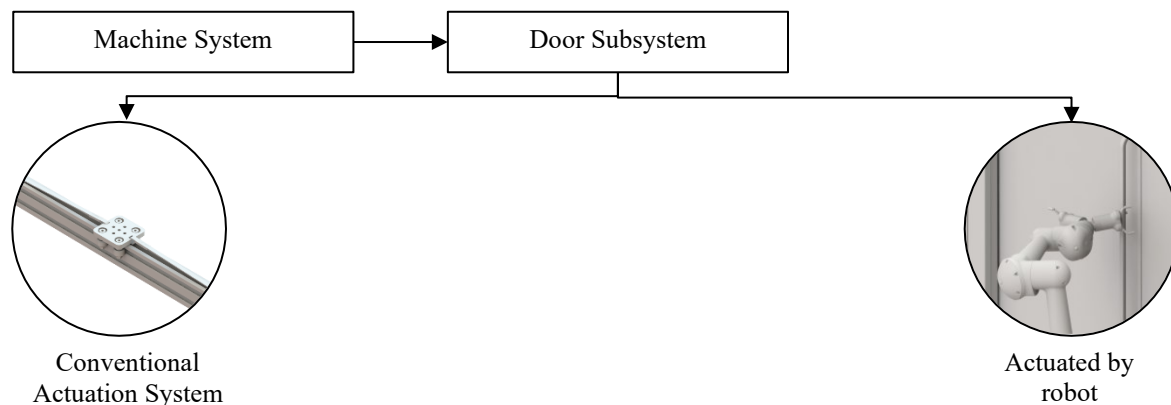


Figure 2.4: Door Subsystem Alternatives

2.1.4 Logistics System

In order to load and unload the machine with the material, a logistic system is required, consisting of the workpiece provision subsystem and the processed part subsystem [36]. Those consist of the material system itself (pallet-free or pallet-based), buffers, and storages, as well as transport devices [53]. Fundamentally, a lathe machine can be fed with either bars or shaft material, depending on the defined products.

Material bars constitute one primary basis for turning operations and are especially suitable for large-volume production. Due to the high retooling effort, NC bar loading magazines are utilized for cycle time optimization [54]. Bar loaders are feeding devices that hand bars from a roller conveyor over to a tooling machine autonomously. The stored bars are firstly separated and then inserted into the feed channel by guiding the workpiece bars with elastic rolls [54, 64]. A telescope slider is used to transport the workpieces, consisting of an outer part and an inner slider [65]. Through the main spindle, which is equipped with a hollow clamping cylinder, bars can be rear-fed and clamped with a collet chuck [53, 66]. When a workpiece has been processed and cut off, the bar is pushed through the opened guiding channel section-wise [54]. Due to the rotation of the bar during processing, a respective bearing (centric rollers, oil guiding systems) is required to avoid vibrations [53, 65]. The inner slider automatically removes the bar rests that cannot be processed [54, 64]. Subsequently, another separated workpiece bar is transported by the insertion system to the guiding channel for processing [54]. By providing sufficient bar storage for, e.g., one whole shift, fully automated or multi-machine operation with minimized personnel of large volumes can be guaranteed [53, 64, 67]. Therefore, most CNC swiss-type lathes, automatic lathes, and rotary cycle centers are usually equipped with a bar feeder, which reduces intervention into the production process to a minimum [53, 64]. Besides economic considerations, especially the process reliability has to be taken into account when adding such a system, usually given for bars larger than 3 millimeters diameter [64]. On the other side, chuck parts can be provided as single or mixed parts, either pallet-based or pallet-free [54, 68]. Pallets are customized workpiece carriers, which position the part either vertically (hole pattern) or horizontally (prism). Those can be further classified into storage and transport pallets and workpiece pallets. On the other side, pallet-free workpiece provision is commonly used for either smaller or middle workpieces as well as for bigger rotational parts with a very small length to diameter ratio [54, 68]. In the simplest form, workpieces can be placed on provision tables, either as a single workpiece or under the use of a pallet or tray [69]. Also, drawers are possible, in which multiple layers of material can be stored. Another option are flow racks with an inclined plane to provide multiple small load carriers or single workpieces in a specific order [69, 70]. Lastly, turntables can be used, e.g., to load from one side and take out the workpieces from the other [69]. Such a system is typical for robotic lathe machine tending since the robot can initiate the turning movement [71]. In order to counterbalance production uncertainties, buffers and storages can be added [53].

Lastly, transport devices are required to move the workpieces between the single positions within multi-machine systems. Those systems can be classified according to their floor bounding (bound or free) and steadiness (steady or intermittent). Typical systems for multi-machine operation are conveyor belts, roller conveyors, chain-pulled conveyors or magazines, tugs, lift trucks, rail-bound transport devices, inductive-based forklift trucks, and driverless transport systems (DTS) [53, 72]. The whole classification is enclosed in Appendix 3. For this research, only drawers and provision tables are further considered.

2.1.5 Handling System

2.1.5.1 General Handling Possibilities

In combination with a bar feeder, usually, machine-internal workpiece extraction systems, such as part grippers, collection trays, or small robots with a conveyor track, are used to enable automated operation without door actuation. After gripping the workpiece within the machine, it is transported on the conveyor to a defined position outside of the machine [54]. In exceptional cases, e.g., for very massive bars or workpieces with a very high surface finish, machine-external automation is used.

Chuck part production is mainly automated with machine-external technologies, such as linear or area portal loaders, cranes, or robots. Due to the high machine accessibility resulting from the above-gripping, linear portals constitute the standard automation for lathe machines. The construction consists of the trolley, the x-system, and the z-system. Mounted on the x-guide rails, the trolley can be moved horizontally by the x-drive. In the z-direction, the z-drive moves the lifting unit with the attached gripper vertically. This system is ideal for transporting workpieces between linear arranged machines. Cartesian area portal loaders are used for movements in three directions, which have an additional y-axis integrated. When a broader space in the y-direction needs to be covered, e.g., for big machines, the outrigger is supported on both sides by a crossbeam, also called a bridge [23, 54]. Another automation possibility is crane systems in various construction forms [73]. An overview of all handling possibilities is enclosed in Appendix 4.

2.1.5.2 Robotic-based Machine Tending Possibilities

When it comes to machine tending installations with robots, a wide variety of automation forms are possible, mainly depending on the production type and the respective number of

tended machines. For single machine tending, the following robot installations are possible: inside, from above, on a console, or a socket (see Figure 2.5).

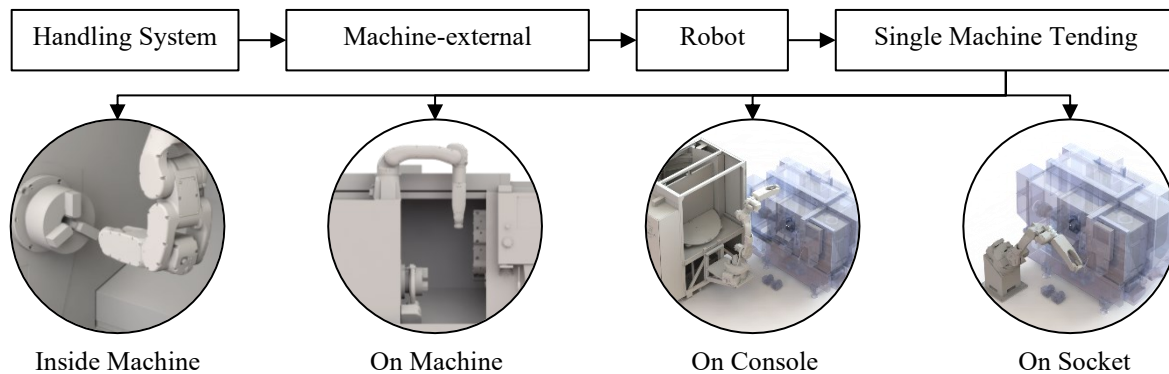


Figure 2.5: Robot Subsystem - Single Machine Tending Installation Possibilities

Usually, small robots with high protection classes (IP class) are used for inside applications, working by the same principle as the previously mentioned workpiece grippers but with higher flexibility [74]. Due to the closed-door operation, human-robot interaction is not required. For tending from above, either standard robots in a ceiling installation or rack-mounted robots are used, often with extended reach below the robot installation base level [12, 75]. Due to the considerable weight and potential to compromise the machine's static structure, smaller robots are preferred for the first variant. Consoles are whole frames in which the system can be integrated as a complete solution. Depending on the robot specifications, ground, angled, wall, or ceiling installations are possible [71]. For socket installations, large robots with a high reach are mounted onto a freestanding angled socket [76]. Such an angled installation (either in one or two directions) is standard within machine tending because it provides better accessibility to the machine. Despite inside robot installation, all other variants are possible with both industrial and collaborative robots and fenced-in and fenceless operation.

When more than one machine must be operated, multiple machine tending is preferred to increase the robot's utilization rate while reducing unproductive waiting times. Therefore, various interlinking technologies are available, such as linear axis, gantry systems, and driverless transport systems (DTS) or rather automated guided vehicles (AGV) [77]. Multi-machine systems describe multiple single machines interconnected by interlinking technology to achieve an automated workpiece flow. Within the overall system, an increase in productivity and flexibility is pursued [53]. Due to the high reach of large robots, those can be installed between two frontside-arranged or three triangular-arranged machines,

providing a small footprint [76]. Another more uncommon option is to connect a middle-sized robot with a two-axis positioner [76]. The most usual interlinking solution for linear arranged machines is robots onto a linear axis to add more degrees of freedom to the robot to enable it to access positions out of its reach [12]. Floor installations require a higher footprint with low installation cost, while gantry systems are more space-saving due to the pillar footprint but demand vast and cost-intensive steel constructions [26]. Recent innovations in mobile robotics provide the highest flexibility regarding machine arrangements and application fields while requiring high investments and IT integration effort [12, 26]. Mobile robots are the most sophisticated option in terms of footprint and utilization rate because the robot occupies only space at one machine simultaneously and reacts to order deviations. Fundamentally, all these installation principles can be potentially executed with an industrial and collaborative robot or rather with or without a fence (see Figure 2.6). For this research, robots on consoles and sockets are further considered.

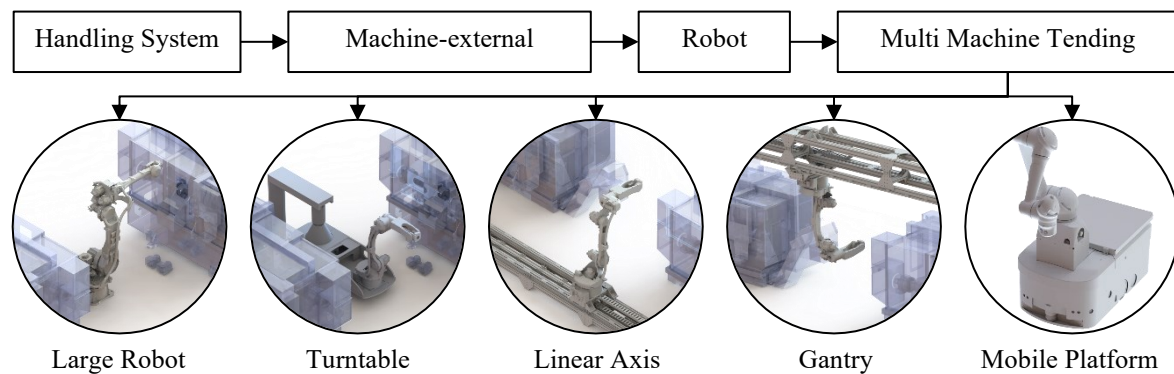


Figure 2.6: Robot Subsystem - Multi-Machine Tending Installation Possibilities

2.2 Robotics

2.2.1 Robot Installation Development and Application Fields

According to [26] and [78], the continuous average growth rate (CAGR) of global robot installations was between 7 % to 19 % since 2010 or rather 2012. One of the leading exporting and integration nations is Germany, due to close connections between industrial and research clusters with the automotive industry as an innovation driver, the direct logistic access to the European market, the demographic employee development, and the increasing digitalization and automation in terms of Industry 4.0 [78]. Recent developments in the technical features and integration simplification and growing accessibility to robotics technicians can be considered enablers for this development [26]. Robot production prices

have been decreasing dramatically since 1990, while labor cost, on the other side was highly increasing since then [26, 79]. By using robots, customers expect, among others, a qualification shift in their current staff, increase in efficiency, quality, precision, and production time, as well as cost decrease [78]. While the automotive industry focuses mainly on flexibility and safety optimization, companies of the electronics sector consider quality and productivity improvements as essential benefits of industrial robots. The main challenges for the robot manufacturers are the Total Cost of Ownership (TCO) of a robot, the heterogenous variety of programming options and interfaces, the global distribution of system integrators, and the difficulties in retrofitting existing systems [26].

The International Federation of Robotics (IFR) [80] publishes an annual report about the internationally sold robot units, clustered them by countries, robot types, and applications. To get a more in-depth market understanding, the domains Global, Europe, and Germany are considered with a focus on articulated robots [80]. Figure 2.7 shows the industrial segmentation in all three market scopes in 2018. Since the latest reports of 2019 to 2021 are biased by the corona pandemic, the 2018 numbers are considered more representative and are therefore analyzed. As can be seen, articulated robots are primarily installed in the manufacturing industry (dotted area), independent of the observed domain.

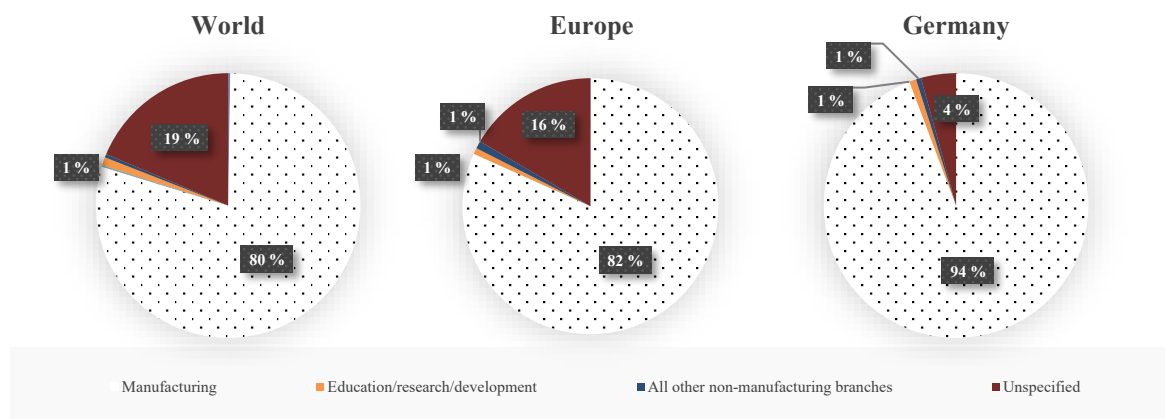


Figure 2.7: Industry Segment Robot Installations in 2018 based on [80]

The robot installation base in the manufacturing sector is distributed into single sub-industries, where automotive and metal are the strongest (Figure 2.8, stippled areas).

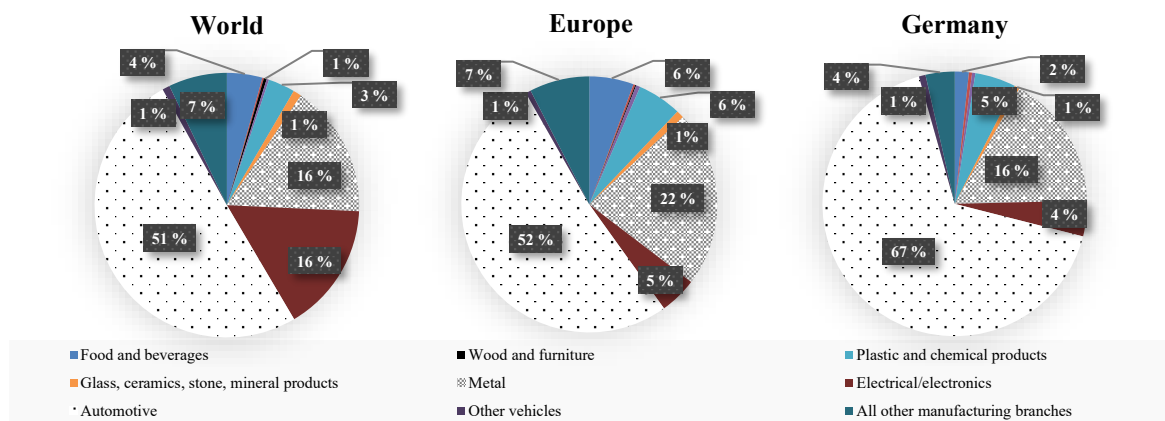


Figure 2.8: Robot Installations by Industry in 2018 based on [80]

Material Handling & Machine Tending (dotted area) are revealed as dominant fields by analyzing different applications (see Figure 2.9).

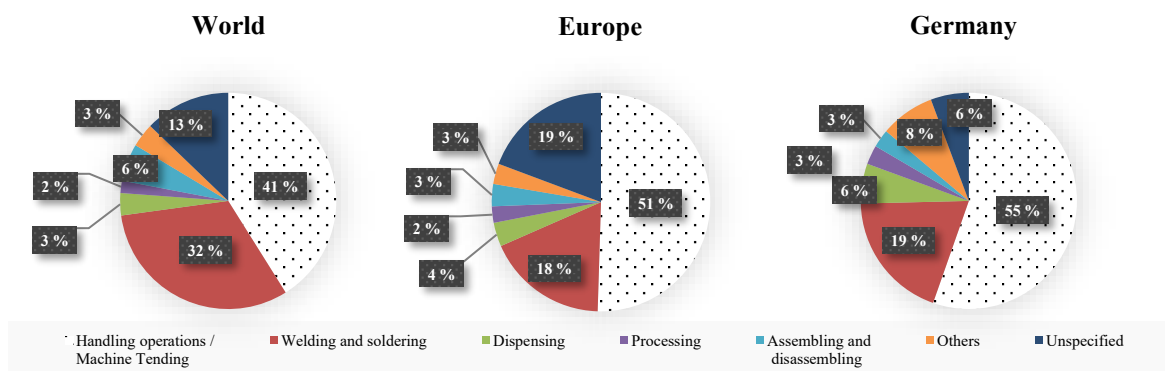


Figure 2.9: Robot Installations by Application in 2018 based on [80]

By sub classifying this wide application field, the main areas “material handling” (Figure 2.10, MH, dotted white area) and “handling operations at machine tools and other machines” can be identified (Figure 2.10, MT, dotted grey area). In the designated IFR application coding, “114 handling operations at machine tools” and “115 handling operations for other processes” are separate streams. According to the [81], those must be considered mutually recently due to changes in the reporting behavior.

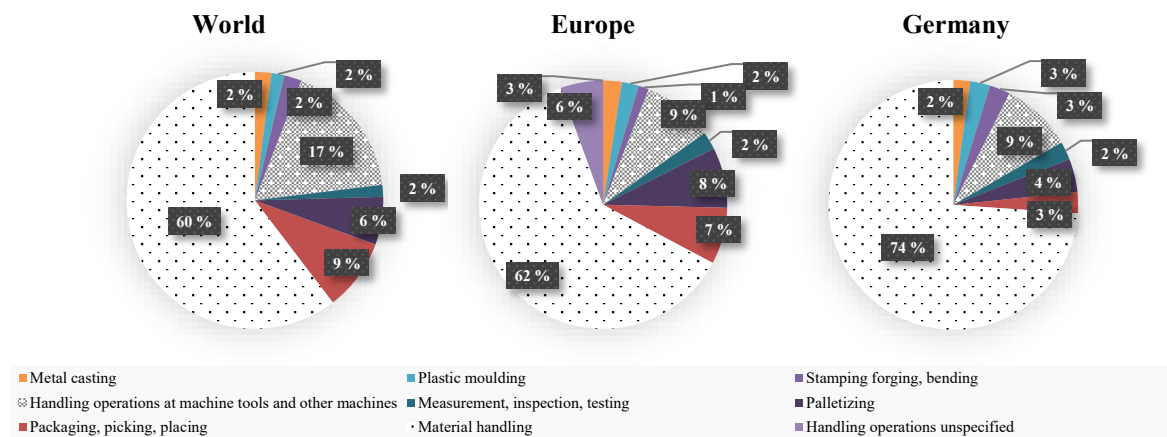


Figure 2.10: Robot Applications in Handling Operations/ Machine Tending in 2018 based on [80]

Figure 2.11 illustrates the installation development between 2017 and 2018 in general, for material handling & machine tending and machine tending in particular for all three domains. In contrast to the World and European markets, Germany's strong focus on handling and machine tending applications can be noted, making this application field ideal for in-depth research.

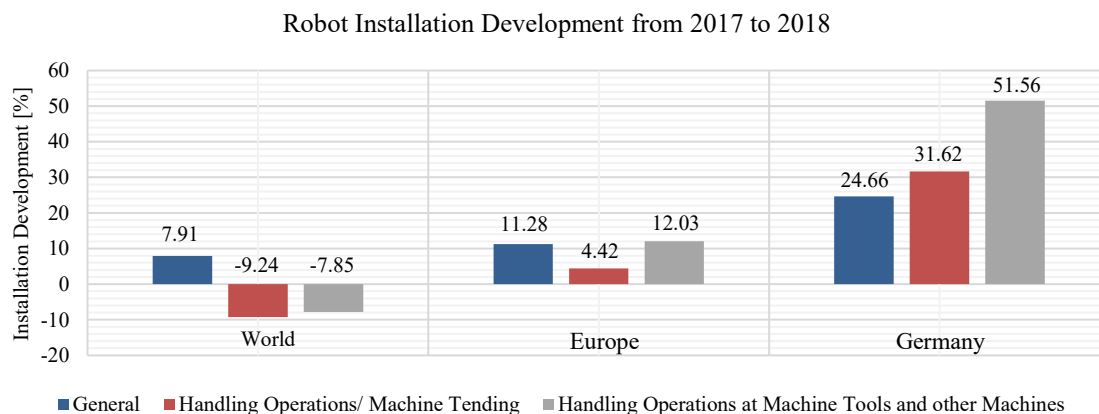


Figure 2.11: Robot Installation Development from 2017 to 2018 based on [80] and [81]

After reviewing industrial robots in general, the development of collaborative robots is focused on as follows. According to [81], the cobot market space promise long-term growth potentials, especially in new branches and for SMEs due to simplified programming and integration. For this market, strong growth with over 100,000 units in 2020 was forecasted by [26]. End of 2020, the cobot market leader Universal Robots reported the 50,000th sold unit [82]. Therefore, forecast and reality mismatch can also be traced back to the corona pandemic's bias regarding investment hesitation. According to [3], the electrical and

electrotechnical, automotive, and polymers industries were forecasted as the leading sectors for cobots from 2015 to 2021. As main applications fields, material handling, machine tending, and small parts assembly have been stated. Recent studies and expert statements comply with this forecast. According to [25], cobots are typically used in small- and middle-series production of small workpieces with low weight for assembly or handling tasks, such as pick & place or machine tending. Similar results show a study conducted by [83] with primary applications in the assembly area and part manufacturing in the automotive and electrotechnical industry. Growing application areas are retail trade, food industry, measurement, and laboratory applications [13]. Examples for lab automation with industrial and collaborative robots were published in [84–86], while a quality test example is given in [87]. As application reasons, the following have been stated commonly: economic considerations in terms of higher productivity, improved ergonomics and skilled labor shortage to intercept demographic developments, new process possibilities, and innovation strategic aspects [19, 83]. Further benefits are direct integration due to fenceless operation with a small footprint, requirements in precision and ergonomics, flexible process adaption, job enlargement, or rather job enrichment by rearranging work contents [13]. According to [78], the essential requirements for human-robot cooperation are rentability, usability, employee qualification, robot O.E.E., functionality, and safety. Furthermore, a production-based infrastructure, value-stream-oriented digitalization, spatial shop-floor conditions, and IT infrastructure are also necessary. Pursued targets are highly flexible production processes to encounter the demands of mass customization, efficient and low-cost installation effort due to simplified programming and on-board safety, the direct integration to the workstation with minimal modification, and the optimal combination of human and robot abilities to improve ergonomics [25, 26, 88]. Based on the market overview provided by [89], the payload-reach-distribution of multiple commercially available cobots of 22 manufacturers is illustrated in Figure 2.12. As can be seen, collaborative robots are concentrated on smaller reaches of 400 mm to 1500 mm and payloads from 0.5 kg to 20 kg. Due to scaling, the Comau Aura with 2,790 mm reach and 170 kg is not included in this diagram.

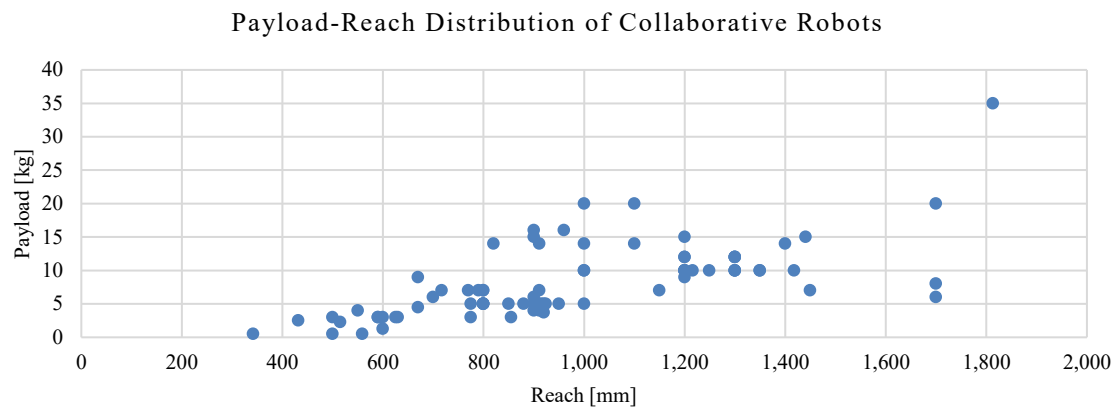


Figure 2.12: Payload-Reach Distribution of Collaborative Robots based on [89]

2.2.2 Fenceless Industrial and Collaborative Robots

According to [90], an industrial robot is defined as an “*automatically controlled, reprogrammable, multipurpose manipulator, programmed in three or more axes, which can be either fixed in place or mobile for use in industrial automation applications.*” Fundamentally, robots can be classified based on their kinematic chain: open for serial robots or closed for parallel ones. Furthermore, hybrid types are available, which combine the characteristics of both types [91]. [92] further classifies serial kinematics into the types SCARA, robots with 4/5 axis, and six axes; additionally, 7-axis robots must be considered (see Figure 2.13). Furthermore, robots can be differentiated by their weight between lightweight robots and classical industrial robots [93]. The mass is directly affecting the robustness, reach, and payload of the robot. [94] divide single and dual-arm robots. For this research, only 6-axis robots are further considered.

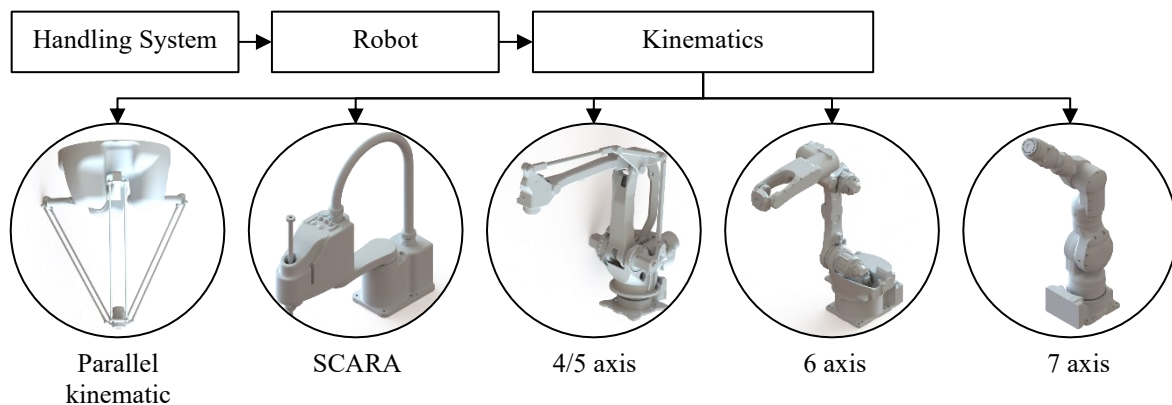


Figure 2.13: Robot Subsystem - Kinematic Possibilities

Most important for this doctoral thesis is the subdivision between industrial and collaborative robots, according to [95]. To better comprehend the conceptual progression of human-robot collaboration, it is valuable to take a step back into classical industrial robotics to understand the core of safety measures. On this basis, the following paragraph deals with the clarification of and the distinction between the terms “collaborative application” and “collaborative robot”. From an occupational safety point of view, robots constitute a risk potential to injure an operator. The robot installer is obligated to guarantee the operator's safety by adding respective safety measures to prevent accidents. The classical way of safeguarding is safety fences, which separate the robot physically from the operator. Entrance doors that shut the robot down as they are opened, guaranteeing safe access to the robot's operating space, e.g., for maintenance. The main advantages of that solution are simplicity, small footprint, and high shielding from the robot itself and potentially flying objects. The downside is the static installation without transformation possibilities and restricted logistic and human interaction possibilities [96]. Propelled by the beforementioned Industry 4.0 development, modern and future factories require flexible and transformable production systems that directly integrate the robot without static fencing. This vision of fenceless automated manufacturing comes along with various expectations and targeted improvements compared to traditional fenced-in solutions [2, 97]:

- 1) Cost and space savings,
- 2) ergonomic improvements,
- 3) safety,
- 4) cycle time improvements, and
- 5) simple programming and flexibility.

For technical realization, human-robot collaboration plays a vital part. In [98], a collaborative application is defined as a “*state in which [a] purposely designed robot work in direct cooperation with a human within a defined workspace.*” Even though the actual “collaboration” with a cobot does not always occur, other HRC forms, such as coexistence and cooperation, are likewise suitable to operate fenceless. Therefore, the term “human-robot collaboration” is too narrow and should be extended to “human-robot-interaction” (HRI) to incorporate all types, which are explained as follows. According to [99], HRI can be clustered by the interaction grade into collaboration, cooperation, and coexistence. On the one side, collaboration implies direct interaction between human and robot, which can only be achieved with cobots with internal sensors. On the other side, coexistence describes that

robot and operator work without spatial separation next to each other but interact infrequently or never. In the middle, there is cooperation, where robot and human share a mutual workspace and can interact with each other. Hence, coexistence and cooperation are possible with both collaborative and industrial robots. Other taxonomies have been published, among others, in [83, 93, 100–104].

For the realization of the single types, various safety technology options are possible. [94] subdivide the safety subject into strategies, areas, and functions. Possible approaches are crash, active, or adaptive safety and the definition of safe, warning, and unsafe areas under the use of software-based tools of the safety controller. Safety monitoring has been classified into safety distance & collision, force & torque path planning, and safety by design by [93]. [105] subdivide hardware safety devices into physical guards (fenced-in) and electro-sensitive or pressure-sensitive safety sensors (fenceless). The safety controller takes place on the software side, implying various functions, such as the definition and restriction of work areas and operating speeds and the position and axis data monitoring [93, 106]. According to DIN EN 954-1, the safety controller must be redundant so that two independent systems control each other and induce a safety stop in the event of contradiction (two-channel design) [106, 107].

After this general summary of safety possibilities and requirements, the following paragraphs explain the technical subtleties. [98], [90] and [108] define four methods of human-robot collaboration, or rather interaction, that can be used as a standalone solution or in combination with each other: safety-rated monitored stop (SRMS), hand-guiding (HG), speed and separation monitoring (SSM) and power and force limiting (PFL) (see Figure 2.14). In the latest standard draft, the ISO/DIS 10218-2 [109], SRMS is no longer considered a human-robot collaboration method. For the sake of completeness, this mode is going to be explained in detail, though.

In SRMS mode, an external safety device (e.g., laser scanner) monitors the presence of an operator within the designated interaction area to stop the robot before the operator enters the zone. Before entering and after leaving this area, the robot operates in full-speed (FS) industrial mode; only during the presence phase, the robot cannot operate. The HG mode enables the operator to physically guide the robot by applying force in the desired direction, measured, computed, and controlled by the robot system accordingly. This mode is not further considered since it is only required for the teaching process and does not affect the actual operation.

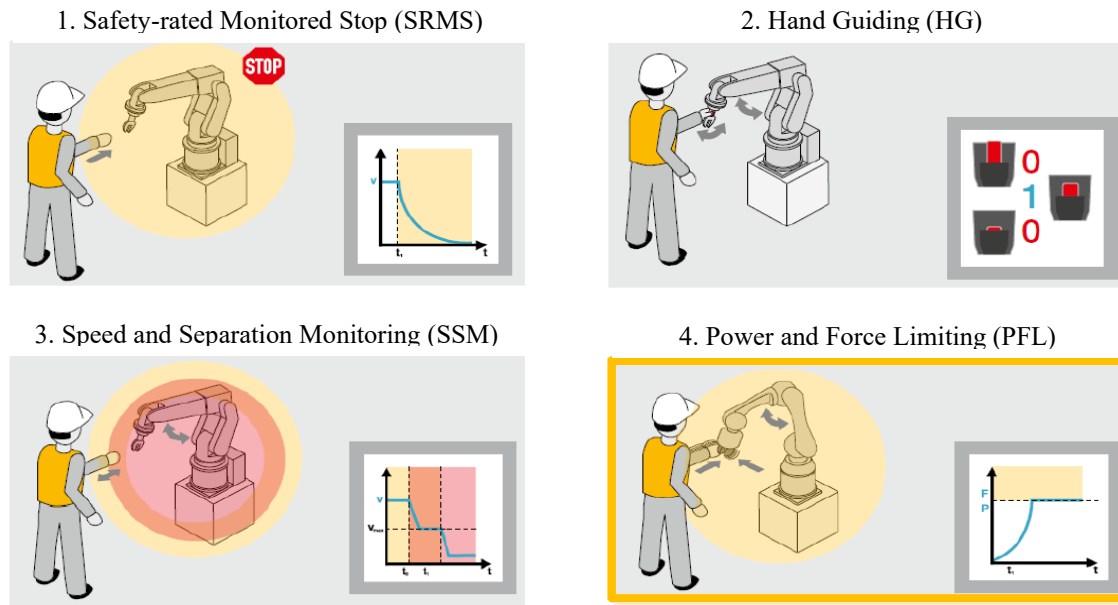


Figure 2.14: Four Modes of Human-robot-interaction [110]

In SSM, the robot speed is adjusted according to the proximity of the operator based on position monitoring with external safety devices. That means that the robot decelerates when the operator approaches and accelerates again with increasing human distance. To enable this mode, the robot must have a safety-rated monitored speed function according to ISO 10218-1, 5.6.4 [98], and a safety-rated monitored stop function. If needed, a safety-rated soft axis and space limitation can be used to limit the robot's motion range. Used as standalone solution, a separation distance to the operator must be maintained. In the case of violation of this distance, the robot must execute a protective stop (stop category 0) or start active safety-related functions according to ISO 10218-2, 5.11.2g [90]. This condition is avoidable by executing an alternative motion path or mode combination with either a safety-rated stop or power and force limiting. SRMS and SSM can be used with both industrial and collaborative robots. For their realization, different safety technologies are worth considering, such as safety curtains, laser scanners, or vision-based systems [77, 96, 111–114]. Light curtains are light-based barriers that map a specific planar area to automatically detect operators moving into the robot operating space [115, 116]. It consists of a sending unit that emits several light beams and a receiving unit that senses them, while the received beams trigger the two outputs [117]. As soon as an operator breaches the light curtain and breaks the light beams, the two outputs are de-energized, which activates the control circuit. Those outputs serve as an input signal for the robot for immediate and safe shutdown [116, 117]. Depending on the selected light source, the system is affected by disruptive factors, such as sunlight [115]. Laser

scanners monitor 2D areas from the installed point by defining various safety zones [96]. The configuration of these zones enables the mode assignment of either reducing the robot speed (warning protection field) or stopping the robot's motion (shutdown protection field), which offers a wide variety of safety concepts [96, 118]. The downside of this technology is the high space consumption and opacities within the scanning area (objects, blind angles) [96]. When a safety-based stop of the robot has occurred, the operator needs to confirm the action of leaving the operating zone (e.g., by pushing a safety button) to ensure the safe restart of the robot. Recent developments in laser scanning technology enable an automatic restart. An integrated logic circuit checks if the safety zones are triggered in the opposite way at leaving the operating space as at entering it [119]. Consequently, it is ensured that nobody is within the robot's operating space. The latest safety innovations imply radar systems that enable the definition of three-dimensional zones. Areal overlaps ensure the comprehensive coverage of the defined room [120]. Camera-based systems use multiple-oriented cameras covering a three-dimensional space of predefined safety areas (warning and protection fields). Therefore, technological enablers are stereo camera sight, stereo algorithms, and virtual fences [93, 121]. Changes in contrast allow the detection of multiple undefined entities to calculate the physical distance between robot and operator [93, 107]. Depending on the camera resolution and installation height, even single body parts can be detected for more accurate results [107]. In the event of field violation, digital signal outputs are used to reduce the robot's speed or even stop its movement based on the operator's proximity [93, 107, 122]. While camera systems are quick to install and cover a wide area, this technology is still expensive and implies problems in process reliability due to person masking and light changes. [123] presents a zone-based control algorithm that can be combined with different sensor technologies.

The PFL mode can be used with either collaborative, inherently safe robots or come with a safety-related control system or with industrial robots by adding additional sensors directly on the manipulator (e.g., sensitive skins). The control system needs to limit the occurring contact forces below the threshold values defined in ISO/TS 15066 [90, 98, 108, 124–126]. To operate the robot in PFL mode, passive and active measures are described in ISO/TS 15066. Passive ones imply increasing the potential collision area, reducing occurring forces, and the robot mass. Therefore, commercially available cobots come with rounded edges without clamping areas in the robot kinematic (safety-by-design) and lightweight construction. Active measures include the previously mentioned functionalities (limitation

of force/ torque, speed, energy and space, safety-rated soft-axis, SRMS) and sensing devices. In the area of active sensing technologies, robot manufacturers pursue different approaches, such as motor current monitoring, force and/ or torque sensors, sensitive skins, or the combination of different systems (see Figure 2.15) [95, 127–130].

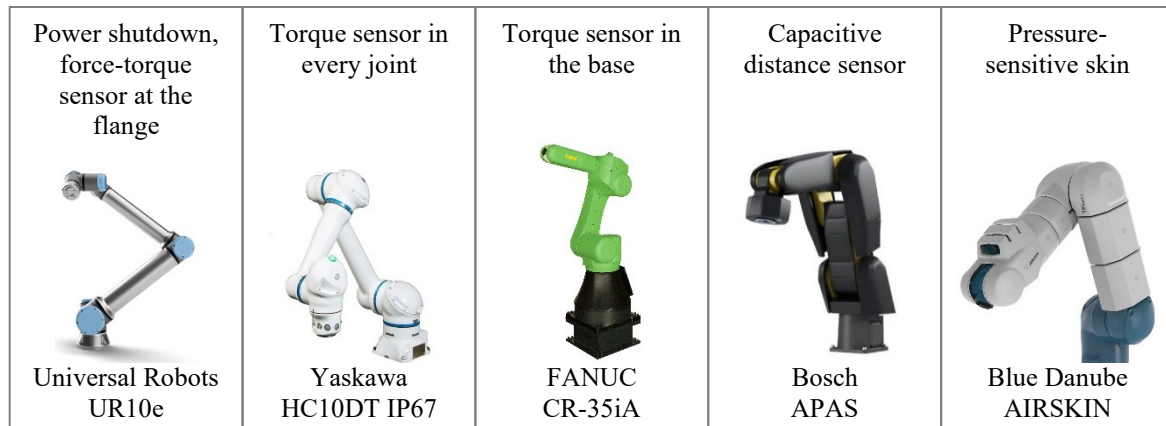


Figure 2.15: Cobot Representatives with different active Safety Technologies [131–135]

A novel approach has been patented at the Technical University Chemnitz by developing a joint with an integrated spring that absorbs the collision energy [136]. In the following, some available solutions are presented. Electric motors provide current data that is used to indicate the present torque of the drive [129]. Changes in the current behavior can be interpreted as collisions [127]. However, the measurement result is not representative due to the dissipation of the mechanical system [129]. Much more exact information is delivered by torque sensors that are not biased by the behavior of the gearboxes [129]. Instead, these sensors monitor the occurring moments directly at the installed joint [127]. Force/torque sensors provide even more correct data by measuring 3-dimensional forces and moments each [127, 129]. As shown in Figure 2.15, these sensors can be differently installed, e.g., at the flange, in each joint, or the base. Current safety skin technology utilizes, among others, capacitive or resistance-based sensors [128]. While capacitive sensors can detect approaching objects within a distance of a few centimeters, resistance-based skins require a collision that deforms the elastic skin element in order to measure the applied force [127, 128]. In [137], an industrial robot has been equipped with a combination of force sensors, a vision system, and sensitive skin to enable close human-robot collaboration. Based on the previously mentioned safety technologies in all three modes, an overall morphology can be concluded, enclosed in Appendix 5.

Even though these “cobots” are called collaborative, most applications end up coexistent or cooperative [81]. A study conducted by the Fraunhofer IAO shows that over 57 % of the analyzed applications were coexistent, while only 10 % can be considered collaborative [83]. In another study [138], 32 % coexistent, 31 % cooperative and 28 % collaborative applications were identified. With the given overview of human-robot interaction in mind, it can be summarized that there is no “collaborative robot” per se since it is an incomplete machine. The application is designated as collaborative by integrating a robot into a work cell by incorporating one or multiple modes of HRI. As described previously in this subchapter, cobots can work exclusively in PFL mode or the so-called hybrid operation by using multiple modes. Suitable combinations are FS – PFL or FS – SSM – PFL, while FS – SRMS or FS – SSM – SRMS are unreasonable due to lacking utilization of the PFL mode and should be used for classical industrial robots instead. Hence, a so-called cobot can coexist without true collaboration but still work in a so-called collaborative work cell. This example demonstrates the unclear definition of terms. The overall context between the HRI grade and the utilized robot and safety technology is illustrated in Figure 2.16.

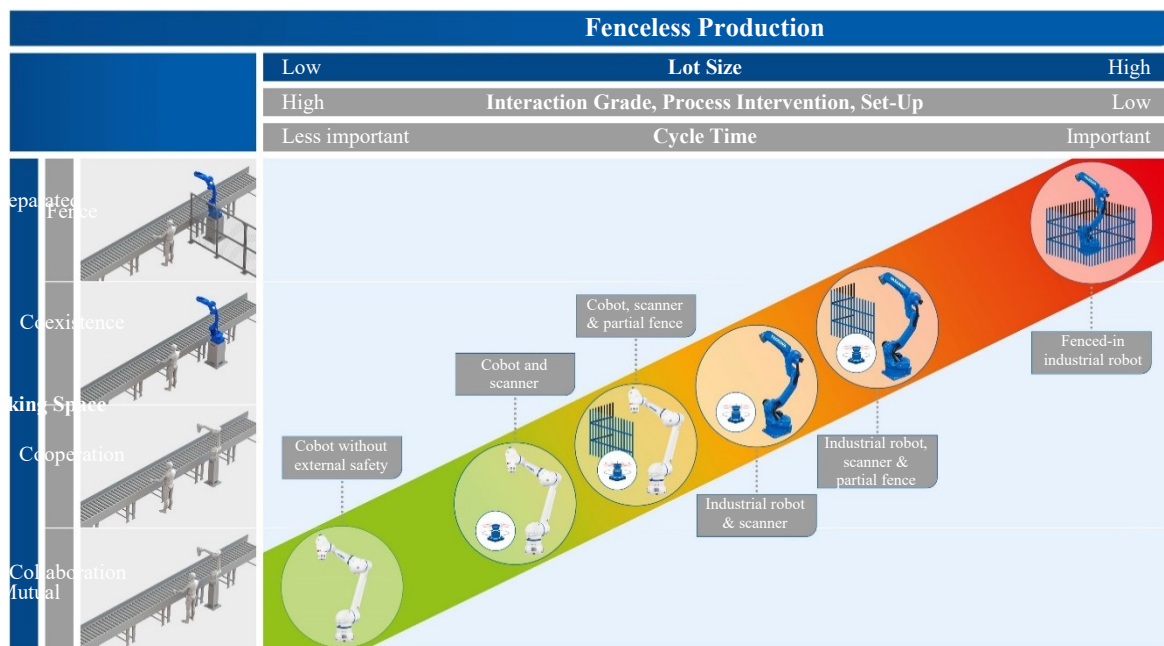


Figure 2.16: Human-Robot Interaction Classification regarding Robot and Safety Technology [139]

Besides the mentioned criteria, the single options are arranged by lot size suitability and cycle time priority since cobots usually have a lower maximum speed than industrial robots and must operate at a reduced collaborative speed during PFL operation. To better

understand this context, chapter “2.3 Planning and Evaluation Methods” will clarify requirements on safety compliance in PFL mode with a strong emphasis on the allowed operating speeds.

For this research, industrial robots in FS - SSM - SRMS mode and cobots in exclusive PFL operation and hybrid mode with FS - SSM - PFL mode are further considered.

2.2.3 Robot Grippers

As a robotic counterpart to the human hand, actuated grippers are used to handle a workpiece. According to [38], grippers can be classified according to the tool compliance (stiff, elastic, plastic, articulated), the tool power (electric, hydraulic, pneumatic, mechanical, thermal), the tool use, contact, and interaction as well as different force characteristics (e.g., force transfer, force magnitude, force type, force application, and process speed) [38]. Grippers consist of the flange, the case, the power unit, the drive side, and the actual holding system, which are explained as follows [140]. The flange connects the gripper with the robot and provides the interconnections of compressed air, vacuum, and electrical power and signals. The power unit and drive side, responsible for the gripper actuation, are integrated within the case. Actuation describes the transformation of primary energy into usable movement energy, either fluidic pressure-based or electrically powered. The integrated gearbox predefines the finger stroke and the actual clamping force. Depending on the construction form, lifespan and precision are mainly affected. Cases can be realized in monolithic or multi-part construction, providing either robustness and reliability (monolithic) or are open for customization by adding various materials or gripping concepts. Usually, grippers are made of steel, aluminum, or plastic. In order to grip and touch the part, the holding system is required, by using different physical principles, such as adhesive bond (adhesive tape, capillary gripper, freezing gripper), traction (friction, magnetic or electrostatic forces, negative pressure) and/ or form closure (surface interlocking, pairing form elements [140, 141]. Typical gripper forms are mechanical grippers (such as parallel grippers) and vacuum grippers.

Mechanical grippers consist of two or more jaws, which move toward each other. The simplest design is two-jaw grippers with a parallel kinematic. The movements are synchronized to the middle point of the gripper and are executed by short-stroke cylinders and pressure springs to achieve the stroke and return stroke [142]. Two-jaw grippers usually touch two points of the shell surface by gripping from the side, providing relatively reliable

handling. When using straight jaws contact surfaces, the workpiece can still rotate in one direction leading to inaccurate workpiece positioning (force closure). For counterbalance, custom rounded contact surfaces can be used to match the respective workpiece's diameter (form closure). Three-jaw grippers, however, grip the workpiece on the face side by touching three points of the shell surface, leading to a coverage of all degrees of freedom. Hence, jaw customization is avoided, leading to higher application flexibility. Due to this argumentation and the industrial predominance of this approach in lathe machine tending, face-sided gripping with a three-jaw-gripper is further considered. In collaborative applications, particular design thoughts must be undertaken, resulting from the contact geometries in the collision case between the robot system and operator. Therefore, the potential tool contact geometry must have a design that reduces the contact forces in the collision case, e.g., by rounded edges or the addition of elastic outer skin. Lastly, gripping forces need to be reduced and monitored [108, 143]. Figure 2.17 gives an overview of gripping technologies.

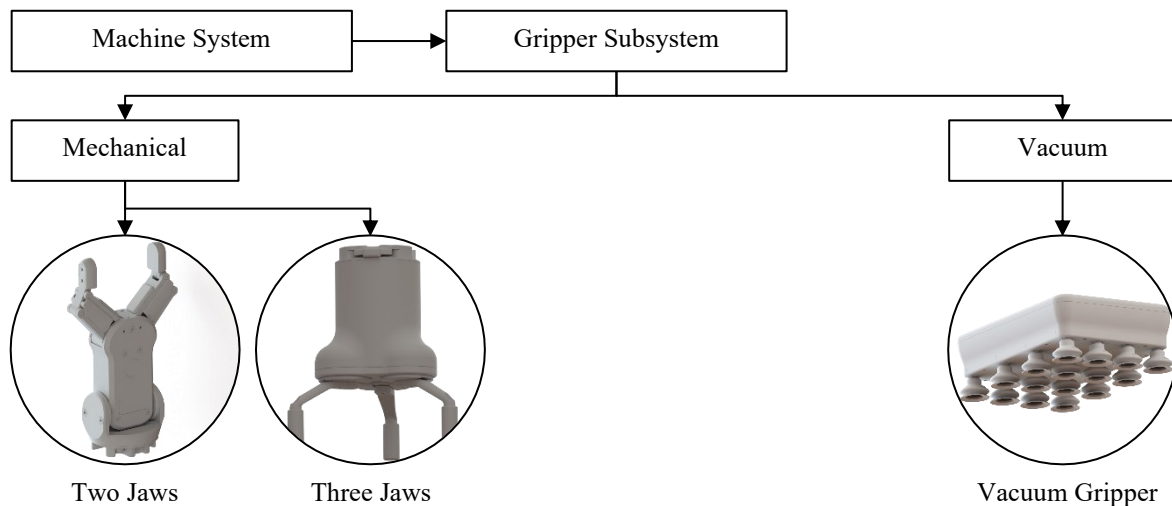


Figure 2.17: Gripper Subsystem Possibilities

2.3 Planning and Evaluation Methods

2.3.1 Planning of General and Manual Workstations

On the most abstract system level, a factory consists of the general system, subsystems, and elements, which can be described by their structure, function, and relation to each other. While single process elements such as machines can be merged to processes, binary relations between the elements are considered as structures [144, 145]. By extending this model, every system can be defined by its frame structure (input-output relationships between the system

and its environment) and its system constraints (definition of the overall system and its sub- and part systems). According to [146], flow systems in manufacturing and production are planned in five steps:

- 1) production plan preparation,
- 2) function determination,
- 3) dimensioning,
- 4) structuring, and
- 5) layout design.

Firstly, possible resources are defined, and an information base is collected for the following steps, such as specifications regarding the produced products, lot sizes, and targeted cycle times. Secondly, the product structure is analyzed to conclude the production steps and manufacturing methods. This information leads to the manufacturing process and functioning scheme. For dimensioning, the quantities of personnel, equipment, and material are obtained statically, followed by dynamic, spatial, and cost-based dimensioning. After that, the system is temporarily and spatially organized and statically and dynamically structured. Lastly, the layout is designed, starting with an ideal layout that is refined under the addition of restrictions to various real layout variants [146]. According to [147], the ideal layout can be characterized as an optimal spatial assignment of a group of elements by considering complex bilateral relations. The mentioned relations are expressed with transport intensities described by quantitative or qualitative methods, such as structural graphs and material flow matrices [72]. These graphs serve as input information to conclude the transport matrix, where the sending elements are enlisted in rows and the receiving ones in columns to collect the ongoing transports. For element arrangement, the single objects are positioned in a logistic-optimal way with the triangulation method. Therefore, a triangular pattern in multiple rows is used to place the single elements on the intersection points based on the transport intensities identified earlier [72, 146].

The machine space requirements can be calculated based on the machines' footprint on a more detailed machine level. Several calculation schemes are offered, such as area factors, supplement factors, substitution area, or functional area classification. The last-mentioned method is most detailed regarding abstraction level and data quality since it is based on statistical research of SME workshops [146, 148]. In the following, this method is further explained to support comprehension of the structure of machine areas (see Figure 2.18). As input information for this method serves the machine's width B_M [m] and depth T_M [m]. By

adding the clearance for operation and safety Z_1 [m] and clearance for maintenance Z_2 [m], the total width B_{MA} [m] and depth T_{MA} [m] can be calculated, which delivers the machine station area F_{MA} [m²] by multiplication of both factors. Further calculations deliver the manufacturing area F_F [m²], the intermediate storage area F_{ZL} [m²], the transport area F_T [m²], the additional area F_Z [m²] and the workshop space F_W [m²] [148].

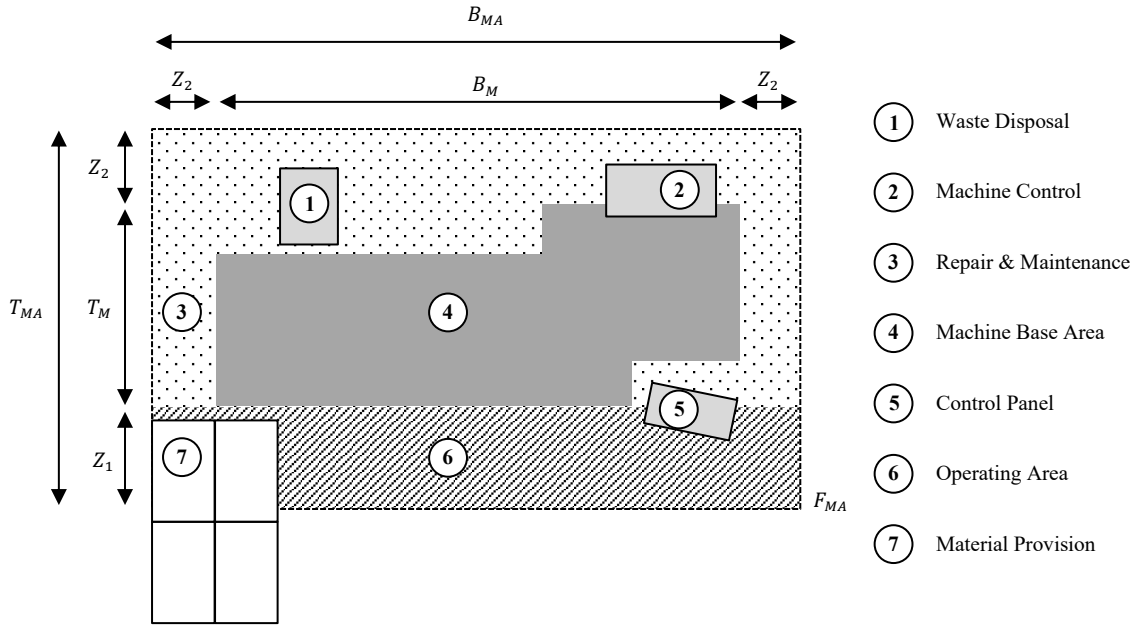


Figure 2.18: Layout Structure of a Machine Station based on [148, 149]

Since this doctoral thesis deals primarily with the rough planning phase, these detailed calculations are not further investigated. However, they provide valuable insights into the planning fundament of manual machine workstations and the required distances and areas, especially regarding safety and material provision. Since robot systems are fixed installed and limited in their reach, these side conditions and restrictions must be considered when planning the movements and positioning of the robot to execute reachability studies.

On the most detailed level, the single processes and motions are considered. Workstations can be examined using the work analysis method and described by the following organizational characteristics: structure, sequences, evaluation, requirements, and safety [150]. According to [151], various methods are suitable to describe process sequences, e.g., flow diagrams, structured analysis, net plans, process chain diagrams, petri nets, or event-based process chains (EPC). EPCs consist of events, functions, organization units, and information objects set into relation with the connectors AND, IOR, and XOR [152–154]. REFA, Methods-Time-Measurement (MTM), and digital human models are suitable to

assess the cycle times of the single process elements in manual execution. The REFA analysis consists of 39 methods to improve work conditions regarding ergonomics by subdividing the task into the process types human, equipment, and the subject of labor [155–158]. MTM is a tool to plan time capacities by splitting complex human motions into single motion types. Therefore, the basic movements reach, grasp, release, and move are distinguished. Furthermore, three basic movements of the finger-hand-arm-system, two eye movements, and body movements are added. For each motion type, a specific empirically determined execution time (TMU) is assigned for theoretical cycle time calculation [16, 159, 160]. In digital engineering, anthropometric models have been created to simulate human motions and sequences virtually. Movement building blocks enable the planner to configure the desired manual process supplemented by three-dimensional position data of the used handling objects [161]. Besides the 3D representation of the work execution, digital human models are based upon MTM motion blocks and deliver cycle time calculation for the respective use case in parallel [161, 162].

2.3.2 Cell Planning for Fully Automated and Hybrid Robot Systems

In robot system planning, graphical robot simulation software is accepted broadly in the industry [163]. To avoid a production standstill during on-site programming, e.g., by unpredicted dangers and errors during commissioning, offline programming is a suitable tool to plan, design, and program robot systems in advance [164]. Those systems visualize the robot cell in a graphical way and model the robot movements with emulators, enabling the designer to plan and program motion paths offline [163–165]. According to [165], [163], robotic cell development includes the following planning contents:

- 1) equipment selection and design,
- 2) task allocation,
- 3) material flow, process and layout planning,
- 4) robot movement programming and
- 5) fine planning, optimization, and cycle time calculations.

As input data for offline programming and simulation serve CAD models of the engineered workstation [164]. To plan the robot motions, these systems assist with visualized robot envelope curves and joint movements to execute reachability, collision, and cycle time studies [163]. Another approach lies in calculating the robot execution times instead of simulation, called Robot Time and Motion (RTM). This method can be understood

as the robotic counterpart to MTM, where movements are subdivided into single elements. Under the usage of the pick and place coordinates, the respective movement distance, type, and speed, the execution time is calculated [166]. Based on the time module-based work of [167–173], [166] develops a cycle time determination method for HRC called MTM-MRK (MRK is the German abbreviation for HRC).

Generally, robot motions can be categorized into linear, joint, and circle movements, which are explained as follows [174, 175]. The robot moves on a direct straight line between two taught points for the linear ones, even though the resulting movement may not be the most convenient variant for the robot. Due to the accurate movement description and limited joint utilization, the operating speed can be adjusted in SI units, e.g., m/s, cm/s, or mm/s. This motion type is used for path-related motion, i.e., arc welding, dispensing, or painting applications. On the other side, joint movements utilize the most convenient and efficient path for the robot by optimizing each joint's motion. The resulting movement is a curve that is also more complex in its description. Due to this complexity and the utilization of all joints, the movement can be adjusted only in percent [%] of the maximum operating speed. For exact speed determination, robot controller-internal calculations can be used. Such movements are suitable for pick & place motions, e.g., to transport a box from a conveyor to the feed position of a pallet in palletizing applications or to move a workpiece from the material deposit to the machine's door in machine tending. Lastly, circular motions move on a circular path that is programmed by giving a minimum of three reference points. [174, 175] Since this path can be precisely described, the speed is also adjustable in SI units. This motion type is mainly used for orbital welding for pipe workpieces. To either optimize the cycle time or guarantee an exact path accuracy, position levels (PL) can be used. When no PL is given, the robot controller shortcuts the motion, passing by the taught position in favor of cycle time. By giving the highest position level ($PL = 0$), the robot will reach all target positions exactly, resulting in a higher cycle time but guaranteeing exact motion accuracy [174]. To compare different robot models regarding their technical specifications, various patterns are used. [176], for example, defines a test cube to execute predefined motions to determine the repeatability of a robot. For cycle time comparisons of SCARA robots in pick & place applications, standard patterns, e.g., the ADEPT pattern developed by OMRON, are used. With a predefined motion set (standard cycle), the robot performance regarding speed, path accuracy, and achieved cycle time can be determined on a general basis [177].

Various general HRI planning procedures were presented by [31, 166, 172, 173, 178–181] with individual focus regarding robot technology, application fields, and optimization targets. In the following, selected approaches that are of particular interest for this doctoral thesis are presented. For the resource selection and layout planning problem, [182] present a respective decision tree using multiple criteria. [183] developed a method for rough planning that considers resource planning, rough layout design, and cost estimation. Resources are assessed using multiple criteria to conclude their suitability. With a discretized positioning patterns, these resources (e.g., robots) are placed iteratively to develop multiple layout alternatives. [184] outlines another method, including feasibility and rough planning of HRC projects. [185] seeks the optimization of operation time and ergonomics with digital human models and offline simulation tools. Furthermore, layout design, task allocation, handover positioning, and cost considerations are included. Models for task allocations have been excessively described by [34, 35, 186–193].

2.3.3 Robot Safety Planning

To give the planner a solid information base to design the safety system, a comprehensive set of standards has been developed by different standard bodies subdivided into A,- B,- and C-standards. A-standards include basic terms, substantial design bids, and general aspects for conception with machine-wide validity. Safety group standards (B) describe safety aspects (B1) or a specific type of safety device (B2) for a wide range of machines. The machine safety standards (C) describe concrete safety demands for a designated machine or machine types [194]. For the operation of a machine and/ or machine system, a risk assessment is required, according to [195]. This procedure consists of the risk analysis and the risk evaluation and identifies present hazards within predefined system boundaries. For the operation mode SRMS, the following conditions apply:

- 1) limited robot motions according to ISO 10218-1, 5.12 [98],
- 2) the robot functionality to execute a protective stop in compliance with ISO 10218-1, 5.5.3 [98],
- 3) distance design of the collaborative workspace regarding ISO 13855 [124],
- 4) deceleration of the robot to perform a safety-rated monitored stop (stop category 2) in accordance to ISO 10218-1, 5.4 [98] as well as IEC 60204-1 [125], and
- 5) initiation of a protective stop (stop category 1) for violation of the stated conditions according to IEC 60204-1 [125].

To calculate the relative constant or variable speeds in SSM mode, ISO 102018-2, 5.2.2, 5.6.4, and annex B [90], ISO 13855 [124] and IEC/TS 62046, 4.4.2.3 [126] serve as the basis. General safety design considerations for HRI with industrial robots are presented by [196].

The specifics of the risk assessment for collaborative applications in PFL mode are defined in ISO/TS 15066 [108]. Currently, the standards committee revises this technical specification ISO/TS 15066 [108] for transfer to the ISO 102018-2 [109]. Hence, the presented risk assessment procedure is under steady development and improvement. Since the PFL mode actively considers potential contacts between both collaboration partners, the occurring collision forces and pressures must be evaluated in advance, either by measurement or by calculation. Contact situations are subdivided into quasi-static (clamping) and transient (collision in free space) ones. ISO/TS 15066 [108] defines a quasi-static contact as a *“contact between an operator and part of a robot system, where the operator body part can be clamped between a moving part of a robot system and another fixed or moving part of the robot cell”*, while RIA TR R15.806 [197] and ISO/DIS 10218-2 [109] states that this contact situation is *“[...] characterized by the robot system contacting a region of the body that is constrained or quickly constrained against a fixed object [...]”*. A transient contact, on the other side, is defined in ISO/TS 15066 [108] as a *“contact between an operator and part of a robot system, where the operator body part is not clamped and can recoil or retract from the moving part of the robot system”*, while RIA TR R15.806 [197] and ISO/DIS 10218-2 [109] characterize this situation *“[...] by the robot system contacting a body region that is not constrained by a fixed object.”* Both definitions describe a quasi-static contact as a clamping situation, in which a specific body region is constrained for either a specific time period or only temporarily. However, a transient contact does not constrain a body region at any time since the possibility of recoiling or moving in the impact direction is given for the respective body part. Therefore, these two contact types must be divided by definition.

Human subject research empirically determined threshold values for the pain entrance level for allowed forces and pressures of both contact types, defined in ISO/TS 15066 [108] for single body parts (see Figure 2.19 and Appendix 6). For each body region, a quasi-static pressure [N/cm^2] and force threshold value [N] is given. For the transient cases, pressure and force multipliers serve to upscale the quasi-static values. Only for the skull, forehead, and face, transient multipliers are not applicable. Those areas should be excluded from

consideration by using safe movement monitoring or organizational measures in the safety design [108]. In [198], several studies are presented to refine and expand these values.

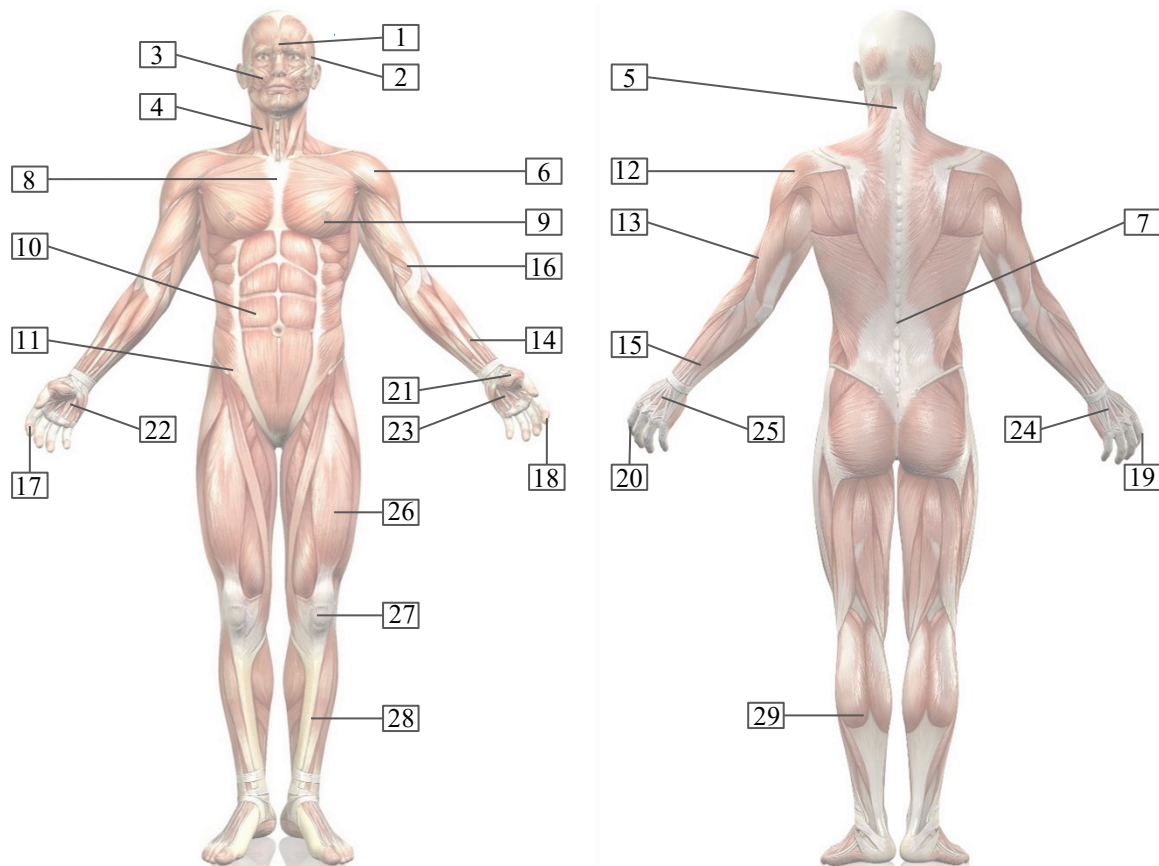


Figure 2.19: Human Anatomy with considered Body Regions for Human-robot-interaction, according to [108], Biomechanical Threshold Values see Appendix 6 [199, 200]

The whole robot system (robot, gripper, and workpiece) is considered for the risk assessment by observing the worst-case scenarios [197]. Due to the rounded edges of cobots and collaborative grippers, the problematic element is usually the workpiece. Quasi-static contacts must be mandatorily measured, while transient cases can be either calculated with the equations provided in ISO/TS 15066 or alternatively measured [108]. The beforementioned threshold values serve as a data basis for comparison to the measurement results to determine the maximum allowed collaborative speed *MACS* [mm/s].

Various designated pressure and/ or force measurement devices (PFMD) are commercially available for the measurement itself, such as the Pilz Robot Measurement System (PRMS) [201] or the GTE CoboSafe CBSF system [202]. An integrated load cell measures the collision forces and delivers the time-dependent force applied to a respective software that generates a force graph over time (see Figure 2.20). For pressure

measurements, pressure indicating films in different resolutions are placed on top of the device. In the case of the PRMS system, which is used for this research, LW foils with a measuring range of $250 - 1200 \text{ N/mm}^2$, and LLW foils with a resolution of $50 - 300 \text{ N/mm}^2$ are available. In addition, a developer layer foil must be placed on top of the measurement foil [203]. During the collision event, small air bubbles burst and discolor the film relative to the intensity. To counterbalance irregularities of the contact surface, a microfiber cloth is added on top of the film. A scanner with respective software digitizes the pressure distribution picture for visualization and further analysis. Besides the actual device, different damping materials (K1) and springs (K2) simulate the single body parts by combination [203]. The German Statutory Accident Insurance (Deutsche Gesetzliche Unfallversicherung, DGUV) [204] proposes values for thickness, K1 and K2 (see Appendix 7).

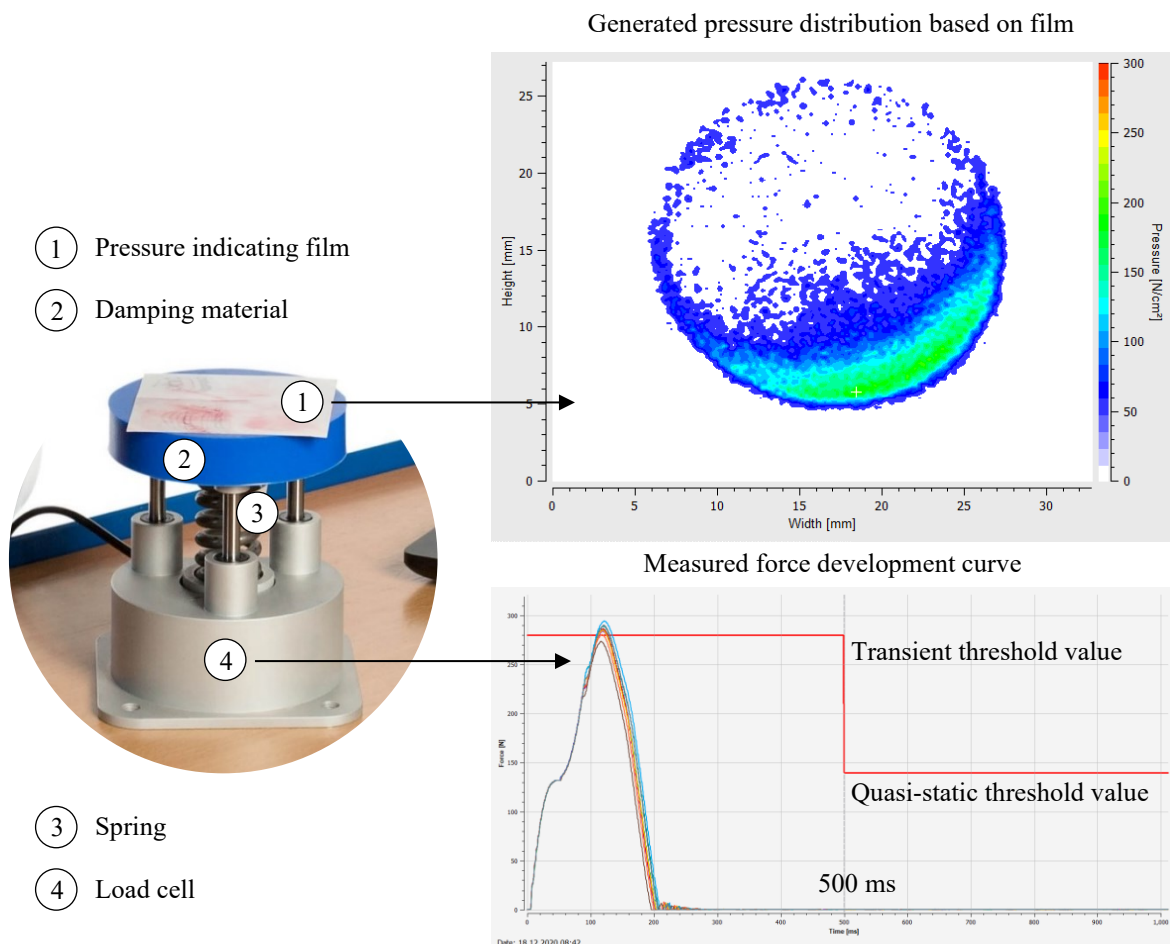


Figure 2.20: Force and Pressure Measurement Setup according to [108]

For measuring quasi-static contacts, ISO/DIS 10218-2 [109] and RIA TR R15.806 [197] define that the measurement device “[...] shall be anchored, stable and adequately

supported on a rigid surface [...]". The setup for transient contacts "[...] shall account for the robot system and body region masses. There is currently one defined method making these measurements, which uses an unconstrained test device with effective mass method. This method requires that the PFMD be allowed to move freely along the direction of contact as well as replicate the human body region effective mass M_H to directly measure force and pressure." [109, 197]. It can be seen that the standard differentiates the required measurement setup by contact case. The DGUV [204] does not explicitly differentiate these two measurement setups; instead, a fixed installation of the measurement device is illustrated for both cases. For this doctoral thesis, the presented differentiation is further considered since it follows the latest research.

To calculate the transient contact case, ISO/TS 15066 [108] provides the following equations with E as transfer energy [J], F or rather F_{max} as maximum permissible force [N], k as effective spring constant [N/mm], μ as the reduced mass of both collision bodies [kg], v_{rel} or rather $v_{rel,max}$ as relative speed between both collision bodies, m_H as effective body region mass [kg], m_R as effective robot mass [kg], M as total mass of moving robot parts [kg], m_L as effective robot system payload, p_{max} as maximum permissible pressure [N/mm²] and A as contact area [mm²].

$$E = \frac{F^2}{2k} = \frac{1}{2}\mu v_{rel}^2 \quad [108] \quad (2.1)$$

$$\mu = \left(\frac{1}{m_H} + \frac{1}{m_R} \right)^{-1} \quad [108] \quad (2.2)$$

$$m_R = \frac{M}{2} + m_L \quad [108] \quad (2.3)$$

$$v_{rel,max} = \frac{F_{max}}{\sqrt{\mu k}} = \frac{p_{max} A}{\sqrt{\mu k}} \quad [108] \quad (2.4)$$

The measurement procedure starts by setting an initial slow cobot operating speed. Then, the respective application's considered movement is executed so that the examined collision element (e.g., workpiece) collides with the measurement device. As a result of this first run, the connected measurement software delivers both force and pressure values. If the results comply with the biomechanical threshold values, further measurements are run with increasing speed until the maximum allowed speed is determined. If the results exceed those values, the speed or the robot sensor sensitivity must be decreased or adjusted in the subsequent runs until it complies with the biomechanical limits. This iterative procedure is individual for each use case.

Particular attention must be paid to the correct interpretation of the standards in terms of utilized force and pressure threshold values and the application of multipliers. As interpretation base serve the beforementioned definitions and the force progression curve over time. Since multipliers must always be applied to the transient case, this contact type is very clear in interpretation. However, for the quasi-static case, the standard does not formulate precisely enough, leaving room for interpretation. This statement can be supported by a survey regarding the risk assessment procedure for HRC conducted by the University of Applied Sciences in Karlsruhe [205]. As a result, a concretization of the ISO/TS 15066 would be beneficial for 19 % of the respondents, while 18 % wish for a more specified measurement procedure. Further assistance in terms of instructions, example applications, decision support tools, or safety measure catalogs was indicated by 49 % of the study participants [205]. In the following, the interpretation that is used for this doctoral thesis is precisely explained. As mentioned before, the force progression can be used as the first indication. Therefore, ISO/DIS 102018-2 [109] and RIA TR R15.806 [197] distinguishes three curve progression cases for quasi-static contacts:

- 1) *“Measurements with sustained pressures or forces over 0.5 seconds”*
- 2) *“Measurements with sustained pressures or forces over 0.5 seconds and with a high peak during the initial 0.5 seconds of contact”*
- 3) *“Measurements with only a high peak during the initial 0.5 seconds of contact”.*

For this research, especially type three is of particular interest, illustrated in Figure 2.20. During the first 500 ms, the standard allows the application of a multiplier for the quasi-static case, while after this time span the defined threshold value without a multiplier applies. The question arises if these multipliers are applicable to force, pressure, or both characteristics. At this point, the standards are imprecise in a clear textual definition, while several charts are used instead. In ISO/TS 15066 [108], chapter 5.5.5.5.-figure 4, a force progression diagram over time is illustrated, while the y-axis is indicated as force or pressure. Further, it is specified in this chapter that *“The limit values for the relevant contact events on the exposed body regions shall be analysed for the most stringent limits. These ‘worst case’ threshold limit values for the transient and quasi-static events shall be used in determining the proper level of risk reduction.”* [108]. On the other side, Annex A.3.5. states: *“In some cases during quasi-static contact, there could be an initial peak in force or pressure, consisting of a very short duration, as m_H and m_R reach an equilibrium energy transfer during the clamping period. If such an initial force or pressure peak exists, and can*

be measured through instrumentation that can distinguish the initial force or pressure from the equilibrium force or pressure, the initial force or pressure value shall be limited by the relevant transient contact value.” [108]. ISO/DIS 10218-2 [109], Annex N, Figure N.7 shows a general force progression graph over time by naming the y-axis force or pressure. When specifying quasi-static case three in Annex N, Figure N.10, however, a similar graph refers only to force. Furthermore, it has been stated in Note 1: “*The maximum force is evaluated using the transient biomechanical limit [...]. The maximum permissible force for hands and fingers is 280 N.*” [109]. Here, only the applicability of the force multiplier is explicitly stated. RIA TR R15.806 [197] illustrates this same case three by only indicating the force on the y-axis with a similar caption as the previously mentioned Note 1. Therefore, it can be summarized that only the applicability of the force multiplier is explicitly mentioned in the standards. Similar charts with a pressure progression over time are not illustrated. In practice, such a time-related pressure progression is also not indicated by the PFMD, at least not for the PRMS that has been used for this research. Hence, the temporal dimension of the pressure p can only be deduced from the force F progression in relation to the contact surface A by the following equation:

$$p = \frac{F}{A} \quad (2.5)$$

When executing such a measurement with the PRMS, the contact case must be set in advance within the software before actually starting the procedure. Therefore, the type of contact must already have been defined within the risk identification process of the risk assessment according to ISO 12100. By setting a quasi-static case in the software, the tool adjusts the allowed forces to the transient thresholds using the multiplier for the first 500 ms and continues then with the normal threshold value. For the pressure, however, consistent utilization of the normal threshold values is set without multipliers. Only if the contact case is modified to a transient one, the multiplier is applied to the pressure value as well. Consequently, the contact case must be categorized by its characteristics according to the previously mentioned definitions and not by its behavior that is identified during the measurement procedure. Based on the analysis of the operating principle of a certified PFMD, the presented argumentation is further underpinned in the following. To understand the physical properties of both contact cases, Figure A.2, as well as the following passages of ISO/TS 15066 [108], seem important:

- Annex A, A.3.6: “*The transient contact between a robot and a human body part is assumed to result in a fully inelastic two-body collision.*”

- Annex A, A.3.4: *“The effective mass values represent a combination of the mass of the body region along the effects of interconnectivity of the body region with adjacent body regions, particularly as it related to the body region’s ability to move in the same vector direction of the contact when contact occurs.”*
- 5.5.5.2: *“Transient contact: This is also referred to as ‘dynamic impact’ and describes a situation in which a person’s body part is impacted by a moving part of the robot system and can recoil or retract from the robot without clamping or trapping the contacted body area, thus making for a short duration of the actual contact. Transient contact is dependent on the combination of the inertia of the robot [...], the inertia of the person’s body part [...], and the relative speed of the two.”*
- 5.5.5.2: *“Quasi-static contact: This includes clamping or crushing situations in which a person’s body part is trapped between a moving part of the robot system and another fixed or moving part of the work cell. In such a situation, the robot system would apply a pressure or force to the trapped body part for an extended time interval until the condition can be alleviated.”*

According to these quotes from ISO/TS 15066, transient contact cases are described as fully inelastic two-body collision. As a result, the human mass m_H would move in the same direction as the robot mass m_R , which is not possible for a quasi-static contact. Further, these passages describe the quasi-static contact regarding its characteristics and not mitigation techniques to reduce the measured force and pressure values to acceptable levels. Another important characteristic is that the operator would be trapped if no retract movement is executed. Therefore, it can be clearly seen that the standard defines the contact cases based on their physical properties and not by the responsiveness in an individual measurement situation. It is not mentioned that a contact type can be reclassified if the measured robot behavior meets a specific characteristic. Consequently, the contact type in the PRMS software cannot be changed from quasi-static to transient to utilize the pressure multipliers after a retraction movement within the first 500 ms has been identified in the measured force progression graph.

Another argument can be found in the risk evaluation for the operator according to ISO 10218-2 [90] and ISO/TS 15066 [108] prior to robot system manufacturing. ISO/TS 15066 [108], 4.3.1 states: *“The integrator shall conduct a risk assessment for the collaborative operation as described in ISO 10218-2:2011, 4.3. Special consideration concerning*

potential intended or reasonably foreseeable unintended contact situations between an operator and the robot system, as well as the expected accessibility of an operator to interact in the collaborative workspace, shall be taken into account.”. This quote describes that the risk assessment of the individual application must be conducted at the design stage by defining the transient and quasi-static contact in advance. At this time, a priori assessment of the robot behavior is not intended, and the contact case must be defined based on the physical characteristics.

Based on this extensive review of the definitions, physical properties, and measurement setup advice of the standards, as well as aligning these statements with the certified PRMS operating principle, it can be concluded that the contact case is classified based on its characteristics instead of its individual behavior during the measurement procedure. Therefore, this doctoral thesis will adhere to the presented argumentation line, backed up by expert interviews with members of the respective standard committees. As a result, the multiplier for the quasi-static contact case will only be utilized for the force during the first 500 ms of the measurement. For the quasi-static pressure threshold, no multiplier will be applied, independent of the measured result.

Since the current risk assessment procedure requires measuring a specific situation, upfront determination of exact compliant velocities is not feasible. Adaptive safety systems that can adjust to dynamic environments (e.g., workpiece change), as presented by [206], would require a thorough understanding of influencing factors and the robot system behavior. In the following, different scientific approaches to analyze quasi-static and transient contact cases are summarized. [207] present a three-dimensional map that illustrates the collision forces relative to the robot’s working space. Based on empirical measurements with the cobot models UR10e and KUKA LBR Iiwa with the last robot joint, the influence of robot pose, distance, and velocity have been investigated. [208] analyzed crash tests with different industrial robots considering the robot mass, velocity, and singularity forces during clamping. [209] introduces the power flux density as a metric under consideration of contact area and duration and transferred energy. The outlined rapid contact model has been tested regarding the influence of robot mass and velocity, radius of curvature, and human stiffness parameters. To reduce collision forces of the robot tool and the attached workpiece, a robotic airbag has been developed by [210] that has been evaluated regarding its effectiveness in empirical crash test dummy tests. Another approach under utilization of ultrasonic sensors as safety technology has been presented by [211]. [212] derive a collision

event pipeline with pre-collision, detection, isolation, identification, classification, reaction, and post-collision. The force direction and intensity can therefore characterize collisions. Classifications utilize the occurrence (accidental, intentional), severity (light, severe), and temporal distribution (permanent, transient, repetitive). Models to calculate quasi-static forces were developed by [213] and [214]. [215] and [216] presented virtual force sensors and simulations. The Fraunhofer Institute for Factory Operation and Automation IFF and the Trade Association Wood and Metal (Berufsgenossenschaft Holz und Metall, BGHM) have developed the Cobotplaner: an online planning tool for safe, collaborative speed estimation [217].

2.3.4 Economic Evaluation Methods

Generally, the economic decision can be made based on one or multiple target figures. Due to the scope of this work, solely economic optimization is pursued. To guarantee the soundness of economic-exclusive decisions, the following assumptions must apply [218]:

- 1) reliability of data and interdependencies,
- 2) predictability and isolated assignability of cash flows and their interdependencies to the single investment objects,
- 3) independence of the investment alternatives, and
- 4) predefinition of the operation life.

According to [219], different key figures can be used for economic modeling that is differentiated between static models (e.g., return on investment, ROI) and dynamic models (e.g., net present value, NPV). Despite the broad acceptance in the industry, the ROI has been criticized regarding its suitability for both strategic and investment decisions due to the utilized accounting methods, the unsatisfactory attention to time-based factors, investments in working capital, and profit determination [220]. According to [221], [222], the ROI is utilized by 20 % to 30 % of the DAX 100 top companies as a target figure. Further critics has been expressed by [223–229]. Due to the described critics on static economic key figures, the net present value representing dynamic models is considered in this doctoral thesis. The NPV considers discounted cash flows over multiple periods. Since industrial systems require an initial investment before the first cash flows occur, these objects can be assigned to investment type one. This type is bound to the assumption of a perfect capital market with unified, effective interest rates.

The NPV [€] consists in its simplified form of the initial net investment I_0 [€], the periodical cash-in flows CIF [€] and cash-out flows COF [€], the discount factor q [%], the time index t [year] and the observed time period T [years] (see (2.6)) [230].

$$NPV = -I_0 + \sum_{t=0}^T (CIF(t) - COF(t)) \cdot q^{-t} \quad [230] \quad (2.6)$$

Decisions between alternatives are executed based on absolute or relative advantageousness: while an $NPV > 0$ is absolutely advantageous, the higher NPV value indicates a relative advantageousness [218]. When determining the profitability of technical systems, the values of the elements mentioned above must be determined. Based on [231], activity-based costing (ABC) is a suitable method to assess process chains economically. According to [232], ABC is “*a method that measures the cost and performance of process-related activities and cost objects*”, that “*assigns cost activities based on their use of resources, and assigns costs and cost objects, such as products or customers, based on their use of activities.*” [233] formulates a general economic assessment approach for hybrid production technologies, which has been adapted to different application fields in further research by [231], [234], and [235]. As calculation base serve machine hour rates, cost functions, and the degree of value creation to compare new production technologies (e.g., industrial or collaborative robots) to existing ones (e.g., manual execution). Based on this approach, a cobot-specific methodology has been concluded by [236] and [237]. To assess hybrid technologies comprehensively, product- and process-related alternatives need to be combined in one model by considering various technology products as well as process chains [233].

2.4 Synthesis - State of the Art and Research

In this section, the state of the art and research have been characterized regarding turning machines and machine tending, robotics, and planning and evaluation methods. By this, the first research question (RQ 1) has been thoroughly answered. In Figure 2.1, the anatomy of a machine tending cell was explained, at least from a hardware perspective, while communication or CNC software systems were not discussed. A comprehensive overview of the possible technical solutions was given in the respective paragraph, including single and multi-machine systems with both classical automation solutions (e.g., linear portal loaders) and robotic solutions. For fenceless robotic lathe machine tending, the following elements are most relevant and therefore further considered in this research: workpiece

system (rotary workpieces classified by the OPITZ system), machine system (CNC lathe machines & turning/ milling machining centers, clamping chucks, door actuation), logistic system (drawers and provision tables) and handling system (industrial and collaborative 6-axis robots installed on sockets or consoles, external safety devices, safety controller, torque sensors and three-jaw grippers) (see Figure 2.21).

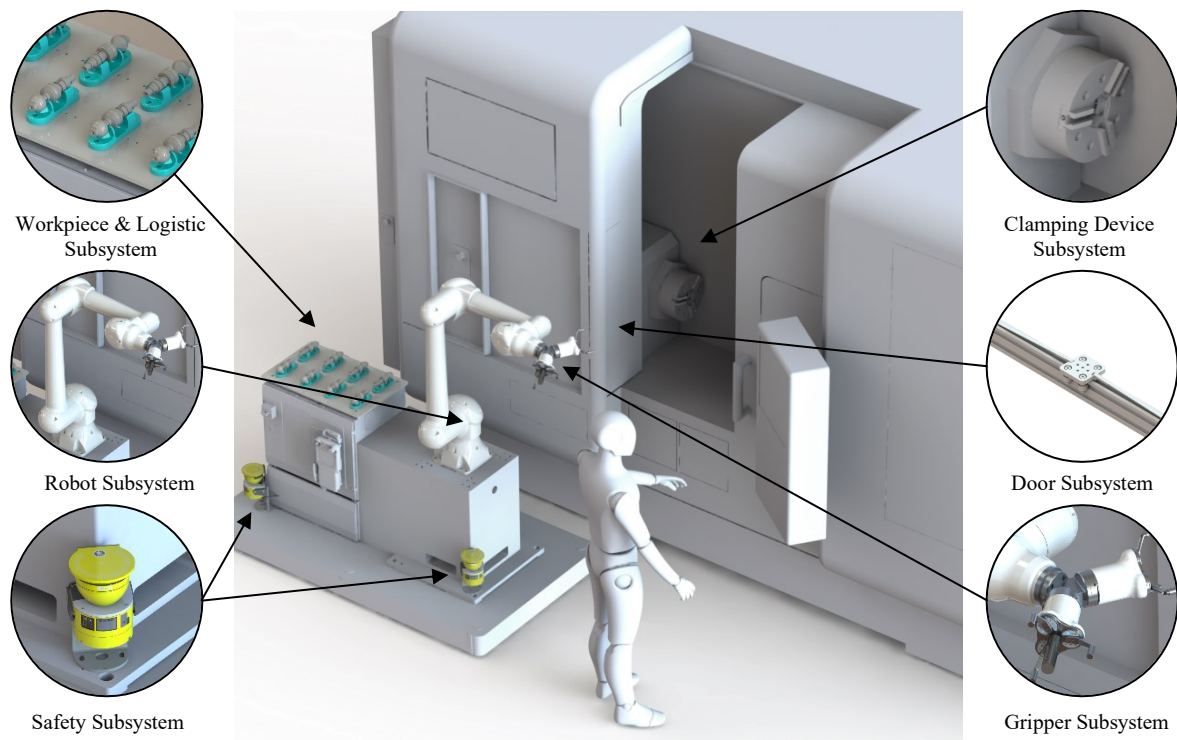


Figure 2.21: Considered Lathe Machine Tending Elements

The second research question (RQ 2) has been answered already partially. Fundamentally, both industrial and collaborative robots can work fenceless in human-robot interaction (HRI), either with internal sensors or with electro-sensitive protective equipment (ESPE). Therefore, the single modes of collaboration and their suitability for the respective robot type were presented. By adding external safety devices (e.g., laser scanners) that detect the presence, absence, or distance to an operator, the modes full-speed (FS), speed separation monitoring (SSM), and safety-rated monitored stop (SRMS) can be combined. That means that the industrial robot operates with maximum speed when no operator is present. As soon as a worker enters the interaction zone, the robot switches to the SSM mode and moves at a reduced velocity. When a critical distance to the robot is reached, the industrial robot activates the SRMS mode and stops safely. With increasing distance between both interaction partners, the robot gradually increases its speed until an operation in full-speed

mode during human absence is possible again. Collaborative robots can utilize a similar approach (hybrid mode) under the substitution of the SRMS by the PFL mode. As a result, the robot does not stop at close proximity to the operator but operates at a safe, collaborative velocity and sensor sensitivity instead. Additional sensors (e.g., internal torque sensors) detect a collision and initiate a safe stop of the cobot. As an alternative to the presented hybrid mode, cobots can also operate in exclusive PFL operation at safe, collaborative speed during the operation. As defined in ISO/TS 15066 [108], these maximum allowed collaborative speeds (*MACS*) must be determined by iterative force and pressure measurements under consideration of body region-specific biomechanical threshold values. While quasi-static contacts (clamping) must be measured, transient ones (collision in free space) can either be calculated or measured. Since a prototypical cell is required to conduct these tests, the project must already be well-advanced to validate the targeted operating times. It can be summarized that the single operating modes are linked to individual speed levels of the robot, which mainly influences the achieved cycle times. When considering each mode individually at 100% execution, a mode-specific cycle time can be calculated. To conclude a realistic cycle time in mixed operation, however, the time slices of each mode operation must be considered and proportioned to each other (interaction grade). Consequently, the hypothesis can be formulated that the achieved velocities of each mode and their temporal relation to each other mainly affect the cycle time and, therefore, the economic feasibility. Statements regarding the main technical influencing factors on the economic feasibility cannot be made at this stage. In the further proceeding of this doctoral thesis, these factors need to be distilled. Various papers have been assessed regarding their used economic structure and methodological coverage to determine these factors to give an overview of further potential influencing factors (see Table 2.3). This analysis gives insights into the considered robot technology, the utilized economic target figure, the used structure to describe the investment, and positive and negative cash flows. For calculating these cash flows, the used reference basis and the cycle time consistency were analyzed regarding the considered operation modes and individual speed levels. As a result, there is no planning method yet, enabling the user to comprehensively plan fenceless workstations neither to compare industrial and collaborative robots to each other. Especially the influence of different operation modes on the cycle time by actively incorporating the differences in the speed levels and their combination has not been covered from an economic point of view.

Table 2.3: Methodological Economic Coverage of HRI in Present Literature

		Bouchard, 2017 [178]	Gopinath et al., 2018 [196]	Selevsek et al., 2018 [184]	Malik et al., 2017 [179]	Ore et al., 2017 [173]	Michalos et al., 2018 [183]	Göze et al., 2015 [236]	Schneider et al., 2018 [31]	Schröter, 2018 [166]	Zhang et al., 2017 [172]	Presented Approach
Technology Focus	Robots in General	●	○	○	○	○	○	○	○	○	○	●
	Industrial Robots	○	●	○	○	●	●	○	●	●	●	●
	Collaborative Robots	○	○	●	●	○	○	●	●	●	●	●
Target Figure	Net Present Value (NPV)	○	○	○	○	○	○	●	●	○	○	●
	Return on Investment (ROI)	●	○	○	○	○	○	○	○	○	○	○
Investment Structure	Equipment	●	○	○	○	○	●	●	●	○	○	●
	Project Planning	●	○	○	○	○	○	○	○	○	○	○
	Commissioning	○	○	○	○	○	●	●	●	○	○	●
	Disposal	○	○	○	○	○	○	●	○	○	○	○
	Training	●	○	○	○	○	○	●	○	○	○	○
	Software	○	○	○	○	○	○	●	○	○	○	○
Positive cash-flows	Labor release	●	○	○	○	○	○	○	●	○	○	●●
	Value creation	●	○	○	○	○	○	○	●	○	○	●
	Capacity increase	●	○	○	○	○	○	○	●	○	○	●●
	Quality increase	●	○	○	○	○	○	○	●	○	○	○
	Experience for future projects	●	○	○	○	○	○	○	○	○	○	○
Negative cash-flows	Production cost	●	○	○	○	○	○	○	●	○	○	○
	Labor cost	○	○	○	○	○	○	●	●	○	○	●
	Maintenance	○	○	○	○	○	○	●	●	○	○	○
	Energy consumption	○	○	○	○	○	○	●	●	○	○	○
	Space occupation	○	○	○	○	○	●	●	○	○	○	○
Reference values	Output	●	○	○	○	●	○	●	●	○	○	●●
	Working Time	●	○	○	○	●	○	●	○	○	○	●
	Number of operators	●	○	○	○	○	○	●	○	○	○	●
Cycle Time	Robot general	●	○	○	●	○	○	○	○	○	○	●
	Industrial robot general	○	○	○	○	●	●	○	●	●●	●●	●●
	Industrial robot full speed	○	○	○	○	○	○	○	●	●●	●	●●
	Industrial robot SSM	○	○	○	○	○	○	○	○	●●	●●	○
	Collaborative robot general	○	○	○	○	○	○	○	○	●●	●●	●●
	Collaborative robot full speed	○	○	○	○	○	○	○	●	●●	●●	●●
	Collaborative robot SSM	○	○	○	○	○	○	○	○	●●	●●	○
	Collaborative robot PFL	○	○	○	○	○	○	○	●	●●	●●	●●
	Manual execution	●	○	○	●	●	●	○	●●	●●	●	●
Operating Speeds and Time Slice	SSM Speed	○	○	●	○	○	○	○	○	●	●	○
	PFL Speed	○	○	○	○	○	○	○	○	●	●●	●●
	Interaction Grade	○	○	●	○	○	●	○	●	○	●●	●●
●● deeply considered ● considered ○ not considered												

The third research question (RQ 3) was also partially answered by giving an overview of various engineering methods. Based on Table 2.3, possible determination methods for

single economic factors were assessed regarding their practical suitability. To determine manual execution times, the methods MTM, REFA, and digital human models are conventional. Robot cycle times are either calculated or simulated with offline programming software, while RTM or virtual sensors are not broadly accepted in the industry. As an input value, the actual operating speeds are required. Speed and separation monitoring velocities can be calculated. The collaborative speed can be measured or calculated. Scientific proposals were the evaluation with virtual collision models or virtual sensors. Lastly, the interaction grade can be determined with a parallel robot and human digital modeling or virtual reality environments. Even though [166] and [172] described all factors in their methodologies, practical validity is not given. Some of the used methods are still in the theoretical concept phase and neither accepted by industry nor applicable. Although those methods have been presented in theory, their readiness for industrial practice is questionable. Simulations with virtual reality, sensors, or collision models are possible but rarely accepted. Lacking accuracy and mismatching with practical results lead to unsharp economic outcomes that endanger the realization of automation projects. Firstly, digital human simulation requires a tremendous modeling effort, especially when synchronizing the motions with a robot. Therefore, planning costs are higher than for classical fenced-in robot cells, where the operation speeds and execution times can be simulated and optimized without external influencing factors. Secondly, virtual sensors systems are available but still must be designed according to the use case. Using virtual inputs and outputs (I/Os) is already possible in offline programming to switch between operating speeds and to simulate different scenarios. As data input, the determined operating speeds according to the zone definition and design are a prerequisite, though. Lastly, virtual collision models are not that accurate yet to replace the force and pressure measurements that are required by ISO/TS 15066. The model would have to cover the whole system behavior, consisting of a robot, gripper, workpiece, and collision surface for the collision in free space and the clamping scenario. Factors such as pose-dependent kinematic behavior, rigidity, and yielding of all single components would need to be simulated. According to the state of research, exact behavior modeling of the robot in collision cases is still insufficient. At this stage of the doctoral thesis, available methods were collected and critically assessed regarding their practical suitability. Statements about the transfer possibilities to a frontloading planning approach are not feasible yet but are targeted in the further proceeding of this work. Regarding research questions RQ 4 and RQ 5, no statements can be made yet.

3. Solution Approach

3.1 Need for Research and General Solution Approach

As summarized in the previous chapter, a research gap has been identified in the preliminary economic evaluation of and comparing collaborative and industrial robotic lathe machine tending systems. For RQ 3, various methods were presented to determine the economic-affecting factors, while a modification approach to frontload the required information to the project beginning has not been considered yet. RQ 4, which targets the formulation of an integrated rough planning methodology, was not assessed at this stage. To investigate these questions further, consideration of the classic planning procedures serves as starting point. In Figure 3.1, a simplified form of a comprehensive HRI planning methodology, presented by [7], has been derived.

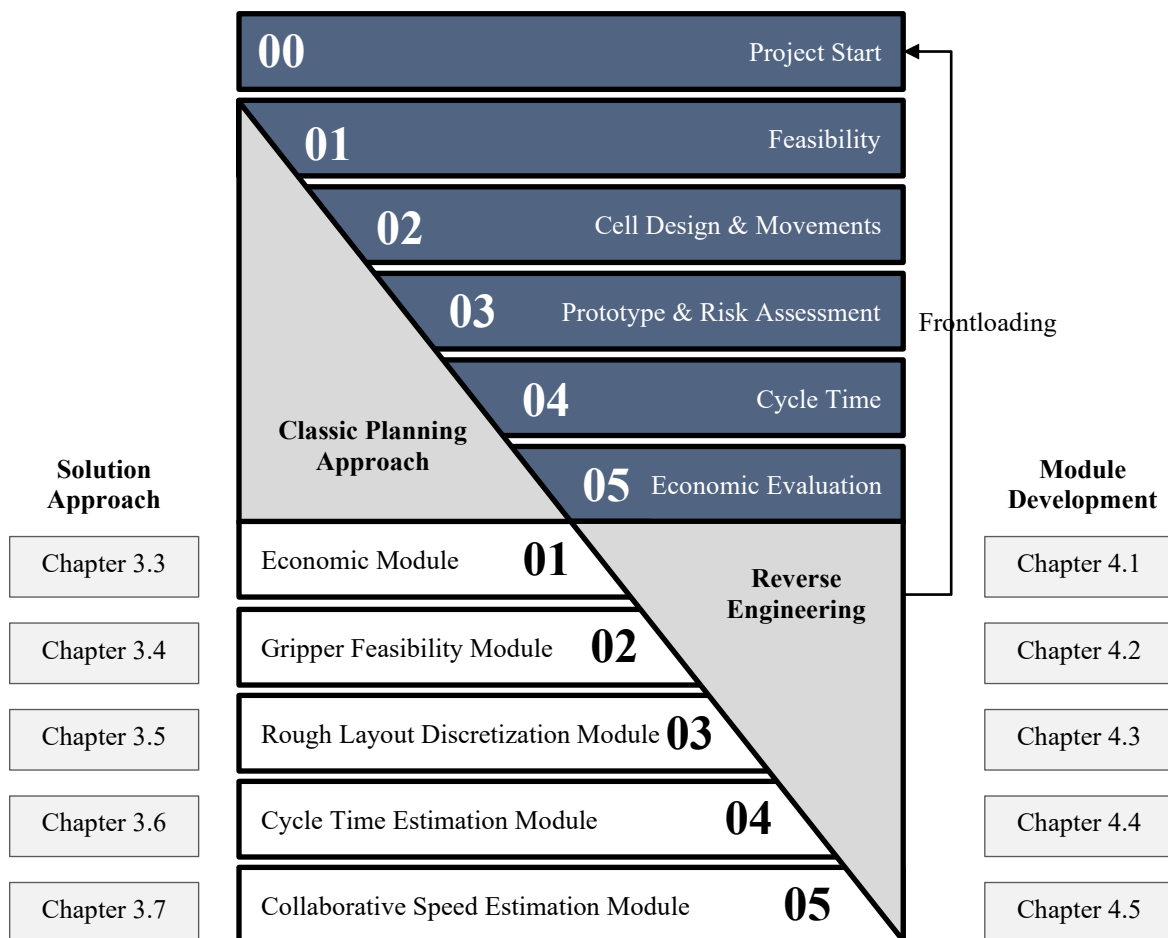


Figure 3.1: Solution Approach - Reverse Engineering to Frontload Planning Information to the Project Start based on the Classic Planning Approach

Firstly, the technical feasibility is checked regarding the ability of a specific robot-gripper combination to handle the workpiece. At this stage, suitable robot and gripper models can already be defined or excluded (01). Secondly, the cell is designed on a rough layout level to define possible positions of the robot depending on the relative machine and material locations. This layout is usually designed in CAD for import to simulation software to generate the required movements. With these simulations, the single motions can be modeled to conclude the technical feasibility of the preselected possible positions regarding their reachability (02). To conclude the cycle times of each motion (04), the achievable operating speeds must be inserted into the simulation. Therefore, a risk assessment takes place (03). For industrial robots, the achievable speeds in the single modes FS – SSM – SRMS can be either derived from the technical specifications (full speed based on given maximum speed stated by the robot manufacturer) or calculated with the equations provided in the standard (SSM speed), while speed 0 is valid for SRMS. A prototypical cell can be used for verification but is not mandatorily required for industrial robots at this stage. Collaborative robots, on the other side, require force and pressure measurements as part of the risk assessment to conclude the maximum allowed operating speeds in PFL mode. Therefore, a prototypical cell is mandatorily required to execute these tests. Operating speeds for FS and SSM operations can be derived by the same procedure as stated before. Equipped with this information base, the fine simulations with the actual operating speeds in the several modes take place to determine the achieved cycle times (04). Since the cycle time mainly influences the achieved workpiece output and the time slice that an operator is relieved from its original work, this data is mandatory to calculate the cash-in flows. With the investment information and the cash-out flows of each automation alternative, the net present value can be calculated to conduct the economic evaluation (05).

Analysis of the classic planning approach shows that the relevant information, such as layout, operating speeds, and cycle times, is produced in a well-advanced planning stage of the project. Therefore, the whole planning procedure must be undertaken with a quite long development time before the first economic result is available. While this process can be conducted entirely offline for industrial robots, cobots require a test setup to execute the risk assessment. Since reference values of realistic speeds are lacking, the whole pre-study requires intensive planning measuring resources. If the economic result is unsatisfactory, efforts regarding time and financials have already been invested, impeding a shift to an industrial robot to start the planning from scratch. Instead, additional fencing is added to

compensate for the cycle time, as stated at the beginning of the problem statement of this doctoral thesis. Since this planning procedure is highly resource-binding, considerations of simpler automation alternatives, such as linear portal loaders, are also impeded. Consequently, this planning issue can be designated as an optimization problem that requires a mutual calculation basis. Therefore, this doctoral thesis seeks to categorize, systematize and describe the considered technical system. In parallel, a modularization of the planning system is targeted to identify the most crucial factors. With deductive, simulative, and empirical system analysis, the statistical assessment is pursued for data-based approximation and prediction of the single factors. Due to the multidisciplinary and complexity of the planning problem, a tension field between data granularity, approximation precision, computability, and usability for the user can be noted, which will be addressed in this research.

A reverse engineering approach is used as a solution approach that derives the single information modules from the overall economic objective (see Figure 3.1 bottom). Reverse engineering means that the single planning modules of the technical-based topics are derived from the economic planning result. The single steps were rearranged in a proper order instead of exactly reversing the classic procedure. Firstly, an economic module is developed that includes a mutual calculation scheme that collects all economic planning information for both industrial and collaborative robots. Secondly, the technical feasibility regarding the handling ability of the workpiece is investigated, delivering valuable data for further simulations and prototypical tests by narrowing down the workpiece spectrum. In the third step, the layout possibilities are discretized by creating a suitable positioning pattern for all entities (machine, robot, material). Step four deals with the actual robot movements by analysis, differentiation, and definition of single motion modules. Based on the previous positioning pattern, respective cycle time simulations are executed. Since the achievable operating velocities are unknown at this stage, studies on the speed-dependent cycle time development are conducted. Lastly, a risk assessment is conducted to derive potential hazards in step five. For the individual cases, suitable experimental setups are developed to conduct the force and pressure measurements. As a result, the maximum allowed collaborative operating speeds are available. With this methodological toolset, the single planning information can be frontloaded to the project begin. Since this doctoral thesis deals with rough planning at an early project stage, approximation models are targeted instead of exact values. The information granularity is sufficient for the considered planning situation

and provides substantial assistance. The considered use case is analyzed further in the following subchapter for preliminary consideration of the module development. Furthermore, the planning focus is specified. Each module is described regarding its procedure within the next subchapters and is developed in chapter 4 (see Figure 3.1).

3.2 Use Case Delineation and Planning Focus

At first, a solid understanding of the process is required as a fundament for automation. In Figure 3.2, the process of lathe machine tending has been described regarding manual and robotic execution with both robot types.

A comprehensive process pipeline has been derived by analyzing common structures in the individual process steps and sequencing. To guarantee practical applicability, existing customer projects and expert interviews with manufacturing engineers of the industrial research partner have been conducted for feasibility backup. The result is the following process map, illustrated in Figure 3.2. As can be seen, the processes are distinguished between cognitively challenging and repetitive tasks, which are executed either exclusively manually by the operator (M) or automated with an industrial (IR) or collaborative (CR) robot. As described earlier, suitable methods to determine the execution times for the alternatives are MTM for the manual tasks and offline simulation studies for the robotized execution [238, 239]. Furthermore, there are lathe machine-based processes (L), which are neutral to the execution form. For both robotized process chains, the manual process “robot program adjustment” (P3, M) is added, which includes tasks such as tool center point (TCP) measuring or reteaching points. As a condition, it is set that the doors stand open at the beginning and are operated by an actuation system in all three execution forms. Furthermore, a maximum automation level is pursued so that the automated process chains include only those manual processes that must remain in that execution form.

As technology representatives, a collaborative and industrial robot with nearly equal technical specifications is compared. It must be noted that the maximum operating speeds of both robots differ due to kinematic individualities. Cost-relevant factors, such as space occupation, maintenance effort, and energy consumption, are presumed equal, leading to the same cash-out flows. For cycle time optimization, double grippers are used to handle raw and machined parts simultaneously.

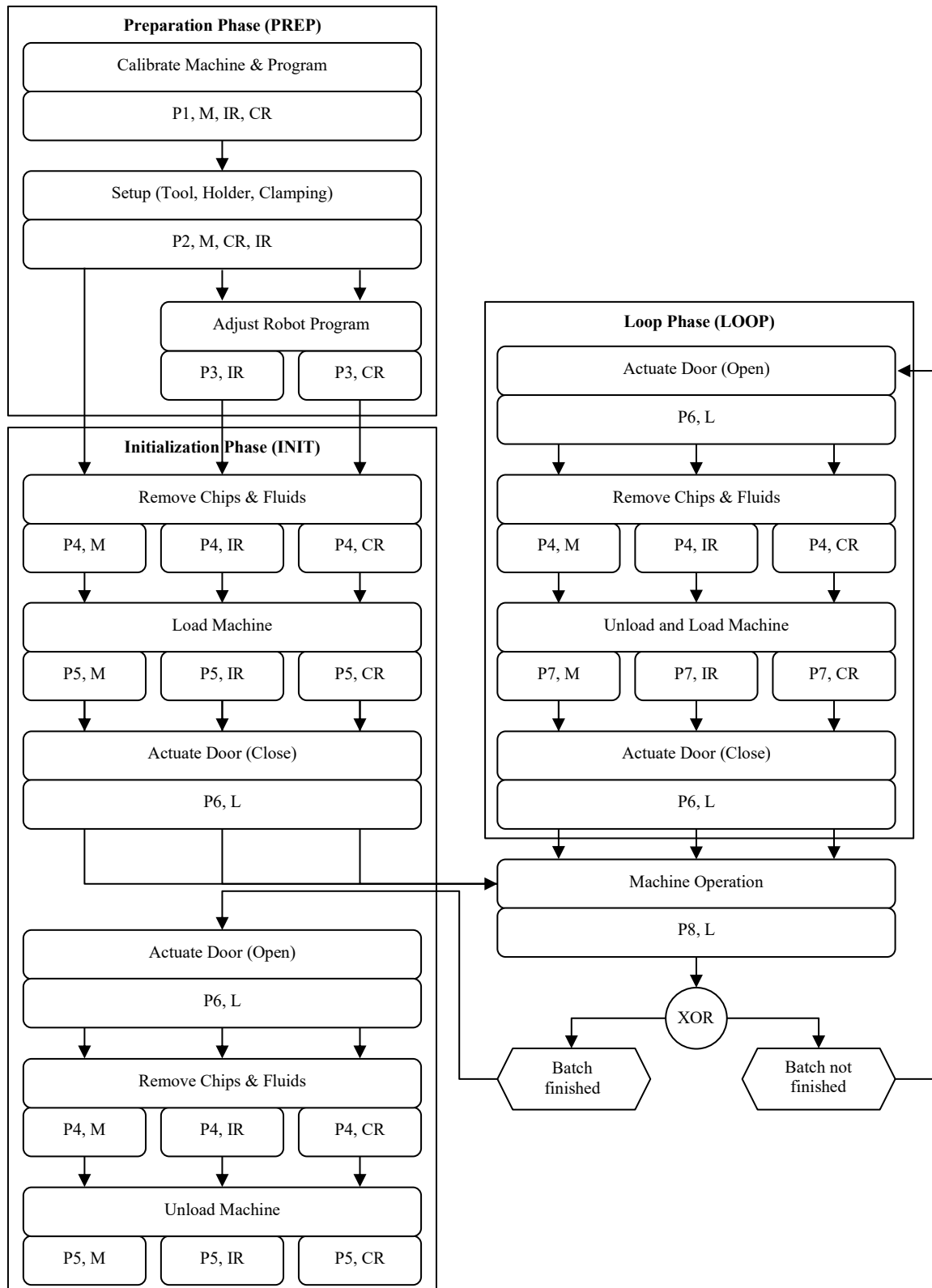


Figure 3.2: Process Pipeline for CNC Lathe Machine Tending

The following three alternatives are used for this doctoral thesis based on the previously described fenceless robotic options by incorporating different operation modes (see Figure

3.3). Concept one shows a collaborative robot without external safety devices for exclusive operation in PFL mode with the permitted collaborative speed. In the middle picture, additional safety devices (e.g., laser scanners) are added to enable the cobot to switch between operation speeds according to the operator's proximity (FS – SSM – PFL). During human presence in the white zone, the cobot works in industrial mode with full speed (FS). As soon as the operator enters the yellow zone, speed and separation monitoring decelerate the robot accordingly (SSM). When the green zone is entered, collaborative speed is activated (PFL). In contrast to the first two, concept three uses an industrial robot instead. Fundamentally, the setting is the same as the previous one, only with the difference that this robot must stop in the inner zone (red area, safety-rated monitored stop, SRMS).

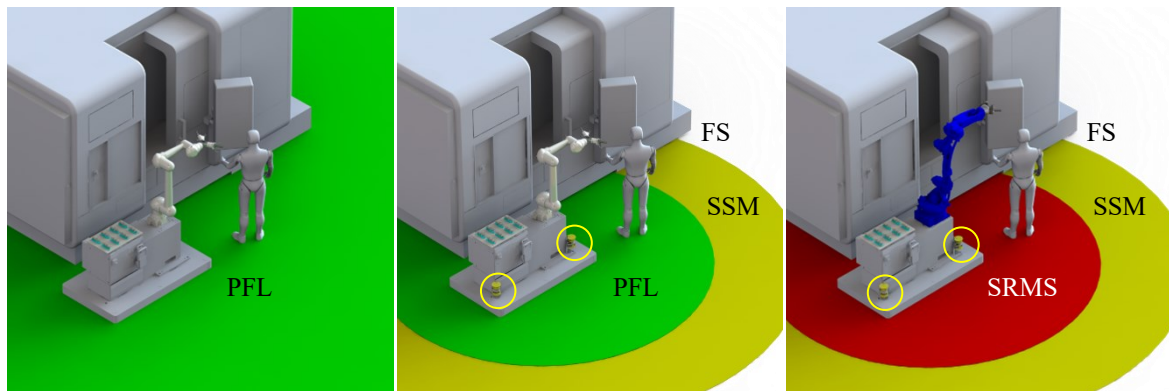


Figure 3.3: Technical Options for Fenceless Lathe Machine Tending – Collaborative Robot in Exclusive PFL Operation (CR, PFL, left), Collaborative Robot in Hybrid Mode (CR, HM, middle) and Industrial Robot (IR, right)

The main advantage of concept 2 compared to concept 3 is the work continuation in the inner zone. Although this approach seems superior at first glance, a deeper consideration of the achievable speeds and investment cost leads to an optimization problem. The main differences in the robot technologies are the lower maximum speeds of cobots and their higher investment. For this research, only full-speed operation (white zone), SRMS (red zone), and PFL (green zone) are considered. SSM (yellow zone) is excluded to limit this research's scope and ensure controllable complexity of the presented economic algorithm. In future research, this gap must be closed by considering the required distances and allowed speeds concerning the robot's stopping times. Therefore, the following three technical alternatives are further considered: “Collaborative Robot in exclusive PFL operation” (CR, PFL), “Collaborative Robot in Hybrid Mode” (CR, HM), and “Industrial Robot” (IR).

In the following, the development focus (F) of the presented modules is further refined. Since automation solutions pursue a substantial improvement toward manual execution, both execution options must flow into the toolset for economic comparison. According to [39], working systems can be classified based on the used system for handling, including operators and robots in HRI (see the last column of Table 3.1).

Table 3.1: Handling Execution-based Working Systems based on [39]

	Fully manual	Fixed interlinked	Robotized	Flow automated	Mechanized	Robot-supported	Manual-mechanized/robotized	Mechanic-automated	Automated	Operator-supported automation
Operator	•				•	•	•			•
Feeding device		•			•	•	•	•		•
Robot			•			•	•	•	•	•
Conveyor technology				•			•		•	•

The HRI system must be executable manually and automated, e.g., regarding handling workpieces at the material deposit. Therefore, the focus of this work lies on the evaluation of partially automated systems instead of fully automated ones, even though both solutions can be probably calculated with the same scheme with slight adjustments, leading to:

- *F1: Focus on the incorporation of manual and robotic automated execution regarding economic profitability for comparison.*

According to [146], manufacturing systems can be hierarchically differentiated into the following five levels with increasing complexity:

- 1) manufacturing station (e.g., single machine),
- 2) manufacturing group (e.g., multiple machines),
- 3) manufacturing section (e.g., several entities with similar production technology),
- 4) manufacturing area and
- 5) manufacturing plant.

As described in the state of the art and research, multi-machine tending (levels 2 to 3) is a complex topic requiring interlinking technology and, therefore, line balancing. To limit the complexity of the presented approach in favor of higher research depth, manufacturing stations (level 1) are considered in this doctoral thesis. Multiple machines can also be planned with the pursued method with the limitation of one robot's assignment to one machine each. Further research can extend the presented approach to include different interlinking technology and the line balancing problem. The second focus implies:

- *F2: Focus on single machines.*

The production program is analyzed in the first step of the earlier presented general factory planning framework (data preparation) [39, 72, 146, 148, 149]. Production programs can be assigned to the following product range-based groups [148]:

- 1) definite ones for mass production and high volumes,
- 2) aggregated ones for medium volume, and
- 3) general ones for small volume/ single-piece production.

From an HRI automation point of view, only aggregated programs are considered since high volumes are usually automated with fenced-in solutions for maximum performance, and single-piece productions are not economically feasible [146, 240]. This leads to focus three:

- *F3: Focus on middle-volume production systems.*

In order to reduce the planning effort for various products, the information is aggregated by using workpiece representatives: substitute workpieces that cover a broad characteristics range. In the second step of the before-mentioned planning method, function- and process determination, necessary production stages, functions, and manufacturing technologies are determined [146]. Hence, it can be stated that the considered product variety is directly linked to the utilized machine types. To ensure the controllability of the research problem, a workpiece focus is needed that likewise limits the scope of manufacturing technologies. From a workpiece perspective, the fundamental distinction lies between prismatic ones, which can have all kinds of regular and irregular shapes, and rotary ones characterized by rotational-symmetric character. From a technological point of view, the following automation obstacles occur when automating a milling machine in comparison to a lathe:

- 1) the number of clamping position possibilities,
- 2) clamping complexity regarding automation,
- 3) variety of gripping strategies, and
- 4) classification potentials of outer shapes for simplified PFL speed determination (see force and pressure measurements).

As a result, the following focus applies:

- *F4: Focus on rotary workpieces, lathe machines, and turning/ milling machining centers.*

As described in the state of the art, there are various automation options to tend a turning machine. For bar material, the standard automation is a combination of bar feeders,

collection tray, part gripper, and conveyor band as the most feasible and profitable one by avoiding operating the machine doors. Chuck parts, on the other side, are tended machine-externally. As insertion and/ or extraction point, the main and/ or counter spindle takes place. To limit the research scope, main spindle tending is focused. In future work, motion types for counter spindle extraction can be added. Focus five is, therefore:

- *F5: Focus on chuck parts that are machine-externally fed from the main spindle with a robot.*

The simulations and measurements are executed with selected robot and gripper models to refine and concretize the presented abstract picture. By this, concrete planning values can be created, and the applicability of the presented modules can be demonstrated. In further research, other models can be tested in the same way to conclude a mutual database that supports comparison. The payload-reach overview of cobots (see Figure 3.4) serves as the first indication to identify suitable robot models, demonstrating that cobots have, on average, around 1,000 mm reach and 10 kg payload. In addition, the installed base of Yaskawa robots in machine tending applications from 2015 to 2018 has been analyzed regarding payload and reach (see Figure 3.4). The following bubble diagrams illustrate this context in two different scales.

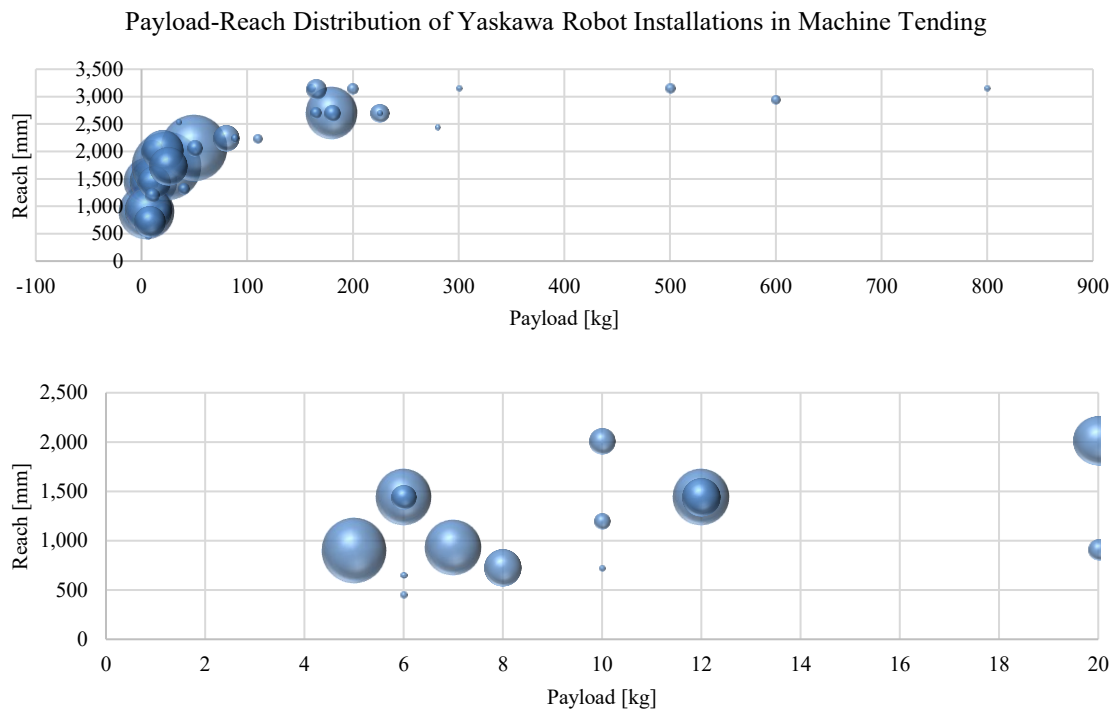


Figure 3.4: Payload-Reach Distribution of Yaskawa Robot Installations in Machine Tending

As can be seen, there are some single applications for high payload robots, while the highest concentration lies in the field up to 100 kg and around 200 kg. Due to the focus on cobots, which are concentrated in a low payload and low range area, nearly equal representatives within these specifications must be selected. Therefore, the industrial robot Yaskawa GP12 (1,440 mm reach, 12 kg payload) and the collaborative robot HC10DT IP67 (also known as HC10DT XP, 1,200 mm reach, 10 kg payload) are used [241, 242]. Two respective grippers are selected to simulate the exact mass properties attached to the robot flange: a collaborative OnRobot 3FG15 and an industrial Schunk PZN-plus 100-1-SD, which have similar weights [243, 244]. As turning machine representatives, the latest DMG Mori portfolio is analyzed. The CAD system SolidWorks and the simulation software Yaskawa MotoSize for payload simulations and MotoSim (see software description in Appendix 8) for offline programming are used as software tools. Therefore, the last focus is:

- *F6: Focus on the robots Yaskawa GP12 and HC10DT IP67, the grippers OnRobot 3FG15 and Schunk PZN-plus 100-1-SD, the DMG Mori machine portfolio, and the software tools SolidWorks, MotoSize, and MotoSim.*

3.3 Economic Module – Solution Approach

In this research, only economic optimization is pursued under the use of the net present value (*NPV*) as a target figure by neglecting further dimensions, such as social or ecological ones. The presented results of this subsection, of “4.1 Economic Module – Module Development” and of “5.6 Economic Evaluation” were published in [245]. [236] presents a target system that serves as the basis to select particular factors that are further considered for this work. To identify the optimal robot technology, three separate *NPV* values are calculated for the alternatives “CR, PFL,” “CR, HM,” and “IR”. By comparing those values, an economic-based decision about the advantageousness can be made. While the initial investment I_0 and the cash-in flows *CIF* show individualities when comparing robot systems, cash-out flows *COF* can be cut down due to the assumptions mentioned above, leading to the following simplified equation:

$$\Delta NPV = -I_0 + \sum_{t=0}^T CIF(t) \cdot q^{-t} \quad (3.1)$$

Therefore, cash-in flow determination is emphasized in this doctoral thesis. The most important factors have been summarized in the following Ishikawa diagram to get a more detailed observation of the economic system's complexity (Figure 3.5). As reference basis serves the manual operation. The factors labor release grade *LRG* [%] and the annual output

deviation ΔO [workpieces] are proposed to determine the positive cash flows. For a more comprehensive economic consideration, this target system can be extended in further research. The *LRG* describes the percental time slice that the operator is relieved from its task due to automation, making him available to conduct other, more value-adding activities within this gained time. On the other side, the annual output deviation ΔO describes the change in produced units that come with automation. Considering the specifics of human-robot interaction, the following approach emphasizes the switching between operating modes depending on the operator's proximity, which influences the robot's velocities and cycle times. To describe the time slices of the operator's absence and presence, the interaction grade α [%] is introduced. This factor implies the percental time slice of potential interaction, in which the industrial robot stops and the cobot operates at a safe, collaborative speed and serves as a metric to set the execution times ET [h] in the single modes into ratio to each other. Consequently, preliminary consideration of α -affected (α) and α -unaffected processes (α^*) is recommended (see Figure 3.2).

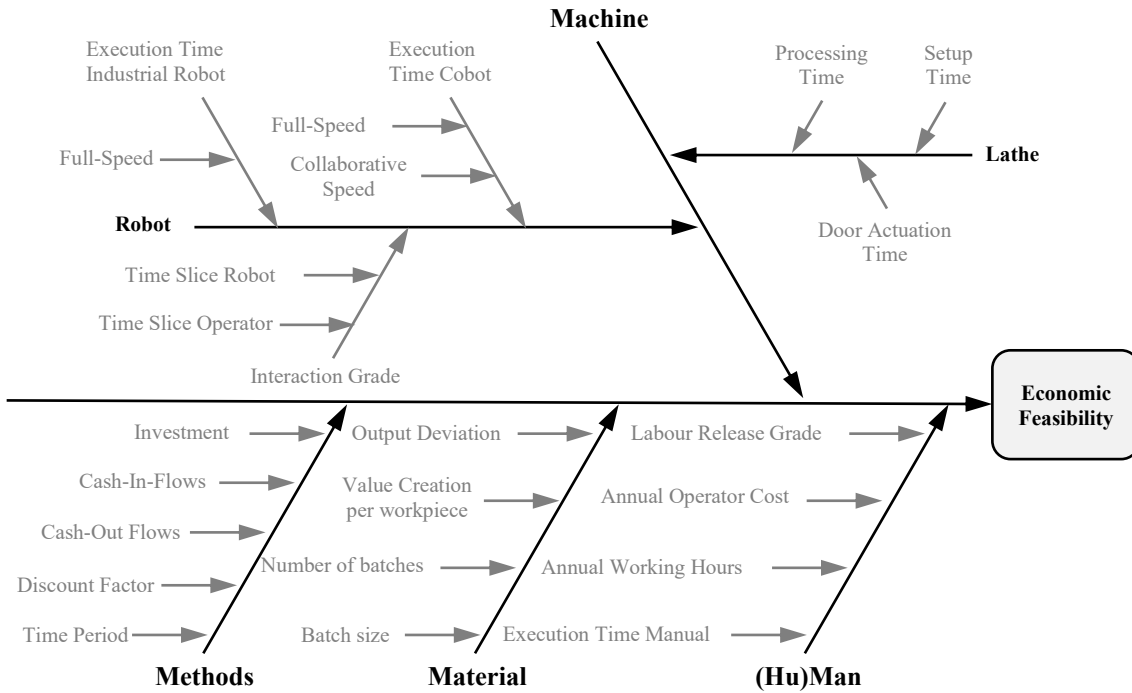


Figure 3.5: Ishikawa Diagram for Economic Module based on [7]

To calculate the factors *LRG* and ΔO , a suitable deduction is presented as follows (see Figure 3.6). As information base serves the manual execution time for one batch B_n , resulting from the addition of the *ETs* of all required manual processes. Together with the annual

working time W [h], the total number of produced batches N can be calculated. Furthermore, potential rest capacities R [h] must be considered, in which a batch share N_+ can be completed. The addition of the product of the batch number B_n and batch size S_n [workpieces] with the lot share or rather the rest output O_R [workpieces] delivers the total annual output O_A [workpieces]. As the basis for the *LRG*, the annual execution time *AET* [h] in manual operation is used, describing the operator's temporal binding to the machine.

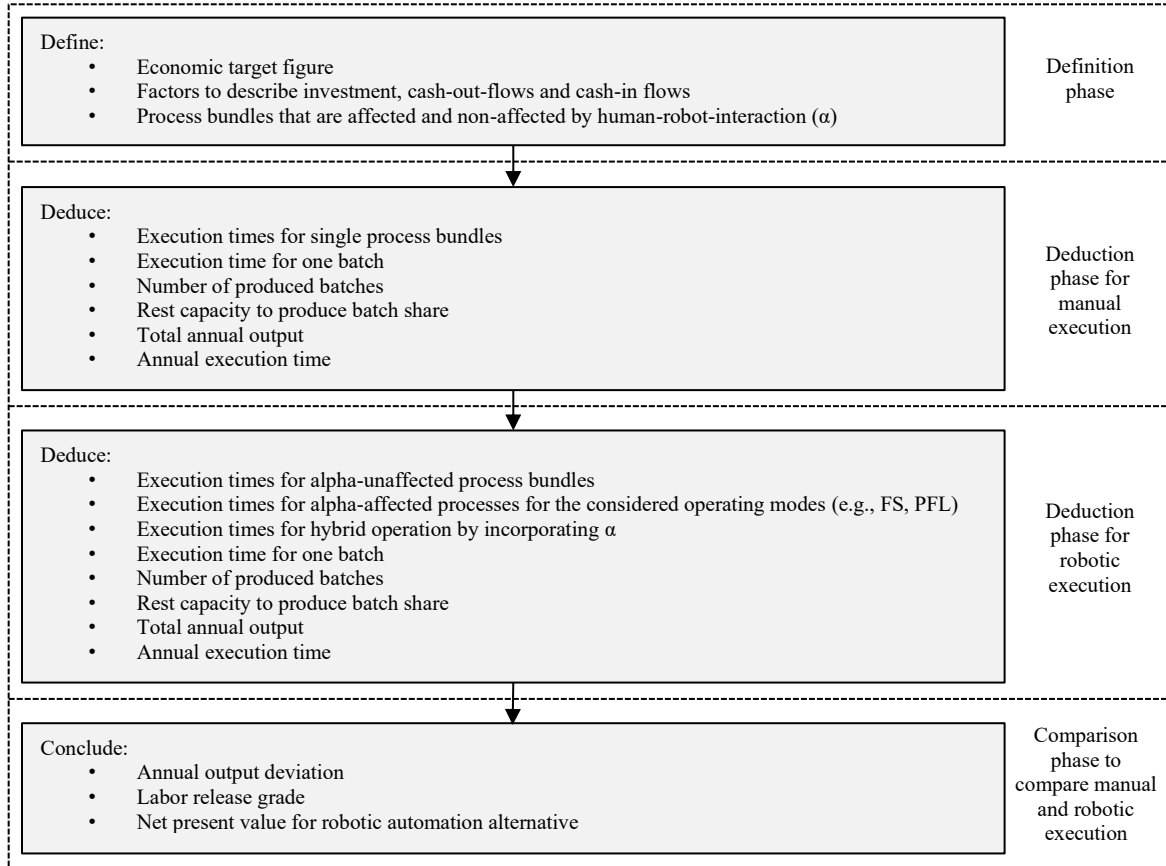


Figure 3.6: Deduction Procedure for Economic Module

In the next step, a similar calculation scheme is used for the robotic execution that extends the complexity by the single operating modes. At first, the execution times for α -unaffected processes are calculated. Secondly, the α -affected *ETs* in FS and PFL mode at collaborative speed CR are calculated, assuming 100 % exclusive operating in each mode to describe extreme scenarios. By incorporating the interaction grade α , these scenarios are combined to conclude an interaction-dependent cycle time. The addition of the α -unaffected and α -affected *ETs* delivers the *ETs* for one batch in hybrid mode. Based on this data, the same procedure regarding the number of batches, rest capacity, batch share, and total annual output is applied as described before. Only the setup times (initialization phase) must be

considered for the annual execution time in the robotic execution form. To calculate the CR, PFL alternative, the interaction grade's influence is not considered since the robot always operates at a safe, collaborative speed independent of the operator's proximity. Therefore, the calculation scheme can be simplified.

Lastly, manual execution is compared to the considered automation alternative regarding temporal operator binding (LRG) and ΔO via division and subtraction. The cash-in flows result from the multiplication of the LRG with the annual operator cost and multiplying the ΔO with the value creation per workpiece to conclude the monetary human resource-saving and production capacity increase. Figure 3.6 summarizes the presented procedure.

3.4 Gripper Feasibility Module – Solution Approach

One main technical feasibility criterion in robotic system integration is the robot's ability to handle the gripper-workpiece system in all positions and speed levels. Robot payloads are always specified as the absolute mass that the robot can handle. This indication can be understood as a point mass at the tool center point TCP. The actual payload depends on the lever of the attached mass and the moment of inertia of the combination of gripper and workpiece [246, 247]. Robot manufacturers provide diagrams to their customers that show the allowable wrist load depending on the x-y-distance of the moment of inertia from the center of rotation [241]. Gripper manufacturers specify the accessible, gripping forces depending on the jaw length in respective diagrams and define the allowable moments in forces [248].

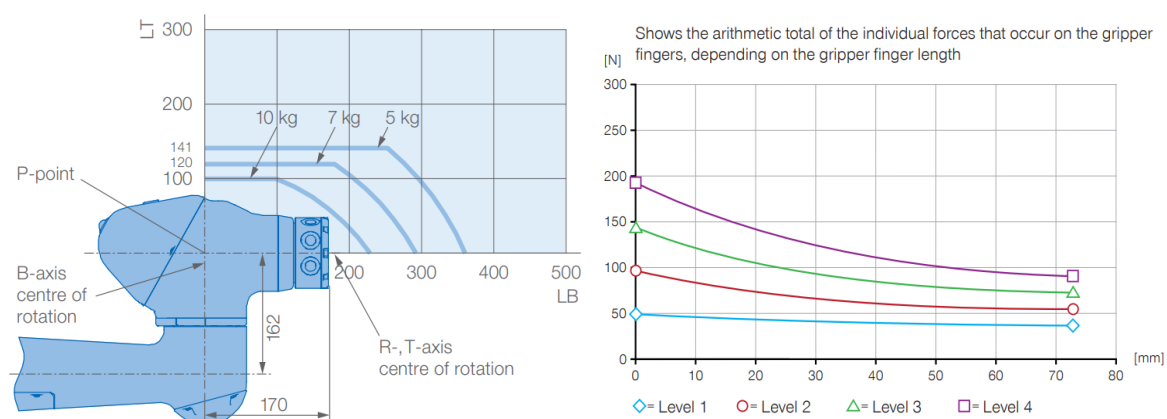


Figure 3.7: Allowable Wrist Load Diagram, Allowable Forces and Moments, and Gripper Force Diagram [241, 248]

Although this information is provided to the planner, it is not feasible to make generalized statements about the gripping feasibility of a specific workpiece or workpiece spectrum, making further engineering effort mandatory. The gripper planning and design process starts with a basic concept that is further specified during rough and fine planning up to actual testing and practicability verification. This whole engineering process requires several iteration loops and, therefore, temporal resources. Hence, the decision if a gripper is feasible can be finally made in the well-advanced fine planning stage of the project [178]. At this point, engineering efforts have already been undertaken, which also increases the overall project cost. Negative feasibility results or decision changes toward another robot model or technology make a new gripper feasibility study necessary. To reduce the project cost, a frontloading model is demanded that enables the planner to make a preliminary decision about feasible gripper solutions at the beginning of the project in the rough planning phase. Therefore, the main influencing factors must be identified and simulated to create a knowledge base.

For simplification of the planning procedure, this module deals with the provision of gripping feasibility information of workpiece-specific diameter-length combinations of a selected gripper model. This tool is intended to be used in the rough planning phase, which requires a low complexity and has an easy-to-use character. A knowledge base of various simulations builds the foundation to conclude the feasible combinations for collaborative and industrial robots. As a result, the factors diameter and length are focused on by iterating the feasible length at predefined diameter values within several simulations.

The main influencing factors of the stated problem are, as discussed previously, the moment of inertia and the mass that is attached to the TCP and the robot characteristics. The following paragraph explains how the single subcomponents influence those factors and how the respective values can be determined. A multi-level consideration of the subdivided systems robot, gripper, jaws, and workpiece is suggestive to get a more in-depth view of the problem. The lowest level (level 1) implies the interface between jaws and the workpiece, which is mainly influenced by the gripping strategy. Rotary workpieces, assumed as raw parts, can be described by their length l [mm], diameter d [mm], and material with the density $\rho \left[\frac{\text{kg}}{\text{m}^3} \right]$, delivering the weight m [kg]. Jaws, on the other side, are defined by their length and contact surface. Besides the standard jaws provided by the gripper manufacturer, custom solutions can be designed for special gripping situations. Especially for form closure, this is typical because the jaws form the geometrical counterpart to the workpiece's outer contour.

Jaw customizations also influence the moment of inertia due to mass distribution deviation from the standard solution. Level 2 assumes the jaw-workpiece system (level 1) as set and takes the gripper into account regarding the required forces and the gripper stroke. The overall design (case and jaws) and used materials (steel, aluminum, synthetic) of the single gripper components mainly influence the mass distribution and, therefore, the moment of inertia. For machine tending, double grippers must be considered, which require a special dual flange attached to the robot's 6th axis. On the highest level (level 3), the interface between the robot and the subsystem gripper-jaw-workpiece (level 1 & 2) is analyzed. From this robot-oriented perspective, the mentioned subsystem is assumed as a whole by assigning one mutual mass and moment of inertia to it. On the robot side, especially its kinematics, rigidity, reach, and payload highly influence the ability to handle different loading situations. Figure 3.8 sums up the mentioned influencing factors on the robot-based gripping feasibility in an Ishikawa diagram clustered by the three Ms machine, methods, and material (workpiece). The two Ms “(hu)man” and “measurement” are excluded from lacking manual or measurement-based influences.

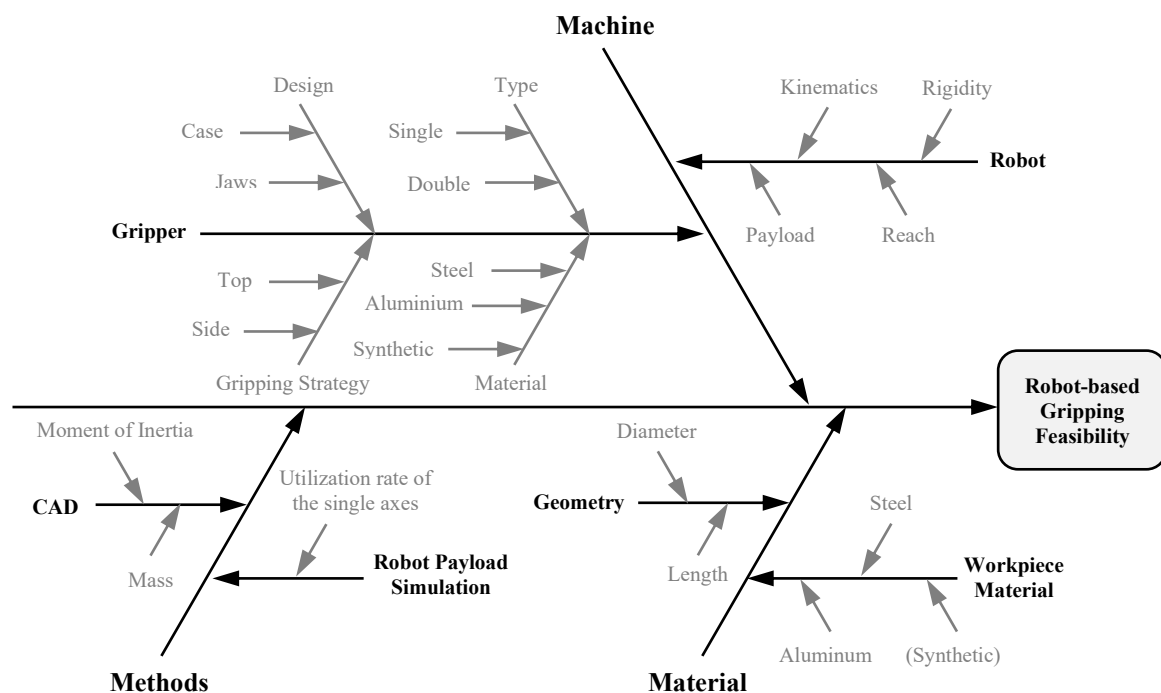


Figure 3.8: Ishikawa Diagram for Robot-based Gripping Feasibility Module

For the simulation study, collaborative and industrial grippers are used. It is assumed that collaborative grippers are exclusively used for cobots and industrial grippers only for

industrial ones. ISO/TS 15066 [108] demands the gripping force limitation to 140 N and rounded edges to reduce occurring forces at the potential collision event. Therefore, cobots can only be operated with collaborative grippers (assuming they operate in PFL mode). Industrial fenceless robots, however, can exclusively work in coexistent or cooperative mode. Theoretically, industrial robots could be equipped with both types of grippers, which is not the case in practice because of the following reasons. Firstly, the cost of cobot grippers is higher than industrial ones. Lower sales figures and more complicated case manufacturing (due to the rounded edges) make them unprofitable in combination with an industrial robot. Secondly, the reduction to 140 N limits the application field of the robot unnecessarily. Hence, this assumption is based on valid practical argumentation. All models are tested as a double gripper. For dual operation, respective flanges have been individually designed. As gripping strategies, gripping from the top is considered. As workpiece material, steel (S235JRG2), aluminum (3.1645 EN AW-2007), and polyoxymethylene (POM) are used.

At first, the diameters that need to be simulated are predefined for each gripper model. The maximal opening width OW [mm] and the minimal closing width CW [mm] serve as the first indications. In combination with the robot repeatability R_R [mm] and gripper repeatability R_G [mm], the minimal workpiece diameter WD_{min} [mm] and maximal workpiece diameter WD_{max} [mm] are calculated. The following equations illustrate the context:

$$WD_{min} = CW + (R_R + R_G) \quad (3.2)$$

$$WD_{max} = OW - (R_R + R_G). \quad (3.3)$$

In the following, the general simulation procedure is presented (see Figure 3.9). To determine the moment of inertia and the masses of a gripper-jaw-workpiece combination, CAD systems are suitable. The robot manufacturer usually provides robot payload simulation tools. At first, a CAD volume model of the gripper is required, containing the mass properties of the assembly. To receive realistic mass results, the used materials must be assigned to the single subcomponents. The rotary workpiece is designed by defining the diameter and length and assigning the respective material to the model in the next step. Then, the gripping strategy is defined, and the single subcomponents are assembled. Based on the previously designed gripping situation, the respective mass properties of the gripper-jaw-workpiece assembly are evaluated regarding the payload behavior of the robot. Therefore, the CAD software offers the calculation of this information. The gripper's interface point to

the robot flange must be used to cover the robot-dependent payload utilization as the reference point. Besides the mass m [kg], the mass center from the flange L_x , L_y and L_z [m] and the moment of inertia I_{xx} , I_{yy} , I_{zz} , I_{xy} , I_{xz} and I_{yz} [kg * m²] are relevant (see (3.4)).

$$\begin{bmatrix} \text{Mass Center} & \text{Moment} & \text{Moment} \\ \text{from} & \text{of} & \text{of} \\ \text{Flange} & \text{Inertia} & \text{Inertia} \end{bmatrix} = \begin{bmatrix} L_x & I_{xx} & I_{xy} \\ L_y & I_{yy} & I_{xz} \\ L_z & I_{zz} & I_{yz} \end{bmatrix} \quad (3.4)$$

In the simulation software, this data is inserted after selecting the correct robot type. As a result, the software delivers the percental utilization of the maximum allowed load at the 6th axis, 5th axis, and 4th axis as maximal occurring moments $M_{\%Max}$ [%] and moments of inertia $MI_{\%Max}$ [%]. Furthermore, a color indication is given by the software signaling the load utilization of each axis: green for unproblematic operation in all directions, yellow for minor limitations, purple for significant limitations, and red for unfeasibility.

$$\begin{bmatrix} M_{6,\%Max} & MI_{6,\%Max} \\ M_{5,\%Max} & MI_{5,\%Max} \\ M_{4,\%Max} & MI_{4,\%Max} \end{bmatrix} \quad (3.5)$$

Figure 3.9 illustrates the utilized approach. As the procedure's starting point, an initial diameter-length combination is chosen, and the first simulation is executed. Then, the workpiece length is variated depending on the previous result, and the simulation is executed again. This process is repeated until the identified lengths, delivering a green and a yellow result within the predefined workpiece length interval. The length value that delivers the last green result before it turns yellow is set as the threshold length value for the respective diameter. Then, the next diameter is chosen, and the procedure is repeated. This procedure is applied to all simulation runs that have been defined. In this way, a database is created that delivers supporting points for feasible diameter-length combinations.

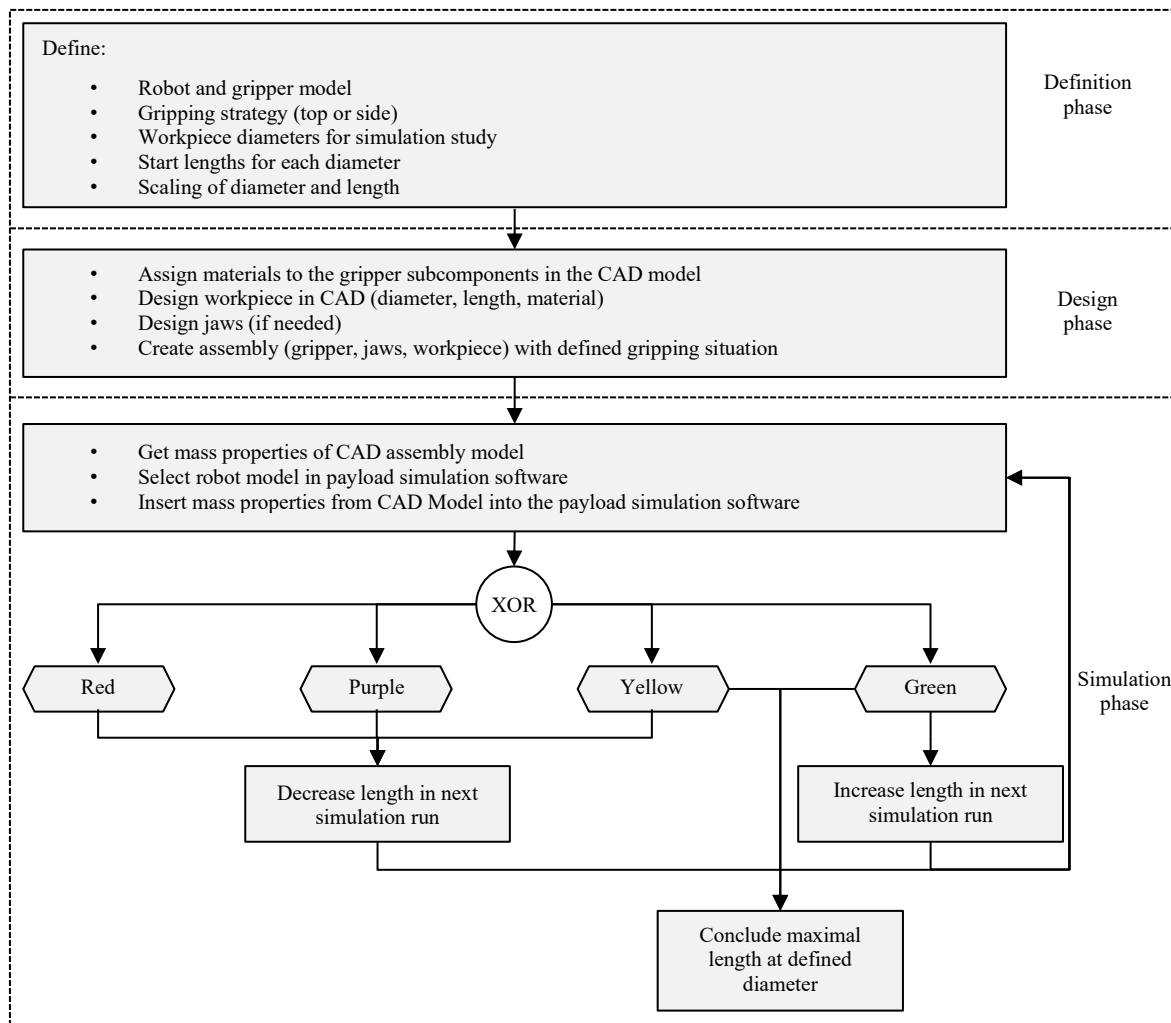


Figure 3.9: Simulation Procedure for Gripper Feasibility Module

3.5 Rough Layout Discretization Model – Solution Approach

As mentioned in state-of-the-art, optimized layouts are designed based on transport matrices that indicate the intensities between single entities. The triangulation method serves as a spatial arrangement framework to position the single elements in optimal material flow to each other. The following module picks up this approach and modifies it for the purpose of lathe machine tending. Therefore, a standardized pattern should be developed that includes suitable positions within the application context. To understand factors worth considering, the following Ishikawa (see Figure 3.10) diagram assists.

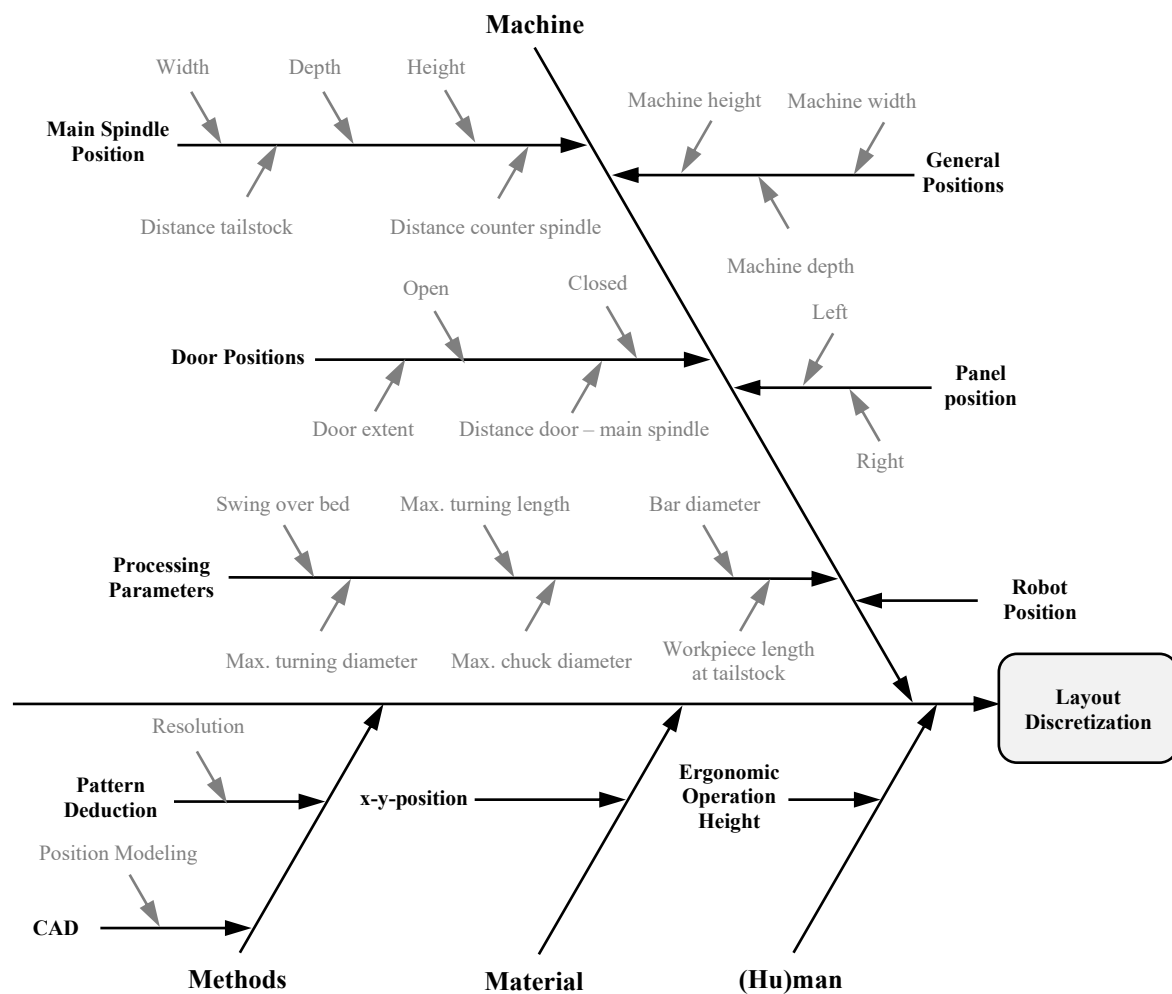


Figure 3.10: Ishikawa Diagram for Layout Discretization Module

Figure 3.11 illustrates the following modeling procedure. As the first step, the dimensional character of lathe machines through the example of the latest DMG MORI machine portfolio is described by analyzing the criteria described in Figure 3.10: general, main spindle, door, and panel positions as well as processing parameters. Based on this analysis of machine dimensions, the abstraction of a general arrangement pattern is pursued, covering a broad range of machines and enabling the planner to describe the use-case-specific machine. At first, all positions (doors, main and counter spindle, maximum turning length) for each machine are three-dimensionally generated in CAD, referring to the x-y coordinate of the left door position of the machine as the zeroing point. Secondly, the single models are layered and transferred to one mutual model leading to a machine pattern. With two-dimensional fields in a suitable resolution, the single positions are discretized. Therefore, an average height must be defined resulting from analysis of the collected

machine parameters or realistic assumptions, e.g., anthropometric data. To cover the robot installation positions, further fields with the same or another resolution are added in front and left of the machine at different distances.

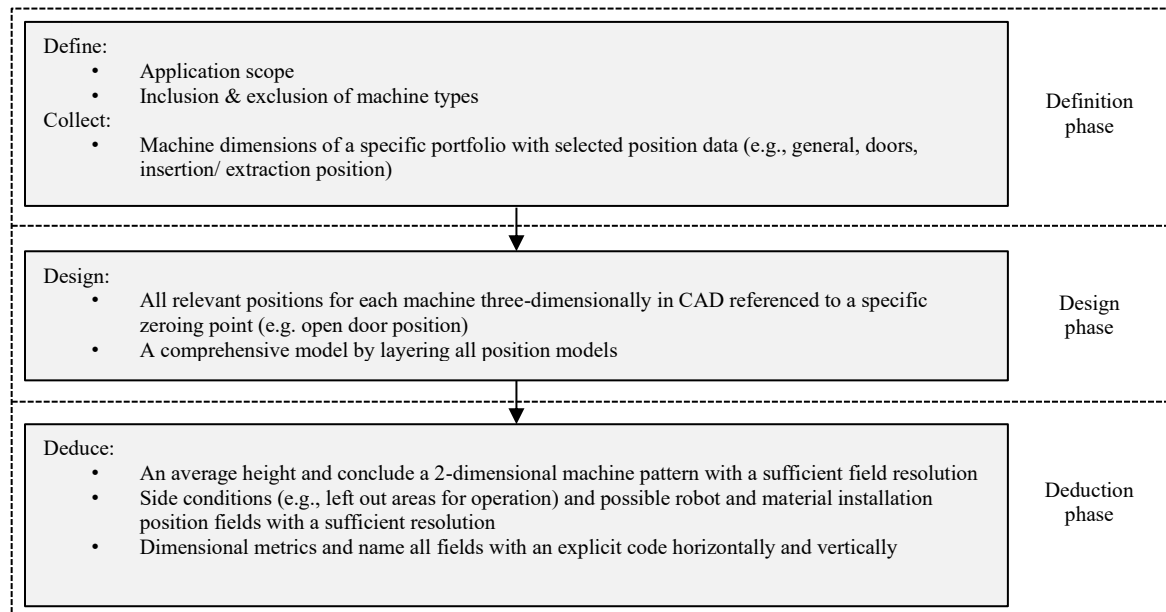


Figure 3.11: Modeling Procedure for Rough Layout Discretization Module

The first line directly in front of the machine is spared since this space provides accessibility to the operator for setup activities (see Figure 2.18). By conducting a reachability study of the single robot installation possibilities, feasible positions are identified within the mentioned pattern. The primary condition is the reachability of the main spindle without colliding with the machine door on both sides. As feasible material positions, the neighbor fields of those robot installation options are chosen. All positions are named horizontally with letters and vertically with numbers. Door and machine positions have lowercase letters, while the robot and material positions have capital ones.

Due to the wide structural variety of lathe machines and turning/ milling machines, the following exclusion criteria were used to limit the observation scope and streamline the results. Special machines for crankshaft machining imply a high workpiece weight that cannot be handled with the selected robots. Workpieces that must be additionally supported with steady rests or require either a door extent over 1,200 mm or the utilization of two machine doors indicate high workpiece lengths with high weights, levers, and reaches that are not feasible with these robots. Multi-spindle machines for high-volume production or the usage of internally installed robots have already been excluded in the use case delineation.

Vertical machines and machines with a double spindle oriented to the front require a different loading and unloading (LUL) strategy. Furthermore, machines with no inclined bed or a left-sided panel orientation are excluded due to their individuality. Figure 3.11 illustrates the presented modeling procedure.

3.6 Cycle Time Estimation Module – Solution Approach

A crucial factor in the economic evaluation of robot systems is the achieved cycle time. Various methods are available to determine these times for both manual and automated operations as described in state-of-the-art. While MTM is a recognized tool with broad acceptance in the industry to determine manual execution times, offline programming and simulation software is broadly used in robot planning, even though there is no predominant software solution. Advantageous of these software tools is their accuracy in modeling the robot's kinematics and specifics regarding singularities for reachability studies. On the other side, RTM systems, described in [166], allow a robot-independent calculation of cycle times based on the distance information between two points. While the simplicity of this method is advantageous, consideration of robot model-specific factors is lacking. Hence, the comparability of differences in robot models of different manufacturers is impeded, e.g., for supplier selection throughout project planning. As a solution approach, this doctoral thesis presents a planning method based on reference simulations in a predefined positioning pattern for different motion modules under the incorporation of the utilized operating speed. With this database, the complexity of the problem is discretized to provide the planner a fair understanding and overview. Since simulations need CAD information for programming the robot paths, a precedent layout planning effort is required. Therefore, the rough layout must already be known to design the single-cell elements and implement the considered robot positioning options. To identify the optimal robot position, the manipulator's motions are individually programmed for each position to conclude the respective cycle time. Due to the individualities regarding robot kinematics and singularities for each position, it is challenging to determine suitable positions in advance or select the best position. As planning assistance, reference simulations in a predefined positioning pattern can assist as a database. For a better understanding of the problem complexity, the following Ishikawa diagram assists (Figure 3.12).

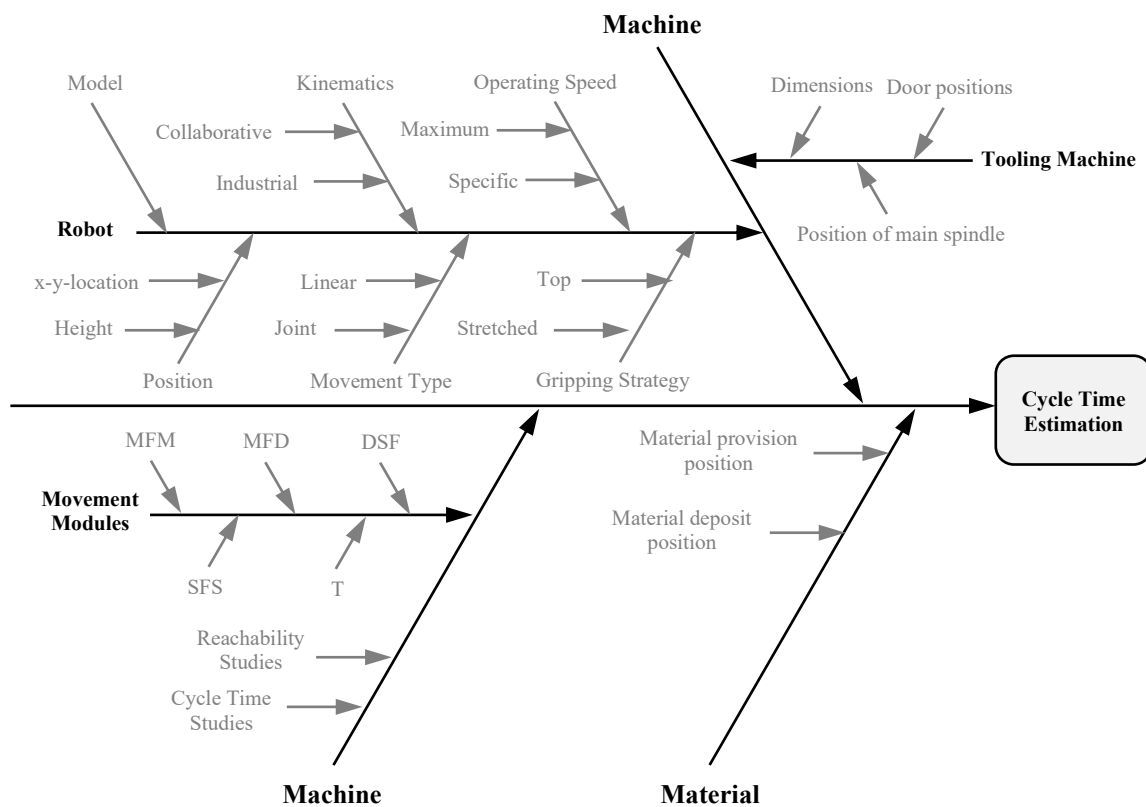


Figure 3.12: Ishikawa Diagram for Cycle Time Estimation Module

On the machine side, both robot and tooling machines must be considered. Its dimensions can mainly characterize the machine model. As insertion and extraction points for the machine tending operation, the main spindle position serve. Side conditions are the door positions that define the robot's reachability. While reaching into the machine, collisions with the door and the machine interior must be avoided. The robot model can be described by its kinematics, which predefines motion possibilities. The robot operating speed during the single motions is a primary influencing factor for the cycle time determination. To simplify the use case-specific cycle time determination, the high-level processes (illustrated in Figure 3.2) "P7 Unload and Load Machine", "P5 Load Machine", and "P5 Unload Machine" are broken down into movement sub-elements. One option is utilizing the MTM motion types; another is creating application-specific ones for turning machine tending, which aligns with the previously described process pipeline, which is focused on in this doctoral thesis. For "Loading Machine", it is assumed that the machine is empty and that one initial workpiece of the new batch must be loaded. Similarly, the last workpiece must be taken out in the process "Unloading Machine". For "Unloading and Loading Machine", it is assumed that a previous machining cycle has been executed and the

workpiece lies machined in the main spindle. Generally, the process consists of recurring positions and movements.

Therefore, this problem can be discretized by using the following robot motion elements: “Material Feed – Material” (MFM), “Material Feed - Door” (MFD), “Door – Spindle Feed” (DSF), “Spindle Feed – Spindle” (SFS) and “Turning” (T), which are illustrated in Figure 3.13 and explained in the following. Based on the before-mentioned assumptions, the process starts with picking up the raw material with a linear movement, starting from a material feed position to the actual deposit. These feed positions depend on the deposit height and the workpiece length. When gripped, the robot moves in front of the machine with a joint movement, waiting for the signal that the machining is finished and the door is opened. Then, the robot moves into the machine to a spindle feed position with a linear movement and executes then a linear feed motion to grip the processed workpiece. A spindle feed position must be chosen to guarantee a collision-free trajectory and sufficient space for the feed motion, with sufficient distance to the main spindle. This distance must be larger than the sum of workpiece length and feed motion length. The door position can be concluded based on this position since the robot moves from the door to the spindle feed position with a linear motion. When the workpiece is gripped, the same feed motion is executed in the opposite direction, followed by a joint turning movement around the 6th axis to change to the gripper with the loaded raw material. The same linear feed motion is executed to position the material into the chuck. After placing, the robot moves back to the feed position and then to the door position. At this point, a signal is sent to the machine that the robot left the machine operating space, and the door can be closed to start machining. With a joint movement to the material deposit feed position, the finished workpiece is positioned and then placed at the deposit target position with a linear motion. Lastly, the robot moves back into the deposit feed position and executes a joint movement to the initial position to initiate the next loop.

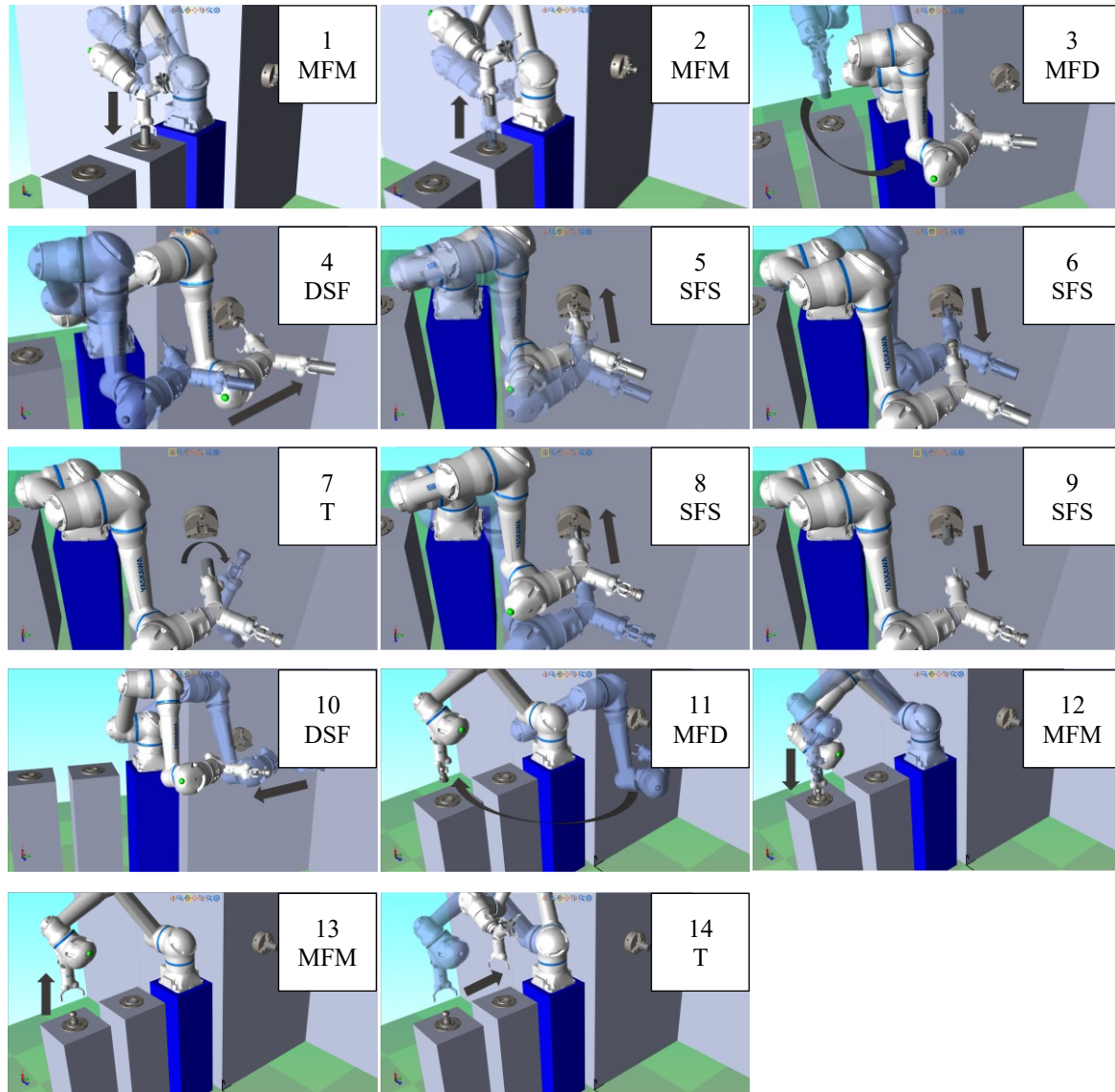


Figure 3.13: General Workflow of Lathe Machine Tending

By analyzing this process, another condition for the economic model becomes clear. For the actual cycle time calculation of the module “Unloading/ Loading Machine,” only those movements need to be considered that are executed within the machine. All motions needed to pick a raw part or position the finished one are executed simultaneously while the machine operates. Therefore, the condition must be set that the sum of these movements needs to be smaller than the processing times in order to avoid waiting times between robot and lathe machine. If not avoidable, these times must be added to the overall cycle time. Only for the initial “Loading Machine” and the final “Unloading Machine” this time parallelization is not applicable. To cover different gripping strategies with different reachability, “Top Gripping”

(T) and “Stretched Gripping” (S) are used, which differ in the positioning of the 6th axis, as illustrated in Figure 3.14.

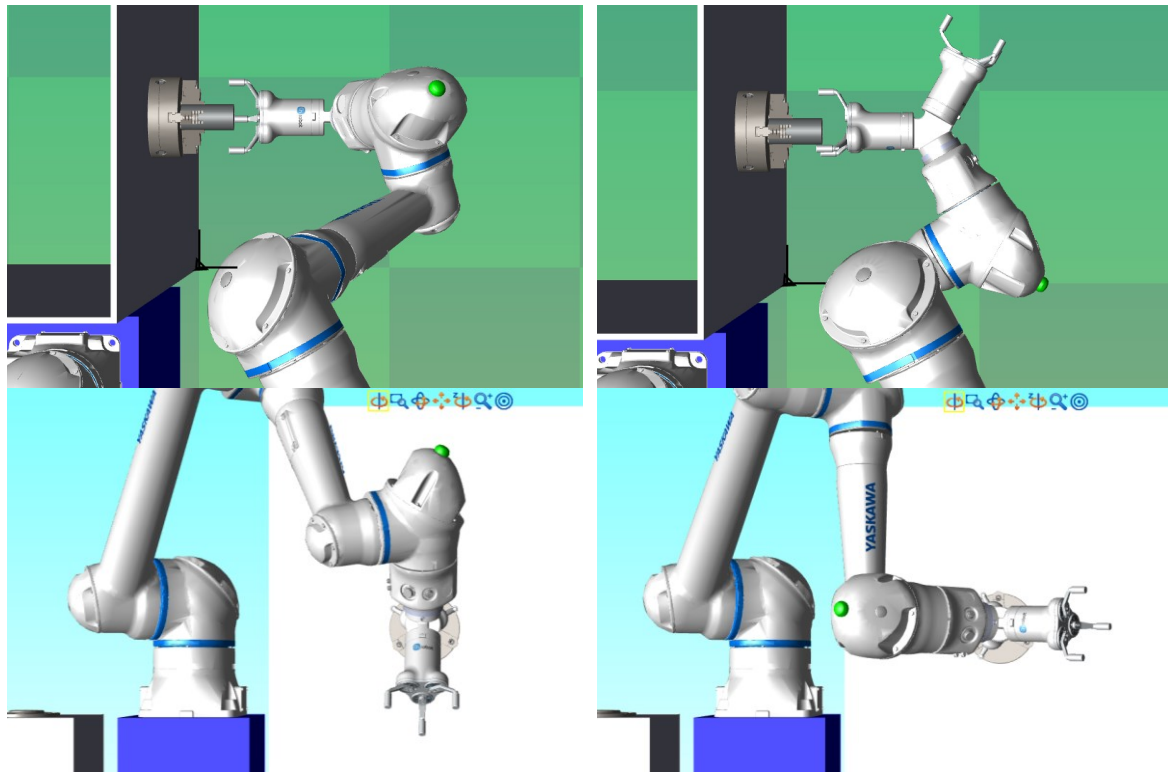


Figure 3.14: Top (left) and Stretched (right) Gripping

Those apply only for motions within the machine since the feed motion for material picking and placing is the same. Both reachability and cycle time studies can be executed within the robot offline programming software, while the first-mentioned ones serve as a feasibility check for the further proceeding. The material arrangement for workpiece provision and deposit serves as input information to simulate moving to the pick position. Comparisons regarding the automation-based productivity increase require a parallel manual motion assessment with MTM.

To determine each motion sub-element cycle times, all considered positions (robot, material, doors, main spindle) are three-dimensionally designed in CAD in simplified ways. For each simulation run, the robot is placed in another position. Then, all combinations between material feed and material, material feed and door, door and spindle feed, and spindle feed and spindle are simulated. As a result, the individualities in cycle times and hypothetical behavior outliers can be identified. To ensure feasibility, reachability studies are executed in order to verify if the robot can reach these positions. For the feasible

positions, the individual movement is simulated at different speed levels in the offline programming software, and the reached cycle time is measured. In this way, a velocity-dependent cycle time diagram for each motion sub-element can be concluded for all combinations.

As mentioned earlier, the simulations are conducted with two selected robot models to demonstrate this method's applicability and increase the significance of this approach with actual simulation results. For the collaborative robot HC10DT IP67, a maximum speed of 1 m/s is technically possible, while the classic industrial GP12 can achieve 1.5 m/s. The simulation is executed for the whole speed range, starting from 100 mm/s and increasing up to the maximum speed in 100 mm/s steps. Furthermore, no tool data is defined because the individual loading situation is use case-specific. Hence, the simulations represent a solid average value. Since the cycle time depends on the use-case specific workpiece regarding mass and geometrical properties, with high individualities that are complex in modeling, tool data are neglected. As a result, an average error is assumed over the whole simulation study, which is acceptable for rough planning. Figure 3.15 sums up the simulation process.

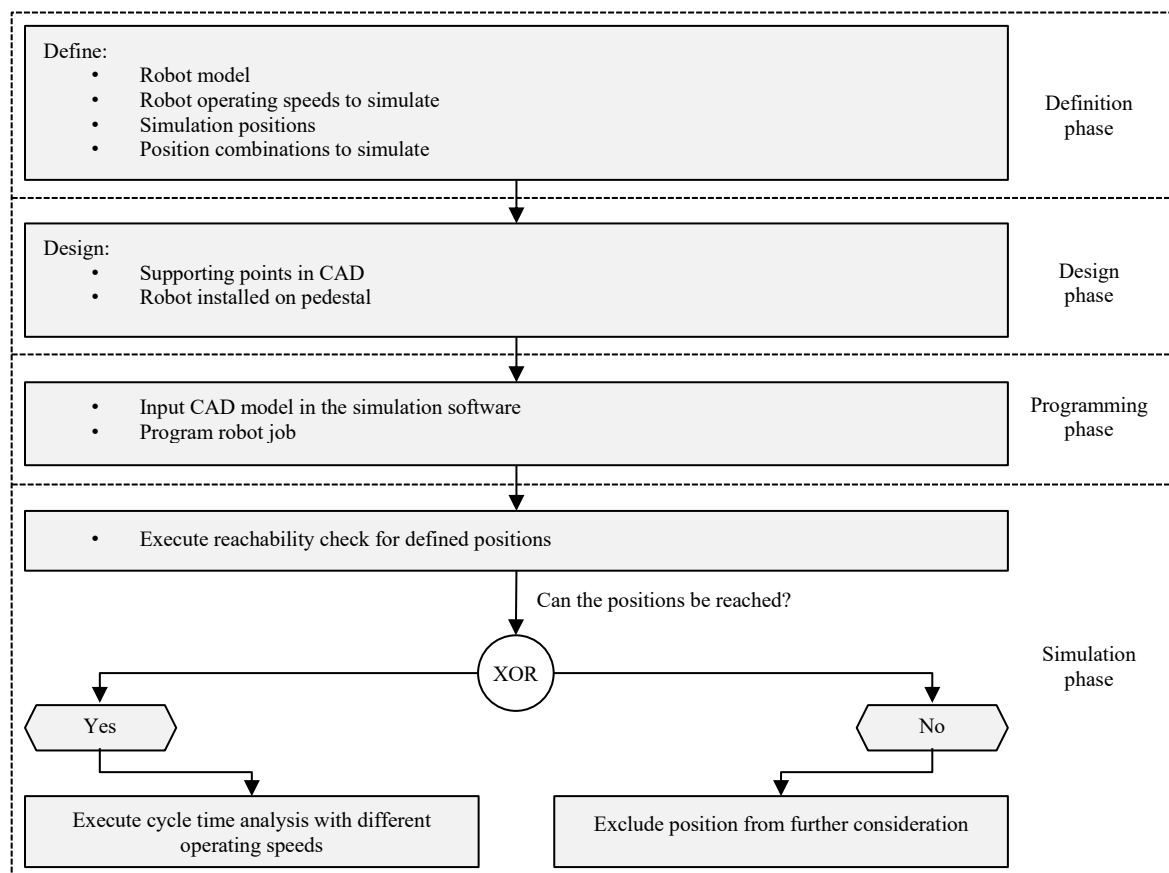


Figure 3.15: Simulation Procedure for Cycle Time Estimation Module

3.7 Collaborative Speed Estimation Module – Solution Approach

3.7.1 General Approach

Based on the state of the art and research, estimating the maximum allowed collaborative speed according to ISO/TS 15066 in advance is currently not feasible. The exact process needs to be planned and set up to execute the time-intensive force and pressure measurements for determination. The problem's multi-dimensional character and insufficient description of the system behavior regarding the extent of influencing factors on the results impede a preliminary assessment of the allowed speed and the economic project feasibility. This research focuses on developing a model that provides the planner an approximation of the allowed collaborative operating speed value for simplification. The method should be simple to reduce applicability efforts to a minimum in the rough planning phase. Model development is executed in two steps: firstly, the system is analyzed to identify the influence of the single factors, and, secondly, the data is statistically evaluated to conclude approximation equations. As database serves a set of exemplary measurements for different scenarios based on combining several influencing factors. Specific criteria combinations are selected and iteratively measured to determine the relevance of selected factors regarding the maximum compliant velocities. This project has received funding from the European Union's Horizon 2020 research and innovation program under grant agreement No 779966 and has been supervised by the Fraunhofer IFF institute.

As potential risk situations, three cases have been concluded from the movement sequence illustrated in Figure 3.13 (see Figure 3.16). Case 1 implies a clamping situation during placing the workpiece on the material deposit (Material Feed – Material, MFM, see sequences 1 and 12). A quasi-static contact can occur if the operator holds his hand between the workpiece and the provision plate when the robot moves downwards. In the second case, the robot could collide with the operator's hand during moving from the material feed position to the machine door (Material Feed – Door, MFD, see sequences 3 and 11). The hand's non-dominant side (ND) is used as the considered body part for both cases. The third case implies a collision during the feed motion to insert and take out the workpiece (Spindle Feed – Spindle, SFS, see sequences 5, 6, 8, and 9) and during the movement from the machine's door to the spindle feed position (Door – Spindle Feed, DSF, see sequences 4 and

10). Assuming a robot installation on a pedestal, the motions will likely be executed at the operator's shoulder height, which is the considered body part for this case.

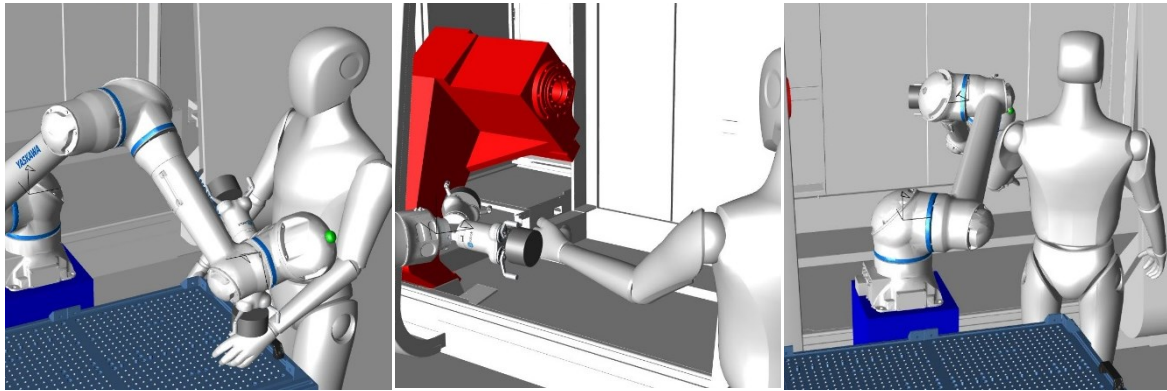


Figure 3.16: Identified Risk Scenarios – Quasi-static Contact with Hand (left), Transient Contact with Hand (middle), and Transient Contact with Shoulder (right)

Please note that the illustrated process in Figure 3.13 shows a dual gripper, which is the preferred solution in machine tending applications. For simplification reasons, to limit the considered factors, and for the sake of factor isolation, this research focuses on single grippers. In future research, a separate study on the influence of the gripper installation angle must identify a conversion factor between both gripping options.

To understand the most critical influences on the measurement results, a list of potential influencing factors has been developed, building the basis for measurement planning and execution. For collection, the following Ishikawa diagram (Figure 3.17) gives an overview by clustering them in the 5 Ms machine, method, material, (hu)man, and measurement. On this general basis, influencing factors have been specified with respective characteristics. To guarantee reproducibility for future similar studies, the experimental conditions are specified in the following. The robot was operated with software version YAS4.12.01A(EN/DE)-00, which should be used when conducting similar experiments. Firstly, the measurement device is firmly installed on a plate for quasi-static contacts. Potentially occurring vibrations need to be minimized by mounting the robot (with pedestal) and the measurement setup on one mutual massive base plate. Secondly, the distance between the start point of the movement (feed position) and the collision point must be high enough to reach the operating speed. Furthermore, the programmed endpoint needs to lie below or behind the collision point to ensure realistic results. If the endpoint of the robot program lay on the collision point, the robot would decelerate to reach the taught point with zero speed, which distorts the result. The robot must be configured with correct tool data for exact results, and the torque sensors

should be calibrated regularly. Furthermore, the cobot needs to operate in a collaborative mode with the respective safety functions activated (e.g., anti-clamping function, retract function, pushback function).

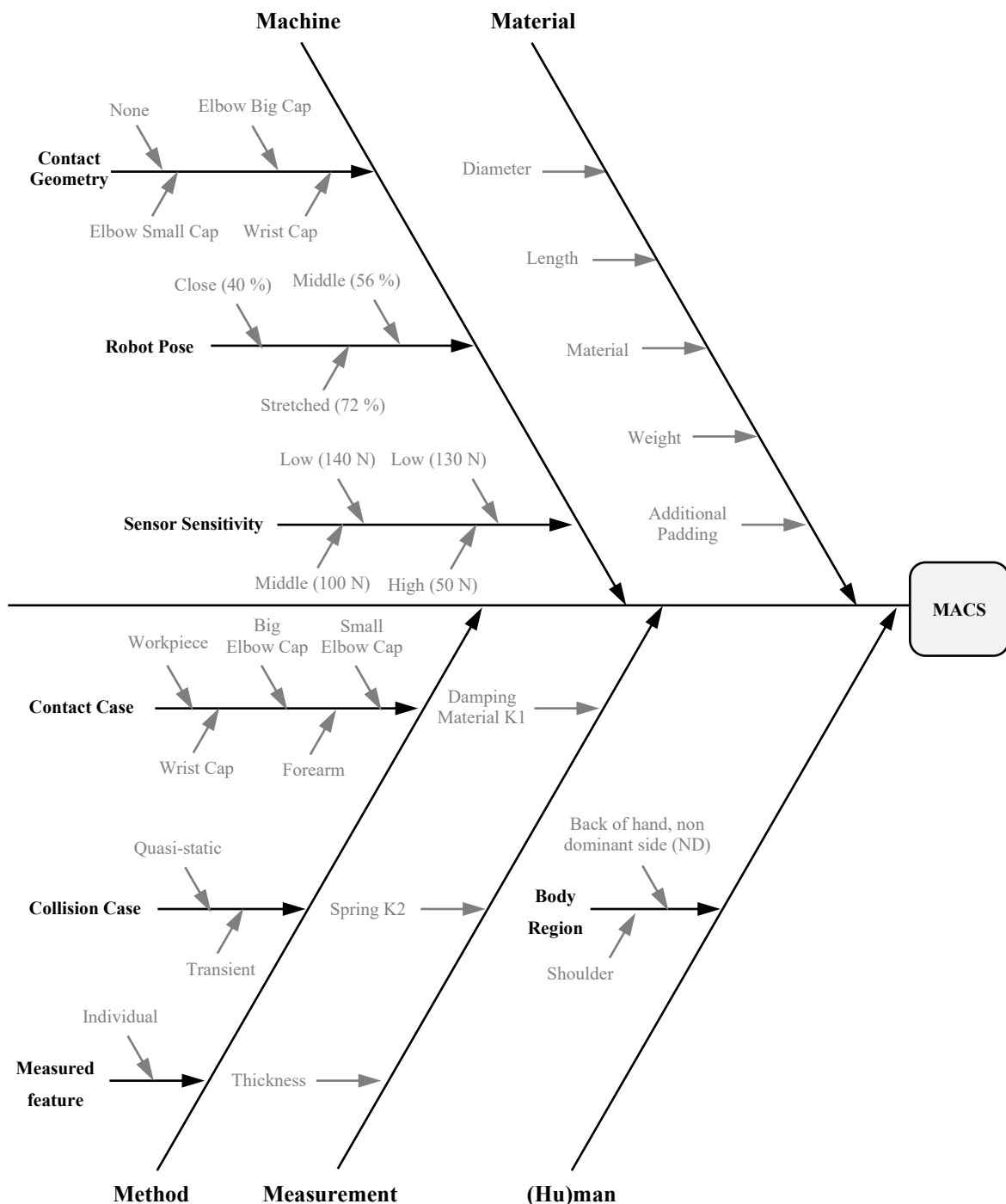


Figure 3.17: Ishikawa Diagram for the Collaborative Speed Estimation Module

It is recommended to run the tests under the same environmental conditions as the system will be used in practice. The pressure-sensitive foils' limiting conditions are specified as 17 °C to 38 °C temperature range and relative humidity of 35 % to 80 % [201]. For these tests, an average temperature of 21 °C and a humidity of 60 % were measured. For the tests' documentation, the PRMS sets three force measurement runs by default to counterbalance the device's inaccuracy [201]. For scientific and proven results, ten runs per series are used for this research. Outliers, defined as the minimum and maximum value of one series, are excluded from further consideration. The remaining eight values are averaged and used as an information base to compare with the threshold values defined in ISO/TS 15066 [108]. It is recommended to wait 30 minutes between collision and scanning for optimal results for the pressure foils. The experiment specifications are listed in Table 3.2. In Figure 3.18, the general measurement procedure is illustrated.

Table 3.2: General Experiment Specifications for Collaborative Speed Estimation Module

Category	General Criteria	Specifications	Criteria characteristics
Machine	Software version	YAS4.12.01A(EN/DE)-00	-
Measurement	Positions	Distance start to collision point	High enough to reach defined speed
		End point position	Below collision point
	Robot configuration	Tool data	Individually configured for each payload situation
		Sensor calibration	Regular
		Safety settings	Required functions activated
	Environmental conditions	Temperature	21 °C
		Humidity	60 %
	Data collection	Number of measurement runs	10
		Dealing with outliers	Exclude MIN & MAX value from consideration
		Final result	Averaging 8 remaining values

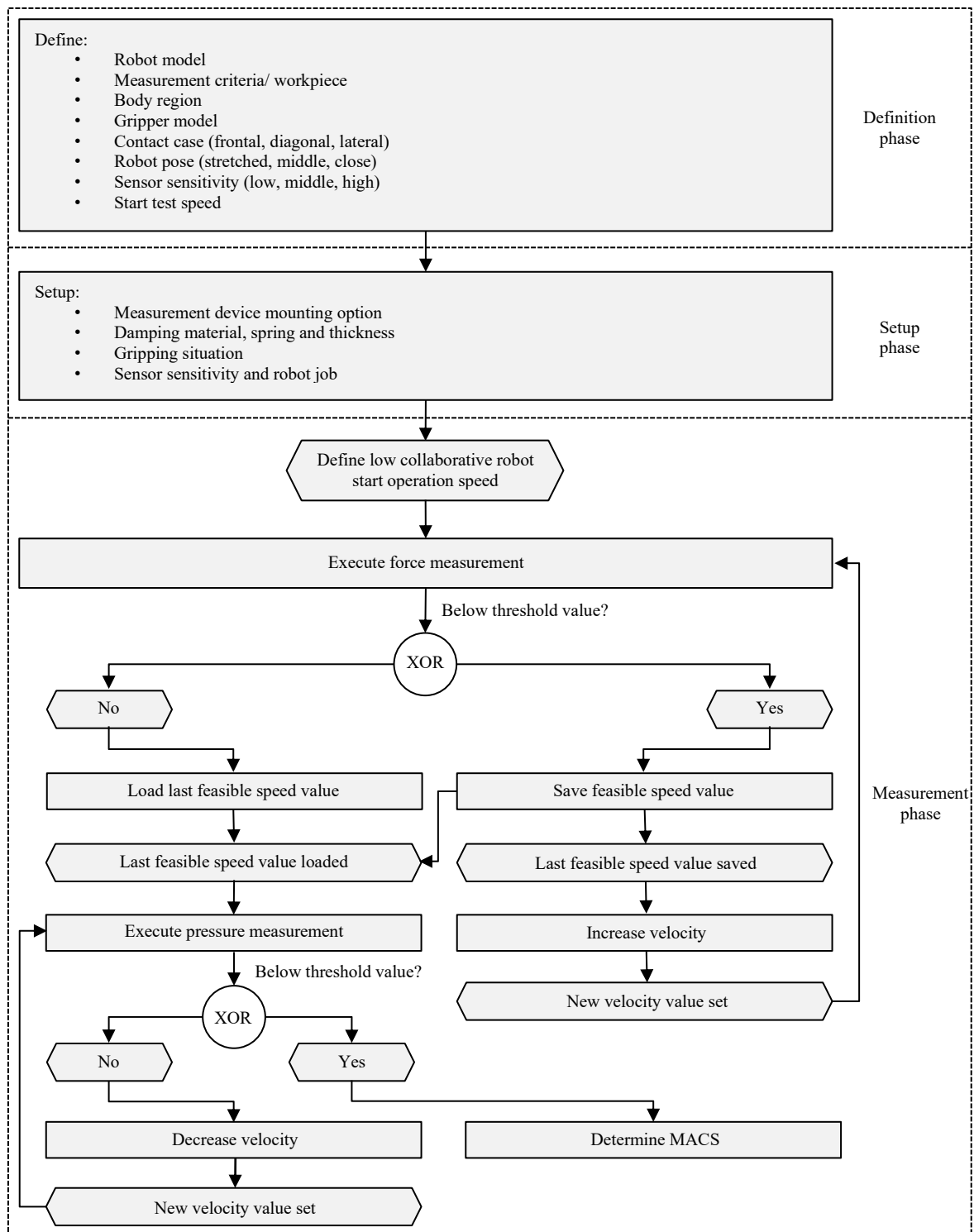


Figure 3.18: Measurement Procedure for Collaborative Speed Estimation Module

3.7.2 Case 1: Quasi-static Contact with Hand

In this paragraph, the measurements for the quasi-static contact with the hand are specified. The presented results of this subsection and of “4.5.2 Case 1: Quasi-static Contact with

Hand” were published in [249–251] and [252]. A customized setup has been designed to measure the quasi-static contact with the hand, illustrated in Figure 3.19. As base serves a solid metal plate, on which the robot pedestal with the collaborative robot Yaskawa HC10DT IP67 and a rigid frame is mounted. An adapter plate is installed on the top plate of the frame, where the measurement setups can be fixed. Four different drilling patterns enable fixing the sole measurement device for the quasi-static measurements on three different positions and the rail construction for the transient ones (see following subchapter). Quasi-static measurements are executed by moving the robot from the top of the device to measure the pressure and force.

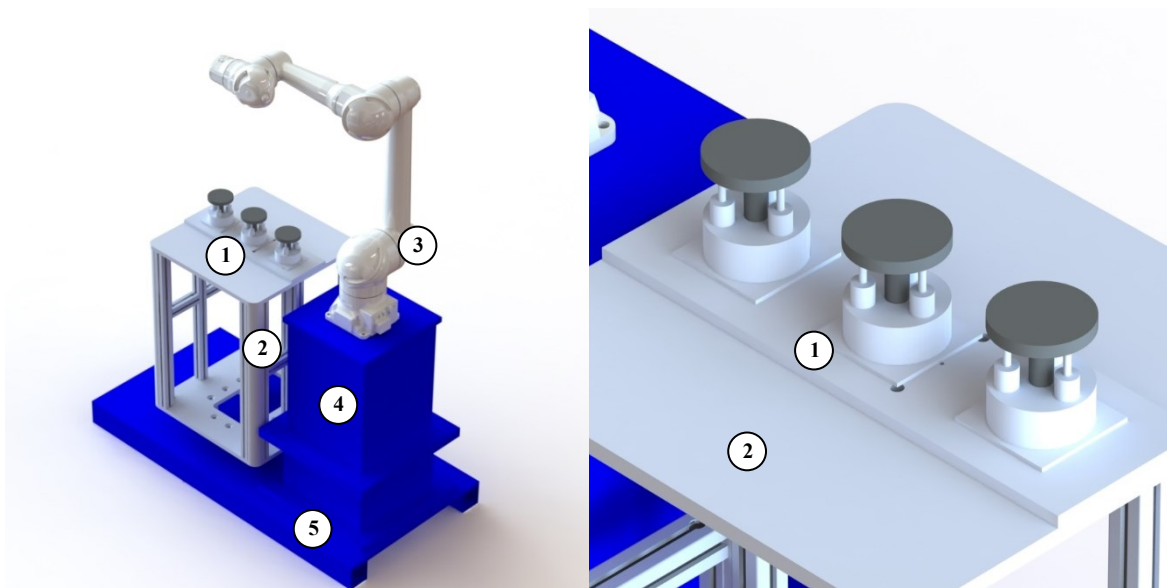


Figure 3.19: Measurement Setup for Case 1 - Quasi-Static Contact with Hand, with 1 – Adapter Plate with Measurement Device, 2 – Rigid Frame, 3 – Robot, 4 – Pedestal, 5 – Base Plate

As machine-dependent factors, the robot's pose and the sensor sensitivity come into further consideration - individualities in the robot's kinematic lead to a position-dependent sensor behavior, especially close to singularity positions. Hence, the sensor's responsivity can vary in specific poses. To cover this factor, measurements in different robot poses must be executed. As a metric, the percental reach utilization is based on the measurement positions resulting from the experiment design. For this research, 40 % (close), 56 % (middle) and 72 % (stretched) are defined. Based on the reach of 1,200 mm of the selected robot model, the close position lies at a distance of 480 mm from the robot base, while the middle and stretched positions are 672 mm and 864 mm distant. The sensor sensitivity itself is adjustable by the force limits to define the responsivity of the system. As force limits, 140

N (low), 130 N (low), 100 N (middle), and 50 N (high) are used, whereby the sensitivity extent is indirectly proportional to the force limit number. As described earlier, the body region emphases lie on the back of the hand (non-dominant side), which has a defined quasi-static threshold value of 140 N force and 190 N/cm² pressure (human-dependent factors). Hence, this area is assessed in more detail by using force limit settings at 140 N and 130 N. To analyze the impact of high sensitivities, 100 N and 50 N settings are considered in addition. To receive precise results, the operating speed is adjusted in 1 mm/s steps, which is the measurement accuracy simultaneously. The quasi-static tests with frontal contact (method-based factors) are executed by incorporating the workpiece diameter, length, material, and weight (material-based factors). Table 3.3 summarizes the experiment specifications for case 1.

Table 3.3: Experiment Specifications for Case 1 – Quasi-static Contact with Hand

Category	General Criteria	Criteria	Criteria characteristics
Machine (Robot)	Robot pose	Close, middle, stretched	40 %, 56 %, 72 %
	Sensor sensitivity	Low, middle, high	140 N, 130 N, 100 N, 50 N
Method	Measured feature	Individual for the measurements	-
	Collision case	Quasi-static	-
	Contact case	Frontal	-
(Hu)Man	Body region	Hand and fingers non-dominant side (ND)	190 N/cm ² Pressure, 140 N Force
Measurement	Damping material K1	-	Shore A 70
	Spring K2	k	75 N/mm
	Thickness	-	7 mm
	Result resolution	Speed adjustment interval	1 mm/s
Material (Workpiece)	Measured feature	Diameter d	[mm]
		Length l	[mm]
		Material	Steel, Aluminum, POM, PLA
		Mass m	[kg]

3.7.3 Case 2: Transient Contact with Hand

This paragraph deals with the measurements for the transient contact with the hand. The presented results of this subsection and of “4.5.3 Case 2: Transient Contact with Hand” were published in [249, 250] and [252, 253]. Since ISO/TS 15066 provides the before-mentioned equations, transient measurements are not mandatorily required. To compare the generally formulated calculation scheme with actual measurements, the presented approach pursues the description of hypothetical optimization potentials in the compliant robot velocity. Furthermore, the realistic modeling of transient contact scenarios is further investigated by testing a measurement setup provided by the Fraunhofer IFF. Theoretically, a transient contact is characterized by the recoil of an elastic system, in this case, the respective body region. For this reason, ISO/TS 15066 [108] specifies masses for each region that are picked up by the defined equations. To actively incorporate this factor, the Fraunhofer IFF provided

technical drawings of a designated rail construction based on their latest research (see Figure 3.20). This doctoral thesis contributes to developing the upcoming standard revision by testing this measurement setup by providing the first practical experimental results.

The guide rail is mounted with four screws on the adapter plate to connect it with the frame. On top, a rail carrier is installed, whose movement is stopped at each side with a mechanical stop. The holding construction connects the carrier with the adapter plate, which has various drilling patterns to install the measurement device on one side and the locating bolt on the other. On the bolt, different weight plates can be mounted. This setup aims to simulate the collision between robot and operator in free space on different body parts. In reality, the respective body region would recoil due to the collision energy simulated with the guide rail. Depending on the body region where the collision occurs, different body masses are moved, simulated with adjustable weight plates. Hence, the collision case is reproduced realistically.

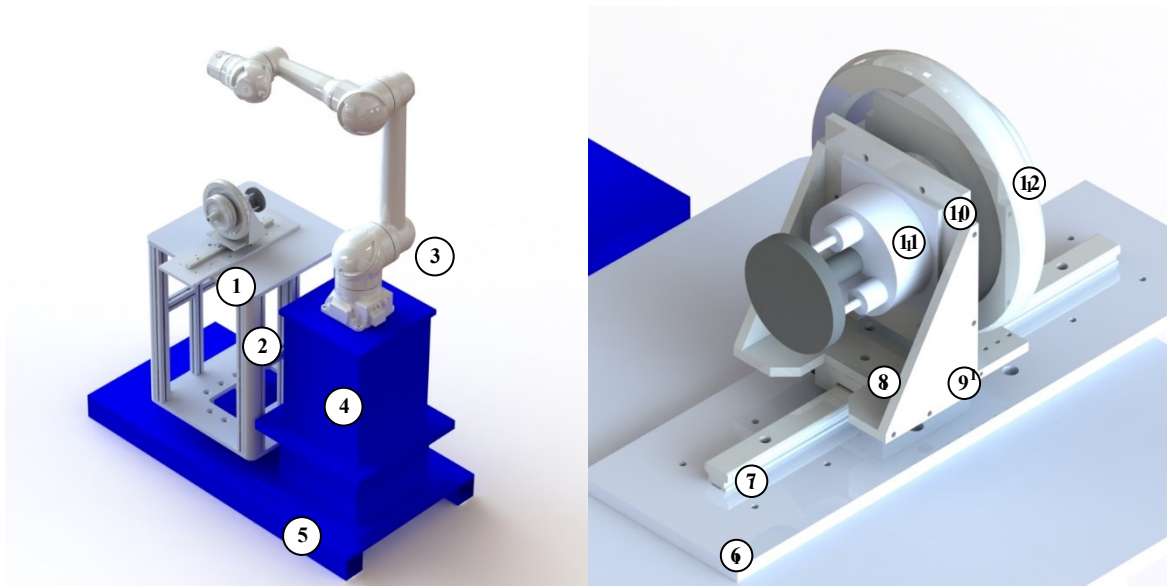


Figure 3.20: Measurement Setup for Case 2 - Transient Contact with Hand, with 1 – Measurement Setup, 2 – Rigid Frame, 3 – Robot, 4 – Pedestal, 5 – Base Plate, 6 – Adapter Plate, 7 – Guide Rail, 8 – Rail Carrier, 9 – Holding Construction, 10 – Adapter Plate for Measurement Device and Locating Bolt, 11 – Measurement Device and 12 – Weight Plates

Since ISO/TS 15066 [108] states a hand mass of $m = 0.6 \text{ kg}$, additional weight plates are not required for this experiment because the whole setup already weighs 3.8 kg, which can be considered reality mismatching. Please note that a setup design at 0.6 kg is not realistic due to the own weight of the measurement device and required stability to ensure replicable results. In future research, a conversion factor must be determined to deduce more

realistic measurement results. To match the characteristics of the back of the hand non-dominant side (ND), a spring with $k = 75 \text{ N/mm}$, black silicone damping material with shore A 70 hardness, and a thickness of 7 mm is used. For realistic collision simulation with a workpiece, the maximum payload steel shaft from the quasi-static measurements is used that matches the length and mass characteristics ($d = 110 \text{ mm}$, $l = 230 \text{ mm}$, $m = 6.041 \text{ kg}$) of an industrial gripper with a small chuck part. As collision cases, two different realistic scenarios have been derived from the beforementioned motion sequence:

- 1) plane contact with a round surface and
- 2) edge contact.

Since diameters from 110 mm to 20 mm are considered for case 1, the worst-case scenario with $d = 20 \text{ mm}$ is used for this study. Due to the low contact area of this diameter, the most critical pressure is expected for this case. In the second case, the robot was tilted by 45° while maintaining the same collision position. A granularity of 1 mm/s is used for the plane contact since force is expected to be the dominant metric. However, for the edge contact, the scaling has been increased to 10 mm/s because it is expected that the pressure is the dominant criterion. Due to the high measurement efforts of scanning the sensitive foils, this limitation is set for effectiveness reasons. Furthermore, the same sensor settings were used as for case 1. The experimental specifications for case 2 are summarized in Table 3.4.

Table 3.4: Experiment Specifications for Case 2 – Transient Contact with Hand

Category	General Criteria	Criteria	Criteria characteristics
Machine (Robot)	Sensor sensitivity	Low, middle, high	140 N, 130 N, 100 N, 50 N
Method	Measured feature	Individual for the measurements	-
	Collision case	Transient	-
	Contact case	Frontal, lateral (edge)	-
(Hu)Man	Body region	Hand and fingers non-dominant side (ND)	380 N/cm ² pressure, 280 N force
Measurement	Damping material K1	-	Shore A 70
	Spring K2	k	75 N/mm
	Thickness	-	7 mm
	Result resolution	Speed adjustment interval	1 mm/s (frontal), 10 mm/s (lateral)
Material (Workpiece)	Measured feature	Diameter d	20 mm
		Length l	230 mm
		Material	Steel
		Mass m	6.041 kg

3.7.4 Case 3: Transient Contact with Shoulder

In this subsection, the transient collision case with the shoulder is emphasized. The respective results of this subsection and of “4.5.4 Case 3: Transient Contact with Shoulder” were published by [254]. For realistic reproduction of the described contact case, a particular design is required that guarantees free oscillation and is adjustable in weight to match the

shoulder mass properties of 40 kg (see Figure 3.21). As mentioned in the previous subchapter, transient cases must be measured with a fixed load cell installation. Even though the described guide rail offers the possibility of adding weight plates to simulate different body regions, feasibility problems occur when considering the upper body. Firstly, suitable weight plates usually have a big diameter, making attaching them to the locating bolt difficult. Secondly, the one-sided loading of the setup tilts the holding construction, leading to the jamming of the adapter plate with the rail. Lastly, enormous friction negatively influences the measurement result and impedes comparability to measurements with lighter body regions, e.g., the hand. Consequently, this subsection presents a suitable measurement setup that picks up the described challenges to contribute to developing a proper measurement procedure in the future.

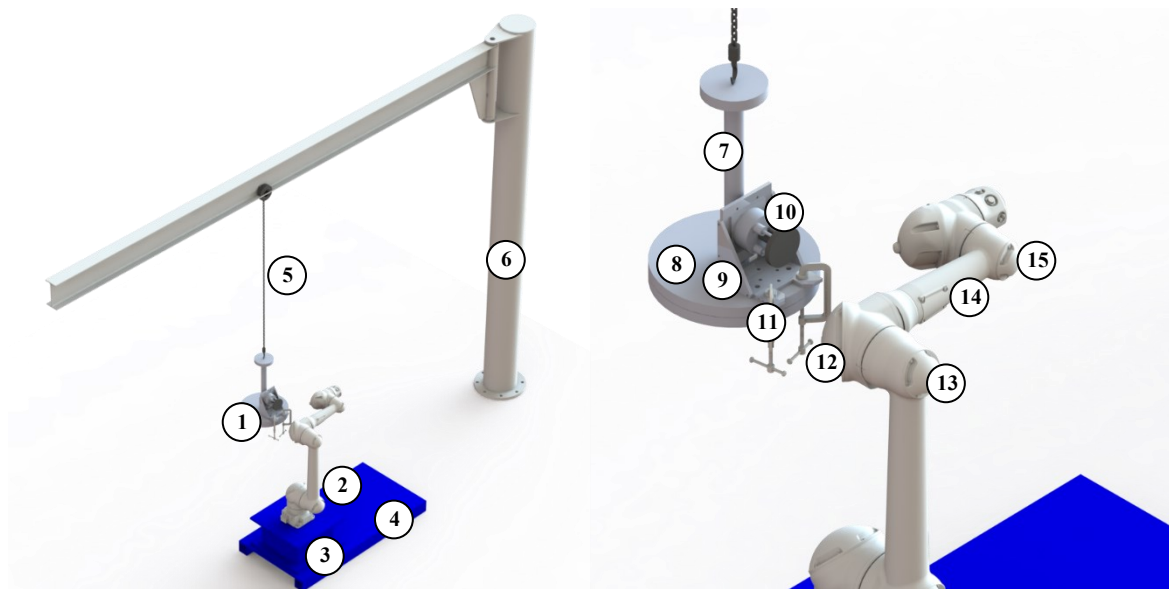


Figure 3.21: Measurement Setup for Case 3 - Transient Contact with Shoulder, with 1 – Measurement Setup, 2 – Robot, 3 – Pedestal, 4 – Base Plate, 5 – Chain with Hook, 6 – Crane, 7 – Locating Bolt, 8 – Weight Plates, 9 – Holding Construction, 10 – Measurement Device, 11 – Screw Clamp, 12 – Elbow Big Cap, 13 – Elbow Small Cap, 14 – Forearm and 15 – Wrist Cap

Therefore, a large locating bolt with a thread was used to install different weight plates with a screw nut. This unit was connected to a 0.5 t crane steel tracks, minimizing friction and providing a sufficiently long pendulum. On top of the plates, the measurement device has been fixed using screw clamps. The pedestal crane combination has been adjusted to simulate a realistic shoulder height of 1,450 mm. Ropes were attached to the device to guide the recoil movement and maintain a certain rebound angle for reproducible results.

Four different robot outer contours have been tested regarding collision forces and pressures: the two elbow caps, the forearm, and the wrist cap of the cobot (see Figure 3.21). This setup was designed to deliver insights on worst-case scenarios where one of the robot's least favorable edges collides with the measurement device. While the hard edge has been used for tests with the big elbow cap, this type of collision was not reproducible for the smaller caps since the cap radius does not allow a collision with the cap edge. Instead, contacts with the round outer contour of the small caps were targeted. Therefore, the big elbow cap delivers a smaller contact area than the small caps. It is expected that the pressure distribution is critical for this contact area. To counterbalance the effect on the pressure results and to provide a solution for *MACS* optimization, different protective measures have been added: no protection, neoprene padding (thickness: 5 mm), and foam padding (expanded polyethylene foam profile, thickness: 140 mm). For comprehensibility, this padding was also used for all considered robot contact areas. While the neoprene protection was attached with a velcro fastener, the foam protection had to be attached with adhesive tape. Using these three different paddings, the impact of the damping characteristics regarding material and thickness on the *MACS* is analyzed.

As can be seen in Figure 3.13, different movement types are assigned to the respective contact areas. While tests with the big elbow cap utilize mainly the 2nd robot axis for linear movement execution, the other cases predominantly use the 1st axis. When having a closer look at the big elbow cap, a hard edge can be seen. To match the biomechanical shoulder conditions, a spring constant of $k = 35 \text{ N/mm}$, blue silicone damping material with shore A 30 hardness, and a thickness of 14 mm was used. For worst-case scenario consideration, the same workpiece as described in case 2 was used. Due to the high time consumption of the pressure measurements, a velocity scaling of 10 mm/s was used. As force limits, 100 N and 50 N were considered. Table 3.5 summarizes the experimental specifications for case 3.

Table 3.5: Experiment Specifications for Case 3 – Transient Contact with Hand

Category	General Criteria	Criteria	Criteria characteristics
Machine (Robot)	Sensor sensitivity	Middle, high	100 N, 50 N
Method	Measured feature	Individual for the measurements	-
	Collision case	Transient	-
	Contact case	Robot collision geometry	Elbow big cap, elbow small cap, forearm, wrist cap
(Hu)Man	Body region	Shoulder	320 N/cm ² pressure, 420 N force
Measurement	Damping material K1	-	Shore A 30
	Spring K2	k	35 N/mm
	Thickness	-	14 mm
	Result resolution	Speed adjustment interval	10 mm/s
Material (Workpiece)	Additional protective measure	Padding	None, neoprene, foam
	Attached workpiece	Diameter d	20 mm
		Length l	230 mm
		Material	Steel
		Mass m	6.041 kg

3.8 Synthesis – Solution Approach

This section dealt with presenting a solution approach to simultaneously plan fenceless machine tending systems with both industrial and collaborative robots. Firstly, the research gap has been clearly defined by reviewing the state of the art and research and the latest planning methodologies. It can be stated that a comprehensive method is lacking for the preliminary economic evaluation of lathe machine tending systems with collaborative and industrial robots that enables the planner to approximate the economic and technical feasibility of both alternatives. Hence, the optimal robot technology cannot be selected in advance, leading to incorrect utilization of the available HRI methods. Important planning information is obtained at a well-progressed project stage, forcing the end-user to add additional partial fencing to the collaborative work cell to guarantee profitability. Single solution modules were presented to break this complex problem down, derived from observing the classical planning procedure. With a reverse engineering approach, planning contents were rearranged to allow front loading of the required planning to the project beginning. Since this method is intended for the early rough planning phase, approximation models are pursued, providing sufficient accuracy while guaranteeing low complexity and ease of use. As an information base, the use case has been delineated by deriving a general process pipeline.

For further specification, the planning focus has been defined to make the stated complexity manageable. By reviewing the four modes of collaboration and its combinatorics, the technical options “Collaborative Robot in Exclusive PFL Operation” (CR, PFL), “Collaborative Robot in Hybrid Mode” (CR, HM), and “Industrial Robot” (IR)

were defined. After illustrating this abstract picture, the single modules were further specified regarding the considered influencing factors and the modeling procedure. As a result, the following overall planning methodology can be concluded, illustrated in Figure 3.22. It shows the entire context and the interrelations of the modules to each other, leading to a comprehensive decision tree to determine the optimal robot technology.

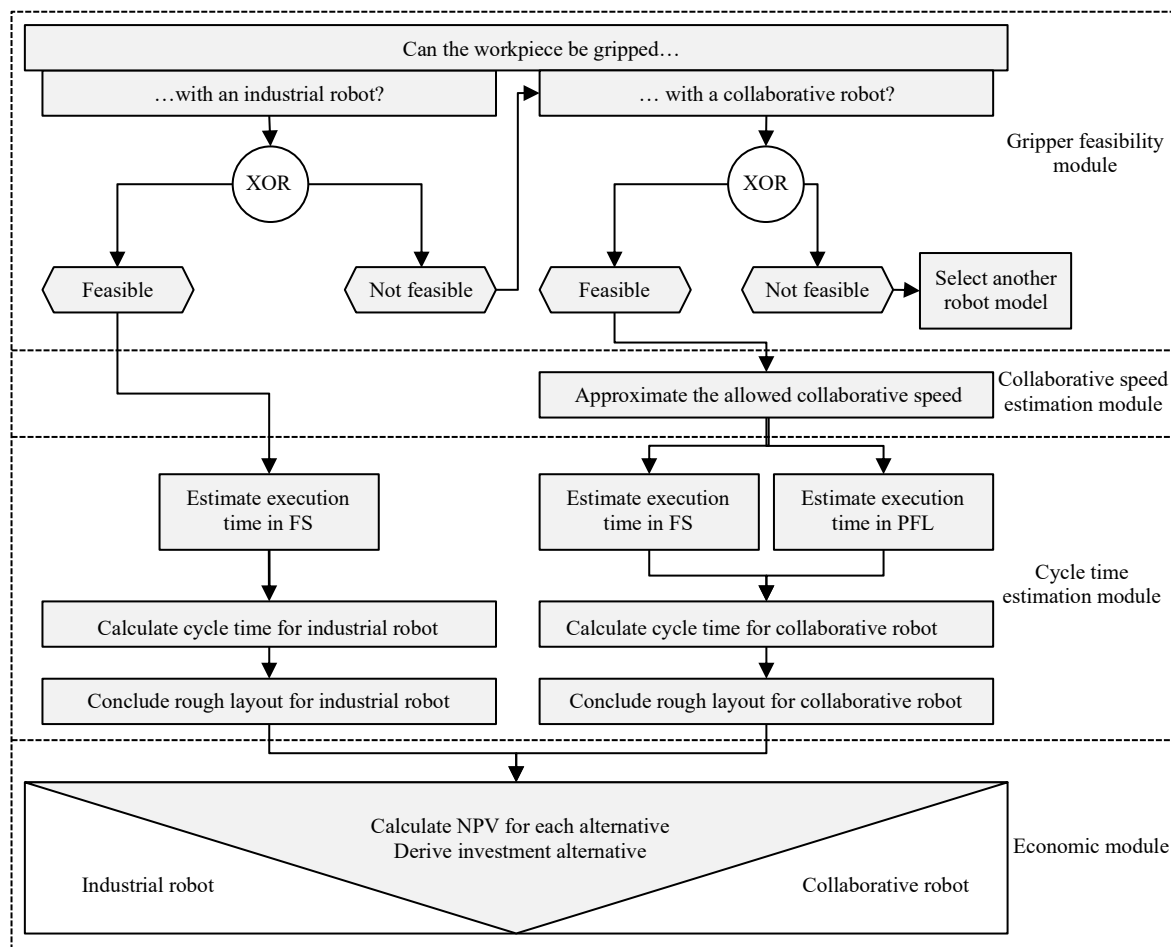


Figure 3.22: Overall Presented Approach and Interrelations of the Single Modules

In this section, RQ 2 has been further answered regarding the available technical alternatives for HRI. Hypotheses about the main technical influencing factors on the economic feasibility were stated by analyzing the economic structure of an automation project and refining these factors regarding their consistency. These factors will be specified and modeled with suitable measurement and determination tools in the following chapters, as presented in the single modules. In the practical validation, the overall context between considered alternatives, net present value, and interaction grade will be clarified. Consequently, this RQ is still not answered thoroughly. To answer the third research

question (RQ 3), currently available and accepted methods have been presented to determine the mentioned influencing factors. Furthermore, several modules were presented that demonstrate respective modeling procedures to frontload the individual planning information. In the following chapters, the specific execution of these procedures will be explained with exemplary practical results for the considered robot models and grippers. In the validation section of this doctoral thesis, the practical applicability of these modules will be tested and demonstrated at an actual customer project. As a result, this RQ is still insufficiently dealt with. The fourth research question (RQ 4) has been partially answered by proposing an overall planning approach, as shown in Figure 3.1 and Figure 3.22. Reverse engineering has been chosen as a suitable method to frontload all information under the utilization of approximation models. By merging the single modules, an overall planning and decision process has been derived, which will be further specified in the following chapter and practically tested in the validation section. Hence, this research question is partially answered and will be further refined. The last research question (RQ 5) cannot be answered yet. At this point of the doctoral thesis, the single influencing factors are neither modeled nor brought into economic relation to each other. In the next chapter, when the modules are specified, a glance at the required circumstances will be given. A final statement is going to be made when considering the practical customer project as an example. Therefore, this research question has not been considered yet.

4. Module Development

4.1 Economic Module – Module Development

4.1.1 General Approach

Based on the deduction procedure illustrated in Figure 3.6, this subchapter deals with the actual development of the economic calculation scheme. For evaluation of the single alternatives, the process times P [h] of each process module p must be gathered, which can be executed either manually (M), on the lathe (L), with an industrial robot in full-speed (IR, FS) or with a cobot in full-speed (CR, FS) or collaborative speed (CR, CS). This leads to the following variables: $P_{P,M}$, $P_{P,L}$, $P_{P,IR,FS}$, $P_{P,CR,FS}$ and $P_{P,CR,CS}$. For better understanding, the execution time calculation in the manual state is demonstrated first. Then, the economic calculation structure for the three automation alternatives is developed.

4.1.2 Calculation Scheme for Manual Operation

At first, the production order is cut down to single batches B_n , which includes a specific number of workpieces per batch n : the batch size S_n [workpieces]. Before a batch can be produced in the loop phase (LOOP), the framing preparation (PREP) and initialization (INIT) phase take place before and after. The sum of all three steps delivers the execution time.

$$ET_{PREP,Bn,M} = \sum_{p=1}^2 P_{p,M} \quad (4.1)$$

$$ET_{INIT,Bn,M} = 2 * \sum_{p=4}^5 P_{p,M} + 2 * P_{6,L} \quad (4.2)$$

$$ET_{LOOP,Bn,M} = 2 * P_{6,L} + P_{4,M} + P_{7,M} \quad (4.3)$$

$$ET_{Bn,M} = ET_{PREP,Bn,M} + ET_{INIT,Bn,M} + ((ET_{LOOP,Bn,M} + P_{8,L}) * S_n) \quad (4.4)$$

After calculating the execution times for one batch, the total number of produced batches N can be concluded. The available annual working time W implies the plain working time, while breaks are taken additionally.

$$N_M = \frac{W}{ET_{Bn,M}}, N_M \in \mathbb{N} * \quad (4.5)$$

The available rest capacity R equals the time that is left over after subtracting the execution times of all produced batches ET_N .

$$R_M = W - N_M * ET_{Bn,M} \quad (4.6)$$

Within this remaining time R , a batch share can be completed in the loop phase. Therefore, the PREP and INIT phase need to be executed first. The leftover capacity can be used to process a specific output O_R . Based on the result, either no or one batch share N_+ can be produced.

$$O_{R,M} = \frac{R_M - (ET_{PREP,Bn,M} + ET_{INIT,Bn,M})}{(ET_{LOOP,Bn,M} + P_{8,L})}, O_{R,M} \in \mathbb{N} \rightarrow N_{+,M} \{0; 1\} \quad (4.7)$$

By adding up the batch sizes S_n of the single batches B_n with the remaining batch share O_R , the total annual output O_A is calculated.

$$O_{A,M} = S_n \cdot N_M + O_{R,M} \quad (4.8)$$

As a calculation base for the *LRG*, the manual annual execution time *AET* is calculated, delivering the operator's temporal binding to the machine. In the manual state, this factor is quite high since all operations are executed by hand. Only during the machine's processing time, the operator is relieved.

$$AET_M = (ET_{PREP,Bn,M} + ET_{INIT,Bn,M}) \cdot (N_M + N_{+,M}) + ET_{LOOP,Bn,M} \cdot (S_n \cdot N_M + O_{R,M}) \quad (4.9)$$

4.1.3 Calculation Scheme for Collaborative Robots

For calculations of the robotized execution times, mixed operations at different speed levels must be considered. To cover the time slice, in which the operator stays within the robot's working space for potential interaction, the human-robot interaction grade α is used with $0 \leq \alpha < 1$. For simplification, it is assumed that the operator stays either out of the robot's operating space (white area) or within (red or green area). Passing through the safety zones in between (yellow area) and the associated speed reduction in terms of SSM is not considered. Zone penetration events are either planned activities (e.g., setup, programming) or unplanned ones (e.g., troubleshooting, in-process workpiece measurements). The behavior of this factor and its influence on the robot's performance depends on the used technology and assumed consideration period. A linear interaction-speed relation is noted for cobots because the robot gradually decreases from full to collaborative speed. Hence, the execution times of both modes are set in ratio to each other for mixed operation calculations. The following equations demonstrate the same procedure as for the manual operation by incorporating the interaction grade and the different operating modes.

$$ET_{PREP,Bn,CR} = \sum_{p=1}^3 P_{p,CR} \quad (4.10)$$

$$ET_{INIT,Bn,CR,\alpha*} = 2 * P_{6,L} \quad (4.11)$$

$$ET_{INIT,Bn,CR,\alpha,FS} = 2 * \sum_{p=4}^5 P_{p,CR,FS} \quad (4.12)$$

$$ET_{INIT,Bn,CR,\alpha,CS} = 2 * \sum_{p=4}^5 P_{p,CR,CS} \quad (4.13)$$

$$ET_{INIT,Bn,CR} = ET_{INIT,Bn,CR,\alpha*} + ET_{INIT,Bn,CR,\alpha,FS} \cdot (1 - \alpha) + ET_{INIT,Bn,CR,\alpha,CS} \cdot \alpha \quad (4.14)$$

$$ET_{LOOP,Bn,CR,\alpha*} = 2 * P_{6,L} \quad (4.15)$$

$$ET_{LOOP,Bn,CR,\alpha,FS} = P_{4,CR,FS} + P_{7,CR,FS} \quad (4.16)$$

$$ET_{LOOP,Bn,CR,\alpha,CS} = P_{4,CR,CS} + P_{7,CR,CS} \quad (4.17)$$

$$ET_{LOOP,Bn,CR} = ET_{LOOP,Bn,CR,\alpha*} + ET_{LOOP,Bn,CR,\alpha,FS} \cdot (1 - \alpha) + ET_{LOOP,Bn,CR,\alpha,CS} \cdot \alpha \quad (4.18)$$

$$ET_{Bn,CR} = ET_{PREP,Bn,CR} + ET_{INIT,Bn,CR} + ((ET_{LOOP,Bn,CR} + P_{8,L}) \cdot S_n) \quad (4.19)$$

$$N_{CR} = \frac{W}{ET_{Bn,CR}}, N_{CR} \in \mathbb{N} * \quad (4.20)$$

$$R_{CR} = W - N_{CR} \cdot ET_{Bn,CR} \quad (4.21)$$

$$O_{R,CR} = \frac{R_{CR} - (ET_{PREP,Bn,CR} + ET_{INIT,Bn,CR})}{(ET_{LOOP,Bn,CR} + P_{8,L})}, O_{R,CR} \in \mathbb{N} \rightarrow N_{+,CR} \{0; 1\} \quad (4.22)$$

$$O_{A,CR} = S_n \cdot N_{CR} + O_{R,CR} \quad (4.23)$$

For cash-in flow observation, the annual output deviation between the automated and the manual execution as well as the labor release grade is used.

$$\Delta O_{A,CR,M} = O_{A,CR} - O_{A,M} \quad (4.24)$$

$$AET_{CR} = ET_{PREP,Bn,CR} \cdot (N_{CR} + N_{+,CR}) \quad (4.25)$$

$$LRG_{CR} = 1 - \frac{AET_{CR}}{AET_M} \quad (4.26)$$

Finally, the *CIF* is calculated comprehensively by multiplying the *LRG* with the annual labor cost *C* on the one side and the ΔO_A with the value creation per workpiece *VC* [€] on the other.

$$CIF(t)_{CR} = LRG_{CR} \cdot C + \Delta O_{A,CR,M} \cdot VC \quad (4.27)$$

Lastly, the *CIF* and I_0 values for each automation alternative are inserted into the *NPV* equation.

$$NPV_{CR} = -I_{0,CR} + \sum_{t=0}^T CIF_{CR}(t) \cdot q^{-t} \quad (4.28)$$

When using the collaborative robot in exclusive PFL operation, the calculations can be strongly simplified since the allocation of the α -affected ET s can be neglected. Hence, the same calculations can be used by cutting out the allocations.

4.1.4 Calculation Scheme for Industrial Robots

Industrial robots, on the other side, stop in the event of safety zone violation. As a counterpart for the execution time in 100 % full speed, the actual value in a 100 % stop situation cannot be calculated, which impedes time estimation in mixed operation. Theoretically, the order would never be completed in the 100 % stop scenario and the execution time converges to infinity with the expression:

$$P_{p,IR} = \frac{P_{p,IR,FS}}{1-\alpha} \quad (4.29)$$

Example calculations verify this exponential behavior. Due to the increasing share of stopping periods, the robot must subsequently compensate. Therefore, the entire operating time (e.g., one year) is assumed, in which stopping events occur irregularly and need to be compensated for finishing the batch. When considering a short period of time (e.g., one shift) with regular stopping times (planned activities), the expected waiting times of the next cycle are not included. Instead, the execution time results from adding the unproductive time slice to the theoretical ideal execution time at full speed:

$$P_{p,IR} = P_{p,IR,FS} \cdot (1 + \alpha) \quad (4.30)$$

However, this calculation is theoretically correct and an idealistic assumption, which is not transferrable to the unpredictable circumstances of production. Therefore, (4.29) is used for the further procedure.

$$ET_{PREP,Bn,IR} = \sum_{p=1}^3 P_{p,IR} \quad (4.31)$$

$$ET_{INIT,Bn,IR,\alpha*} = 2 * P_{6,L} \quad (4.32)$$

$$ET_{INIT,Bn,IR,\alpha,FS} = 2 * \sum_{p=4}^5 P_{p,IR,FS} \quad (4.33)$$

$$ET_{INIT,Bn,IR} = ET_{INIT,Bn,IR,\alpha*} + \frac{ET_{INIT,Bn,IR,\alpha,FS}}{(1-\alpha)} \quad (4.34)$$

$$ET_{LOOP,Bn,IR,\alpha*} = 2 * P_{6,L} \quad (4.35)$$

$$ET_{LOOP,Bn,IR,\alpha,FS} = P_{4,IR,FS} + P_{7,IR,FS} \quad (4.36)$$

$$ET_{LOOP,Bn,IR} = ET_{LOOP,Bn,IR,\alpha*} + \frac{ET_{LOOP,Bn,IR,\alpha,FS}}{(1-\alpha)} \quad (4.37)$$

$$ET_{Bn,IR} = ET_{PREP,Bn,IR} + ET_{INIT,Bn,IR} + (ET_{LOOP,Bn,IR} + P_{8,L}) \cdot S_n \quad (4.38)$$

$$N_{IR} = \frac{W}{ET_{Bn,IR}}, N_{IR} \in \mathbb{N} * \quad (4.39)$$

$$R_{IR} = W - N_{IR} \cdot ET_{Bn,IR} \quad (4.40)$$

$$O_{R,IR} = \frac{R_{IR} - (ET_{PREP,Bn,IR} + ET_{INIT,Bn,IR})}{(ET_{LOOP,Bn,IR} + P_{8,L})}, O_{R,IR} \in \mathbb{N} \rightarrow N_{+,IR} \{0; 1\} \quad (4.41)$$

$$O_{A,IR} = S_n \cdot N_{IR} + O_{R,IR} \quad (4.42)$$

$$\Delta O_{A,IR,M} = O_{A,IR} - O_{A,M} \quad (4.43)$$

$$AET_{IR} = ET_{PREP,Bn,IR} \cdot (N_{IR} + N_{+,IR}) \quad (4.44)$$

$$LRG_{IR} = 1 - \frac{AET_{IR}}{AET_M} \quad (4.45)$$

$$CIF(t)_{IR} = LRG_{IR} \cdot C + \Delta O_{A,IR,M} \cdot VC \quad (4.46)$$

$$NPV_{IR} = -I_{0,IR} + \sum_{t=0}^T CIF_{IR}(t) \cdot q^{-t} \quad (4.47)$$

As a result, three net present values were calculated, one for each automation alternative. For decision assistance, these variants are compared to each other to conclude relative advantageousness.

$$NPV_{IR} > NPV_{CR}: \text{Industrial Robot preferable} \quad (4.48)$$

$$NPV_{IR} < NPV_{CR}: \text{Collaborative Robot preferable} \quad (4.49)$$

4.2 Gripper Feasibility Module – Module Development

As gripper representatives, the collaborative gripper OnRobot 3FG15 combined with the dual flange gripper and the flange model H and the industrial gripper Schunk PZN-plus 100-1-SD were used. The model selection is based on the premise that the gripper should match the robot's protection class IP67 since coolant fluids characterize the operating environment. For collaborative robots, the OnRobot is one of a few merchantable models. The particular gripping strategy allows only gripping chuck workpieces from the top, touching the shell surface. For comparison, an industrial gripper with IP67 protection and with similar mass properties was selected. For correct mass properties, the respective information documented in the manual was used. While the OnRobot mass information is only available, including the delivered standard jaws, Schunk provides this information only without jaws since the jaw design is usually customized for the individual use case. Consequently, two different information bases were used, leading to an accuracy error of the results. Due to the low share

of the jaws on the considered overall system weight, this error is acceptable for rough planning. As a simulation result, the following diagram (Figure 4.1) has been derived, illustrating the feasible workpiece diameter-length combinations for the collaborative (CR) and the industrial robot (IR) for steel, aluminum, and polyoxymethylene (POM).

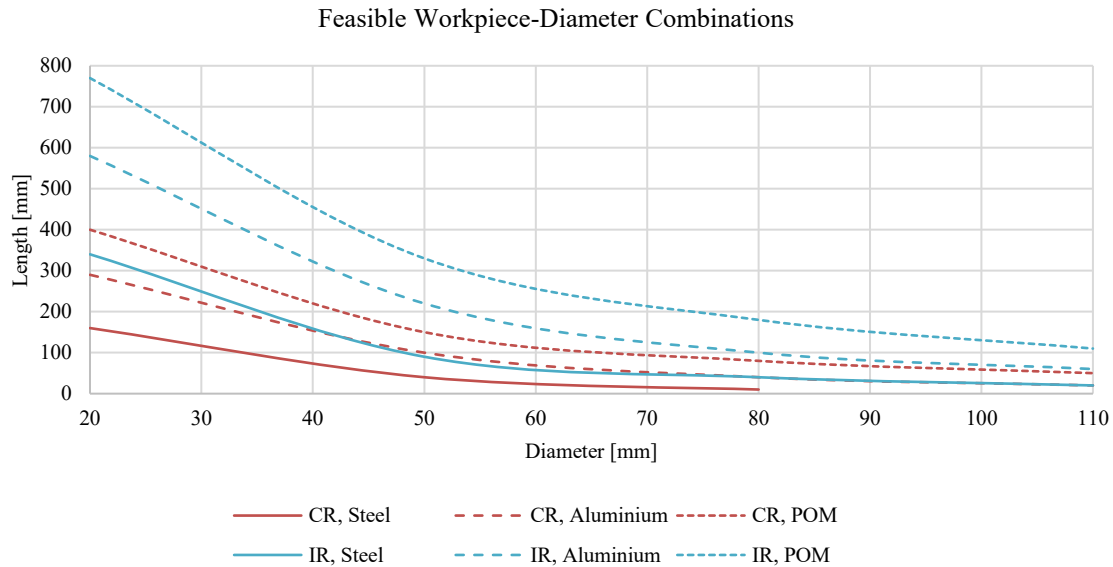


Figure 4.1: Feasible Workpiece Diameter-Length Combinations for Collaborative (CR) and Industrial (IR) Robots and Different Materials

It can be clearly seen that all curves decrease exponentially. Since the industrial robot has 2 kg more in payload and a significantly higher weight with increased stiffness, higher diameter-length combinations are achievable compared to the collaborative robot. Due to the high density of steel, comparatively lower payload, and lightweight cobot design, a maximum of 80 mm diameter can be achieved for CR. This approach illustrates that a significant database of robot payload utilization studies facilitates the feasibility check by providing an overview diagram, as it is often used in factory planning. The derived curves can serve as a first overview to assess an automation project's technical feasibility and dig further into the fine gripper planning. Computability of the results can be given under the utilization of regression equations for each curve.

4.3 Rough Layout Discretization Module – Module Development

4.3.1 General Approach

The dimensional character of 34 DMG MORI machines has been analyzed as an information base, illustrated in boxplot diagrams in Appendix 9. Based on this analysis of machine

dimensions, a general arrangement pattern was abstracted, covering a broad range of machines and enabling the planner to describe the use-case-specific machine. At first, all positions (doors-red and yellow, main and counter spindle-dark blue and green, maximum turning length-turquoise) for each machine were three-dimensionally generated in CAD, referring to the left side and the front of the machine. Secondly, the single models are layered and transferred to one mutual model using the x-y coordinate of the left door (red sphere) as zeroing point, illustrated in Figure 4.2 from an isometric perspective.

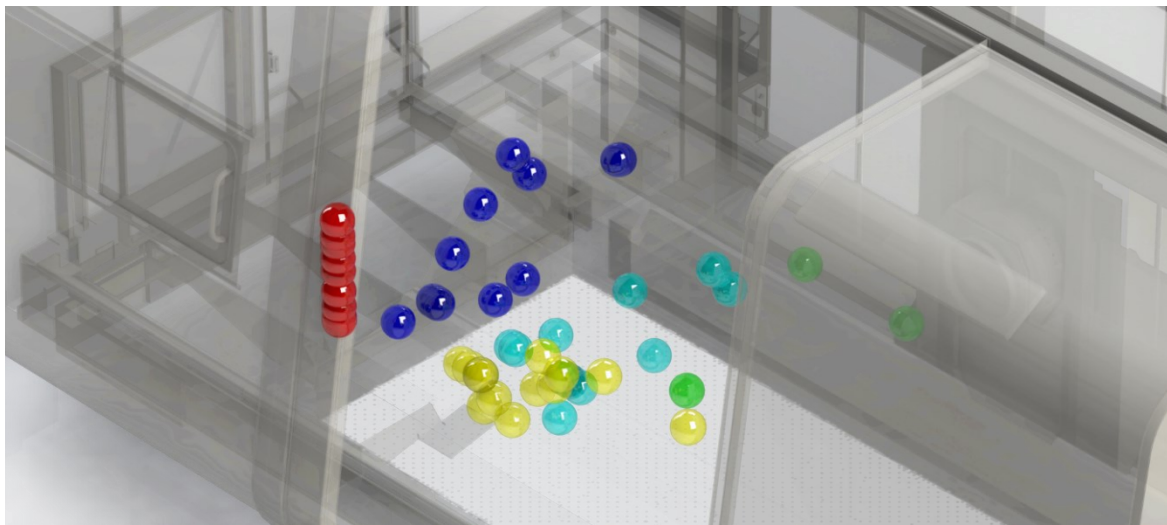


Figure 4.2: 3-dimensional Representation of Relevant Machine Coordinates (Door Closed and Open – Red and Yellow, Main Spindle – Dark Blue, Counter Spindle – Green, Maximum Turning Length – Turquoise)

4.3.2 Two-Dimensional Layout Pattern

With a 200 mm x 200 mm pattern, the single positions were discretized in a two-dimensional plane, as enclosed in Appendix 10. Between the first and second positioning patterns, a distance of 150 mm is added. In a reachability study, the robot installation possibilities were varied to identify feasible positions to access the main spindle. Based on these positions, accessible material was concluded. Further 400 mm x 400 mm fields were added in front and left of the machine to cover both entities. The first line directly in front of the machine is spared since this space provides accessibility to the operator for setup activities. By averaging the heights of the collected positions, a door height of 1,300 mm and a spindle height of 1,100 mm have been calculated. Therefore, both entities were positioned at a z-value of 1,100 mm, since the spindle position determines the spindle feed and door position as described before. Since collision-free and short trajectories are pursued, motions in one plane are used. As the installation height of the robot, a merchantable pedestal of 900 mm is

used. This model has been chosen to grant a preferably horizontal robot operation of the spindle to optimize accessibility while ensuring an ergonomic height for direct teaching. Furthermore, the material depots should be reached easily by the robot and operator. According to [255], lightweight materials should be provided at a height between 400 mm to 600 mm and 1,100 mm to 1,400 mm, while heavy parts should be available in between both intervals. On average, an ergonomic height of 1,125 mm is recommended. To transfer these considerations to the presented models, possible workpiece cases must be observed theoretically first. As demonstrated in “4.2 Gripper Feasibility Module – Module Development”, the available workpiece length range is relatively high. All workpiece length possibilities at each material deposit height would be required to cover these cases comprehensively in the simulations. Due to the combinatory complexity, simplifying assumptions take place. Fundamentally, there are two variables to manage this problem: robot and material provision. Either the robot program is changed each time a new workpiece length is used, which leads to tremendous program adaption effort, or flexible material systems are used that are adjustable in height. For this research, the second option is chosen for simplification reasons, explained as follows. To provide sufficient space between material feed and material position, a linear movement length of 200 mm is set. A high z-value for the feed position is set to 1,500 mm to consider different workpiece lengths, providing a maximum deposit height of 1,300 mm by subtracting the feed motion (assuming a workpiece length of 0). By this, different workpieces can be positioned at an ergonomic height, e.g., 200 mm long chucks at the height of 1,100 mm and 900 mm long ones at 400 mm. Based on these assumptions, one MFM motion is used for the simulations, moving from 1,500 mm to 1,300 mm in height. Consequently, the material positions are modeled with these two z-values in the CAD representation. In Figure 4.3, the two-dimensional representation of the described pattern is illustrated, while Figure 4.4 shows the transfer to the CAD system in 3D.

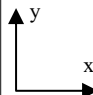
							a	b	c	d	e	f	g	h								
							0	0	100	300	500	700	900	900				1100	1100	1300	1300	1500
40	1050						a40	b40	c40	d40	e40	f40	g40				1050					
30	850						a30	b30	c30	d30	e30	f30	g30				850					
	850																850					
20	650						a20	b20	c20	d20	e20	f20	g20				650					
	650																650					
10	450	a10	b10	c10	d10	e10	f10	g10	450													
	450								450													
	250								250													
00	0								b00	c00	d00	e00	f00	g00	h00		0	00				
	0																0					
01	-100	EE01	DD01	CC01	BB01	AA01											-100	01				
											-400											
02	-400	EE02	DD02	CC02	BB02	AA02	A02	B02	C02	D02	E02	-400	02									
	-800											-800										
03	-800	EE03	DD03	CC03	BB03	AA03	A03	B03	C03	D03	E03	-800	03									
	-1200											-1200										
04	-1200	EE04	DD04	CC04	BB04	AA04	A04	B04	C04	D04	E04	-1200	04									
	-1600											-1600										
05	-1200	EE05	DD05	CC05	BB05	AA05	A05	B05	C05	D05	E05	-1200	05									
	-2000											-2000										
	-2000	-1600	-1600	-1200	-1200	-800	-800	-400	-400	0	0	400	400	800	800	1200	1200	1600	1600	2000		
	EE	DD	CC	BB	AA	A	B	C	D	E												

Figure 4.3: Discretized 2D General Layout Pattern

4.3.3 Three-Dimensional Layout Pattern

Figure 4.4 shows the transfer of the beforementioned pattern into a 3D representation with an example. The machine space is limited on both sides with beams, representing the maximum door opening width and serving for reachability studies in terms of collision detection. Inside the machine, the single fields are modeled with black cuboids arranged on a cylinder positioned at the average height of the main spindle. While the cuboids serve as an end stop, the cylindric geometry facilitates the exact positioning of the robot within the simulation model. A position is reached when the footprint of the gripper (without fingers) touches the cuboid. In this way, a finger-independent representation is guaranteed since jaw design is use case-individual.

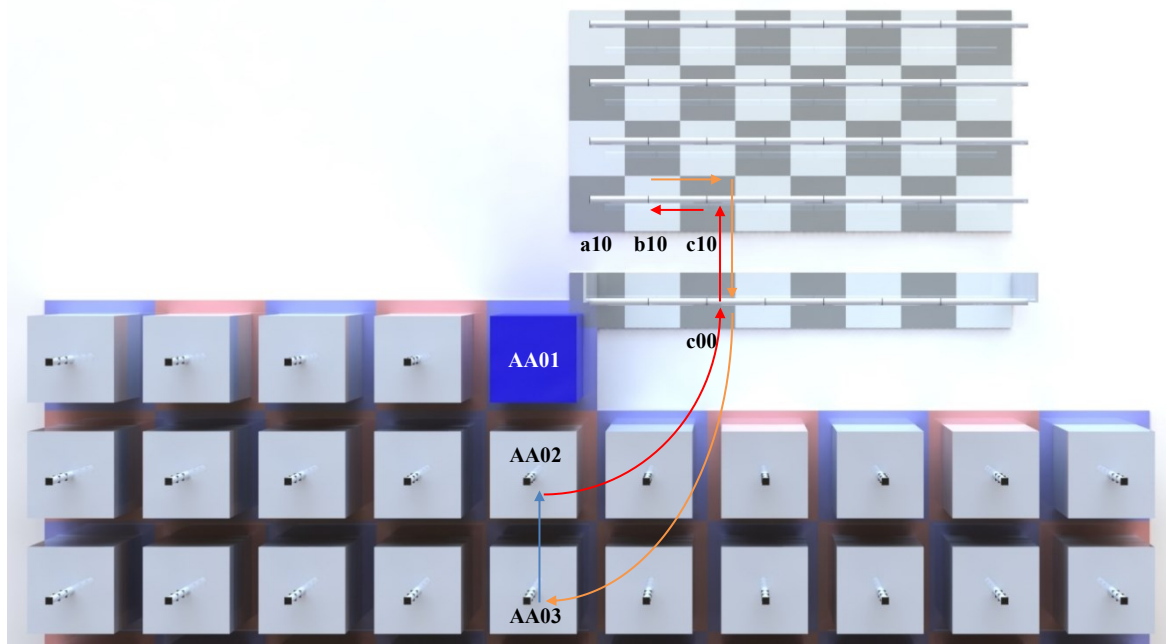


Figure 4.4: 3D Representation of the Layout Pattern and Application Example

For a better understanding, an application example is given. It is assumed that the main spindle is located within the a10 field and that the raw material is provided at AA02, and the material deposit for finished parts lies at AA03. The raw and finished workpiece is approximately 200 mm long. At first, a feed motion of one field (200 mm) is required to provide a collision-free trajectory, leading to field b10. Due to the workpiece length of 200 mm, this distance needs to be bridged to the spindle position, leading to c10 as feed position. Hence, the robot moves between the positions c10 and b10 to position the workpiece in a10 (SFS). In order to reach the feed position, the door position c00 is used for linear movement (DSF). As material pick and place movements, the motions between the AA02 and AA03 and c00 are used (MFD). In this example, the robot is positioned at AA01.

4.4 Cycle Time Estimation Module – Module Development

4.4.1 General Approach

In this subchapter, the cycle time estimation module is developed. At first, a reachability study is conducted to determine feasible positions and limit the combinatory complexity. The simulation results for all movements are presented regarding the general velocity-dependent cycle time behavior based on this data. Statistical analysis with nonlinear regression methods is used to provide approximation equations to calculate the respective

cycle time at a particular operating speed. Due to the enormous data amount, the results are explained in detail in the example of the DSF movement because this dataset includes many simulation runs that are well-presentable in one mutual diagram. The same procedure is applied to the other motion types, which are explained briefly.

4.4.2 Reachability Study

In the first step, a reachability study has been executed for the whole machine space, including the door, spindle and spindle feed positions, and material positions. Therefore, both robot models, the cobot (C) and the classic industrial one (I) were tested for both gripping options, top (T) or side (S) gripping. By iterating the robot position, the feasibility of reaching the respective position has been concluded. Table 4.1 shows exemplary results for the door positions; the whole result is documented in Appendix 11.

Table 4.1: Feasible Reachable Door Positions based on Robot Position

		Robot Position						
		AA01	AA02	A02	B02	C02	A03	B03
Door Positions	b00	CT, CS	CT	CT, CS, IT, IS	CT, IT, IS	CT, IT, IS	CS, IT, IS	CS, IT, IS
	c00	CT, CS		CT, CS, IT, IS	CT, CS, IT, IS	CT, IT, IS	IT, IS	CS, IT, IS
	d00	CT, CS		CT, CS, IT, IS	CT, CS, IT, IS	CT, IT, IS	IS	CS, IT, IS
	e00			CS, IT, IS	CT, CS, IT, IS	CT, IT, IS		IT, IS
	f00			IT, IS	CT, CS, IT, IS	CT, IT, IS		IS
	g00				IT, IS	IT, IS		

As it can be seen, the positions A02 to B03 can be used by both robot models with individual reachability possibilities. The main difference lies in the positions AA01 and AA02, which are located on the left side of the machine, which is only accessible with the collaborative robot. The simulation studies show that the position AA01 (left picture series in Figure 4.5) is problematic for the industrial robot in floor installation due to collision with the door, while the kinematic difference of the cobot avoids this problem.

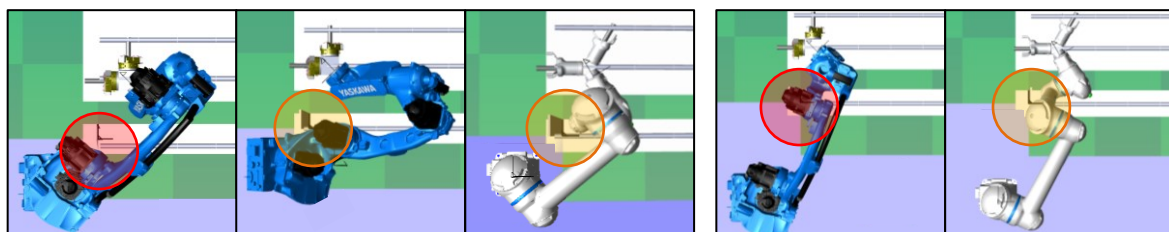


Figure 4.5: Reachability Differences between Collaborative and Industrial Robot (top view)

By tilting the industrial robot by 45° , these collisions can be avoided. For the AA02 position, the same behavior can be registered (right picture series in Figure 4.5). Consequently, industrial robots with similar kinematics should be installed in a tilted way when these positions should be used. In future research, the tilting angle on the cycle time and multi-directional tilting need to be analyzed. When installing the cobot on the AA01 position, material positions in the same row, such as BB01 or CC01, are not feasible since the robot would collide with its 1st axis with the machine.

4.4.3 Simulation Results

For the DSF movements, all possible linear door-spindle feed position combinations were simulated for both gripping strategies (T and S) and robots (CR and IR). The covered distance in the y-direction can cluster the simulation runs, e.g., b00-b10 for one field or d00-d30 for three fields. In Figure 4.6, the velocity-dependent cycle time behavior for both robots for one field is illustrated; Appendix 12 to Appendix 14 summarizes all simulations for one to three field distance.

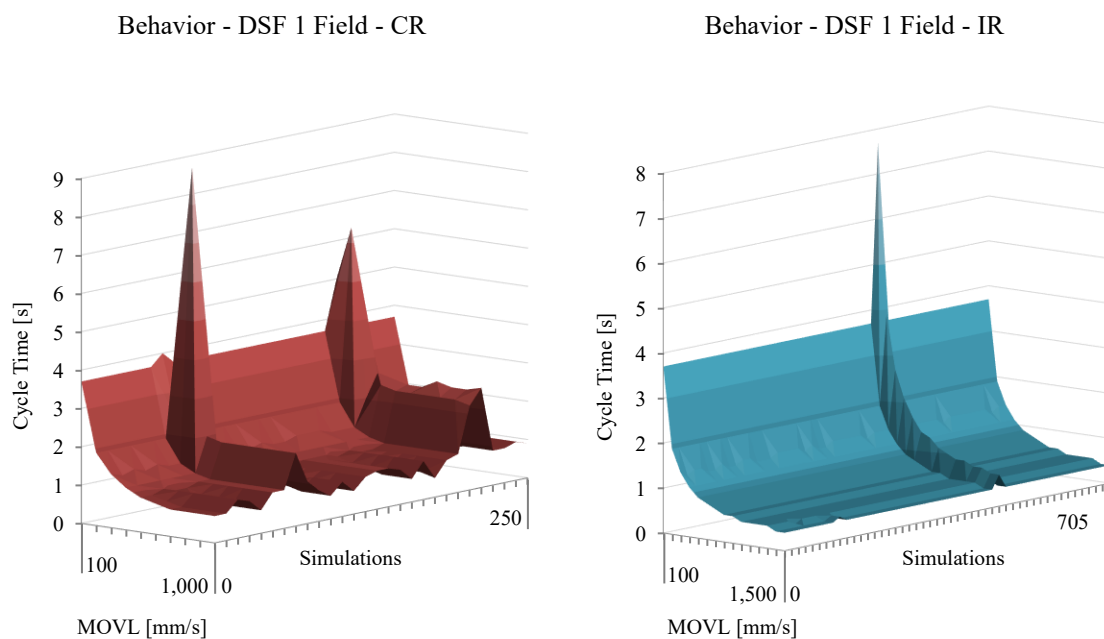


Figure 4.6: Door-Spindle Feed (DSF) Simulation Results for Collaborative (CR) and Industrial Robot (IR) and 1-Field Distance in y-Direction relative to Operating Speed MOVL, Achieved Cycle Time and Simulation Runs

In theory, the cycle time should decrease exponentially with increasing operating speed to a particular value and remain linear at this value. Especially for small distances, the cycle time cannot be further decreased after a certain speed level because the robot already needs

to decelerate before even reaching its maximum speed. This behavior can be validated for the industrial robot. Further, it can be seen that the overall cycle time increases stepwise with a higher field number. Within one movement module, e.g., IR1, the behavior remains consistent with only selected outliers. On the other side, the collaborative robot is much more inconsistent in its behavior, with a higher irregularity and number of outliers. It can be stated that IR is position- and pose-independent, while CR is highly affected by these parameters. When examining this behavior in greater detail, focusing on a specific field coverage is recommended. Therefore, a 1-field movement in the y-direction is presented as representative (see Figure 4.7). When analyzing the collaborative robot outlier behavior, it becomes apparent that the cycle time increases rapidly at different speed levels. The industrial robot shows only one outlier that is consistent in behavior but requires more execution time than the other simulation runs. Those differences regarding position sensitivity can be explained with the kinematic characteristics of both models. Comparing the relations between the single-axis speeds shows that, e.g., the ratio of 4th to 3rd axis speed of the IR is much higher than of the CR (see Table 4.2). Consequently, these kinematic individualities lead to significant differences, depending on which axis is mainly responsible for the movement.

Table 4.2: Axis Speed Differences between Collaborative and Industrial Robot

Speed [%/s] Robot	1 st Axis	2 nd Axis	3 rd Axis	4 th Axis	5 th Axis	6 th Axis
Collaborative	130	130	180	180	250	250
Industrial	260	230	260	470	470	700

For statistical analysis and behavior modeling, these outliers must be excluded. Consequently, the initially presented reachability study must be adjusted by excluding these possibilities likewise. As outliers for this particular movement, b00-b10bA03-S, d00-d10-B03-S, and e00-e10-A02-S were identified for CR, while e00-e10-B02-T must be excluded for IR. The mentioned coding inherent the following parameters and is used throughout this analysis: Start Position – End Position – Robot Position – Gripping Strategy.

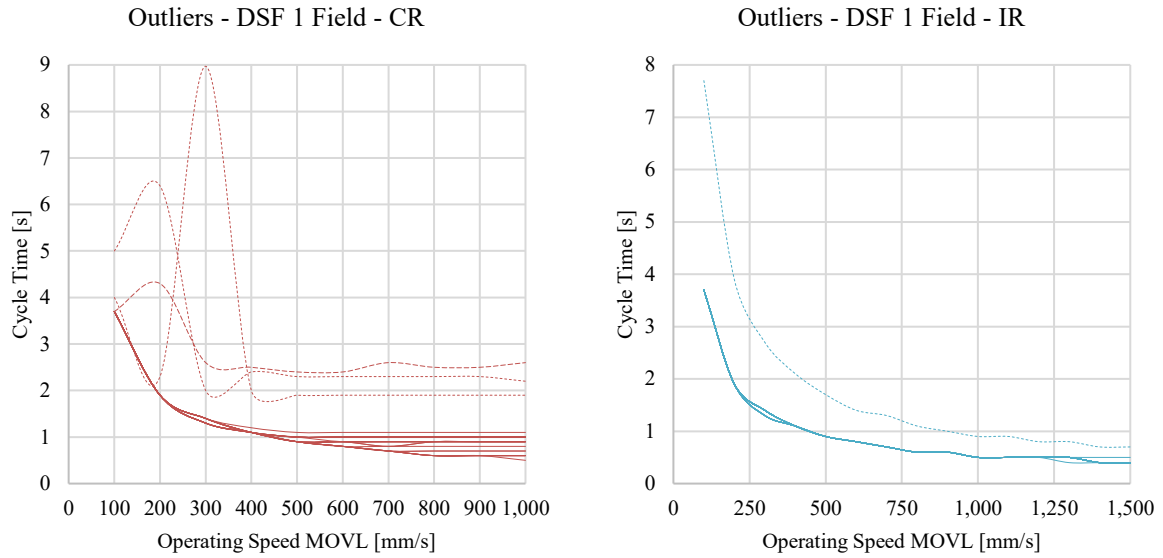


Figure 4.7: Behavior Analysis of all Door-Spindle Feed (DSF) Movement Simulations for 1-Field in y -Direction for both Robots

After adjusting the database, the feasible positions are statistically evaluated to conclude an approximation equation to calculate the achieved cycle times CT based on the utilized robot velocity v [m/s]. Since both graphs decrease exponentially, nonlinear regression is used with the form:

$$CT = n + av + bv^2 + cv^3 + dv^4 + ev^5 + fv^6 \quad (4.50)$$

The following coefficients were determined for the considered case (1-field in y -Direction, DSF movement) (see Table 4.3).

Table 4.3: Nonlinear Regression Coefficients for Door-Spindle Feed (DSF) Movement Simulations for 1-Field in y -Direction for both Robots

	n	a	b	c	d	e	f
$CT_{DSF,1y,CR}$	8.57481	$-7.41726 \cdot 10^{-2}$	$3.19283 \cdot 10^{-4}$	$-7.41317 \cdot 10^{-7}$	$9.50144 \cdot 10^{-10}$	$-6.30266 \cdot 10^{-13}$	$1.68612 \cdot 10^{-16}$
$CT_{DSF,1y,IR}$	7.34645	$-5.09959 \cdot 10^{-2}$	$1.69766 \cdot 10^{-4}$	$-2.93905 \cdot 10^{-7}$	$2.72008 \cdot 10^{-10}$	$-1.27406 \cdot 10^{-13}$	$2.37002 \cdot 10^{-17}$

In Figure 4.8, the nonlinear regression progression relative to the input values is illustrated. Furthermore, the deviations between actual and calculated values are presented as residuals for all simulation runs. It can be seen that the regression accuracy is very high for both robots within the scope of rough planning. While CR has a maximum deviation of 0.358 mm/s, IR shows only a maximum delta of 0.105 mm/s. The statistical results for all DSF field movements are enclosed in Appendix 12 to Appendix 14. Please note that 4-field DSF motions were excluded due to either data inconsistency or lacking data amount.

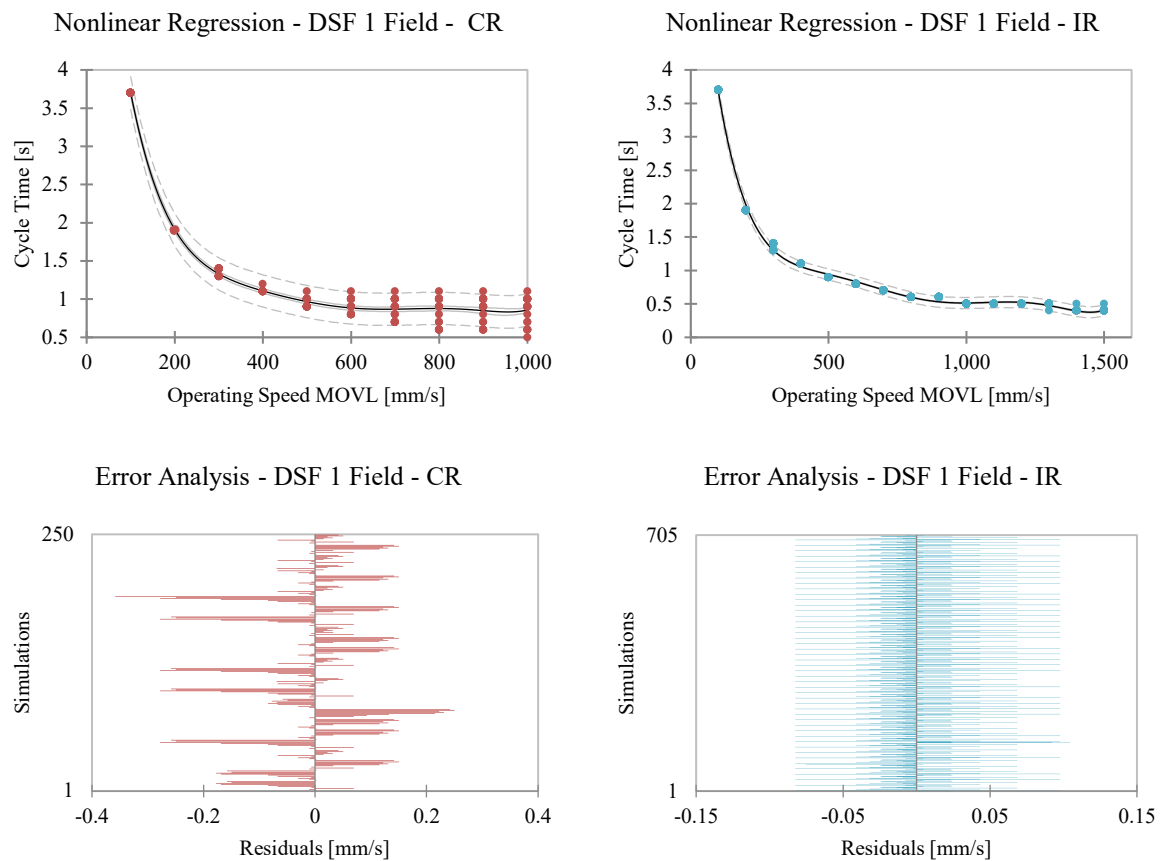


Figure 4.8: Nonlinear Regression Progression and Error Analysis of Door-Spindle Feed (DSF) Movement for 1-Field in y-Direction for both Robots

The same statistical evaluation procedure has been applied for the remaining movement modules, briefly presented as follows. The spindle feed-spindle (SFS) movement must be analyzed by the covered field distance in the x-direction because the combinatory possibilities led to a high number of simulation results that are not displayable in one mutual diagram. Therefore, one x-field movement is illustrated in Figure 4.9 as representative of this motion type. When examining the data consistency, the same behavior as for the DSF motion can be seen. While the CR has many outliers with unexpected progression behavior and peak cycle times, the IR is entirely consistent. Only at the slowest and highest operating speeds, small peaks can be seen that can be traced back to rounding errors in the data analytics process, which can be neglected for the statistical analysis. These individualities of the CR can also be explained with the kinematic conditions mentioned before. In Appendix 15 to Appendix 19, the complete statistical analysis for this one x-field motion and the other SFS field motions is enclosed.

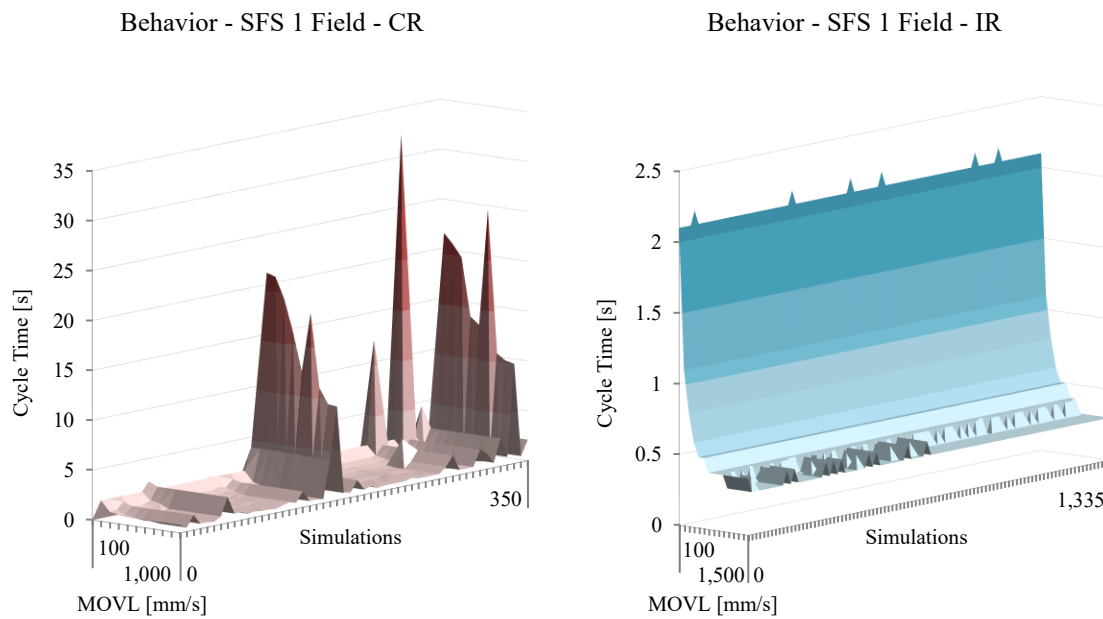


Figure 4.9: Spindle Feed-Spindle (SFS) Simulation Results for Collaborative (CR) and Industrial Robot (IR) and 1 Field Distance in x-Direction relative to Operating Speed MOVL, Achieved Cycle Time and Simulation Runs

The motion pattern T behaves differently from the previous ones because only the 6th axis is in action instead of parallel multi-axis movement like for the other movements (see Figure 4.10). Both robot types operate at all positions, and gripping variations are the same with only a few deviations. Overall, both graphs progress nearly parallel to each other with a start point difference of 3.4 seconds. Since this is a single-axis movement, the effect of the individual axis speeds can be seen very clearly here. While the CR has a maximum 6th axis speed of 250 °/s, the IR operates at 700 °/s maximum. The complete statistical analysis is enclosed in Appendix 20.

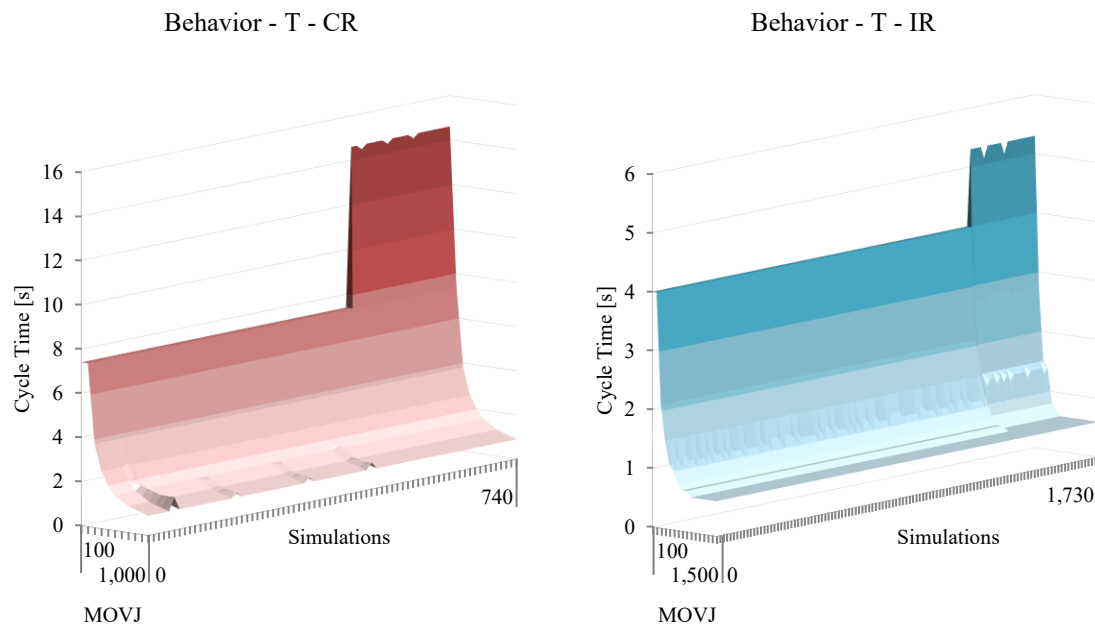


Figure 4.10: Turning (T) Simulation Results for Collaborative (CR) and Industrial Robot (IR) relative to Operating Speed MOVJ, Achieved Cycle Time, and Simulation Runs

The theoretic number of possible simulations is very high for the MFM simulations because there are multiple robot positioning options with respective feasible material positions. To reduce the simulation effort, position AA03 was chosen as representative because this position has a distance of 2 fields in all directions. Based on the assumption that material is arranged one to three fields away from the robot, the simulations within this circle around the AA03 field were executed. These exemplary simulation sets can be transferred to all other robot positions since the resulting robot pose is identical. As a result, it can be seen that the CR behaves irregularly while the IR is very consistent (see Figure 4.11 and Appendix 21).

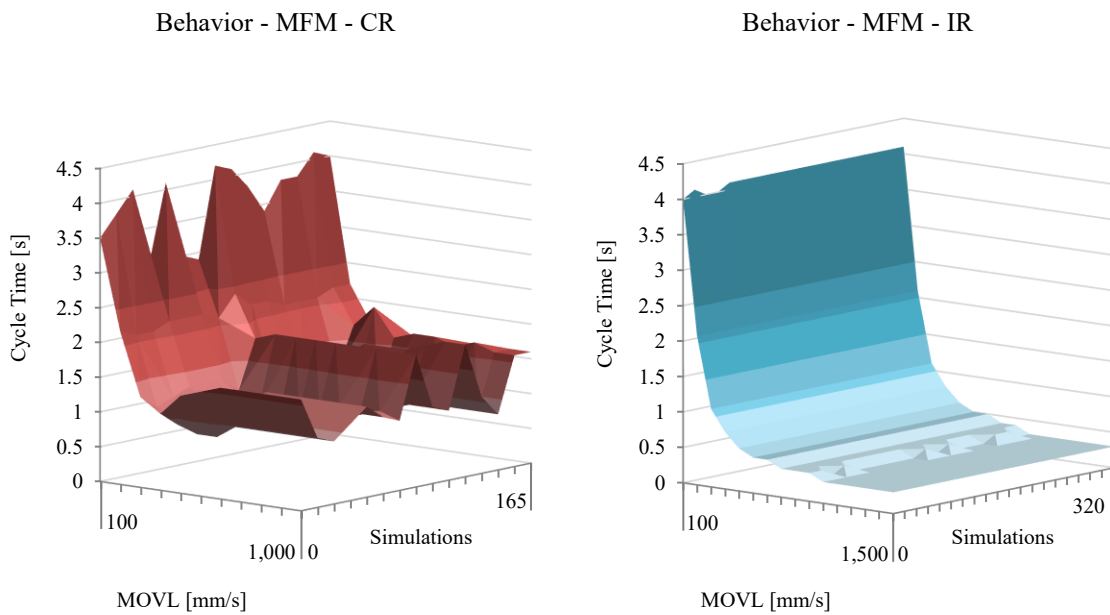


Figure 4.11: Material Feed-Material (MFM) Simulation Results for Collaborative (CR) and Industrial Robot (IR) relative to Operating Speed MOVL, Achieved Cycle Time, and Simulation Runs

For the MFD motion module, no pattern has been identified due to the individuality of each case. The path behavior is case-dependent since the transport movement between material feed and door is executed as a joint movement. For joint movements, the robot calculates the most convenient path, in this case, a curve, which is not generally classifiable in length and shape. Furthermore, the high combinatory character of the position bundle robot-material feed-door leads to very individual cases with individual curves. Therefore, this movement remains a side condition that must be identified by simulation. During the main time, a processed workpiece is tended by the robot. However, the side times start when the machine's door is closed, and the subsequent processing cycle begins. Within this time, the workpiece must be transported to and exchanged at the material deposit. By subtracting one T and four MFM movements from the processing time, the MFD threshold value for both ways can be determined. This limit describes the allowed time for an MFD motion to arrive back at the machine's door before the next cycle begins. If this is not possible, waiting times must be added to the Gantt chart.

4.5 Collaborative Speed Estimation Module – Module Development

4.5.1 General Approach

This section deals with the conduction of a large-scaled empirical study for the beforementioned risk cases. For case 1, the impact of different influencing factors on the *MACS* is analyzed. On this basis, the most relevant factors are used to conclude a *MACS* approximation equation utilizing statistical methods. For the second and third cases, the *MACS* is calculated based on the equations provided by ISO/TS 15066 [108]. For comparison, measurements with the beforementioned setups are executed to analyze the difference between theory and practice. As a result of this chapter, reference values for the most relevant risk cases in lathe machine tending in cobot PFL operation are presented.

4.5.2 Case 1: Quasi-static Contact with Hand

4.5.2.1 Test on Gripper and Material

The first measurement series was executed with different 110 mm diameter chuck workpieces, either cut from bar material or 3D printed in 30 mm and 50 mm length. As materials, PLA (Polylactic acid), POM (Polyoxymethylene), aluminum, and steel were used. Each workpiece was gripped with a Schunk Co-act EGP-C gripper with custom-made aluminum jaws that fit the 110 mm workpiece diameter. This gripper model was used for other cobot tests with the previous HC10DT version, which has an internal media routing. Due to the robot protection class redesign, the HC10DT IP67 has an external media routing, which made customization of the flange necessary to lead the wires from the inside of the gripper to the outside of the robot. However, with this gripper setup, the single workpieces were gripped to execute the tests. This gripper is intended for small workpieces and could not hold the 50 mm long steel material reliably. A screw clamp was used to increase the applied pressure for the measurements as a countermeasure, which led to asymmetric mass distribution. A representative solution was needed to avoid this influence factor and the limitation to one gripper model, simplifying the setup and making the measurement results universally valid, independent of the gripper model. Therefore, an aluminum basis workpiece was manufactured with similar mass characteristics and the same length as the sum of Schunk gripper, including flange and the steel workpiece with 30 mm length. The described setup is illustrated in Figure 4.12.



Figure 4.12: Selected Tested Gripper and Workpiece Setups - Schunk Gripper with 50 mm long POM Material (left), Schunk Gripper with 50 mm long Steel Workpiece and Screw Clamp (middle) and Aluminium Basis Workpiece (right)

As shown in Table 4.4, the mass between Schunk gripper and 30 mm long steel and the aluminum basis workpiece differs by 158 g and is therefore comparable (marked green). Hence, both situations can be measured and compared to evaluate the influence of the gripper. Another steel basis workpiece was designed and manufactured with the highest weight that can be handled to cover the robot's maximum possible load, determined in iterative loops in payload simulation software. As a result, the following workpieces with individual masses are used for the first measurement series.

Table 4.4: Weights of the Tested Workpieces for the D110 mm Measurement Series

Material	PLA		POM		Aluminum			Steel		
Diameter d [mm]	110		110		110			110		
Length l [mm]	50	30	50	30	50	30	Basis workpiece	50	30	Basis workpiece
Mass m (without gripper) [kg]	0.148	0.097	0.674	0.403	1.34	0.8	3.584	4.449	2.222	6.796
Mass m (with gripper) [kg]	1.352	1.301	1.878	1.607	2.544	2.004		5.653	3.426	

For comparison, the *MACS* for 110 mm diameter for the positions close, middle, and stretched and sensor sensitivities 140 N, 130 N, 100 N, and 50 N were determined for the 110 mm x 30 mm steel workpiece with Schunk gripper and the aluminum basis workpiece (see Figure 4.13).

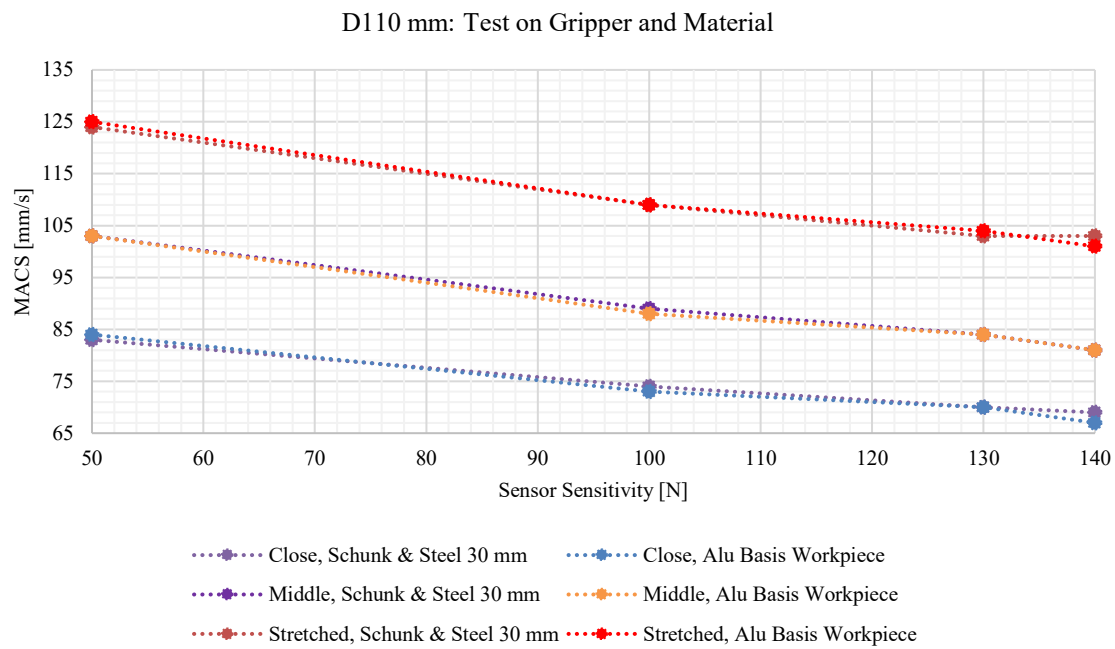


Figure 4.13: Test on Gripper and Material for 110 mm - Comparison of Schunk Gripper with 30 mm Steel Workpiece and Aluminium Basis Workpiece

The measurement results show that there is a minimal deviation between the two setups. Therefore, the material itself can be excluded for further research if the surface quality and rigidity characteristics are identical. Only the weight properties, which come along with the material, will be analyzed in more detail. Secondly, the gripper does not influence the measurement if the gripper guarantees reliable holding, and the gripper-jaw-workpiece system can be considered stiff. Under this assumption, only the mass properties have an influence. For simplification, for the following measurement series with 80 mm, 50 mm, and 20 mm diameter, only the aluminum and steel basis workpiece and a 50 mm long POM material with the Schunk gripper is used. The workpieces and basis workpieces are turned on the contact side by a few millimeters to the desired diameter to keep the results comparable. Hence, the mass properties vary slightly between 110 mm, 80 mm, 50 mm, and 20 mm workpieces. In Table 4.5, the weights of these workpieces are summed up.

Table 4.5: Weights of the Tested Workpieces for the D80 mm to D20 mm Measurement Series

Material	POM		Aluminum basis workpiece		Steel basis workpiece		
Diameter d [mm]	80	50	80	50	80	50	20
Length l [mm]	50	50					
Mass m (without gripper) [kg]	0.54	0.423	-		-		
Mass m (with gripper) [kg]	1.744	1.627	3.484	3.414	6.483	6.195	6.041

4.5.2.2 Test on Minimum Required Collaborative Speed (MRCS)

In this test, the robot was operated at very slow speeds to identify a lower threshold operating speed needed to comply with the defined forces: the minimum required collaborative speed, called *MRCS* [mm/s], in the further proceeding. A selected experiment shows this effect very clearly: at an operating speed of 10 mm/s, the quasi-static forces were exceeded (144 N), while 11 mm/s lies below the defined threshold values (137.4 N) (see Figure 4.14).

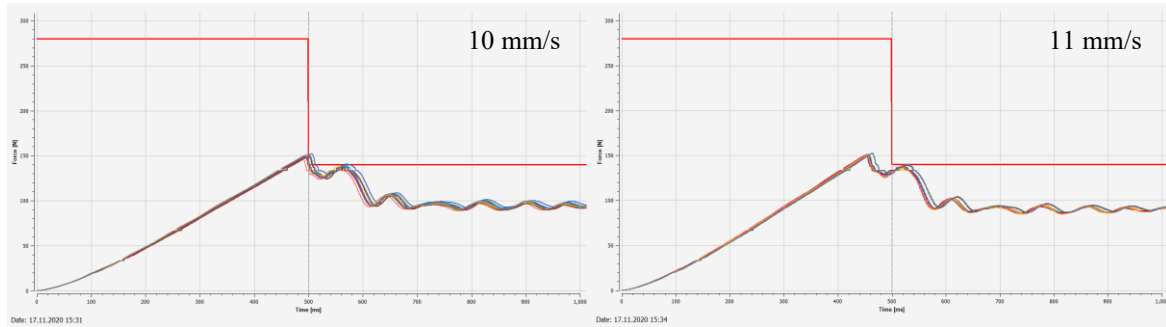


Figure 4.14: Force measurements to identify the Minimum Required Collaborative Speed (MRCS)

Equivalent experiments were executed for all measurement series at 140 N force limit setting. This effect has been verified for 92 % of all measurement series, leading to a slight *MRCS* increase with a higher robot range (see Appendix 22). When reducing the sensor sensitivity to 130 N, only 3,8 % of all measurement series do require an *MRCS*. For the settings 100 N and 50 N, this behavior was not measured. To simplify the sensor setting selection complexity in the future, settings below 140 N should be used to avoid considering the *MRCS*. Comparing the *MACS* for 140 N and 130 N force limit setting independent of whether an *MRCS* is required or not, only a slight average deviation of 2,6 % can be noted, which is equivalent to an absolute average deviation of 2 mm/s (see Appendix 23). Due to this negligible *MACS* decrease, force limit settings below 140 N are recommended.

4.5.2.3 Test on Sensor Sensitivity, Robot Pose, and Workpiece Diameter

Overall, it can be noted that the robot retracts already after about 180 ms within the transient contact area, leading to higher acceptable threshold values. Therefore, an actual clamping does not occur (see Figure 4.15).

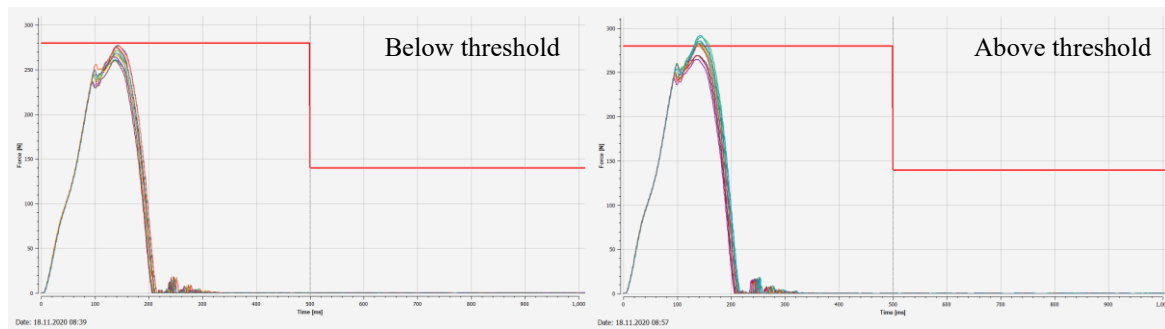


Figure 4.15: Force Development Behavior over Time for Quasi-static Contact Cases

For the workpiece diameter 110 mm to 20 mm, the sensor sensitivity's influence on the *MACS* was measured for all measurement series. With increasing sensitivity (decreasing force limit in N), the speed value increases with a nearly linear progression. The single measurement sets concentrate on three value bundles representing one position each (see Appendix 24). Furthermore, the diameters of the measurement series do not show a specific pattern. The 20 mm diameter series, for example, delivers the highest *MACS* values for the close position while lying in the middle of the other diameters for the middle and stretched position. Analysis of the overall minimum and maximum *MACS* values over diameter deliver a nearly linear even progression. Therefore, the workpiece diameter can be excluded as an influencing factor if the pressure values are not affected (see Appendix 25). Later in this paragraph, the pressure distribution will be analyzed in further detail, showing that pressure measurement with a 20 mm diameter does not exceed the respective thresholds.

4.5.2.4 Test on Tool and Workpiece Weight

To determine the attached weight's influence, the previously mentioned workpieces from diameter 110 mm to 50 mm were used for measuring the *MACS* for different robot poses and sensor sensitivity settings. Diameter 20 mm is considered separately later due to the particular pressure considerations. Overall, an increasing weight impact can be noted, mainly depending on the robot pose and sensor sensitivity setting. While the close positions are nearly unaffected by the increasing weight, the *MACS* slightly decreases at the middle position and is highly impaired at the stretched position. This behavior can be explained by the increasing lever taking effect on the robot kinematic and sensors. Furthermore, it can be seen that higher sensor sensitivity (lower force limit value in N) compensates for the weight influence better, underlined by the increasing negative slope of the trend curves at higher sensitivity (see Appendix 26). By highlighting the used materials of each measurement series

(which are indirectly delivering the attached weights) to the same diagram as Appendix 24, the previously mentioned weight influence can clearly be seen in Appendix 27. The heaviest steel workpieces occupy the lower *MACS* area due to the lever's influence, while the lightweight workpieces take the upper area. Please note that the close position's upper red steel measurement series is the 20 mm diameter measurement, which was only executed with steel. However, the *MACS* is nearly linear, decreasing with increasing robot range and decreasing sensor sensitivity (higher force limit). A deviation analysis between the MIN and MAX values is illustrated in Appendix 28. While the close and middle positions have a nearly equal weight compensation for the single force limits, the stretched position is highly affected by the sensor sensitivity used to compensate for weight influences. In Appendix 29, the relationship between *MACS* and robot pose is illustrated for the single sensor sensitivity force limit settings. Analysis of the MIN and MAX *MACS* deviation over all diameters by robot pose for the single sensor sensitivity force limit settings shows that 50 N force limit setting compensates weight influences best independent of the used robot pose (see Appendix 30). For the remaining settings, the deviation increases exponentially with the higher robot range.

4.5.2.5 Test on Pressure

Pressure tests have been exemplarily executed with foils of the type LLW for each diameter set, emphasizing the 50 mm and 20 mm diameter steel and aluminum workpieces. As an operating speed basis for the tests, the *MACS* identified by the iterative force measurements were used. Therefore, the pressure results should either serve as validation for the force-based measurement result if the pressure complies with ISO/TS 15066 or indicate iterative speed decreasing until the pressure thresholds comply. Diameter 110 mm did not show any pressure results as expected since the contact surface is equivalent to the measurement device's diameter, leading to even pressure distribution. Also, the 80 mm diameter did not show significant pressure results since the contact surface was too large. First, significant pressures were measured at 50 mm diameter, which still complies with the threshold values at the respective force-compliant operating speed. Hence, the entire 50 mm measurement series results were validated by the pressure measurements. At 20 mm, however, the pressure firstly exceeds the defined values at the force-compliant operating speed. Figure 4.16 shows

the difference in pressure distribution between 50 mm and 20 mm for one selected measurement series.

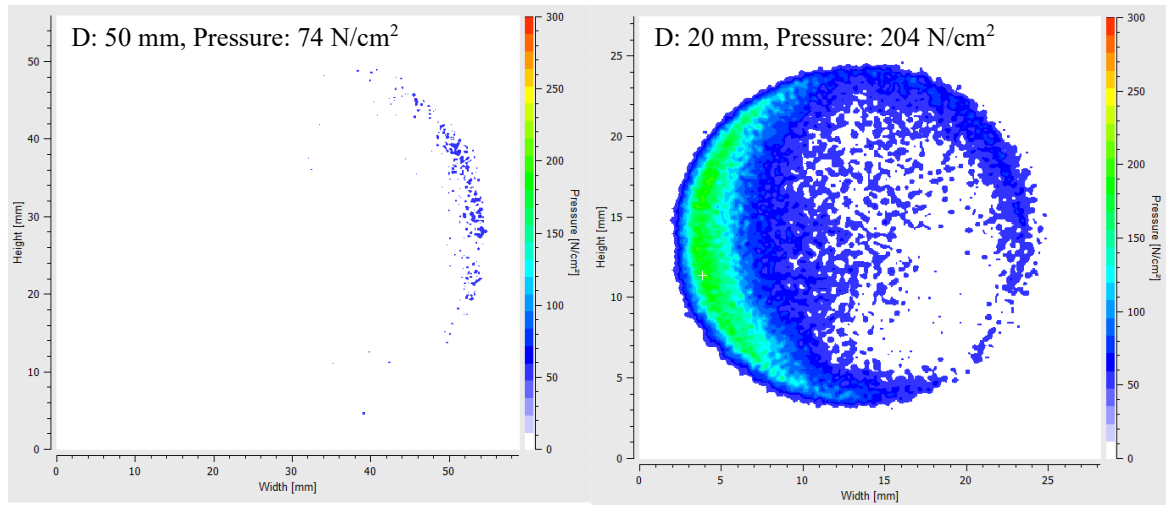


Figure 4.16: Exemplary Pressure Foil Results for 50 mm (left) and 20 mm (right) Diameter

While the left result of 74 N/cm^2 complies with the threshold value of 190 N/cm^2 , the D20 mm workpiece exceeds this defined value. Picture arrangement differences come from different insertion positions of the pressure foil into the scanning device. The unequal pressure distribution can be traced back to unideal measurement conditions. That means that even though the robot flange is oriented nearly parallel to the measurement device, slight irregularities occur during the collision. This explains the higher-pressure application on one side of the contact surface. This irregularity does affect the result negatively, even though these effects also occur in practice and are consequently an accurate representation of industrial risk assessment procedures. Therefore, errors in pressure measurements are analyzed with a strong emphasis on the workpiece's tilting angle. The robot program has been adjusted by modifying the rotation around the Y-axis (R_y) in 0.5 steps in both directions (see Appendix 31). The optimal rotation was identified at $+0.5$ with the lowest pressure values, leading to complying pressure results. Further tilting at -1.5 , -0.5 , $+1$ and $+1.5$ leads to increased pressure values.

4.5.2.6 Conclude MACS Approximation Tool

To provide the planner an approximation tool to calculate the *MACS* for the quasi-static contact, all 216 measurement series based on 2160 force and 36 pressure measurements have been statistically analyzed. Therefore, the position, force limit, and weight characteristics have been assigned to the respective measurement series' individual speed value. In

Appendix 32 and Appendix 33, it can be seen that the *MACS*-sensor sensitivity correlation and the *MACS*-position correlation can be assumed as linear. To include all parameters in one mutual model, multiple linear regression have been used to deliver an approximation equation with the parameters position p [%], sensitivity force limit setting s [N], and workpiece weight m [kg] with a coefficient of determination of $R^2 = 0.964902$:

$$MACS = 53.1107 + 1.15885p - 0.2283s - 0.4578m \quad (4.51)$$

Since this equation is based on statistical evaluation considering the correlations of different parameters, the respective values must be inserted without SI units. A physical connection between those factors, leading to a consistent unit consideration, is not present. The calculated result, the *MACS*, is given in mm/s. The following three-dimensional diagram (Figure 4.17) illustrates the context considering the *MACS*, force limit, and position relative to reach using averaged values (see Appendix 32 and Appendix 33).

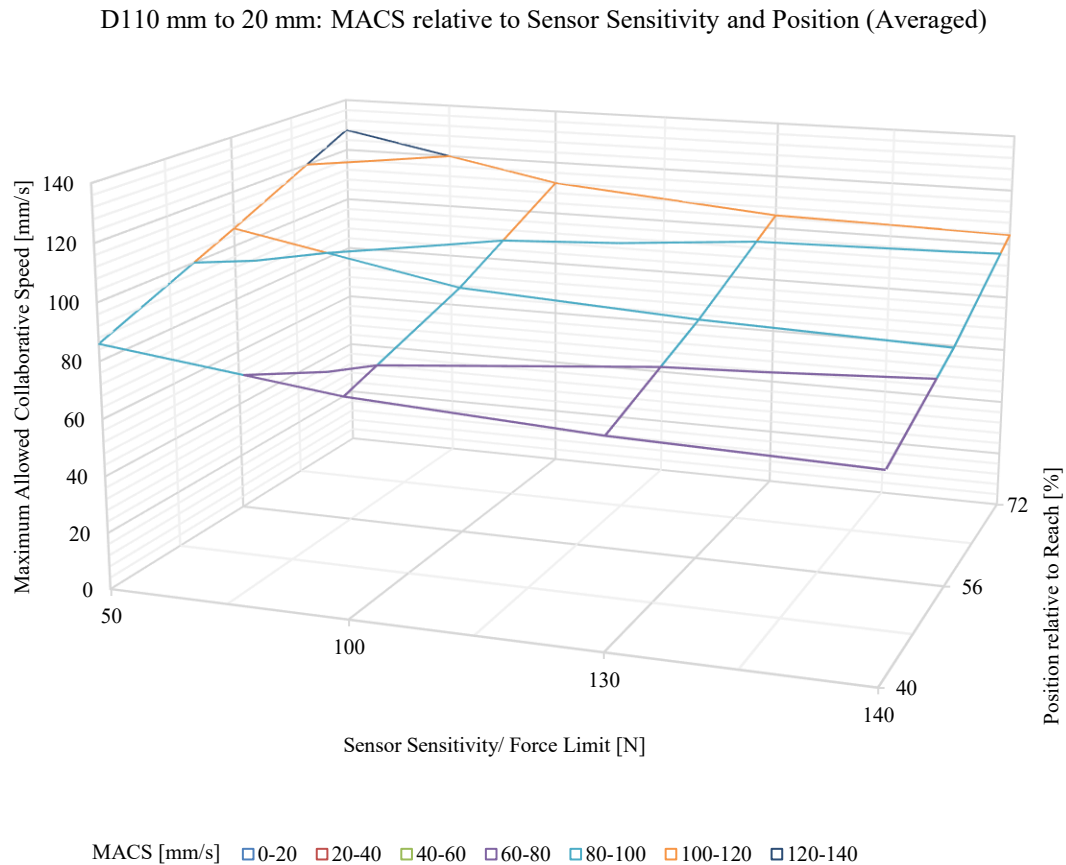


Figure 4.17: Maximum Allowed Collaborative Speed (MACS) relative to Sensor Sensitivity Setting/Force Limit and Robot Pose for Workpiece Diameters 110 mm to 20 mm

4.5.3 Case 2: Transient Contact with Hand

4.5.3.1 Theoretical Considerations

At first, the contact situation is theoretically investigated. A robot mass m of 58 kg was assumed for calculation, including the whole robot, while ISO/TS 15066 describes the mass of moving robot elements. Since the exact masses of the affected robot parts are not known, this assumption takes place. The following general information serves as input values: transfer energy E , effective body region mass m_H , total mass of moving robot parts M , effective robot system payload m_L , maximum permissible force F_{max} and maximum permissible pressure p_{max} [108].

$$E = 0.49 J = 0.49 \frac{kg \cdot m^2}{s^2} [108] \quad (4.52)$$

$$m_H = 0.6 kg; M = 58 kg; m_L = 6.041 kg; d = 0.02m [108] \quad (4.53)$$

$$F_{max} = 280 N; k = 75,000 \frac{N}{m}; p_{max} = 2,800,000 \frac{N}{m^2} [108] \quad (4.54)$$

Based on this data, the effective robot mass m_R and the reduced mass of both collision bodies μ is calculated [108]. For the pressure-based velocity calculation, the considered contact area A is determined for the plane contact.

$$m_R = \frac{M}{2} + m_L = \frac{58 kg}{2} + 6.041 kg = 35.041 kg \quad (4.55)$$

$$\mu = \left(\frac{1}{m_H} + \frac{1}{m_R} \right)^{-1} = \left(\frac{1}{0.6 kg} + \frac{1}{35.041 kg} \right)^{-1} = 0.61045 kg \quad (4.56)$$

$$A_{Plane} = \frac{\pi}{4} * d^2 = \frac{\pi}{4} * 0.02 m^2 = 3.142 * 10^{-4} m^2 \quad (4.57)$$

Consequently, the following relative speed values for the transient plane contact Pl are calculated based on the respective reference basis: energy-based speed $v_{rel,E}$, force-based speed $v_{rel,F}$ and pressure-based speed $v_{rel,Pr}$.

$$E = \frac{1}{2} \mu v_{rel}^2; v_{rel,E} = \sqrt{\frac{2E}{\mu}} = \sqrt{\frac{2 * 0.49 \frac{kg \cdot m^2}{s^2}}{0.61045 kg}} = 1.267 \frac{m}{s} \quad (4.58)$$

$$v_{rel,F} = \frac{F_{max}}{\sqrt{\mu k}} = \frac{280 N}{\sqrt{0.61045 kg * 75,000 \frac{N}{m}}} = 1.3085 \frac{m}{s} \quad (4.59)$$

$$v_{rel,Pr,Plane} = \frac{p_{max} * A_{Plane}}{\sqrt{\mu k}} = \frac{2,800,000 \frac{N}{m^2} * 3.1416 * 10^{-4} m^2}{\sqrt{0.61045 kg * 75,000 \frac{N}{m}}} = 4.111 \frac{m}{s} \quad (4.60)$$

Depending on the used reference basis, different speed values were calculated. Generally, the *MACS* exceed the maximum linear speed of the cobot of 1 m/s. While the energy- and force-based calculations lead to nearly similar results, the pressure-based measurement is nearly three times higher. Consequently, the forces and energies are the limiting factors, while pressure could be enormously increased.

For the edge contacts *Ed*, calculations based on maximum permissible force and energy yield the same results. Therefore, only the calculations based on allowable pressures lead to different results since the size of the collision surface is significantly smaller in this case. The collision area can be simplified assumed as a rectangle. Due to the small collision surface, pressure is the dominant criterion.

$$A_{Ed} = 0.002 m * 0.010 m = 2 * 10^{-5} m^2 \quad (4.61)$$

$$v_{rel,Pr,Ed} = \frac{p_{max} * A_{Edge}}{\sqrt{\mu k}} = \frac{2,800,000 \frac{N}{m^2} * 2 * 10^{-5} m^2}{\sqrt{0.61045 kg * 75,000 \frac{N}{m}}} = 0.266 \frac{m}{s} \quad (4.62)$$

4.5.3.2 Test on Plane Transient Contact and Comparison to Theory

To analyze the difference between theoretic and practical, exemplary measurements were executed. Therefore, the guide rail setup is mounted on the middle position of the frame, and the measurement device is positioned at the end of the mechanical stop. For the exact speed setting, a linear robot movement is used. The practical results deliver a much slower *MACS* of 645 mm/s to 647 mm/s compared to the theoretically calculated values (see Appendix 34). This deviation can be traced back to the experiment design regarding the weight of the guide rail's measurement setup and friction effects. According to ISO/TS 15066 [108], the defined hand mass is defined at 0.6 kg, while the moving setup weight, including the measurement device, weighs 3.664 kg. Consequently, the recoiling mass is much higher, which distorts the result. In the future, a weight compensation coefficient must be determined for adjustment. Furthermore, it is interesting to see that the sensor sensitivity does not affect the results. Due to the high contact energies, the robot stops immediately at the collision moment. In contrast to the quasi-static measurements, where the device is mounted firmly on the frame, the rail moves in the transient case after the collision. Therefore, the sensitivity takes no effect. For this experiment, measurements with a 50 N force limit setting were not

possible since the torque sensors were triggered by the robot's acceleration due to the high sensitivity, leading to a secure stop of the robot.

According to the theoretical results, the force is the restrictive factor, while the pressure could be highly increased. However, the measurements show for the 130 N force limit that the averaged force value at 646 mm/s of 278.13 N lies very close to the threshold of 280 N, while the pressure value of 293 N/cm² undercuts the threshold of 380 N/cm² by 87 N/cm². Consequently, theoretical and practical results differ from each other.

4.5.3.3 Test on Edge Transient Contact and Comparison to Theory

For this experiment, the robot was tilted by 45° to guarantee a collision with the edge of the 20 mm diameter steel basis workpiece. Due to the small collision surface, pressure is the dominant criterion. For the whole sensor sensitivity area, an equal *MACS* of 80 mm/s has been identified (see Appendix 35). According to the theoretical calculations, the force is the restrictive factor, while the pressure could be highly increased. The practical measurements, however, show the opposite. Appendix 36 illustrates the occurring forces and pressures at 80 mm/s and 90 mm/s operating speed relative to the threshold values. Forces are strongly undercutting the allowed values for both velocities and 90 mm/s (full) operating speeds. On the other side, pressures are very close to the threshold at a speed of 80 mm/s but exceed those limits at 90 mm/s. Irregularities in the pressure results can be traced back to the inaccuracy of the pressure-sensitive foils. Therefore, the slightly exceeding pressure value at 130 N can be considered as within the tolerance. An exemplary pressure distribution within the allowed specifications is enclosed in Appendix 36.

4.5.4 Case 3: Transient Contact with Shoulder

4.5.4.1 Theoretical Considerations

Firstly, the maximum allowable collaborative speed will be determined by applying the respective equations defined in ISO/TS 15066. For the human shoulder joint, the following input data was obtained:

$$E = 2.5 J = 2.5 \frac{kg \cdot m^2}{s^2} [108] \quad (4.63)$$

$$m_H = 40 kg; M = 58 kg; m_L = 6.041 kg; d = 0.02 m [108] \quad (4.64)$$

$$F_{max} = 420 N; k = 35,000 \frac{N}{m}; p_{max} = 3,200,000 \frac{N}{m^2} [108] \quad (4.65)$$

This leads to calculating the required auxiliary variables and contact areas A of the robot geometries elbow big-cap Elb , forearm Arm , and the elbow small and wrist caps Cap .

$$m_R = \frac{M}{2} + m_L = 35.041 \text{ kg} \quad (4.66)$$

$$\mu = \left(\frac{1}{m_H} + \frac{1}{m_R} \right)^{-1} = 18.678 \text{ kg} \quad (4.67)$$

$$A_{Elb} = 0.0035 \text{ m} * 0.03 \text{ m} = 1.05 * 10^{-4} \text{ m}^2 \quad (4.68)$$

$$A_{Arm} = 0.02 \text{ m} * 0.08 \text{ m} = 1.6 * 10^{-3} \text{ m}^2 \quad (4.69)$$

$$A_{Cap} = \frac{\pi}{4} (0.035 \text{ m})^2 = 9.621 * 10^{-4} \text{ m}^2 \quad (4.70)$$

Based on this information, the relative speed of the transient contact case based on the different reference bases is calculated.

$$E = \frac{1}{2} \mu v_{rel}^2; v_{rel,E} = \sqrt{\frac{2E}{\mu}} = 0.517 \frac{\text{m}}{\text{s}} \quad (4.71)$$

$$v_{rel,F} = \frac{F_{max}}{\sqrt{\mu k}} = 0.519 \frac{\text{m}}{\text{s}} \quad (4.72)$$

$$v_{rel,Pr,Elb} = \frac{p_{max} * A_{Elb}}{\sqrt{\mu k}} = 0.415 \frac{\text{m}}{\text{s}} \quad (4.73)$$

$$v_{rel,Pr,Arm} = \frac{p_{max} * A_{Arm}}{\sqrt{\mu k}} = 6.332 \frac{\text{m}}{\text{s}} \quad (4.74)$$

$$v_{rel,Pr,Cap} = \frac{p_{max} * A_{Cap}}{\sqrt{\mu k}} = 3.808 \frac{\text{m}}{\text{s}} \quad (4.75)$$

While the energy- and force-based calculations lead to nearly similar results, the pressure-based calculations deviate with a factor between 0.8 and 12.3 compared to those values. Consequently, the forces and energies are the theoretical limiting factors, while pressure could be enormously increased.

4.5.4.2 Test on Transient Contact with Different Robot Geometries and Comparison to Theory

At first, the big elbow cap was measured (see Figure 4.18). Without protective measures, the maximum speed is mainly restricted by the pressure limit, surpassing at 70 mm/s, leading to a *MACS* of 60 mm/s. However, with protective measures, the *MACS* climbs up to 720 mm/s with neoprene and 770 mm/s with foam. This can be explained by an even pressure distribution on a greater surface compared to measurements without protection. Furthermore, the *MACS* with a force limit of 50 N was slightly higher than measurements

with 100 N for protective measures while not being affected when using no padding.



Figure 4.18: Setup for Transient Contact with the Elbow Big Cap – without Padding (left), with Neoprene (middle), and with Foam (right)

Secondly, experiments with the small elbow cap were conducted (see Figure 4.19). The pressure threshold has not been reached in this experiment for all three setups, while the force has been exceeded at 890 mm/s to 920 mm/s depending on the used padding. Measurement results with 50 N deliver higher *MACS* than the 100 N force limit, irrespective of the protective measures. No clear tendency on the dependency of *MACS* and the protective measure could be identified.



Figure 4.19: Setup for Transient Contact with Elbow Small Cap – without Padding (left), with Neoprene (middle), and with Foam (right)

In the next experiment, the forearm was tested (see Figure 4.20). Pressure thresholds were undercut with all measurement series. The highest *MACS* have been registered for 100 N force limit and measurement without protection at 750 mm/s. With a force limit of 50 N, the *MACS* could not be reached for neoprene and foam protection since the high torque sensor sensitivity triggers a protective stop of the robot during high acceleration.



Figure 4.20: Setup for Transient Contact with Forearm – without Padding (left), with Neoprene (middle), and with Foam (right)

Lastly, the wrist cap was measured (see Figure 4.21). As expected, observed *MACS* are lower than those of the small elbow cap because the collision point is further away from the robot base resulting in a higher lever. The highest *MACS* was registered for the 50 N force limit in combination with foam protection. Without protection, results were lower for both sensor sensitivities.



Figure 4.21: Experiment on Transient Contact with Wrist Cap – without Padding (left), with Neoprene (middle), and with Foam (right)

Additional padding on the respective collision surface can drastically increase the maximum allowed collaborative speed if critical areas with small surfaces (big elbow cap) are present. For the other three cases, an evident influence of protective measures on the *MACS* could not be verified (see Figure 4.22). Whereas the neoprene cover could not reduce occurring force compared to the setup without protection, attaching EPE foam profiles on the collision surface showed significant force reduction. Overall, the pressure threshold has been exceeded only for the big elbow cap without padding.

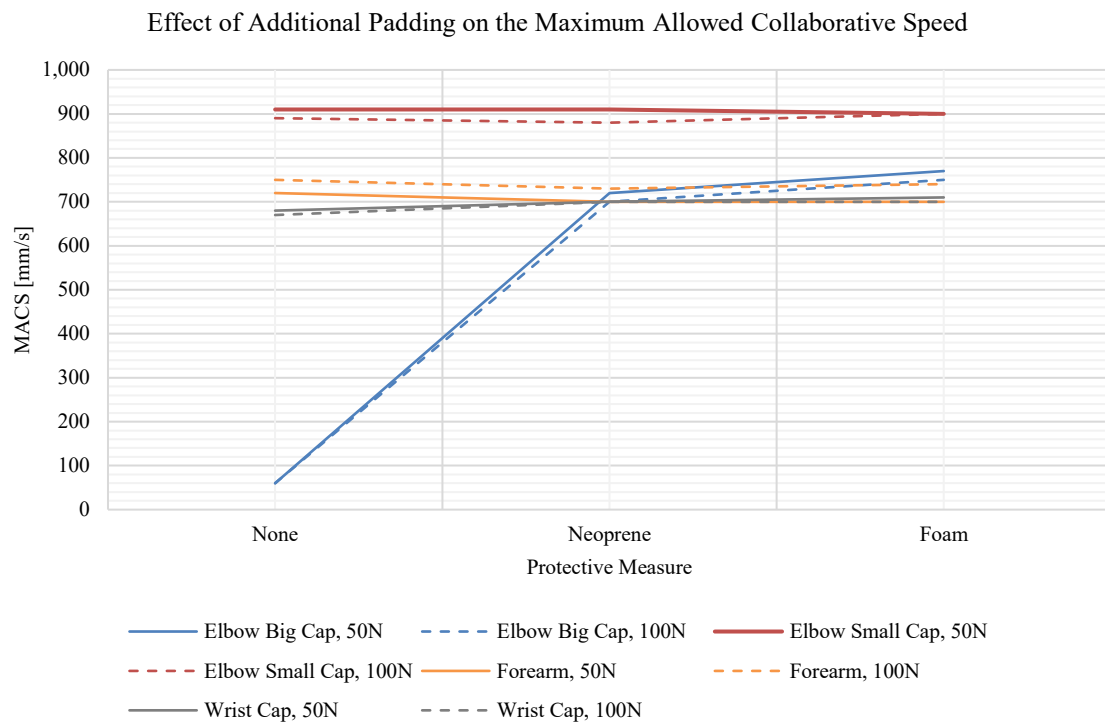


Figure 4.22: Maximum Allowed Collaborative Speed (MACS) by Protective Measure for Different Sensor Sensitivities/Force Limits and Robot Outer Contact Geometries

4.6 Synthesis – Module Development

This chapter dealt with the development of the single modules according to Figure 3.1. At first, an economic calculation scheme was derived under the utilization of the net present value (NPV) as the target figure. As an information basis, calculations for the manual execution were presented to determine the annual execution time and total annual output. Then, further calculation schemes for the three technical options “Collaborative Robot in Exclusive PFL Operation”, “Collaborative Robot in Hybrid Mode”, and “Industrial Robot” was developed. To calculate the NPV for each alternative, cash-in flow determination was emphasized because the investment data are use-case specific and therefore not generally describable, and cash-out flows were assumed as equal for both robot types. These cash-in flows consist mainly of the labor release grade and the annual output deviation by comparing the individual automation option to the manual execution. To calculate these factors, the execution times of the processes build the central factor. For human-robot interaction, the different modes of collaboration must be actively incorporated for realistic results. Therefore, the ETs for 100 % operation in either PFL or FS mode are calculated. With the interaction grade α , these times are brought into ratio to each other.

Secondly, planning assistance for the determination of payload utilization and gripping feasibility was given. Several iterative simulations were conducted in this module for different grippers, workpiece materials, diameters, and lengths. As a result, a diagram has been derived that indicates feasible diameter-length combinations for a selected gripper-material pair. By this, a tool is given to the planner to preliminary select a feasible robot-gripper combination for a selected workpiece or workpiece spectrum.

In the third step, typical rough layouts of lathe machine tending cells have been discretized to a specific pattern. As input data serve the analysis of 34 DMG MORI machines regarding different required positions, which were three-dimensionally modeled and layered. As a result, a 200 mm x 200 mm two-dimensional pattern has been derived to cover the machine's door and main spindle positions. Further fields with a 400 mm x 400 mm resolution were added for robot positioning representing the robot installation and material provision locations. To assign realistic heights to the single entities, analyzed machine data and ergonomic recommendations were used. For robot offline programming, this pattern was transferred to a three-dimensional model. With an exemplary position and motion situation, the application of this method is illustrated. The advantage of this method is the discretization of an individual lathe machine tending application to a simple pattern. Usually, the exact positions must be designed and transferred to a 3D model for import to simulation software. When robot or material positions are changed or iterated, a new model must be created. The planner can easily assign the use-case-specific positions to the respective fields within the pattern and conclude a first rough robot trajectory by applying the presented approach. Even though the result is only a rough approximation of the problem, it makes the problem manageable at the project beginning and builds substantial planning assistance.

For further characterization of this identified robot trajectory, the cycle time estimation module was further developed. A reachability study of feasible robot positions to reach the main spindle for tending serves as an information base. In various simulation runs, all identified possibilities for each motion module were described by stepwise increasing the operating speed to conclude a respective cycle time. With statistical analysis, this data was characterized in great detail. In the example of the DSF movements, the statistical procedure was illustrated. At first, the general behavior over simulation runs regarding operating speed and cycle time consistency was analyzed with surface diagrams. Overall, it can be noted that the collaborative robot behaves much more inconsistently than the industrial one. As a

second step, all simulation runs of an individual movement element were analyzed regarding consistency to identify outliers that were excluded for further analysis. For the remaining datasets, approximation equations were derived using nonlinear regression. An error analysis shows the residuals: the absolute deviation of simulated and calculated value for each simulation run. Generally, slight deviations with a high data coverage have been achieved that are sufficiently precise within the rough planning context. The coefficients for all approximation equations for each movement module are summarized in Appendix 37 to Appendix 38.

As the last unknown variable, the operating speed remains. As mentioned before, the cycle times were determined velocity-dependent to develop a universally valid model. While the velocity values in FS mode are obtainable from the technical specifications of the robot model, the allowed speeds in PFL operation are not a priori determinable. To give the planner a solid indication, reference values were developed. The previous chapter presented suitable measurement setups for quasi-static and transient contacts to execute compliant velocity studies under consideration of various influencing factors. In this chapter, these parameters and their impact on the allowed speed were empirically described. For quasi-static cases, sensor sensitivity, robot pose, and tool/ workpiece weight were identified. The used gripper and material are not relevant if the gripper-jaw-workpiece system can be assumed as a stiff unit and the workpiece diameter lies between 110 mm to 20 mm because the pressures are still compliant. Therefore, only the forces must be measured for quasi-static cases within this diameter range, while the pressure measurements serve only as validation. Based on these identified key factors, an approximation equation was determined using multiple linear regression. For the transient cases, theoretic considerations were conducted first based on the equations provided in ISO/TS 15066. For most of the measurements, tremendous differences between theory and practice were revealed. The transient contacts were classified in three cases: plane contact with the hand, edge contact with the hand, and contact between robot outer contours and shoulder. The first case shows that only the force must be measured since the pressure complies as already identified in the quasi-static experiments. In the second case, only the pressure is relevant due to the small contact surface of the edge. The risk assessment shows very slow allowed velocities. Experiments on the third case clearly showed that the critical contact surface is the edge of the big elbow cap. With additional padding as a protective measure, the forces and pressures can be drastically decreased, leading to a highly increased compliant speed. No hard edge has been identified for the other

robot contact geometries, leading to nearly similar results between 700 mm/s to 900 mm/s. As a result of the round geometry, additional padding showed a low effect. The summarized results of this study are enclosed in Appendix 39. Furthermore, this table shows the worst and best-case values for each situation for simplification.

By inserting the measured *MACS* reference values into the respective movement approximation equations, standard values for each element can be calculated. This approach seeks to build a movement time database for collaborative and industrial robots, emphasizing the PFL operation in direct human-robot interaction. Up to now, it was not possible to define a precise value for a cobot movement in advance since the movement behavior and the compliant speeds were not known. Therefore, this research contributes to an MTM-alike reference value database for HRI. In Table 4.6, the values are summarized.

Table 4.6: Determined Standard Time Values for Different Motions

		Speed [mm/s]	CT_{MFM} [s]	$CT_{SFS,1x}$ [s]	$CT_{SFS,2x}$ [s]	$CT_{SFS,3x}$ [s]	$CT_{SFS,4x}$ [s]	$CT_{SFS,5x}$ [s]	$CT_{DSF,1y}$ [s]	$CT_{DSF,2y}$ [s]	$CT_{DSF,3y}$ [s]	CT_T [s]
CR	Quasi-static - Hand – Worst Case	65	3.15	-	-	-	-	-	-	-	-	-
	Quasi-static - Hand – Best Case	132	1.73	-	-	-	-	-	-	-	-	-
	Transient - Robot Geometry – Worst Case	60	-	2.85	5.75	8.54	11.3	14.02	5.13	7.82	10.68	12.41
	Transient - Robot Geometry – Best Case	900	-	0.55	0.79	0.99	1.21	1.58	0.85	1.08	1.28	0.86
	Transient – Workpiece Edge	80	-	-	-	-	-	-	-	-	-	9.79
	Maximum Speed	1,000	1.27	0.56	0.8	0.99	1.21	1.5	0.86	1.07	1.25	0.94
IR	Maximum Speed	1,500	0.33	0.31	0.48	0.62	0.75	0.91	0.51	0.7	0.9	0.61

In this chapter, answering the research question RQ 2 was further concretized. Based on the technical alternatives defined in the previous chapter, the main technical influencing factors on the economic feasibility were further distilled. Setting the *NPV* as an information base, especially the cash-in flows, characterizes profitability, consisting of the labor release grade and annual output deviation. These factors are multiplied with the annual operator cost and value creation per workpiece to calculate the actual *CIF*. Due to their use-case specificity, the *LRG* and annual output deviation are further examined. The *LRG* is defined by the division of the annual execution times in manual and automated operations. The main influencing factors are the execution times of the individual processes, the time ratio between

setup activities and LUL/ processing activities, and the lot size. These factors determine how often and how long a manual setup activity is required relative to the automated activities. The annual output deviation also depends on these factors because they determine the achievable produced units per year. Setup times and lot sizes are use-case dependent and therefore not generally describable. Hence, the execution times as the main influencing factors are further structured as the primary influence factor. As determined in the simulations and experiments, the cycle time highly depends on the required motion type, e.g., one or two fields in the x- or y-direction, depending on the used machine. More generally, the required time is composed of the mode-dependent operation time and their ratio to each other. An exception is a cobot operating exclusively in PFL mode. These modes are mainly characterized by the utilized robot velocity, either maximum speed in FS or compliant collaborative speed in PFL mode (*MACS*). Consequently, the robot operating speeds mainly influence the cycle time. The *MACS* is mainly characterized by robot position, sensor sensitivity, attached weight, and additional padding on the lowest level. As a result, the following factors can be considered as the primary technical influencing factors on the economic feasibility: labor release grade, annual output deviation, execution time in FS and/or PFL mode, interaction grade α , robot maximum speed, robot position, sensor sensitivity, attached weight, and additional padding. By this, RQ 2 has been thoroughly answered. In the following chapter, a practical use case application will further validate these results.

To answer research questions RQ 3 and RQ 4, suitable methods were developed based on logical deduction, simulation, and empirical measurement studies. The respective procedures proposed in the previous chapter were validated by executing them delivering the mentioned methods. Economic calculation schemes can be derived by structuring the net present value in its single factors, as described before. The gripping feasibility information of a workpiece or workpiece spectrum can be frontloaded by conducting studies on different robot and gripper models by varying the workpiece with the factors material, diameter, and length. As a result, feasible diameter-length combinations can be illustrated in a diagram. To conclude positioning and movement patterns, application-specific layouts can be discretized by analyzing relevant dimensional data, e.g., machine data. These motion patterns can be simulated considering the single positioning possibilities, operating speed, and cycle time to conclude velocity-dependent cycle times. As a result, approximation equations can be derived using statistical regression methods to frontload the cycle time information. As a critical input factor to these equations, reference values for suitable robot velocities are

required, especially for the PFL mode. With empirical measurement studies, the most critical influencing factors can be isolated and statistically evaluated to either conclude an approximation equation or to identify static reference values. By this, velocity information can be frontloaded in structured and categorized ways.

The last research question, RQ 5, cannot be answered yet. Until now, the economic structure of an automation project has been fully presented. Respective sensitivity studies on single parameters can reveal their impact on the overall profitability. In the next chapter, a real-life application is planned. Based on these practical input data, the profitability relations between the three technical alternatives are evaluated in relation to the interaction grade α .

5. Practical Verification

5.1 Use Case Overview

For verification of the proposed planning methodology, a practical use case at a middle-sized company is planned. By this, it can be demonstrated how the methodology is applied to practice and where deficits for future development lie. The customer uses a DMG MORI CTX-1250TC4A machine and plans to produce water rotors on this machine. Table 5.1 summarizes the obtained input data.

Table 5.1: Use Case Input Data for Process, Production, and Investment

Process Times [s]											
Calibration	Setup	Adjust Robot Program		Remove Chips & Fluids				Load or Unload Machine	Actuate Door	Unloading & Loading Machine	Machine Operation
$P_{1,M}$	$P_{2,M}$	$P_{3,IR}$	$P_{3,CR}$	$P_{4,M}$	$P_{4,IR,FS}$	$P_{4,CR,FS}$	$P_{4,CR,CS}$	$P_{5,M}$	$P_{6,L}$	$P_{7,M}$	$P_{8,L}$
900	900	300	300	2	1.5	2	2.5	15	5	30	120
Production Data											
Batch Size			Annual Working Time 2-shift			Annual Operator Cost for 2 workers (company side)			Value Creation per unit		
S_n [units]			W [h]			C [€]			VC [€/unit]		
50			3,440			78,604			8.91		
Investment Data [€]											
	Robot incl. control		Robot Pedestal		Double Gripper		Laser Scanners	Integration Cost	Risk Assessment Cost	Sum	
	Yaskawa GP12	Yaskawa HC10DT IP67	S-RS900	XS-RS900	Schunk PZN-plus 100	OnRobot 3FG15	SICK S3000				
CR, PFL	-	35,000	-	400	-	3,500 *2	-	5,000	5,000	52,400	
CR, HM	-	35,000	-	400	-	3,500 *2	3,000 *2	5,000	5,000	58,400	
IR	28,000	-	990	-	800 *2	-	3,000 *2	4,000	3,000	43,590	

5.2 Gripper Feasibility

In the first step, the robot-sided gripping feasibility of the use case-specific workpieces is evaluated utilizing the presented diagram showing the feasible diameter-length combinations (see Figure 4.1). POM circular blanks with a diameter of 100 mm and a length of 53 mm are used as raw material, while the processed parts are D88 mm x L50 mm. When

inserting these values into the diagram, it can be seen that both workpiece states can be gripped with both robot types. Consequently, this technical side condition is fulfilled.

5.3 Layout Discretization

The single positions are discretized in the second step by assigning them to respective fields within the proposed pattern. The spindle position b30 to b40 and spindle feed position c30 to b40 were concluded from the machine data. Since this is a very large machine, the b40 and c40 positions cannot be reached with the collaborative robot. Therefore, the b30-c30 position combination is used for calculation, and the actual movement is simulated for verification. As door position, c00 was concluded. For robot positioning, the customer preselected either AA02, A02, or B02. According to the reachability study (see Appendix 11), B02 is a suitable position for both robots to access b30 and c30. In reality, the spindle position lies between b30 and b40, making the B02 unfeasible. Iterative reachability adjustments in the simulation identified A02 as the optimal position by shifting the robot pedestal 200 mm further towards the machine. To position the material, 1,300 mm space is available between the machine and the workbench. The A03 position is used for convenient robot gripping, resulting in a 600 mm distance between the robot and material. The concluded discretized layout is illustrated in Figure 5.1.

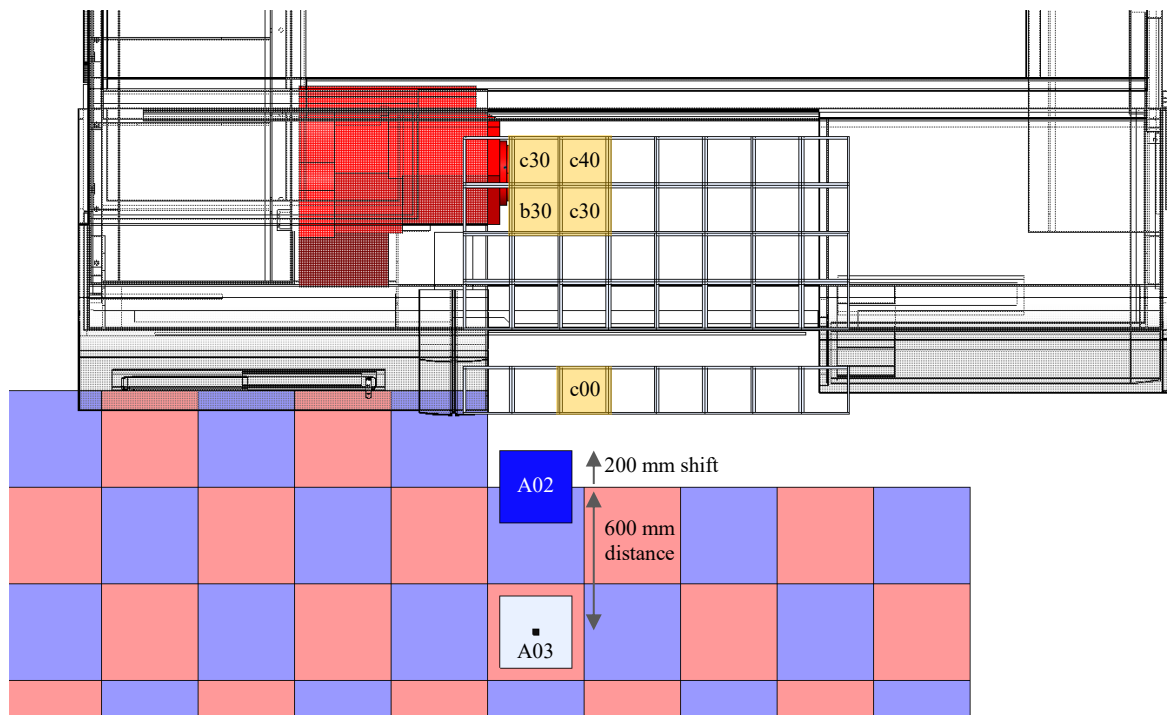


Figure 5.1: Discretized Use Case Layout

5.4 Collaborative Speed Estimation

In the third step, the maximum allowed collaborative operating speeds are preliminary determined. For the quasi-static case, the factors sensor sensitivity s , position p , and mass m are required. As a force limit, 50 N is used for optimal results. The position value is described as the relation between the distance of the occurring clamping situation and the maximum robot reach. To calculate the distance, Figure 5.2 assists.

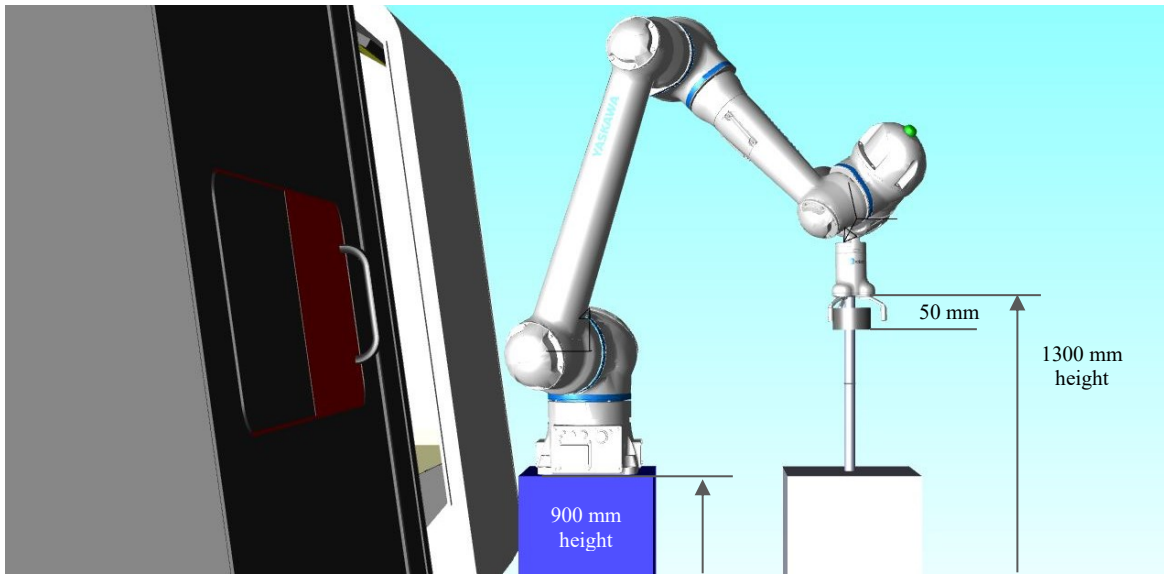


Figure 5.2: Dimensional Relations to Calculate the Position Value

The following position in percent is calculated by setting the hypotenuse ratio to the 1,200 mm reach.

$$p = \frac{\sqrt{600 \text{ mm}^2 + 350 \text{ mm}^2}}{1200 \text{ mm}} * 100 = 57.9 \% \quad (5.1)$$

As double gripper mass, including dual flange, 3.05 kg was calculated in CAD. To conclude the masses of the raw material and the machined workpiece, the volume is multiplied by the material's density.

$$m = m_{\text{Gripper}} + m_{\text{RawMaterial}} + m_{\text{MachinedWorkpiece}} \quad (5.2)$$

$$m_{\text{RawMaterial}} = \left(\frac{\pi}{4} * 10 \text{ cm}^2 * 5.3 \text{ cm} \right) * 1.41 \frac{\text{g}}{\text{cm}^3} = 587 \text{ g} = 0.587 \text{ kg} \quad (5.3)$$

$$m_{MachinedWorkpiece} = \left(\frac{\pi}{4} * 8.8 \text{ cm}^2 * 5 \text{ cm} \right) * 1.41 \frac{\text{g}}{\text{cm}^3} = 429 \text{ g} = 0.429 \text{ kg} \quad (5.4)$$

$$m = 3.05 \text{ kg} + 0.586 \text{ kg} + 0.428 \text{ kg} = 4.066 \text{ kg} \quad (5.5)$$

Based on this information, the *MACS* in mm/s for this specific situation is calculated.

$$MACS = 53.1107 + 1.15885 * 57.9 - 0.2283 * 50 - 0.4578 * 4.066 = 106.9 \text{ mm/s} \quad (5.6)$$

The empirically measured reference values are used for the transient contact cases: 80 mm/s for the workpiece edge contact with the hand and 900 mm/s in average for shoulder contact with the padded robot outer contours.

5.5 Cycle Time Estimation

In the fourth step, the cycle times are estimated using the fields b30, c30, c00, A02, and A03, leading to DSF 3 field and SFS 1 field movements. At first, the main times, including DSF 3 field, SFS 1 field, and T within the machine, are calculated (see Table 5.2).

Table 5.2: Calculated Main Times for all Robots and Operating Modes

		IR	CR, FS	CR, CS
Door-Spindle Feed (DSF) 3 Fields in y	$CT_{DSF,3y}$	0.9 s	1.25 s	1.28 s
Spindle Feed – Spindle SFS 1 Field in x	$CT_{SFS,1x}$	0.31 s	0.56 s	0.55 s
Turning within Machine	CT_T	0.61 s	0.94 s	0.94 s

Secondly, the side times are considered (see Table 5.3). Since no general modeling for the material feed-door (MFD) movement was found, this motion must be simulated. The MFD time serves as a side condition because it determines if the material can be exchanged within the machining time. Furthermore, it must be included in the process time “P5 Load or Unload Machine”. The cycle times for the turning movement above the material deposit and the MFM motion are calculated to determine an MFD threshold value. For PFL operation, robot velocities of either 80 mm/s and 106.9 mm/s were used.

Table 5.3: Calculated Cycle Times for Material Feed-Material (MFM) and Turning (T) Motions above Material Deposit

		IR	CR, FS	CR, CS
Material Feed - Material	CT_{MFM}	0.33 s	1.27 s	2.11 s
Turning above Material Deposit	CT_T	0.61 s	0.94 s	9.79 s

Then, the MFD limit is calculated with the following equations.

$$CT_{MFD,Limit} = \frac{P_{8,L} - 4 * CT_{MFM} - CT_T}{2} \quad (5.7)$$

$$CT_{MFD,Limit,IR} = \frac{120s - 4 * 0.33s - 0.61s}{2} = 59,035 \text{ s} \quad (5.8)$$

$$CT_{MFD,Limit,CR,FS} = \frac{120s - 4 * 1.27s - 0.94s}{2} = 56.99 \text{ s} \quad (5.9)$$

$$CT_{MFD,Limit,CR,CS} = \frac{120s - 4 * 2.11s - 9.79s}{2} = 50.885 \text{ s} \quad (5.10)$$

It can be seen that the MFD limit values are very high, leading to no realistic impairments of the process in terms of waiting times. This assumption has been validated by simulation, delivering 1.12 s for IR, 1.66s for CR, FS, and 13.51 s for CR, CS. On this basis, the process times “P5 Unload or Load Machine” and “P7 Unload & Load Machine” are calculated with the following equations, summarized in Table 5.4.

$$P_5 = 2 * CT_{MFM} + CT_{MFD} + 2 * CT_{DSF,3y} + 2 * CT_{SFS,1x} \quad (5.11)$$

$$P_7 = 2 * CT_{DSF,3y} + 4 * CT_{SFS,1x} + CT_T \quad (5.12)$$

Table 5.4: Calculated Side Times and Process Times P5 and P7

		IR	CR, FS	CR, CS
Load or Unload Machine	P_5	4.20 s	7.82 s	21.39 s
Unload & Load Machine	P_7	3.65 s	5.68 s	5.70 s

For further verification of the developed modules, the customer project was simulated with the exact positions for all three technical alternatives. Comparisons between approximated and exact simulated values are illustrated in Figure 5.3 for the single motion elements.

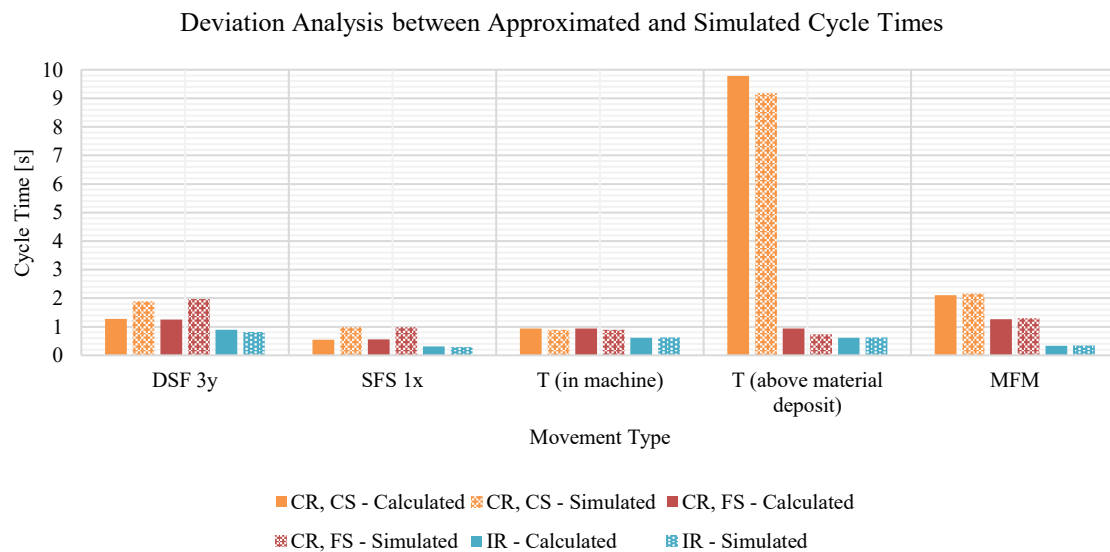


Figure 5.3: Deviation Analysis between Approximated and Simulated Cycle Times for Different Movement Types

It can be seen that the developed model is very close to reality, even though minimum input information is available at this project stage. The absolute deviation ranges from 0.73 s to 0.01 s. Generally, the DSF movement shows the most significant difference because the pattern distance differs from the actual machine. Furthermore, the collaborative robot is much more inaccurate than the industrial one, which can be traced back to the behavior consistency. While all simulation runs lay close together for the IR, the CR was behaving much more diverse. As a result, the residuals are different for both robot types, explaining this mentioned result accuracy. Generally, the model delivers satisfying results when considering the low amount of given input information at the project beginning. For rough planning and preliminary evaluation, the model accuracy contributes significantly to further planning and making sound investment decisions. This information serves as a solid base to refine and optimize the approximated results in the actual cell fine planning.

5.6 Economic Evaluation

Lastly, the three technical alternatives are evaluated regarding their economic advantageousness. Therefore, the process, production, and investment data (see Table 5.1) and the calculated values from this chapter are inserted into the presented calculation scheme. Furthermore, an observed time period T of three years and a discount factor q of 1,08 is used. The net present values were calculated depending on the interaction grade α , delivering the following diagram (Figure 5.4). This diagram shows the α -dependent progression of the single alternatives and two optimal decision areas. Up to an interaction grade of $\sim 30\%$, the industrial robot (IR) is the preferred solution because this robot has the highest velocity, stops occasionally and requires less investment. The IR profitability decreases exponentially with increasing interaction grade because the stopping time slices getting higher, making this alternative increasingly undesirable in dynamic environments. This option is absolute advantageous ($NPV > 0$) until an alpha value of $\sim 82\%$. At an interaction grade of $\sim 30\%$ or higher, the CR, PFL variant is the dominant solution. Since the operating speed difference between CR, FS and CR, CS is very small during the main times, the additional investment of the CR, HM is not beneficial if the robot operates one third of the time at collaborative speed. If the interaction grade lies between $\sim 20\%$ and $\sim 40\%$, the collaborative robot in hybrid mode (CR, HM) is very close to the CR, PFL option. Therefore, it is also a suitable option, because the robot can switch between full- and collaborative speed due to the utilization of external laser scanners. The net present value

decreases linearly and gets closer to the collaborative robot in exclusive PFL operation (CR, PFL) with increasing interaction grade because the operating speeds increasingly converge to those in the PFL operation. Consequently, the decision-maker, in this case, the customer, can make a sound investment decision based on the expected interaction grade.

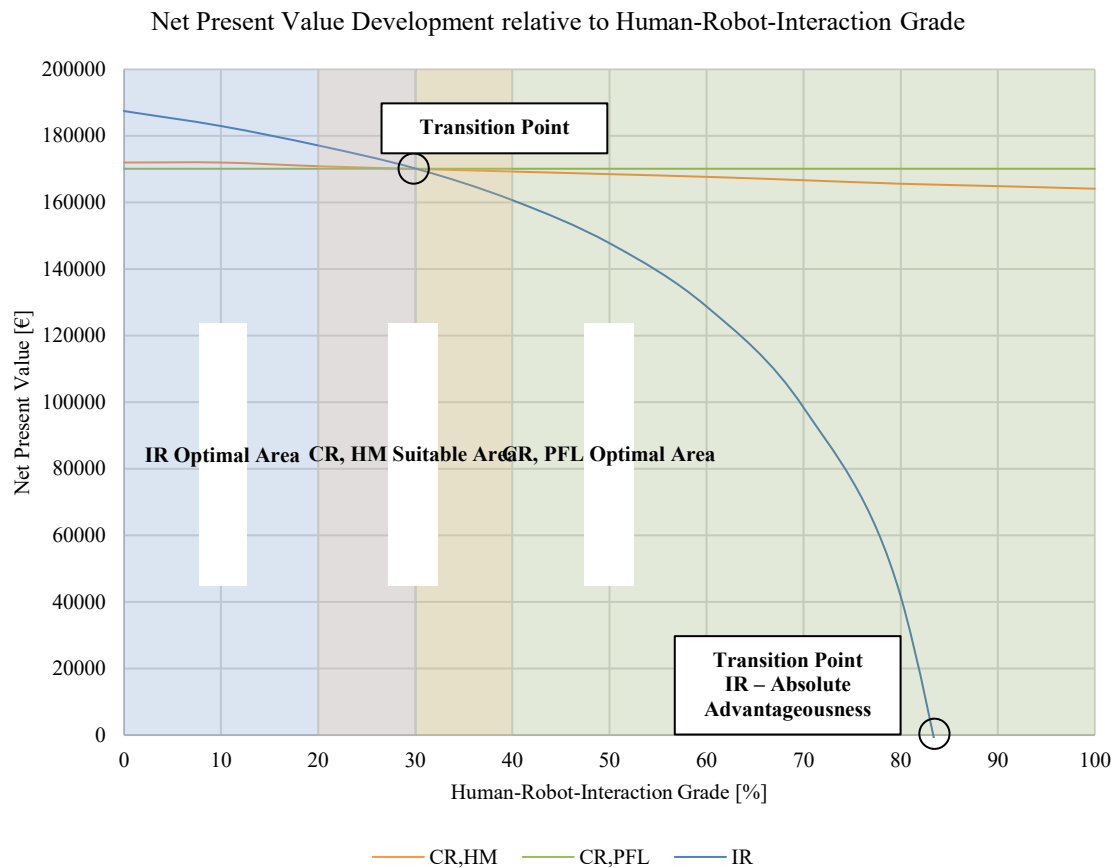


Figure 5.4: Economic Evaluation of the Three Technical Variants Collaborative Robot in Exclusive PFL Operation (CR, PFL), Collaborative Robot in Hybrid Mode (CR, HM), and Industrial Robot (IR)

This analysis has been conducted with the plain operator cost based on the employee's annual salary. For comprehensibility, a labor overhead factor of 1,7 (+ 70 %) has been added to cover the company-sided cost as well. In this case, the transition point shifts from ~30 % to ~20 %. For the IR, the absolute advantageousness shifts from ~82 % to ~88 %.

5.7 Synthesis – Practical Verification

In this chapter, the proposed planning methodology and the individual modules were applied to an actual customer project to demonstrate the applicability of the presented approach. Research question RQ 2 was further refined by calculating the net present values for the three alternatives “Industrial Robot (IR)”, “Collaborative Robot in Hybrid Mode (CR, HM)”

and “Collaborative Robot in Exclusive PFL Operation (CR, PFL).” Besides the technical influencing factors identified in the previous chapter, the significance of the interaction grade α has been highlighted. Depending on this factor, the three alternatives behave differently regarding their profitability. While the CR, PFL variant is unaffected, the CR, HM *NPV* decreases linearly, and the IR *NPV* decreases exponentially with increasing interaction. Consequently, the interaction grade can be designated as the most significant influencing factor in an HRI automation project's economic feasibility. To refine answering the research questions RQ 3 and RQ 4, the proposed modules were practically applied to demonstrate the frontloading of the required planning information to the project beginning. With only a few information available, the gripping feasibility, rough layout positioning, allowed collaborative speeds, cycle times, and economic feasibility can be approximated at an early project stage. The suitability of the proposed approach, which includes deduction of an economic calculation scheme, execution and statistical analysis of simulational and empirical studies, and the conclusion of approximation equations and reference values, has been demonstrated. The resulting accuracy is satisfying for rough planning and contributes to the information acquisition to enable the customer or system integrator to make sound investment decisions based on the available HRI technologies. A posteriori adding of additional fencing to cobot work cells can be avoided by determining the optimal robot type a priori. Lastly, research question RQ 5 was answered at the example of this specific use case. Independent of the utilized interaction modes, the collaborative robot is superior to an industrial robot at an interaction grade of $\sim 30\%$ or higher. Due to the low disturbances up to this factor, the industrial robot can show its strengths in faster operating speeds. Furthermore, the lower equipment cost plays a vital role here. With an interaction grade greater than $\sim 30\%$, the cobot in exclusive collaborative operation is the preferred solution since the increasing frequency of interruptions allows only small time slices of full-speed operation. Between $\sim 10\%$ and $\sim 30\%$ interaction grade, the cobot in hybrid mode is also a suitable alternative with nearly similar profitability as the cobot in exclusive PFL operation. With frequent interruptions of the process, the hybrid mode shows its benefits, enabling the robot to adjust its operating speed to the operator's proximity. The additional uptime can slightly compensate for the higher investment of the internal cobot and external scanner sensor technology. This result applies only to this particular use case. The decision result will also change if other products are manufactured on other machines with a different economic structure. Due to the complexity of the problem, general statements about

economic superiority cannot be made. Instead, a solution approach was presented that equips the planner with a toolset to determine and compare the advantageousness of the different alternatives to each other for a specific use case.

6. Results and Conclusions

6.1 Scientific Findings and Results

This doctoral thesis dealt with the preliminary economic evaluation of lathe machine tending systems for optimal robot technology selection. In contrast to straight economic assessment methodologies that primarily focus on the business side or straight technical planning methodologies with a strong emphasis on the technical refinements of HRI, the presented approach pursued an interdisciplinary understanding of the complexity of human-robot-interaction. According to the state of the art and research, it is currently not possible to determine all required factors at an early project stage. Instead, much relevant information is obtained within the fine planning and prototypical phase, when most of the planning efforts were already invested. Furthermore, parallel assessment of collaborative and industrial robots within a mutual evaluation scheme is lacking. In this doctoral thesis, the project profitability was set as an optimization figure influenced by various technical factors. Therefore, profound engineering knowledge is required to make sound investment decisions. To facilitate the decision process and to give the scientific and industrial community substantial assistance, five research questions were formulated at the beginning. In the following, a summary of results and concrete scientific findings (SF) is presented.

- RQ 1: By which technical systems and subsystems can lathe machine tending cells be classified in general and in particular regarding fenceless robotic systems?

The anatomy of a machine tending cell has been explained from a hardware perspective with a comprehensive overview of the technical possibilities. The overall cell has been subdivided into the systems workpiece, machine, logistic, handling, and interlinking with individual subsystems.

- *SF 1.1: Lathe machine tending cells can be generally subdivided into the systems workpiece, machine, logistics, handling, and interlinking.*
- *SF 1.2: The machine system can be subdivided into tooling machine, clamping device, and door subsystem. The individual technical options have been presented in this research.*

Generally, workpieces are classified into bars and chuck parts. While bars are usually machine-internally tended with, e.g., bar loaders, chuck parts require machine-externally solutions by actuating the machine door. As machine subsystems, the tooling machine itself

and clamping and door subsystems were classified. For this doctoral thesis, chuck part tending has been emphasized.

- *SF 1.3: In the workpiece system, bars and chuck workpieces can be distinguished. For the classification of a workpiece, different systems are available, i.e., the Opitz system.*

Besides classic LUL technologies, such as linear portal loaders, robots play a vital part in handling systems. Since the robot is only an incomplete machine, the addition of gripper and safety technology is required to develop an actual robotic application. As robot representatives, only 6-axis industrial and collaborative robots were further considered.

- *SF 1.4: For the handling system, various classical and robotized options are given. When using a robot, the manipulator, gripper, part recognition, and safety subsystem can be distinguished.*

To feed the machine with new material and to store processed workpieces, different logistic possibilities are offered.

- *SF 1.5: Logistics systems can be subdivided into material provision, processed workpiece logistic, defective workpiece logistic, and chip logistic subsystems. This research presented only options of material provision.*

To further extend the application range, robots can be interlinked to tend multiple machines.

- *SF 1.6: The interlinking system is required when tending multiple machines with one robot.*

For limitation of the observation scope, only single machine tending has been emphasized in this doctoral thesis. A specific set has been selected from the presented subsystems and technological possibilities, representing most of the available lathe machine tending systems, as illustrated in Figure 2.21.

- RQ 2: Which technical alternatives are available to implement human-robot collaboration, and how do they affect the economic feasibility? What are the main technical influencing factors on the economic feasibility of an automation project?

The four modes of collaboration, SRMS, HG, SSM, and PFL, were further examined regarding human-robot interaction and fenceless production systems. As a result, only SRMS and PFL under the addition of full-speed operation (FS) are used. By adding external safety devices, such as laser scanners, the system can detect the presence or absence of an

operator for proximity-based adjustment of the robot velocity. By considering and combining the presented collaboration modes, three technical alternatives were concluded.

- *SF 2.1: The following technical alternatives were identified:*
 - 1) *Collaborative Robot in Exclusive PFL Operation (CR, PFL),*
 - 2) *Collaborative Robot in Hybrid Mode (CR, HM), and*
 - 3) *Industrial Robot (IR).*
- *SF 2.2: When using the CR, PFL option, the robot always operates in collaborative mode, achieving only low to medium operating speeds and cycle times. This solution is unaffected by its environment and eventual process interruptions by entering operators. The equipment cost of the cobot is higher due to internal sensors, while external safety devices are spared.*
- *SF 2.3: When using the CR, HM option, the robot works in hybrid mode by switching between full- and collaborative speed. Therefore, this solution reacts to its environment by adjusting the operating speed according to the operator's proximity to achieve the situation-optimal speed. This is the most advanced and most investment-intensive solution since additional equipment costs for internal and external sensors must be considered.*
- *SF 2.4: When using the IR option, the robot works only at full speed when no operator is around. In the case of field violation, a safety-rated monitored stop is required. Therefore, this solution is most profitable at low interaction grades. While the robot cost is comparatively lower due to lacking internal sensors, external sensors must be mandatorily added to enable fenceless operation.*
- *SF 2.5: The utilization and combination of HRI modes, depending on the used robot technology, is crucial for economic feasibility. Therefore, the human-robot-interaction grade α is a crucial factor by setting the modes into ratio to each other.*

The robot's ability to grip and handle the gripper-jaw-workpiece combination must be assessed as a feasibility condition.

- *SF 2.6: The gripping ability of the robot-gripper system for the considered workpiece spectrum is an essential technical feasibility criterion.*

The behavior specifics and characteristics of each mode were extensively described throughout this doctoral thesis. To determine the main technical influencing factors on the economic feasibility of an automation project, the respective economic structure has been

analyzed in detail under utilization of the net present value as the target figure. Since investment data are use-case specific and cash-out flows were assumed equal for both robot types, only cash-in flow determination was emphasized. The labor release grade and the annual output deviation were set as the two most significant cash-in flow factors.

- *SF 2.7: The cash-in flows can be calculated using the labor release grade and the annual output deviation. These two factors are mainly influenced by the achieved cycle times based on the operating speeds.*

These factors are mainly influenced by the execution times in the respective operation modes depending on the achieved robot velocity. While FS speeds are stated in the robot manufacturer's technical specifications, the maximum allowed collaborative speed in PFL mode is based on different factors. For quasi-static contact cases, especially the robot pose, sensor sensitivity and attached weight play a role. Transient contacts are mainly influenced by the robot's outer contour and the use of additional padding.

- *SF 2.8: While the full speed is stated in the robot's manual, the maximum allowed collaborative speed must be measured according to ISO/TS 15066 for quasi-static and transient contact cases. The MACS is highly affected by robot pose, sensor sensitivity, and attached weight for quasi-static cases, while the robot outer contours and additional padding are the main factors for transient cases.*

The mode-dependent operating speeds and respective cycle times are set into a ratio to each other by the interaction grade, which describes the time slice in which an operator stands close to the robot in its operating area. During this time, a potential collaboration or collision is possible. Therefore, the industrial robots stop (SRMS) while the cobot continues working at a safe, collaborative speed (PFL). The strong influence of the interaction grade has been demonstrated within the use case. Another factor that indirectly biases the presented main factors is the use-case-specific layout that determines the positions of the main spindle, doors, material, and robot and ultimately defining the required movements. Furthermore, the ratio between manual setup and automated LUL times is essential since these times build the basis for the *LRG* calculation.

- *SF 2.9: The robot pose mainly depends on the machine's dimensions and the robot's positioning. Furthermore, the velocity-cycle time behavior for different positions is much more consistent for the industrial robot compared to the collaborative one.*

➤ *SF 2.10: Main technical influencing factors on the economic feasibility are the layout, cycle time, operating speeds, and the interaction grade.*

- RQ 3: Which methods are currently suitable to determine these influencing factors, and how can they be transferred to a frontloading planning approach?

Various available methods have been presented in the state of the art and research to determine these single factors. Firstly, the handling and gripping feasibility can be determined using the payload and gripping diagrams provided by the robot and gripper manufacturers. Modeling the individual situation in CAD delivers the mass properties that can be inserted into payload simulation software tools to assess the payload utilization of the single robot axis. In this doctoral thesis, exemplary simulations on different robot and gripper models and workpiece materials were conducted by iterating the part lengths at predefined diameter values. A diameter-length diagram has been concluded with a database that frontloads all required information to the project beginning. Instead of time-consuming calculation, modeling, and simulation activities, the planner can use this simple tool to read out if the individual situation is feasible or not.

➤ *SF 3.1: The gripper feasibility is currently determined with CAD and payload simulation tools. For frontloading, iterative simulations of predefined robot-gripper-workpiece combinations can be conducted to build a database and illustrate the workpieces' diameter-length combinations in a suitable diagram.*

Secondly, layout planning is usually conducted under the utilization of classical factory planning methods, especially with the triangulation method as a basic positioning pattern. New scientific approaches also pick up this field-discretization. As a proposed method, the general lathe machine structure of 34 DMG MORI models has been analyzed. By three-dimensional modeling and layering, a machine pattern in a suitable resolution has been concluded. Additionally, material and robot position fields were added. This method enables the planner to simply break down the problem by assigning entity positions to individual fields within the developed pattern. On this basis, the required positions can be concluded that must be reached by the robot. As a result, all required layout information is frontloaded to the project's beginning.

➤ *SF 3.2: The rough layout is currently developed with factory planning methods, such as the triangulation method. The layout can be refined with the iterative*

shifting of the elements' positions or optimization algorithms. For frontloading, application-specific 2D or 3D patterns can be derived from analyzing the machine dimensions to discretize the positioning problem.

Since the positions have been discretized, the robot movement and the respective cycle times can be modeled in the next step. For manual processes, MTM, REFA, or digital human models are suitable methods. Robots are primarily simulated in offline programming software, while RTM is not established in the industry. Due to the high simulation effort of classic planning procedures, a simplified method has been proposed that considers the most significant factors to frontload them to the project beginning. Therefore, the overall LUL process has been broken down into single motion elements based on process analysis and modeling. Each motion element's velocity-dependent cycle time behavior has been collected with exemplary simulations of all position combinations. As basis served a reachability study by iterating the robot positioning. Statistical analysis with nonlinear regression delivered approximation equations for the preliminary calculation of the cycle time related to the robot operating speed. To determine the robot velocity in PFL mode, ISO/TS 15066 requires force and pressure measurements for quasi-static contacts and provides equations for the transient case with the option of measuring. Scientific approaches such as virtual collision models or virtual sensors are under development and not accepted by the standards body yet. To facilitate the measurement procedure and preliminary determine realistic operating speeds, empirical studies were conducted for both contact cases. A suitable measurement setup has been developed to measure the most significant influencing factors for the quasi-static contact. A broad database served as the basis for statistical analysis with multiple linear regression that delivered an approximation equation. The difference between theoretically calculated and empirically measured compliant velocity values has been analyzed for the transient case. Since state of the art prescribes a fixed installation of the measurement device that does not represent the practical collision properties, one measurement setup provided by the Fraunhofer IFF has been tested, and another one has been developed. The results of these tests contribute to the development of the ISO/TS 15066 revision by providing valuable test data. Furthermore, the effect of additional padding on the velocity result has been analyzed by using neoprene and foam material. Based on these experiments, reference values for realistic compliant operating speeds have been presented. As a result, the planner already has a rough speed estimation at the beginning of the project.

- *SF 3.3: The robot manufacturer specifies the full speeds, while the maximum allowed collaborative speed is currently determined by measurement and/ or calculation. For frontloading, exemplary measurement studies delivers a solid database for statistical evaluation to conclude a regression equation and/ or reference values.*

By inserting the speed values into the cycle time approximation equations, suitable standard values for each motion element were concluded, similar to the MTM system for manual execution but with different motion types. Because neither the velocity-dependent cycle time behavior nor compliant speed values were available up to now, such standard values were not producible. With the developed modules, a procedure has been presented to evaluate such values for collaborative robots.

- *SF 3.4: The cycle time is currently identified with MTM, REFA, or digital human models for manual processes and RTM and offline programming tools for robotized execution. For frontloading, a set of exemplary simulations of the single motions can be conducted to deduce the velocity-dependent cycle time behavior. With regression equations, the cycle time can be calculated based on the considered speed.*

To receive an average value that represents a realistic cycle time in mixed operation (combination of different collaboration modes), the interaction grade α has been used. Currently, this factor can be derived from the parallel digital robot and human modeling, virtual reality experiments, empirical or experience values. New determination methods for this variable were not presented in this doctoral thesis. Instead, an α -dependent net present value diagram has been presented for all three technical alternatives within the practical validation. On this basis, solid decision advantageousness assistance is given to the planner to choose an appropriate solution.

- *SF 3.5: The interaction grade is currently not considered in research or industry. In this doctoral thesis, no concrete determination method has been formulated. Instead, the influence of the interaction grade on the profitability of the single technical alternatives has been illustrated in a suitable diagram.*
- RQ 4: How can an integrated rough planning methodology be derived that provides all required economic information at the beginning of the project?

In order to develop such an integrated rough planning methodology that provides all required economic information at the beginning of the project, reverse engineering has been used. The single planning contents have been isolated and rearranged in a logical order by observing the classic robot cell planning procedure. By delineating and focusing on the use case, the system complexity has been limited to make the problem manageable. As a planning basis, a general process pipeline serves, which has been further subdivided into single movement modules. Based on this process, a use case-specific economic calculation scheme has been derived. Single approximation modules have been developed with a wide interdisciplinary methodological variety consisting of analytical, simulational, empirical, experimental, and statistical methods. Stepwise execution of each planning step hands over the relevant information to the next stage, leading to a comprehensive planning methodology that builds up one another. Since the most critical information is available, a rough cell concept regarding technical feasibility and profitability can be developed with minimal information.

- *SF 4.1: An integrated rough planning methodology can be derived with a reverse engineering approach that is based on a use case-specific process pipeline and economic calculation scheme. System consideration of the single planning contents delivers approximation modules that add up to a comprehensive planning approach.*
- RQ 5: Under which circumstances is a collaborative robot economically superior to an industrial one in lathe machine tending applications?

Overall, it can be stated that assessing an HRI cell's economic structure is a complex problem that is dependent on various influencing factors. General statements about the superiority of collaborative robots over industrial ones are complex due to the individuality of each case. In the practical validation section, it has been demonstrated that at low interaction grades, the industrial robot is the most profitable variant, while the cobot with additional safety becomes more advantageous for the middle area, and the cobot in exclusive PFL operation is preferable for frequent interactions.

- *SF 5.1: In the demonstrated use case, a collaborative robot becomes economically superior to an industrial robot at an interaction grade of ~20 % to ~30 %. The economic structure is highly individual on the use case.*

6.2 Critical Appraisal and Outlook

For the sake of scientific depth and comprehensibility, different assumptions and limitations were defined in this doctoral thesis, which is critically discussed in the following. On this basis, an outlook for future research is given.

Generally, the application scope has been focused on single lathe machine tending by including only these machines and turning/ milling machining centers. Further exclusion criteria were given, e.g., regarding the machine and workpiece size. Due to the higher complexity of milling operations regarding workpiece classifications and LUL position possibilities, these applications have been excluded. In future research, the presented methodology can be applied to milling and other machining types or even other applications such as palletizing. One main reason for this limitation was the manageable workpiece spectrum in turning operations since the parts are rotationally symmetrical. Especially for the force and pressure measurements, which represent an essential part of this doctoral thesis, the isolation of the single influencing factors was only possible due to the workpiece's simplicity. Now, that fundamental research has been undertaken, more complex geometries can be analyzed in further research. Further technological options that were not included in this research are comparisons to classic machine tending possibilities and the possibilities of multi-machine tending. These limitation has been set to focus more vital on the individualities in the robot behavior. Classic MT options require a different planning sight, adding unnecessary assessment complexity regarding technical and economic consideration factors. In future research, the pros and cons of, e.g., linear or portal loaders compared to robotics automation can be analyzed. For fenceless multi-machine tending, the layout complexity is a significant challenge to solve. Especially for HRI, experiments on the compliance of the collaborative linear axis would be required. For collaborative gantry systems, a potential collision with the head is possible, increasing the complexity of the safety issue. In future research, these topics can be picked up. Only the main spindle tending has been considered for the LUL process because counter spindles require additional motion modules. As considered robot technologies, only the three presented ones with laser scanners as preferred safety measures were analyzed. Additional research is required regarding implementing other safety technologies, such as camera systems and dynamic space monitoring. SSM operation has also been excluded in this research since the zone design and speed determination are already described in the respective standards. Regarding the

interaction grade α , an additional zone would have to make a three-dimensional scenario observation necessary. Incorporating this zone and the effect of the operator's presence behavior in each of the three zones is up for future investigation, e.g., with empirical or simulation studies.

On the economic side, only one-dimensional decisions based on the net present values can be made. Additional consideration of a utility value that incorporates non-monetary factors can help to make this decision process more comprehensive in the future. For this *NPV* calculation, the cash-out flows were assumed equal for both robots, while specific characteristics regarding, e.g., space or energy consumption, have not been considered. On the other side, the cash-in flows rely only on the *LRG* and the annual output deviation. For a more realistic cell representation, further determinants can be added to this model in the future. As a reference basis for the annual output deviation, a manual execution form is used for comparison. This is only applicable if the cell is currently executed manually or if data about the potential manual operation are obtainable, e.g., with *MTM* or *REFA*. If the cell is planned from scratch, the amount of produced units in robotic execution should be used as an absolute value instead of a difference. In this case, the *LRG* cannot be applied since the reference basis is lacking.

For the robot trajectory simulations, further analysis is required as well. Additional studies on the influence of the robot's tilting installation angle can reveal further optimization potentials regarding the reachability behavior of both robots. In the gripping module, similar workpieces on both sides were presumed. In reality, the processed part has different mass properties than the raw part, leading to unsymmetrical load distribution. Furthermore, the standard jaws were considered for mass calculation for the cobot gripper, while these were excluded for the industrial gripper since this gripper requires jaw customization. This small error is negligible due to the small weight impact of the jaws on the overall result but can be analyzed in future research further. Another limitation of the gripper module is the exclusive observation if the robot can handle the gripper-jaw-workpiece combination. Gripping design studies were not executed that also incorporate the required gripping forces and jaw design regarding force or form closure.

Lastly, different limitations apply to the safety-related module. Generally, single grippers have been used for the measurements in both contact cases, while all other modules assumed double grippers since this is the preferred industrial solution. For more precise results, a conversion factor between single and dual grippers under consideration of the

installation angle should be identified in the future. Only the maximum weight has been used in the transient experiments, while the actual mass influence on the results has not been analyzed. Therefore, the identified reference values can be considered as worst-case figures. For the transient contact with the hand, a weight difference between measurement setup (3.8 kg) and defined hand mass (0.6 kg) has been identified due to design reasons. A conversion factor is required in the future for result scaling.

The most significant limitation of this doctoral thesis is the focus on the selected machine, gripper, and robot models. This focus has been defined for the sake of scientific depth by providing a detailed analysis of the robot's behavior. Especially for the force and pressure measurements, this specific robot model selection was necessary since general models are not available yet. The presented procedure can be applied to other models to generate a more extensive database of reference values in future research. On this basis, robot manufacturers receive valuable insights for product improvement in terms of R&D activities, while end-users and system integrators get a profound information base for optimal robot model selection for their specific application case.

References

- [1] Lazinica, A.; Kawai, H.: Robot Manipulators: New Achievements. InTech, 2010
- [2] Winkelhage, U.: The Digital Transformation of the Automotive Industry: Catalysts, Roadmap, Practice. Springer International Publishing, 2018
- [3] BIS Research: Global Collaborative Robot Hardware Market - Analysis & Forecast, 2016-2021 (Focus on Major Industries and Applications). 04.07.2021, <https://bisresearch.com/industry-report/global-cobots-market-report-forecast.html>
- [4] Brown, P.; Green, A.; Lauder, H.: High Skills: Globalization, Competitiveness, and Skill Formation. Oxford University Press, 2003
- [5] Wilkinson, A.; Redman, T.; Dundon, T.: Contemporary Human Resource Management: Text and Cases. Pearson, 2017
- [6] Bauer, W.; Bender, M.; Braun, M.; Rally, P.; Scholtz, O., Fraunhofer Institute for Industrial Engineering IAO: Lightweight robots in manual assembly - best to start simply! 04.07.2021, <https://www.engineering-produktion.iao.fraunhofer.de/content/dam/iao/tim/Bilder/Projekte/LBR/Studie-Leichtbauroboter-Fraunhofer-IAO-2016-EN.pdf>
- [7] Schneider, C.; Hernandez, F. J.; Suchanek, T.; Bdiwi, M.; Hutter-Mironovová, M.; Putz, M.: Hybrid Workstations: A Simultaneous Planning Method for Economic-oriented Selection between Industrial and Collaborative Robots. Robotix-Academy Conference for Industrial Robotics (RACIR), Saarbrücken, Germany, 16.07.2020, pp. 19–26
- [8] Dispan, J., Hans Böckler Stiftung: Entwicklungstrends im Werkzeugmaschinenbau 2017: Kurzstudie zu Branchentrends auf Basis einer Literaturrecherche. 27.07.2021, https://www.boeckler.de/pdf/p_fofoe_WP_029_2017.pdf
- [9] Blecker, T.; Friedrich, G.: Mass Customization: Challenges and Solution. Springer US, 2006
- [10] Khojasteh, Y.: Production Management: Advanced Models, Tools, and Applications for Pull Systems. Taylor & Francis, 2017
- [11] Autodesk; Kuka: Deciphering Industry 4.0 Part III: Smart Logistics and Mass Customization. 04.07.2021

- [12] Kuka: Ihre Produktivität gesteigert - Automation für Werkzeugmaschinen. 18.07.2021, https://www.kuka.com/-/media/kuka-downloads/imported/9cb8e311bfd744b4b0eab25ca883f6d3/industry_brochure_machine_tool_de.pdf?rev=26d7a469935a42558649f975499b0559&hash=A9DE7CC14C0A4E9C96C56C99D67E67DC
- [13] Autodesk; Kuka: Deciphering Industry 4.0 Part II: Human Robot Collaboration. 04.07.2021
- [14] Volberda, H. W.: Building the Flexible Firm: How to Remain Competitive. New York: Oxford University Press, 1998
- [15] Lödding, H.: Handbook of Manufacturing Control: Fundamentals, Descriptions, Configuration. Berlin Heidelberg: Springer-Verlag, 2013
- [16] Lehto, M. R.; Landry, S. J.: Introduction to Human Factors and Ergonomics for Engineers. CRC Press, 2012
- [17] Kubr, M.: Management Consulting: A Guide to the Profession. Geneva: International Labour Organization, 2002
- [18] PwC: The new hire: How a new generation of robots is transforming manufacturing, 2014
- [19] Deutsche Gesetzliche Unfallversicherung (DGUV): Industrie 4.0: Herausforderungen für die Prävention - Positionspaper der gesetzlichen Unfallversicherung. 04.07.2021, <http://www.dguv.de/medien/inhalt/praevention/arbeitenvierpunktnull/pospap-2-2017.pdf>
- [20] EuropeanCommission: Digital Transformation Monitor: Germany: Industrie 4.0. 04.07.2021, https://ati.ec.europa.eu/sites/default/files/2020-06/DTM_Industrie%204.0_DE.pdf
- [21] Autodesk; Kuka: Deciphering Industry 4.0 for the Engineering Company. 04.07.2021
- [22] Brunet-Thornton, R.; Martinez, F.: Analyzing the Impacts of Industry 4.0 in Modern Business Environments. IGI Global, Business Science Reference, 2018
- [23] MAV Innovation in der spannenden Fertigung, MAV: Wer einmal automatisiert hat, macht es immer wieder. 18.07.2021, <https://mav.industrie.de/automatisierung-von-werkzeugmaschinen/wer-einmal-automatisiert-hat-macht-es-immer-wieder/>

- [24] Kuka: Roboter und Maschine wachsen zusammen. Automationspraxis, 2018, <https://automationspraxis.industrie.de/branchenloesungen/metall-blech/roboter-und-maschine-wachsen-zusammen/>
- [25] Heidecker, D; Hofmann, B.: EMO Hannover 2019: Cobots - Mensch und Roboter gemeinsam zum Erfolg. Maschinenmarkt, 2019, <https://www.maschinenmarkt.vogel.de/cobots-mensch-und-roboter-gemeinsam-zum-erfolg-a-861812/>
- [26] McKinsey & Company: Industrial robotics: Insights into the sector's future growth dynamics. 18.07.2021, https://www.mckinsey.com/~/_media/McKinsey/Industries/Advanced%20Electronics/Our%20Insights/Growth%20dynamics%20in%20industrial%20robotics/Industrial-robotics-Insights-into-the-sectors-future-growth-dynamics.ashx
- [27] ISO 21919-1: Automation systems and integration - Interfaces for automated machine tending - Part 1: Overview and fundamental principles. International Organization for Standardization, 2019
- [28] ISO/TC 184: Automation systems and integration. International Organization for Standardization
- [29] ISO 11161: Safety of machinery - Integrated manufacturing systems - Basic requirements. International Organization for Standardization, 2007
- [30] ISO/ DIS 21919-2: Physical device control - Interfaces for automated machine tending - Part 2: Safety and control interface. International Organization for Standardization
- [31] Schneider, C.; Unger, H.: Methodik zur Grob-und Feinplanung von Arbeitsstationen zur Mensch-Roboter-Kooperation in hybriden Produktionssystemen. Vernetzt Planen und Produzieren (VPP), Chemnitz, Germany, 28.-29.11.2018, pp. 67–76
- [32] Andrisano, A. O.; Leali, F.; Pellicciari, M.; Pini, F.; Vergnano, A.: Hybrid Reconfigurable System design and optimization through virtual prototyping and digital manufacturing tools. International Journal for Interactive Design and Manufacturing (IJIDeM), 2012, vol. 6, pp. 17–27
- [33] Papakostas, N.; Michalos, G.; Makris, S.; Zouzias, D.; Chryssolouris, G.: Industrial Applications with Cooperating Robots for the Flexible Assembly. International Journal of Computer Integrated Manufacturing, 2011, vol. 24, no. 7, pp. 650–660

- [34] Takata, S.; Hirano, T.: Human and robot allocation method for hybrid assembly systems. *CIRP Annals*, 2011, vol. 60, no. 1, pp. 9–12
- [35] Tsarouchi, P.; Matthaiakis, A.-S.; Makris, S.; Chryssolouris, G.: On a human-robot collaboration in an assembly cell. *International Journal of Computer Integrated Manufacturing*, 2017, vol. 30, no. 6, pp. 580–589
- [36] Robotiq: The Machine Tending Playbook. 18.07.2021, <https://blog.robotiq.com/robotiq-ebook-summary-the-machine-tending-playbook>
- [37] Brecher, C.; Kürzel, A.; Herchel, M.; Matthias, B.: Portable Robot Systems for Machine Tending Tasks. 37th International Symposium on Robotics ISR 2006; 4th German Conference on Robotics Robotik, Munich, 15.05.-17.05.2006
- [38] Marvel, J. A.; Falco, J.; Marstio, I.: Characterizing Task-Based Human-Robot Collaboration Safety in Manufacturing. *IEEE Transactions on Systems, Man, and Cybernetics: Systems*, 2015, vol. 45, no. 2, pp. 260–275
- [39] Helbing, K. W.: *Handbuch Fabrikprojektierung*. Berlin Heidelberg: Springer-Verlag, 2010
- [40] Schneider, C.; Klos, M.; Bdiwi, M.; Putz, M.: Machine-To-Machine (M2M) Communication of a Mobile Robotic Platform in Machine Tending Applications. Robotix-Academy Conference for Industrial Robotics (RACIR), Liège, Belgium, 05.06.2019, pp. 1–8
- [41] Mitrofanov, S. P.: *Scientific Principles of Group Technology*. Boston Spa, Yorkshire: National Lending Library for Science and Technology, 1966
- [42] Opitz, H.: *A Classification System to Describe Workpieces: Definitions*. Pergamon Press, 1970
- [43] TNO: Miclass system. TNO Metal Research Institute Technical Center for Metalworking, 1970
- [44] Husain, M.; Leonard, R.: The Design of Standard Cells For Group Technology By The Use Of Machine Tool And Workpiece Statistics. *Proceedings of the Sixteenth International Machine Tool Design and Research Conference*, Palgrave, London, 1976, pp. 87–98

- [45] Groovers, M.; Zimmers, E.: CAD/CAM: Computer-Aided Design and Manufacturing. Pearson India, 1984
- [46] Gallagher, C. C.; Knight, W. A.: Group Technology Production Methods in Manufacture. Ellis Horwood Ltd, 1986
- [47] Jung, J.-Y.; Ahluwalia, R. S.: FORCOD: A coding and classification system for formed parts. Journal of Manufacturing Systems, 1991, vol. 10, no. 3, pp. 223–232
- [48] Wolf, A.; Steinmann, R.; Schunk, H.: Grippers in Motion: The Fascination of Automated Handling Tasks. Berlin Heidelberg: Springer-Verlag, 2005
- [49] Allen, D. K.: Classification Systems. Mechanical Engineer's Handbok: Manufacturing and Management, 2006, pp. 68–109
- [50] Ghosh, T.; Modak, M.; Dan, P.: Coding and Classification Based Heuristic Technique for Workpiece Grouping Problems in Cellular Manufacturing Systems. International Transaction Journal of Engineering, Management & Applied Sciences & Technologies, pp. 53–722011
- [51] Dantale, A.: A Group Technology Based Approach for Application of Design for Manufacturability (DFM) Rules. Master Thesis, Nagpur University, Department of Mechanical Engineering Of the College of Engineering and Applied Science, Nagpur, India, 2015
- [52] Schneider, C.; Suchanek, T.; Klos, M.; Hutter-Mironovová, M., COVR: COVR Project RACOS: Risk Assessment Metamodel for Cobot Operating Speed Determination - Milestone 1. 27.07.2021, <https://covrfilestorage.blob.core.windows.net/documents/casestories%5CRACOS%20Milestone%201.pdf>
- [53] Neugebauer, R.: Werkzeugmaschinen: Aufbau, Funktion und Anwendung von spanenden und abtragenden Werkzeugmaschinen. Berlin Heidelberg: Springer Vieweg, 2012
- [54] Weck, M.: Werkzeugmaschinen 1: Maschinenarten und Anwendungsbereiche. Springer Vieweg, 2005
- [55] Radhakrishnan, P.; Subramanyan, S.; Raju, V.: CAD/CAM/CIM. New Age International, 2008

- [56] Borangiu, T.; Thomas, A.; Trentesaux, D.: Service Orientation in Holonic and Multi-Agent Manufacturing Control. Berlin Heidelberg: Springer-Verlag, 2012
- [57] Smith, G. T.: CNC Machining Technology: Volume 1: Design, Development and CIM Strategies. London: Springer-Verlag, 1993
- [58] Schuhbauer, A.; Kroh, R.: Roboter arbeitet mit Drehmaschine Hand in Hand. Maschinenmarkt, 2008, <https://www.maschinenmarkt.vogel.de/roboter-arbeitet-mit-drehmaschine-hand-in-hand-a-146466/>
- [59] MD 2006/42/EC: Machinery Directive. European Parliament and the Council, 2006
- [60] DIN EN 61800-5-2: Adjustable speed electrical power drive systems - Part 5-2: Safety requirements - Functional. Deutsches Institut für Normung, 2017
- [61] ISO 13849-1: Safety of machinery - Safety-related parts of control systems - Part 1: General principles for design. International Organization for Standardization, 2016
- [62] Macdonald, D.: Practical Machinery Safety. Newnes, 2004
- [63] Löwe, B.: Maschinenschutztüren und die Maschinenrichtlinie 2006/42/EG: Tür zu, dann läuft's. 18.07.2021, <https://www.all-electronics.de/automatisierung/tuer-zu-dann-laeuft.html>
- [64] Heisel, U.; Klocke, F.; Uhlmann, E.; Spur, G.: Handbuch Spanen. Carl Hanser Verlag GmbH Co. KG, 2014
- [65] Weck, M.: Werkzeugmaschinen 4: Automatisierung von Maschinen und Anlagen. Springer Vieweg, 2006
- [66] Hesse, S.: Lexikon Handhabungseinrichtungen und Industrierobotik. expert Verlag, 1995
- [67] Kief, H. B.; Roschiwal, H. A.; Schwarz, K.: CNC-Handbuch: CNC, DNC, CAD, CAM, FFS, SPS, RPD, LAN, CNC-Maschinen, CNC-Roboter, Antriebe, Energieeffizienz, Werkzeuge, Industrie 4.0, Fertigungstechnik, Richtlinien, Normen, Simulation, Fachwortverzeichnis. Carl Hanser Verlag GmbH Co KG, 2017
- [68] Consiglio, S.; Gelingier, G.; Weinert, N.: Development of Hybrid Assembly Workplaces. CIRP Annals, 2007, vol. 56, no. 1, pp. 37–40

- [69] Bullinger, H.-J.; Lung, M. M.: Planung der Materialbereitstellung in der Montage. Vieweg+Teubner Verlag, 2013
- [70] Schneider, M.: Lean Factory Design: Gestaltungsprinzipien für die perfekte Produktion und Logistik. Carl Hanser Verlag GmbH & Company KG, 2021
- [71] HALTER CNC Automation B.V.: HALTER LoadAssistant®. 27.07.2021, <https://maskintek.dk/wp-content/uploads/2020/11/HALTER-Brochure-2017-EN.pdf>
- [72] Pawellek, G.: Ganzheitliche Fabrikplanung: Grundlagen, Vorgehensweise, EDV-Unterstützung. Berlin Heidelberg: Springer Vieweg, 2014
- [73] Bambynek, A.: Flurfreie Fördersysteme im automatisieren Materialfluss. Doctoral Thesis, Technische Universität München, Fakultät für Maschinenwesen, Lehrstuhl für Fördertechnik Materialfluss Logistik, München, Germany, 2001
- [74] DMG MORI: MULTISPRINT-Baureihe. 27.07.2021, https://media.dmgmori.com/media/epaper/multisprint_de/epaper/multisprint_de.pdf
- [75] ABB: IRB 6620LX improves productivity. 27.07.2021, https://search.abb.com/library/Download.aspx?DocumentID=ROB0199EN_B&LanguageCode=en&DocumentPartId=&Action=Launch
- [76] Motoman Robotics Europe AB: MOTOMAN: Robotised machine tending. 27.07.2021, <https://docplayer.net/101529932-Motoman-robotised-machine-tending.html>
- [77] Nof, S. Y.: Handbook of Industrial Robotics. John Wiley & Sons, Inc., 1999
- [78] PwC: Roboter im deutschen Maschinenbau: Einsatzgebiete, Anforderungen und Auswirkungen. 18.07.2021, <https://www.pwc.de/de/industrielle-produktion/assets/pwc-studie-roboter-im-deutschen-maschinenbau.pdf>
- [79] Wilson, M.: Implementation of Robot Systems: An Introduction to Robotics, Automation, and Successful Systems Integration in Manufacturing. Butterworth-Heinemann, 2014
- [80] International Federation of Robotics (IFR): Robot Report Articulated Robots by Applications and Industry. IFR Report, 2019

- [81] Verband Deutscher Maschinen-und Anlagenbau (VDMA): Industrieroboter in Deutschland 2019: Marktdaten und Einsatz von Robotern 2018, Prognosen 2019. VDMA Report, 2019
- [82] Automationspraxis: Universal Robots feiert Meilenstein: 50.000 Cobots verkauft. 27.07.2021, <https://automationspraxis.industrie.de/news/universal-robots-feiert-meilenstein-50-000-cobots-verkauft/>
- [83] Fraunhofer Institute for Industrial Engineering IAO: Lightweight robots in manual assembly - best to start simply! 09.07.2021, http://publica.fraunhofer.de/eprints/urn_nbn_de_0011-n-4151114.pdf
- [84] Schneider, C., Yaskawa Europe GmbH: Automated laboratory tests with robots. 27.07.2021, https://www.yaskawa.eu.com/header-meta/news-events/article/automated-laboratory-tests-with-robots_n10067
- [85] Schneider, C.: Roboter übernehmen Nachtschicht im Labor. Prozesstechnik Online, 2020, <https://prozesstechnik.industrie.de/pharma/roboter-uebernehmen-nachtschicht-im-labor/>
- [86] Schneider, C.; Sonnenberg, V.: Roboter entlasten Personal durch automatisierte Labortests. Maschinenmarkt, 2020, <https://www.maschinenmarkt.vogel.de/roboter-entlasten-personal-durch-automatisierte-labortests-a-917819/>
- [87] Schneider, C.: Gemeinsames Arbeiten von Mensch und Maschine in einer Prüfzelle. messtec drives Automation E-Special Robotik, no. 29, p. 82021, https://issuu.com/ernst-und-sohn/docs/e-special_robotik_mda0421?fr=sYTJmMTEzODQ2Mjc
- [88] Deutsche Gesetzliche Unfallversicherung (DGUV): Industrie 4.0 - Kollaborierende Roboter (80168). Fachzeitschrift für Prävention, Rehabilitation und Entschädigung, no. 32015, https://forum.dguv.de/issues/archiv/2015/02_DGUV_Forum_3_2015.pdf
- [89] CoboticsWorld: The Cobot Comparison Tool. 04.07.2021, <https://www.coboticsworld.com/cobot-comparison-tool/>
- [90] ISO 10218-2: Robots and robotic devices - Safety requirements for industrial robots - Part 2: Robot systems and integration. International Organization for Standardization, 2011
- [91] Zhang, D.: Parallel Robotic Machine Tools. Springer US, 2010

- [92] Ravani, B.: CAD BAsed Programming for Sensory Robots. Berlin Heidelberg: Springer-Verlag, 1988
- [93] Shen, Y.: System für die Mensch-Roboter-Koexistenz in der Fließmontage. Doctoral Thesis, Technische Universität München, Lehrstuhl für Betriebswissenschaften und Montagetechnik, München, Germany, 2015
- [94] Michalos, G.; Makris, S.; Tsarouchi, P.; Guasch, T.; Kontovrakis, D.; Chryssolouris, G.: Design considerations for safe human-robot collaborative workplaces. *Procedia CIRP*, 2015, vol. 37, pp. 248–253
- [95] Gurgul, M.: Industrial robots and cobots: Everything you need to know about your future co-worker. Michal Gurgul, 2018
- [96] Zaeh, M. F.: Enabling Manufacturing Competitiveness and Economic Sustainability: Proceedings of the 5th International Conference on Changeable, Agile, Reconfigurable and Virtual Production (CARV 2013), Munich, Germany, October 6th-9th, 2013. Switzerland: Springer International Publishing, 2014
- [97] Makris, S.: Cooperating Robots for Flexible Manufacturing. Springer International Publishing, 2021
- [98] ISO 10218-1: Robots and robotic devices - Safety requirements for industrial robots - Part 1: Robots. International Organization for Standardization, 2011
- [99] Onnasch, L.; Maier, X.; Jürgensohn, T.: Mensch-Roboter-Interaktion - Eine Taxonomie für alle Anwendungsfälle. *baua: Fokus*, 2016
- [100] Thiemermann, S.: Direkte Mensch-Roboter-Kooperation in der Kleinteilemontage mit einem SCARA-Roboter. Doctoral Thesis, Universität Stuttgart, Fakultät für Maschinenbau, Institut für Industrielle Fertigung und Fabrikbetrieb, Stuttgart, Germany, 2005
- [101] Helms, E.: Roboterbasierte Bahnführungsunterstützung von industriellen Handhabungs- und Bearbeitungsprozessen. Doctoral Thesis, Universität Stuttgart, Institut für Industrielle Fertigung und Fabrikbetrieb, Stuttgart, Germany, 2006
- [102] Spillner, R.: Einsatz und Planung von Roboterassistenz zur Berücksichtigung von Leistungswandlungen in der Produktion. Doctoral Thesis, Technische Universität

- München, Lehrstuhl für Werkzeugmaschinen und Betriebswissenschaften, München, Germany, 2014
- [103] Bdiwi, M.; Pfeifer, M.; Sterzing, A.: A new strategy for ensuring human safety during various levels of interaction with industrial robots. *CIRP Annals. Manufacturing Technology*, 2017, vol. 66, no. 1, pp. 453–456
- [104] Schweidler, P.; Tausch, A.; Oehme, A.; Jürgensohn, T., Bundesanstalt für Arbeitsschutz und Arbeitsmedizin (baua): MRI-Szenarien einfach klassifizieren mit der Kontext-Person-Roboter-Heuristik „KOPROH“. 27.07.2021, https://www.baua.de/DE/Angebote/Publicationen/Fokus/KOPROH.pdf?__blob=publicationFile&v=4
- [105] Gopinath, V.; Ore, F.; Johansen, K.: Safe Assembly Cell Layout through risk assessment - An Application with Hand Guided Industrial Robot. *Procedia CIRP*, 2017, vol. 63, pp. 430–435
- [106] Hesse, S.: Grundlagen der Handhabungstechnik. Carl Hanser Verlag GmbH Co. KG, 2010
- [107] Müller, R.; Franke, J.; Henrich, D.; Kuhlenkötter, B.; Raatz, A.; Verl, A.: Handbuch Mensch-Roboter-Kollaboration. Carl Hanser Verlag GmbH & Co. KG, 2019
- [108] ISO/TS 15066: Robots and robotic devices - Collaborative robots. International Organization for Standardization, 2017
- [109] ISO/DIS 10218-2: Robotics - Safety requirements for robot systems in an industrial environment - Part 2: Robot systems, robot applications and robot cells integration. International Organization for Standardization, 2020
- [110] Pilz GmbH & Co. KG: Mensch-Roboter-Kollaboration. Aber sicher! 18.07.2021, https://www.pilz.com/mam/pilz/content/uploads/flyer_solutions_for_robotics_de_2016_04_low.pdf
- [111] Dhillon, B. S.: Robot Reliability and Safety. New York: Springer-Verlag, 1991
- [112] Zhang, D.; Wei, B: Mechatronics and Robotics Engineering for Advanced and Intelligent Manufacturing. Springer International Publishing, 2017
- [113] Bajd, T.; Mihelj, M.; Lenarčič, J.; Stanovnik, A.; Munih, M.: Robotics. Springer Netherlands, 2010

- [114] Nüchter, A.: 3D Robotic Mapping: The Simultaneous Localization and Mapping Problem with Six Degrees of Freedom. Berlin Heidelberg: Springer-Verlag, 2009
- [115] Riley, F. J.: Assembly Automation: A Management Handbook. Industrial Press Inc., 1996
- [116] Kurfess, T. R.: Robotics and Automation Handbook. CRC Press, 2018
- [117] Stenerson, J.: Programmable Logic Controllers with ControlLogix. Cengage Learning, 2009
- [118] Hesse, S.; Schnell, G.: Sensoren für die Prozess- und Fabrikautomation: Funktion - Ausführung - Anwendung. Springer Vieweg, 2014
- [119] SICK AG: Safe Robotics Area Protection: OPEN ACCESS FOR SAFE PRODUCTIVITY. 27.07.2021, https://cdn.sick.com/media/docs/9/59/959/product_information_safe_robotics_area_protection_en_im0077959.pdf
- [120] Pilz GmbH & Co. KG: Safe protection zone monitoring with radar technology. 18.07.2021, https://www.pilz.com/download/open/Fly_LBK_system_1005275-ENU-01.pdf
- [121] Puls, S.: Situationsverstehen fuer die Risikobeurteilung bei der Mensch-Roboter-Kooperation. Doctoral Thesis, Karlsruher Institut für Technologie (KIT), Fakultät für Informatik, Karlsruhe, Germany, 2014
- [122] Liu, H.: Intelligent Robotics and Applications: 4th International Conference, ICIRA 2011, Aachen, Germany, December 6-8, 2011, Proceedings, Part I. Berlin Heidelberg: Springer-Verlag, 2011
- [123] Bdiwi, M.; Krusche, S.; Putz, M.: Zone-Based Robot Control for Safe and Efficient Interaction between Human and Industrial Robots. ACM/IEEE International Conference on Human-Robot Interaction (HRI), Vienna, Austria, 06.-09.03.2017, pp. 83–84
- [124] ISO 13855: Safety of machinery - Positioning of safeguards with respect to the approach speeds of parts of the human body. International Organization for Standardization, 2010
- [125] IEC 60204-1: Safety of machinery - Electrical equipment of machines - Part 1: General requirements. International Electrotechnical Commission, 2016

- [126] IEC TS 62046: Safety of machinery - Application of protective equipment to detect the presence of persons (withdrawn). International Electrotechnical Commission, 2008
- [127] Liu, H.: Robot Systems for Rail Transit Applications. Elsevier, 2020
- [128] IGI Global: Robotic Systems: Concepts, Methodologies, Tools, and Applications. IGI Global, 2020
- [129] Fumagalli, M.: Increasing Perceptual Skills of Robots Through Proximal Force/Torque Sensors: A Study for the Implementation of Active Compliance on the iCub Humanoid Robot. Springer International Publishing, 2014
- [130] Zeghloul, S.; Laribi, M. A.; Sandoval, J.: Advances in Service and Industrial Robotics: Results of RAAD. Springer International Publishing, 2020
- [131] Universal Robots: Graphic. 27.07.2021, <https://www.universal-robots.cn/media/1802259/ur10e-series-industrial-collaborative-robot.jpg>
- [132] Yaskawa Europe GmbH: Graphic. 27.07.2021, https://www.motoman.com/getmedia/6b426370-1d6b-45c4-b0d6-f5896b7fe992/HC10XP_500.jpg.aspx
- [133] Fanuc: Graphic. 27.07.2021, https://www.fanuc.co.jp/en/product/robot/image/robotcr35ia_large.jpg
- [134] Bosch Rexroth: Graphic. 27.07.2021, https://dc-mkt-prod.cloud.bosch.tech/xrm/media/global/home/product_group/production-assistants-apas_640x360.jpg
- [135] Blue Danube: Graphic. 27.07.2021, https://www.airskin.io/hubfs/product_staubli_header_visual@2x.jpg
- [136] Juschkat, K.: Forscher erfinden neues Robotergelenk. Elektrotechnik Automatisierung, 2020, <https://www.elektrotechnik.vogel.de/forscher-erfinden-neues-robotergelenk-a-959559/>
- [137] Bdiwi, M.: Integrated Sensors System for Human Safety during Cooperating with Industrial Robots for Handing-over and Assembling Tasks. Procedia CIRP, 2014, vol. 23, pp. 65–70
- [138] Hornung, L., Hochschule Karlsruhe, University of Applied Science: Ergebnisse der Umfrage Mensch-Roboter-Kollaboration. 21.08.2021, <https://www.researchgate.net/>

publication/353090533_Ergebnisse_der_Umfrage_Mensch-Roboter-Kollaboration_
<https://www.touringseu>

- [139] Yaskawa Europe GmbH: Graphic. 27.07.2021, <https://www.yaskawa.eu.com/products/robots/smart-series>
- [140] Feldmann, K.; Schöppner, V.; Spur, G.: Handbuch Fügen, Handhaben, Montieren: Handbuch der Fertigungstechnik. München: Carl Hanser Verlag, 2014
- [141] Monkman, G. J.; Hesse, S.; Steinmann, R.; Schunk, H.: Robot Grippers. Wiley, 2007
- [142] Hesse, S.; Monkman, G. J.; Steinmann, R.; Schunk, H.: Robotergreifer: Funktion, Gestaltung und Anwendung industrieller Greiftechnik. München Wien: Carl Hanser Verlag GmbH & Co. KG, 2004
- [143] Nördinger, S.: So greifen Cobots sicher und handzahn. Produktion.de, 2018, <https://www.produktion.de/trends-innovationen/so-greifen-cobots-sicher-und-handzahn-208.html>
- [144] Ropohl, g.: Eine Systemtheorie der Technik: Zur Grundlegung der Allgemeinen Technologie. München: Hanser, 1997
- [145] Schmigalla, H.: Fabrikplanung: Begriffe und Zusammenhänge. München: Hanser, 1995
- [146] Schenk, M.; Wirth, S.; Müller, E.: Fabrikplanung und Fabrikbetrieb: Methoden für die wandlungsfähige, vernetzte und ressourceneffiziente Fabrik. Berlin Heidelberg: Springer Vieweg, 2014
- [147] Enghardt, W.: Groblayout-Entwicklung und -Bewertung als Baustein der rechnerintegrierten Fabrikplanung. Düsseldorf: VDI Verlag, 1987
- [148] Grundig, C.-G.: Fabrikplanung: Planungssystematik - Methoden - Anwendungen. München: Hanser Verlag, 2015
- [149] Wiendahl, H.-P.; Reichardt, J.; Nyhius, P.: Handbuch Fabrikplanung: Konzept, Gestaltung und Umsetzung wandlungsfähiger Produktionsstätten. Carl Hanser Verlag GmbH & Co. KG, 2014
- [150] Nutzhorn, H.: Leitfaden der Arbeitsanalyse. Bad Harzburg: Verlag für Wissenschaft, Wirtschaft und Technik, 1966

- [151] Bullinger, H.-J.; Spath, D.; Warnecke, H.-J.; Westkämper, E.: Handbuch Unternehmensorganisation: Strategien, Planung, Umsetzung. Berlin Heidelberg: Springer-Verlag, 2009
- [152] Brocke, J. V.: Referenzmodellierung: Gestaltung und Verteilung von Konstruktionsprozessen. Berlin: Logos Verlag, 2003
- [153] Staud, J. L.: Geschäftsprozeßanalyse mit Ereignisgesteuerten Prozeßketten: Grundlagen des Business Reengineering für SAP R/3 und andere Betriebswirtschaftliche Standardsoftware. Berlin Heidelberg: Springer-Verlag, 1999
- [154] Kobler, M.: Qualität von Prozessmodellen: Kennzahlen zur analytischen Qualitätssicherung bei der Prozessmodellierung. Berlin: Logos Verlag, 2010
- [155] Bigga, T.; Seelig, C.: REFA und Lean Production: Eine vergleichende Analyse. ZWF - Zeitschrift für wirtschaftlichen Fabrikbetrieb, 2017, vol. 112, no. 6, pp. 382–386
- [156] Hinrichsen, S.: Was Toyota von REFA lernen kann - Ein exemplarischer Vergleich zwischen REFA-Ablaufanalyse und Toyota-Verschwendungssuche. Industrial Engineering - Fachzeitschrift des REFA-Verbandes, no. 2, pp. 4–8 2014
- [157] Liker, J. K.; Meier, D.: Toyota way fieldbook: A practical guide for implementing Toyota's 4P's. New York: McGraw-Hill, 2006
- [158] Ohno, T.; Hof, W.; Stotko, E. C.; Rother, M.: Das Toyota Produktionssystem: Das Standardwerk zur Lean Production. Frankfurt /Main: Campus-Verl., 2013
- [159] Schlick, C. M.; Bruder, R.; Luczak, H.: Arbeitswissenschaft. Berlin Heidelberg: Springer-Verlag, 2010
- [160] REFA: Industrial Engineering: Standardmethoden zur Produktivitätssteigerung und Prozessoptimierung. Hanser, 2015
- [161] Bullinger-Hoffmann, A. C.; Mühlstedt, J.: Homo Sapiens Digitalis - Virtuelle Ergonomie und digitale Menschmodelle. Springer Vieweg, 2016
- [162] Duffy, V. G.: Handbook of Digital Human Modeling: Research for Applied Ergonomics and Human Factors Engineering. Boca Raton: CRC Press, 2008
- [163] Dillmann, R.; Huck, M.: Informationsverarbeitung in der Robotik. Berlin Heidelberg: Springer Verlag, 1991

- [164] Hornung, B.: Simulation paralleler Roboterprozesse: Ein System zur rechnergestützten Programmierung komplexer Roboterstationen. Berlin Heidelberg: Springer-Verlag, 1990
- [165] Banks, J.: Handbook of Simulation: Principles, Methodology, Advances, Applications, and Practice. John Wiley & Sons, Inc., 1998
- [166] Schröter, D.: Entwicklung einer Methodik zur Planung von Arbeitssystemen in Mensch-Roboter-Kooperation. Doctoral Thesis, Universität Stuttgart, Institut für Steuerungstechnik der Werkzeugmaschinen und Fertigungseinrichtungen, Stuttgart, Germany, 2018
- [167] Choi, C. K.; Ip, W. H.: A comparison of MTM and RTM. Work Study, 1999, vol. 48, no. 2, pp. 57–61
- [168] Petzelt, D. J.: Konzept zur rechnergestützten Bestimmung von Sollzeiten in der Montageplanung. Doctoral Thesis, Technische Universität Dortmund, Fakultät für Maschinenbau, Dortmund, Germany, 2010
- [169] Reichenbach, M.: Entwicklung einer Planungsumgebung für Montageaufgaben in der wandlungsfähigen Fabrik, dargestellt am Beispiel des impedanzgeregelten Leichtbauroboters. Doctoral Thesis, Brandenburgische Technische Universität, Fakultät für Maschinenbau, Elektrotechnik und Wirtschaftsingenieurwesen, Cottbus, Germany, 2010
- [170] Zwicker, C.; Reinhart, G.: System for the Estimation of Robot Cycle Times in Early Production Planning Phase. Applied Mechanics & Materials, 2016, vol. 840, pp. 99–106
- [171] Michalos, G.; Makris, S.; Spiliotopoulos, J.; Misios, I.; Tsarouchi, P.; Chryssolouris, G.: ROBO-PARTNER: Seamless Human-Robot Cooperation for Intelligent, Flexible and Safe Operations in the Assembly Factories of the Future. Procedia CIRP, 2014, vol. 23, pp. 71–76
- [172] Zhang, P.; Bauer, S.; Sontag, T. M.: Mensch-Roboter-Kooperation in der Digitalen Fabrik: Konzept zur Planung und Absicherung. Zeitschrift für wirtschaftlichen Fabrikbetrieb (ZWF), 2017, vol. 112, 1-2, pp. 73–78

- [173] Ore, F.; Hansson, L.; Wiktorsson, M.: Method for design of human-industrial robot collaboration workstations. *Procedia Manufacturing*, 2017, vol. 11, pp. 4–12
- [174] Faulkner, L.; Earl Logan, Jr.: *Handbook of Machinery Dynamics*. CRC Press, 2000
- [175] Dinwiddie, K.: *Basic Robotics*. Cengage Learning, 2015
- [176] ISO 9283: *Manipulating industrial robots - Performance criteria and related test methods*. International Organization for Standardization, 1998
- [177] Lenarčič, J.; Wenger, P.: *Advances in robot kinematics: Analysis and design*. Springer Netherlands, 2008
- [178] Bouchard, S.: *Lean Robotics: A Guide to Making Robots Work in Your Factory*, 2017
- [179] Malik, A. A.; Bilberg, A.: Framework to Implement Collaborative Robots In Manual Assembly: A Lean Automation Approach. *Proceedings of the 28th DAAAM International Symposium, Zadar, Croatia, 08.-11.11.2017*, pp. 1151–1160
- [180] Heydaryan, S.; Bedolla, J. S.; Belingardi, G.: Safety Design and Development of a Human-Robot Collaboration Assembly Process in the Automotive Industry. *Applied Sciences*, vol. 8, no. 3442018
- [181] Kurth, J.; Wagner, M.: Neue Planungsmethodik für Anlagen mit Mensch-Roboter-Kollaboration. *Zeitschrift für wirtschaftlichen Fabrikbetrieb (ZWF)*, 2020, vol. 115, no. 10, pp. 698–702
- [182] Tsarouchi, P.; Spiliotopoulos, J.; Michalos, G.; Koukas, S.; Athanasatos, A.; Makris, S.; Chryssolouris, G.: A Decision Making Framework for Human Robot Collaborative Workplace Generation. *Procedia CIRP*, 2016, vol. 44, pp. 228–232
- [183] Michalos, G.; Spiliotopoulos, J.; Makris, S.; Chryssolouris, G.: A method for planning human robot shared tasks. *CIRP Journal of Manufacturing Science and Technology*, 2018, vol. 22, pp. 76–90
- [184] Selevsek, N.; Köhler, C.: Angepasste Planungssystematik für MRK-Systeme. *Zeitschrift für wirtschaftlichen Fabrikbetrieb (ZWF)*, 2018, vol. 113, 1-2, pp. 55–58

- [185] Ore, F.; Vemula, B. R.; Hanson, L.; Wiktorsson, M.: Human-Industrial Robot Collaboration: Application of simulation software for workstation optimisation. *Procedia CIRP*, 2016, vol. 44, pp. 181–186
- [186] Beumelburg, K.: Fähigkeitsorientierte Montageablaufplanung in der direkten Mensch-Roboter-Kooperation. Doctoral Thesis, Universität Stuttgart, Fakultät für Maschinenbau, Institut für Industrielle Fertigung und Fabrikbetrieb, Stuttgart, Germany, 2005
- [187] Dietz, S.; Oberer-Treitz, S.: Mensch-Roboter-Kooperation wirtschaftlich einsetzen. *Maschinenmarkt. MM, das Industriemagazin*, Nr. 30/31, pp. 50–55 2015
- [188] Chen, X.; Bojko, M.; Riedel, R.; Apostolakis, K. C.; Zarpalas, D.; Daras, P.: Human-centred Adaption and Task Distribution utilizing Levels of Automation. *IFAC-PapersOnLine*, 2018, vol. 51, no. 11, pp. 54–59
- [189] Casalino, A.; Cividini, F.; Zanchettin, A. M.; Piroddi, L.; Rocco, P.: Human-robot collaborative assembly: a use-case application. *IFAC-PapersOnLine*, 2018, vol. 51, no. 11, pp. 194–199
- [190] Ranz, F.; Hummel, V.; Sihn, W.: Capability-based task allocation in human-robot-collaboration. *Procedia Manufacturing*, 2017, vol. 9, pp. 182–189
- [191] Fechter, M.; Seeber, C.; Chen, S.: Integrated Process Planning and Resource Allocation for Collaborative Robot Workplace Design. *Procedia CIRP*, 2018, vol. 72, pp. 39–44
- [192] Mateus, J. E. C.; Aghezzaf, E.-H.; Claeys, D.; Limère, V.; Cottyn, J.: Method for transition from manual assembly to Human-Robot collaborative assembly. *IFAC PapersOnLine*, 2018, vol. 51, no. 11, pp. 405–410
- [193] Fasth, A.; Provost, J.; Fabian, M.; Stahre, J.; Lennartson, B.: From Task Allocation Towards Resource Allocation when Optimising Assembly Systems. *Procedia CIRP*, 2012, vol. 3, pp. 400–405
- [194] Riekeles, H.: Machinery for Europe in compliance with European Standards: A manual for enterprises to supplying machinery for Europe. DIN, 2017
- [195] ISO 14121-1: Safety of machinery - Risk assessment - Part 1: Principles. International Organization for Standardization, 2007

- [196] Gopinath, V.; Ore, F.; Grahn, S.; Johansen, K.: Safety-focussed design of collaborative assembly station with large industrial robots. *Procedia Manufacturing*, 2018, vol. 25, 503-510
- [197] RIA TR R15.806: Technical Report for Industrial Robots and Robot Systems - Safety Requirements - Testing Methods for Power & Force Limited Collaborative Applications. Robotic Industries Association, American National Standards Institute, Inc., 2018
- [198] Behrens, R.; Pliske, G., Fraunhofer IFF, Otto von Guericke University Trauma Surgery Clinic: Human-Robot Collaboration: Partial Supplementary Examination [of Pain Thresholds] for Their Suitability for Inclusion in Publications of the DGUV and Standardization, 04.07.2021
- [199] kjpargeter: Graphic. 27.07.2021, https://www.freepik.com/free-photo/human-body-frontal_1079428.htm
- [200] kjpargeter: Graphic. 27.07.2021, https://www.freepik.com/free-photo/human-body_1079429.htm
- [201] Pilz GmbH & Co. KG: Operating Manual-1005182-EN-01. 04.07.2021, https://www.pilz.com/download/open/PRMS_V110_Operat_Man_1005182-EN-01.pdf
- [202] GTE Industrieelektronik GmbH: CoboSafe CBSF: Measuring system for the testing of transient and quasi-static forces and pressure on collaborative robots. 04.07.2021, https://www.gte.de/material/EN_Flyer_Cobosafe.pdf
- [203] Pilz GmbH & Co. KG: Beiblatt PRMS 22225-DE-04. 04.07.2021, https://www.pilz.com/download/open/PRMS_Set_Supplement_22225-2EN-04.pdf
- [204] Deutsche Gesetzliche Unfallversicherung (DGUV): Collaborative robot systems: Design of systems with "Power and Force Limiting" function. 04.07.2021, https://www.dguv.de/medien/fb-holzundmetall/publikationen-dokumente/infoblaetter/infobl_englisch/080_collaborativerobotsystems.pdf
- [205] Hornung, L., Hochschule Karlsruhe, University of Applied Science: Ergebnisse der Umfrage Risikobeurteilung für Mensch-Roboter-Kollaboration (MRK). 21.08.2021, https://www.researchgate.net/publication/353182365_Ergebnisse_der_Umfrage_Risikobeurteilung_fur_Mensch-Roboter-Kollaboration_MRK

- [206] Eder, K.; Harper, C.; Leonards, Z.: Towards the Safety of Human-in-the-Loop Robotics: Challenges and Opportunities for Safety Assurance of Robotic Co-Workers. The 23rd IEEE International Symposium on Robot and Human Interactive Communication, Edinburgh, UK, 25.-29.08.2014, pp. 660–665
- [207] Svarny, P.; Rozlivek, J.; Rustler, L.; Hoffmann, M.: 3D Collision-Force-Map for Safe Human-Robot Collaboration (Preprint)2020
- [208] Haddadin, S.; Albu-Schäffer, A.; Hirzinger, G.: Safe Physical Human-Robot Interaction: Measurements, Analysis and New Insights. Robotics Research, 2010, pp. 395–407
- [209] Vemula, B.; Matthias, B.; Ahmad, A.: A design metric for safety assessment of industrial robot design suitable for power- and force-limited collaborative operation. International Journal of Intelligent Robotics and Applications, 2018, vol. 2, pp. 226–234
- [210] Weitschat, R.: Industrial Human-Robot Collaboration: Maximizing Performance While Maintaining Safety. Doctoral Thesis, Universität Rostock, Lehrstuhl für Mechatronik, Fakultät für Maschinenbau und Schiffstechnik, Rostock, Germany, 2019
- [211] Ostermann, B.: Entwicklung eines Konzepts zur sicheren Personenerfassung als Schutzeinrichtung an kollaborierenden Robotern. Doctoral Thesis, Bergische Universität Wuppertal, Fachbereich D - Architektur, Bauingenieurwesen, Maschinenbau, Sicherheitstechnik, Wuppertal, Germany, 2014
- [212] Haddadin, S.; De Luca, A.; Albu-Schäffer, A.: Robot Collisions: A Survey on Detection, Isolation, and Identification. IEEE Transactions on Robotics, 2017, vol. 33, no. 6, pp. 1292–1312
- [213] Ganglbauer, M.; Ikeda, M.; Plasch, M.; Pichler, A.: Human in the loop online estimation of robotic speed limits for safe human robot collaboration. Procedia Manufacturing, 2020, vol. 51, pp. 88–94
- [214] Kovincic, N.; Gattringer, H.; Müller, A.; Weyrer, M.; Schlotzhauer, A.; Kaiser, L.; Brandstötter, M.: A model-based strategy for safety assessment of a robot arm interacting with humans. Proceedings in Applied Mathematics & Mechanics (PAMM), 2019, vol. 19, no. 1

- [215] Shin, H.; Kim, S.; Seo, K.; Rhim, S.: A Real-Time Human-Robot Collision Safety Evaluation Method for Collaborative Robot. 3rd IEEE International Conference on Robotic Computing (IRC), Naples, Italy, 25.-27.02.2019, pp. 509–513
- [216] Yen, S.-H.; Tang, P.-C.; Lin, Y.C.; Lin, C.-Y.: Development of a Virtual Force Sensor for a Low-Cost Collaborative Robot and Applications to Safety Control. *Sensors*, 2019, vol. 19, no. 11
- [217] Lange, M.: Planungshilfe für die sichere Mensch-Roboter-Kollaboration. all-electronics, 2021, <https://www.all-electronics.de/markt/planungshilfe-fuer-die-sichere-mensch-roboter-kollaboration.html>
- [218] Götze, U.: Investitionsrechnung: Modelle und Analysen zur Beurteilung von Investitionsvorhaben. Gabler Verlag, 2014
- [219] Krischun, S.: Total Cost of Ownership und Ihre Bedeutung für das internationale Beschaffungsmanagement. Diplomica Verlag, 2009
- [220] Rappaport, A.: Creating Shareholder Value: A guide for managers and investors. New York: Free Press, 1998
- [221] Pellens, B.; Tomaszewski, C.; Weber, N.: Beteiligungscontrolling in Deutschland: Eine empirische Untersuchung der DAX-100-Unternehmen. Eschborn: Bochum Inst. für Unternehmensführung und Unternehmensforschung, 2000
- [222] Aders, C.; Afra, S.: Shareholder-Value-Konzepte: Eine Untersuchung der DAX-100-Unternehmen. Value Based Management, 2000
- [223] Rappaport, A.: Selecting Strategies that Create Shareholder Value. *Harvard Business Review*, vol. 59, pp. 139–149 1981
- [224] Bühner, R.: Das Management-Wert-Konzept: Strategien zur Schaffung von mehr Wert im Unternehmen. Stuttgart: Schäffer, Verl. für Wirtschaft und Steuern, 1990
- [225] Buijink, W.; Jegers, M.: Accounting rates of return: comment. *The American Economic Review*, vol. 79, no. 1, pp. 287–289 1989
- [226] Coenenberg, A. G.: Zur Aussagefähigkeit des Return on Investment für betriebliche Planungs- und Kontrollrechnungen. *Management International Review*, vol. 12, 2/3, 35-50 1972

- [227] Dearden, J.: The Case Against ROI Control. Harvard Business Review - HBR, vol. 47, no. 3, pp. 124–135 1969
- [228] Günther, T.: Unternehmenswertorientiertes Controlling. München: Vahlen, 1997
- [229] Solomon, E.: Return on investment: the relation of book-yield to true yield. Fall Meeting of the Society of Petroleum Engineers of AIME, New Orleans, Louisiana, 06.-09.10.1963
- [230] Vernimmen, P.; Quiry, P.; Dallochio, M.; Le Fur, Y.; Salvi, A.: Corporate Finance: Theory and Practice. Wiley, 2017
- [231] Götze, U.; Hache, B.; Schmidt, A.; Weber, T.: Methodik zur kostenorientierten Bewertung von Prozessketten der Werkstoffverarbeitung. Materialwissenschaft und Werkstofftechnik, 2011, vol. 42, no. 7, pp. 647–657
- [232] Lewis, R. J.: Activity-based Models for Cost Management Systems. Greenwood Publishing Group, 1995
- [233] Götze, U.; Schmidt, A.; Symmank, C.: Zur Analyse und Bewertung von Produkt-Prozessketten-Kombinationen der hybriden Produktion. 3. Methodenband der Querschnittsarbeitsgruppe "Energetisch-wirtschaftliche Bilanzierung" des Spitzentechnologieclusters eniPROD, 2014, pp. 21–32
- [234] Götze, U.; Zönnchen, S.: Methoden zur entwicklungsbegleitenden Bewertung von Prozessketten am Beispiel der Herstellung beschichteter Kohlestofffasern. Tagungsband zum 16. Werkstofftechnischen Kolloquium und zur 10. Industriefachtagung "Oberflächen- und Wärmebehandlungstechnik", pp. 298–311 2013
- [235] Köhler, S.; Symmank, C.; Götze, U.: Economic Evaluation of Process Chains for Hybrid Products - Concept for Managing Cost Knowledge. Procedia Manufacturing, 2017, vol. 8, pp. 587–594
- [236] Götze, U.; Schildt, M.; Mikus, B.: Mensch-Roboter-Kooperation - Interaktionsmodell der Zukunft? Tagungsband zur Innteract Conference, Chemnitz, 07.-08.05.2015, pp. 83–93
- [237] Mikus, B.; Götze, U.; Schildt, M.: Kooperation zwischen Mensch und Roboter - ein Beitrag zur nachhaltigen Produktion? Der Betriebswirt, 2016, vol. 57, no. 2, pp. 25–31

- [238] Karger, D. W.; Bayha, F. H.: Engineered Work Measurement: The principles, techniques, and data of Methods-Time Measurement, background and foundations of work measurement and Methods-Time Measurement, plus other related material. New York: Industrial Press, Inc., 1987
- [239] Leon, B.; Morales, A.; Sancho-Bru, J.: From Robot to Human Grasping Simulation. Springer International Publishing, 2014
- [240] Asplund, J.; Brile, J.: Application of Human-Industrial Robot Collaboration. Master Thesis, Chalmers University of Technology, Department of Product and Production Development, Gothenburg, Sweden, 2017
- [241] Yaskawa Europe GmbH: MOTOMAN HC10DT IP67: Human-Collaborative Robots for harsh Environments. 21.08.2021, https://www.yaskawa.eu.com/Global%20Assets/Downloads/Brochures_Catalogues/Robotics/MOTOMAN_Robots/HC10_HC10DT/Flyer_Robot_HC10DT%20IP67_RedDot_E_04.2020.pdf
- [242] Yaskawa Europe GmbH: MOTOMAN GP12: Handling & General Applications with the GP-series. 21.08.2021, https://www.yaskawa.eu.com/Global%20Assets/Downloads/Brochures_Catalogues/Robotics/MOTOMAN_Robots/GP-Series/Flyer_Robot_GP12_E_11.2020.pdf
- [243] OnRobot: Datasheet 3FG15. 21.08.2021, https://onrobot.com/sites/default/files/documents/Datasheet_3FG15_v1.4_EN.pdf
- [244] Schunk: Product Information Universal gripper PZN-plus 100. 21.08.2021, <https://schunk.com/fileadmin/pim/docs/IM0007142.PDF>
- [245] Schneider, C.; Hutter-Mironovová, M.; Klos, M.; Bdiwi, M.; Putz, M.: Collaborative or Industrial Robot? An Economic Calculation Scheme to Determine the Optimal Robot Technology in Fenceless Machine Tending (in publication). Robotix-Academy Conference for Industrial Robotics (RACIR), Birkenfeld, Germany, 22.09.2021
- [246] Niku, S. B.: Introduction to Robotics: Analysis, Control, Applications. Wiley, 2020
- [247] Siciliano, B.; Khatib, O.: Springer Handbook of Robotics. Berlin Heidelberg: Springer-Verlag, 2008

- [248] Zimmer Group: 2-JAW PARALLEL GRIPPERS: HRC-03-080663. 27.07.2021, https://www.zimmer-group.com/fileadmin/pim/MER/GD/PG/MER_GD_PG_HRC-03-080663__SEN__APD__V1.pdf
- [249] Schneider, C., COVR: COVR - Case story: Creating a Metamodel for Determining Safe Cobot Speeds. 27.07.2021, <https://covrfilestorage.blob.core.windows.net/documents/casestories/COVR%20Case%20Story%20-%20RACOS%20Yaskawa%20v4.pdf>
- [250] Schneider, C., COVR: COVR - Appendix. 27.07.2021, https://covrfilestorage.blob.core.windows.net/documents/casestories/COVR%20RACOS%20-%20Milestone%202%20Report%20-%20Appendix_compressed.pdf
- [251] Schneider, C.: Risikobeurteilung für kollaborierende Roboter geht auch einfach. MAV Tagungsreader, MAV Innovationsforum Digital Edition, 21.04.-22.04.2021, p. 40
- [252] Schneider, C.; Rahman, S.; Seizmeir, M.; Suchanek, T.; Klos, M.; Hutter-Mironovová, M., COVR: COVR Project RACOS: Risk Assessment Metamodel for Cobot Operating Speed Determination - Milestone 2. 27.07.2021, <https://covrfilestorage.blob.core.windows.net/documents/casestories/COVR%20RACOS%20-%20Milestone%202%20Report.pdf>
- [253] Schneider, C.; Seizmeir, M. M.; Suchanek, T.; Hutter-Mironovová, M.; Bdiwi, M.; Putz, M.: Empirical Analysis of Velocity Behavior for Collaborative Robots in Transient Contact Cases (in publication). 15th International Conference on Automation and Robotics (ICAR), Bangkok, Thailand, 19.-20.08.2021
- [254] Schneider, C.; Seizmeir, M.; Suchanek, T.; Hutter-Mironovová, M.; Bdiwi, M.; Putz, M.: Empirical Analysis of the Impact of Additional Padding on the Collaborative Robot Velocity Behavior in Transient Contact Cases. INSTICC. Proceedings of the 18th International Conference on Informatics in Control, Automation and Robotics (ICINCO), 06.-08.07.2021, pp. 216–223
- [255] Bosch Rexroth: Ergonomieratgeber für manuelle Produktionssysteme. 04.07.2021, https://www.fmt-utz.de/fileadmin/redakteure/inhalte/Download_Broschueren/FMT/Produktkataloge_Bosch_Rexroth/MPS_Ergonomieratgeber.pdf

- [256] Yaskawa Europe GmbH: MOTOSIm EG-VRC. 25.10.2021, https://www.yaskawa.de/Global%20Assets/Downloads/Brochures_Catalogues/Robotics/software/Flyer_Software_MotoSimEG-VRC_E_08.2017.pdf

List of Appendices

Appendix 1: Overall Machine Tending Morphology	203
Appendix 2: Specific Workpiece Criteria and Characteristics	204
Appendix 3: Logistics System Alternatives.....	205
Appendix 4: Handling System Possibilities.....	206
Appendix 5: Safety System Possibilities	207
Appendix 6: Biomechanical Threshold Values	208
Appendix 7: Proposed Damping Materials and Springs.....	209
Appendix 8: MotoSim Software Description	210
Appendix 9: Dimensional Machine Character.....	211
Appendix 10: 3D Pattern of Machine Dimensions	213
Appendix 11: Simulated Door and Spindle Positions.....	214
Appendix 12: Door-Spindle Feed (DSF) Movement 1 Field in y-Direction	215
Appendix 13: Door-Spindle Feed (DSF) Movement 2 Fields in y-Direction	217
Appendix 14: Door-Spindle Feed (DSF) Movement 3 Fields in y-Direction	219
Appendix 15: Spindle Feed-Spindle (SFS) Movement 1 Field in x-Direction.....	221
Appendix 16: Spindle Feed-Spindle (SFS) Movement 2 Fields in x-Direction	223
Appendix 17: Spindle Feed-Spindle (SFS) Movement 3 Fields in x-Direction	225
Appendix 18: Spindle Feed-Spindle (SFS) Movement 4 Fields in x-Direction	227
Appendix 19: Spindle Feed-Spindle (SFS) Movement 5 Fields in x-Direction	229
Appendix 20: Turning (T) Movement	231
Appendix 21: Material Feed-Material (MFM) Movement	233
Appendix 22: Minimum Required Speed (MRCS)	235
Appendix 23: Absolute and Relative Deviation of the MACS.....	236
Appendix 24: MACS for Workpiece Diameters 110 mm to 20 mm	237
Appendix 25: Minimal and Maximal Values for the MACS.....	238
Appendix 26: Influence of the Attached Weight on the MACS.....	239
Appendix 27: MACS for Workpiece Diameters 110 mm to 20 mm	240
Appendix 28: Absolute MIN/MAX Deviation of the MACS.....	241
Appendix 29: MACS for Workpiece Diameters 110 mm to 20 mm	242
Appendix 30: Absolute MIN/MAX Deviation of the MACS.....	243
Appendix 31: Error Analysis of Pressure by Rotating around Y at 100 mm/s.....	244

Appendix 32: MACS for Workpiece Diameters 110 mm to 20 mm (averaged).....	245
Appendix 33: MACS for Workpiece Diameters 110 mm to 20 mm (averaged).....	246
Appendix 34: MACS for Transient Case with Plane Contact	247
Appendix 35: MACS for Transient Contact with the Edge	248
Appendix 36: Occurring Forces and Pressures for Transient Edge Contact	249
Appendix 37: Coefficients for Approximation Equations	250
Appendix 38: Coefficients for Approximation Equations	251
Appendix 39: Empirically Measured MACS for Quasi-static Contact Cases	252

Appendix

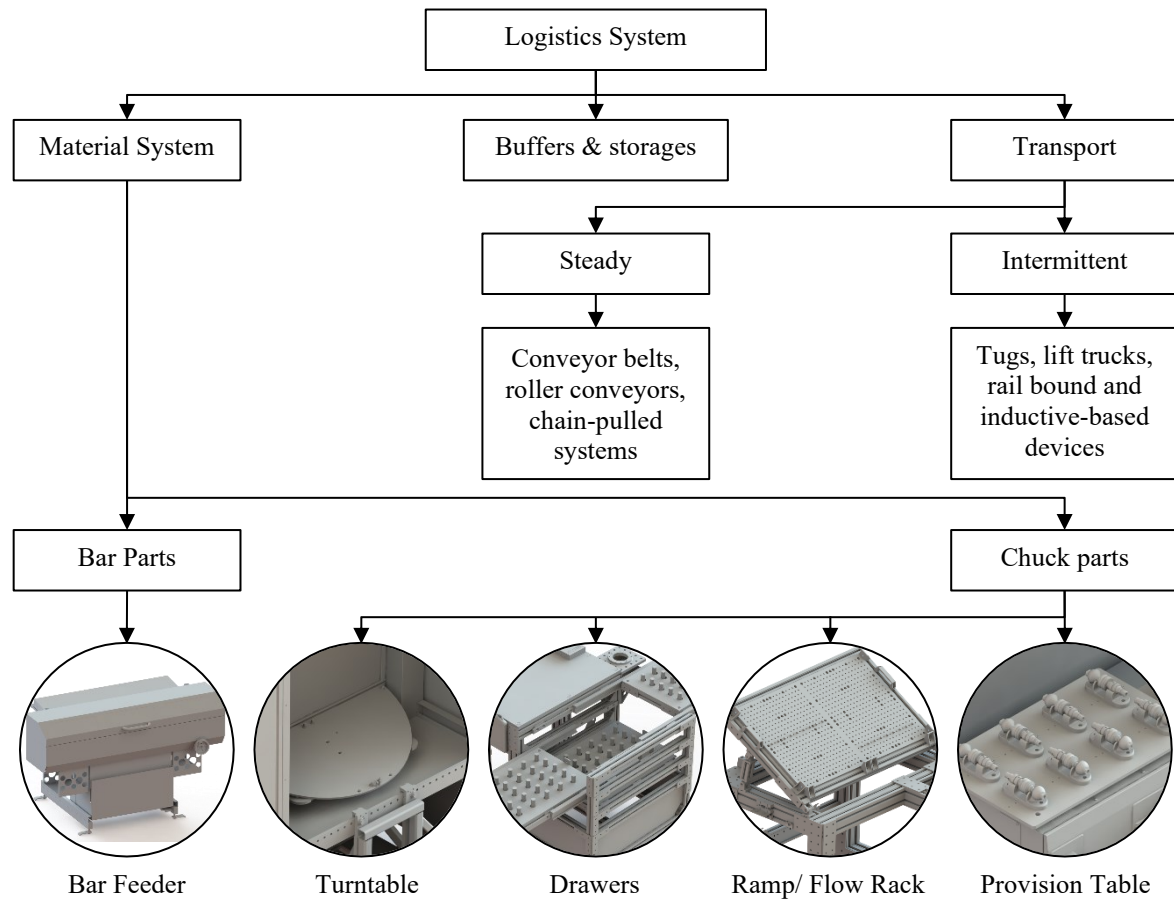
Appendix 1: Overall Machine Tending Morphology

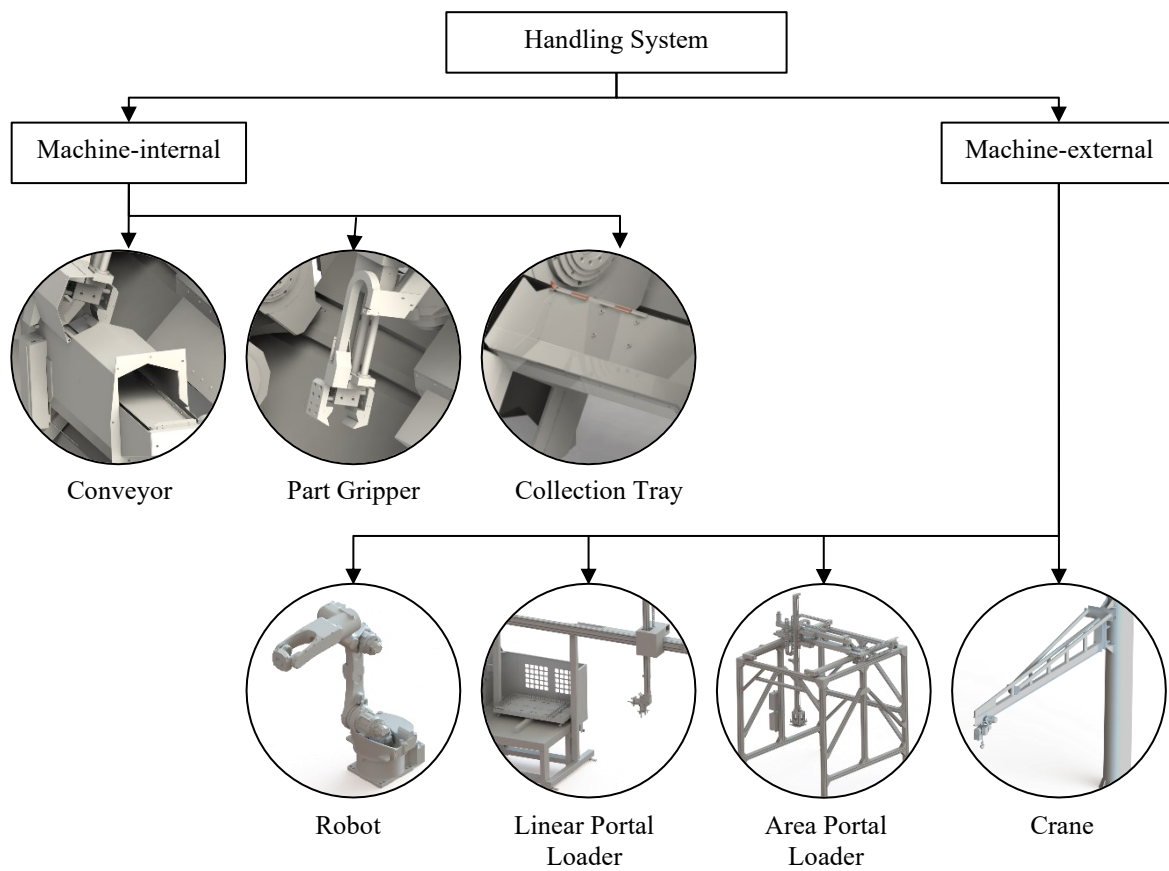
System											
Workpiece System	See Appendix 2										
Machine System	Machine Subsystem	Conventional Tooling Machine	CNC Machine	Machining Centre	Manufacturing Cell	Manufacturing System					
	Clamping Subsystem	Clamping Chuck	Collet Chuck								
	Door Subsystem	Conventional Actuation System	Actuated by robot								
Logistic System	Material System	Bar Feeder	Turntable	Drawers	Ramp/ Flow Rack	Provision Table					
	Buffers/ Storages										
	Transport	Conveyor belts	Roller conveyors	Chain-pulled systems	Tugs	Lift trucks	Rail-bound devices	Inductive-based devices			
Handling System	General	Conveyor	Part Gripper	Collection Tray	Robot	Linear Portal Loader	Area Portal Loader	Crane			
	Robot Subsystem	Single Machine Tending	Inside Machine	On Machine	On Console	On Socket					
		Multi-Machine Tending	Large robots	Turntable	Linear axis	Gantry					
		Kinematics	Parallel kinematic	SCARA	4/ 5 axis	6 axis	7 axis				
		Type	Industrial	Collaborative							
	Safety Subsystem	Software-based	Safety controller								
		Hardware-based	Robot-internal								
			Robot external	Safety Fence	Camera systems	Light curtains	2D laser scanners	3D radar scanners	Safety mats		
	Gripper Subsystem	Two jaw mechanical gripper	Three jaw mechanical gripper	Vacuum gripper							

Appendix 2: Specific Workpiece Criteria and Characteristics

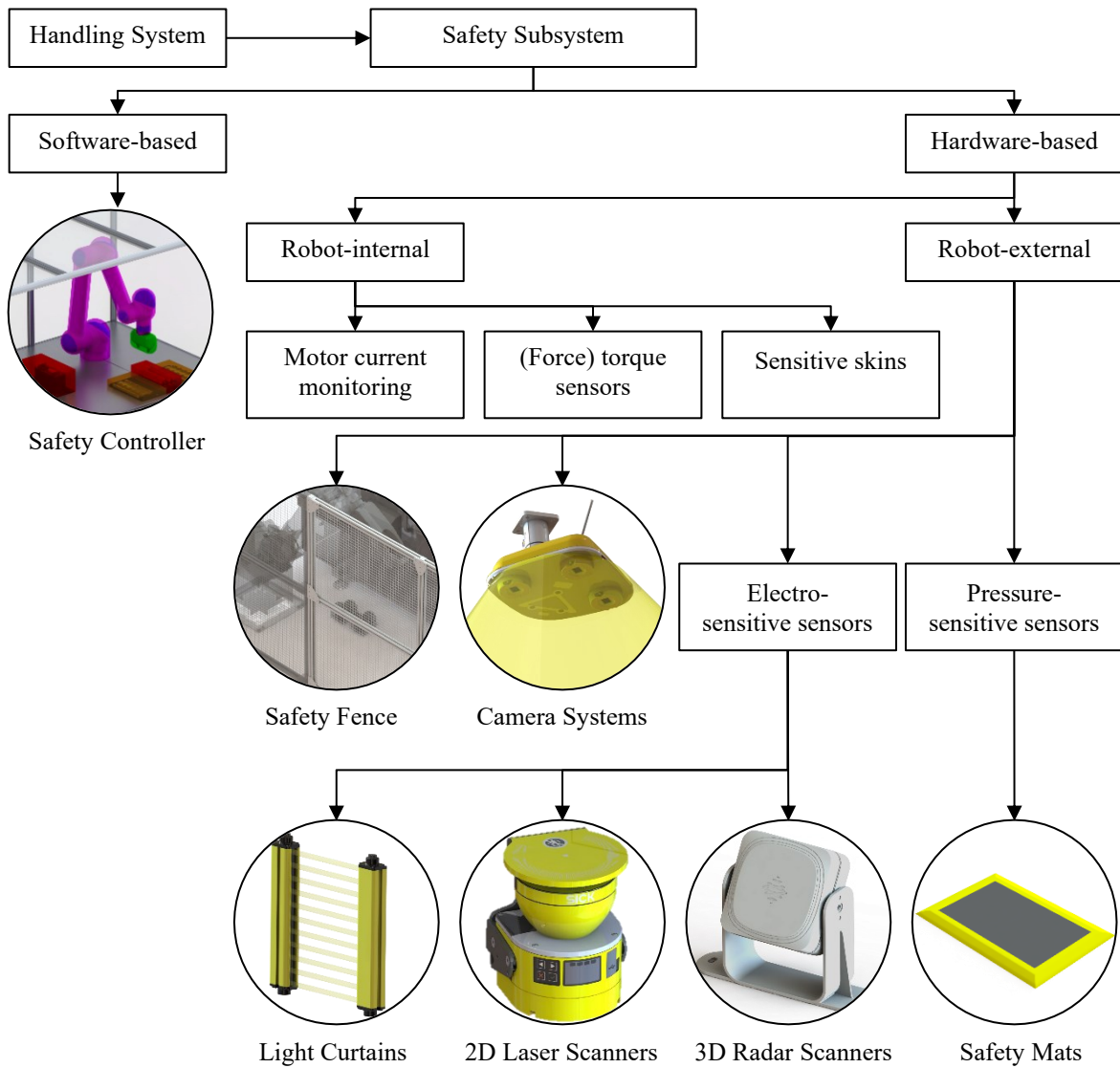
Category	General Criteria	Criteria	Specifications	Criteria characteristics
Material (Workpiece)	Specific Criteria	Base form & footprint	Round rod	-Diameter -Length
			Round tube/ pipe	-Inner diameter -Outer diameter -Length
			Square rod	-Width -Length
			Square tube/ pipe	-Inner width -Outer width -Length
		Surface quality	Low, middle, high	-Average roughness value
		Corners/ edges	Burrs, sharp	-
			Rounded	-Radius
			Chamfer	-Angle -Length
		Knurl	Knurl with axially parallel grooves (RAA), left or right knurl (RBL, RBR), left-right knurl tip-heightened (RGE), left-right knurl tip-deepened (RGV), intersection knurl tip-heightened (RKE), intersection knurl tip-deepened (RKV)	-Nominal diameter -Starting diameter -Width -Division
		Gear teeth	Spur gear teeth	-Gap width -Division -Tooth width -Tooth thickness at the head -Diameter
			Helical gear teeth, worm gear teeth	-Gap width -Division -Tooth width -Tooth thickness at the head -Shift -Diameter
		Drill Holes	Radial hole without drill pattern	-Borehole diameter -Distance from front side -Distance from the outer contour
			Radial hole with drill pattern	-Borehole diameter -Distance from front side -Pattern distance between boreholes -Distance from the outer contour
			Axial hole without drill pattern	-Diameter -Borehole diameter -Angle between reference point and borehole
			Axial hole with drill pattern	-Pattern diameter -Borehole diameter -Pattern angle between boreholes
		Spline	-	-Outer diameter -Inner diameter -Wedge width -Length
		Keyway	-	-Length -Width -Depth -Distance from front side

Appendix 3: Logistics System Alternatives



Appendix 4: Handling System Possibilities

Appendix 5: Safety System Possibilities



Appendix 6: Biomechanical Threshold Values according to [108]

Body region	Specific body area	Criteria characteristics *
Skull and forehead	1 Middle of forehead	130 130 n.a. n.a.
	2 Temple	110 130 n.a. n.a.
Face	3 Masticatory muscle	110 65 n.a. n.a.
Neck	4 Neck muscle	140 150 2 2
	5 Seventh neck vertebra	210 150 2 2
Back and shoulders	6 Shoulder joint	160 210 2 2
	7 Fifth lumbar vertebra	210 210 2 2
Chest	8 Sternum	120 140 2 2
	9 Pectoral muscle	170 140 2 2
Abdomen	10 Abdominal muscle	140 110 2 2
Pelvis	11 Pelvic bone	210 180 2 2
Upper arms and elbow joints	12 Deltoid muscle	190 150 2 2
	13 Humerus	220 150 2 2
Lower arms and wrist joints	14 Radial bone	190 160 2 2
	15 Forearm muscle	180 160 2 2
	16 Arm nerve	180 160 2 2
Hands and fingers	17 Forefinger pad dominant bodyside	300 140 2 2
	18 Forefinger pad non-dominant body side	270 140 2 2
	19 Forefinger end joint dominant bodyside	280 140 2 2
	20 Forefinger end joint non-dominant body side	220 140 2 2
	21 Thenar eminence	200 140 2 2
	22 Palm dominant body side	260 140 2 2
	23 Palm non-dominant body side	260 140 2 2
	24 Back of the hand dominant bodyside	200 140 2 2
	25 Back of the hand non-dominant bodyside	190 140 2 2
Thighs and knees	26 Thigh muscle	250 220 2 2
	27 Kneecap	220 220 2 2
Lower legs	28 Middle of shin	220 130 2 2
	29 Calf muscle	210 130 2 2
*A B C D A = Quasi-static contact, Maximum permissible pressure [N/cm ²] C = Transient contact, Maximum permissible pressure multiplier n.a. = not applicable		
B = Quasi-static contact, Maximum permissible force [N] D = Transient contact, Maximum permissible force multiplier		

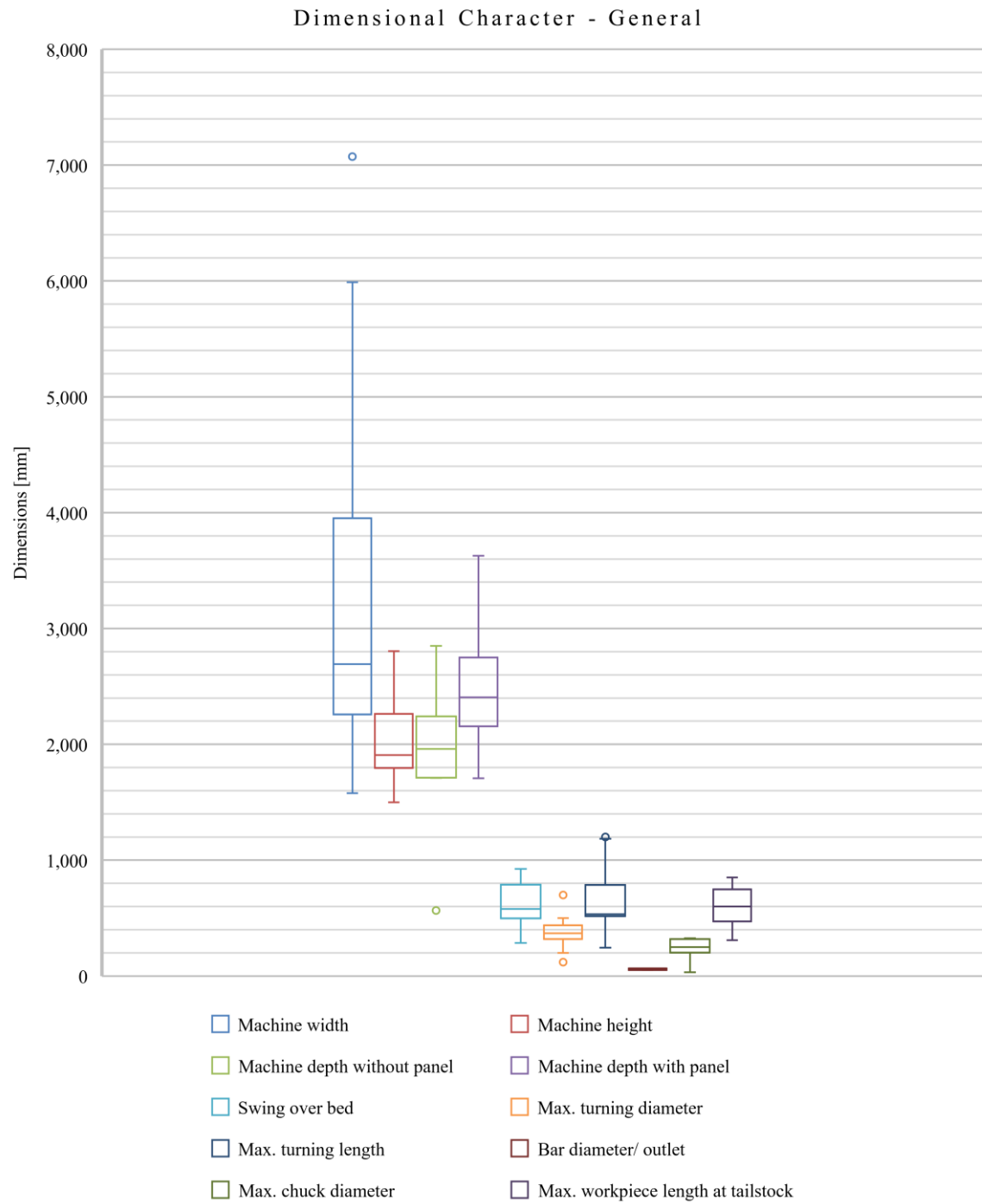
Appendix 7: Proposed Damping Materials and Springs according to [204]

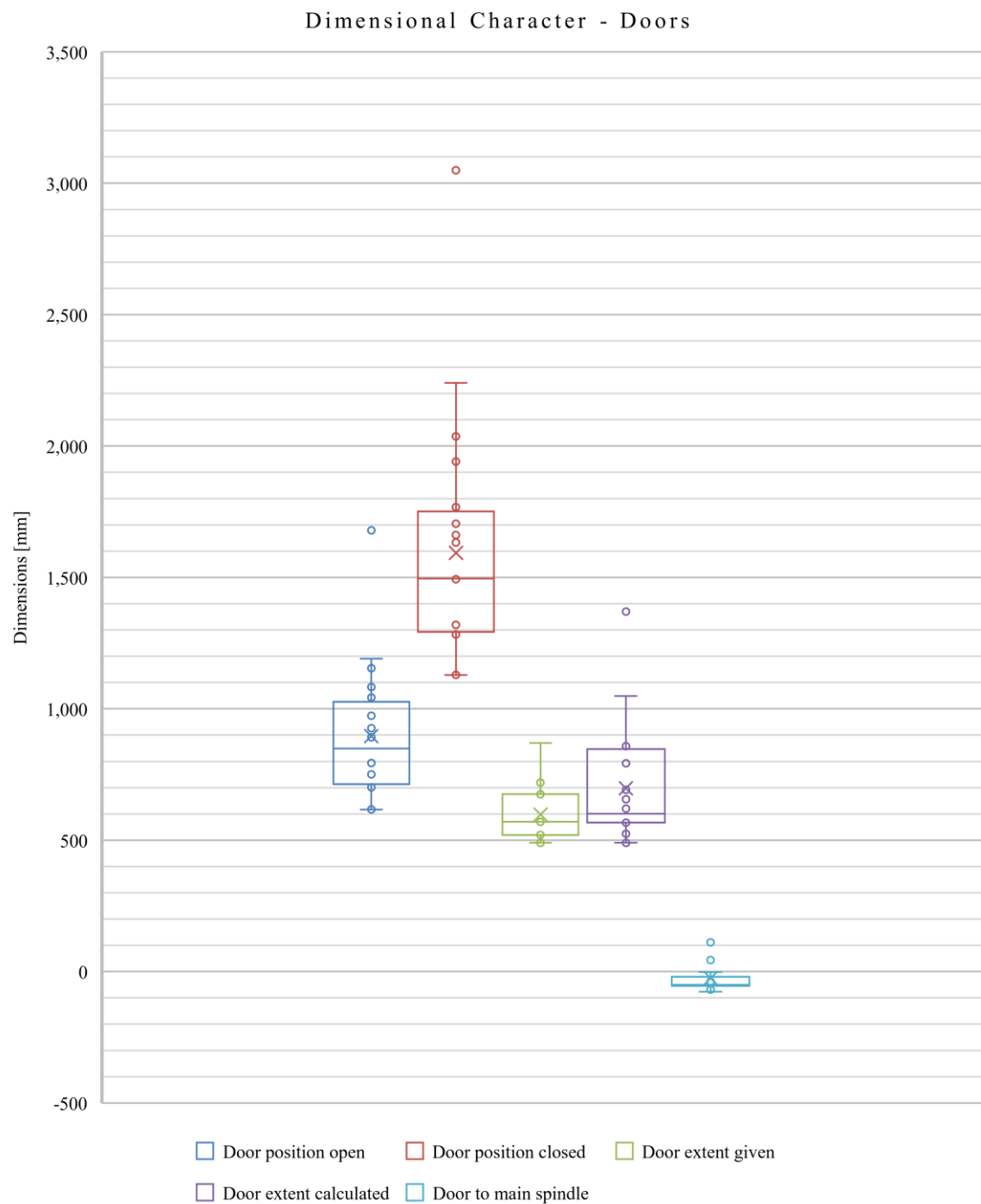
Body region	Damping material K1	Thickness [mm]	Spring K2: k [N/mm]
Hand and finger	70	7	75
Neck			50
Lower arm and wrist			40
Chest			25
Pelvis			25
Lower leg	30	14	60
Thigh and knee			50
Back and shoulders			35
Upper arm and elbow			30
Abdomen	10	21	10

Appendix 8: MotoSim Software Description [256]

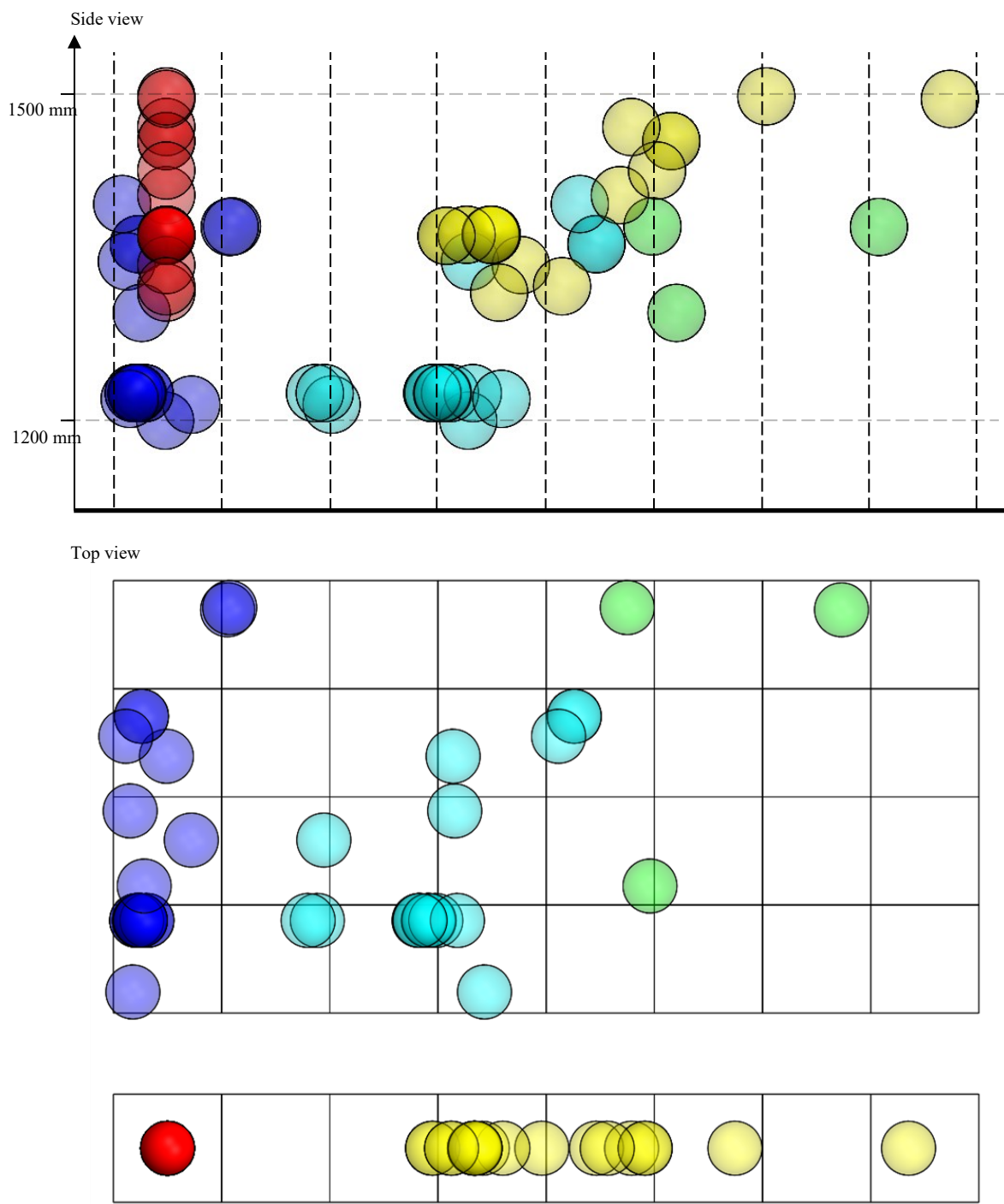
Criterion	Specification
Software Name	MotoSim EG-VRC
Type of Simulation Software	Offline Robot Simulation
Controllable Devices	Yaskawa Motoman Robots, Gantries, Tracks, Positioners
Compatible Controller Types	YRC1000, YRC1000micro, FS100, DX200, DX100, NX100
Supported Cell Import File Formats	IGES, STEP, Inventor, ProE/Creo, SolidWorks, Catia V5, SAT, Parasolid, HSF, HMF, STL, 3DS, RWX, DXF, WRML, PLY
Applicable Applications	Arc Welding, Spot Welding, Cutting, Handling, Painting
CAD/CAM Support	Yes
Safety Controller Support	Yes, Functional Safety Unit
Programming Language Support	INFORM
Applicable Simulation Contents	Motions, Collisions, Reach, Cycle Time
Robot Motion Simulation	Robot Path Calculation and Visualization
Supported Motion Types	Linear, Joint and Circular Motions
Adjustable TCP Velocities	Yes
Motion Blending	Yes, with Position Levels
Multi-Robot Support	Yes
Synchronized Robot Motion Support	Yes
Transferring Offline Program to Real Controller	Yes, without Compilation
Used Input Parameters	Robot Model, Axis Positions, Motion Points, Motion Type, Velocity, Position Level
Used Output Data	Robot Path, Reach, Singularity Assessment, Cycle Time

Appendix 9: Dimensional Machine Character



Appendix 9 (Continuation)

Appendix 10: 3D Pattern of Machine Dimensions (Top: View from Above, Bottom: View from Front, Door Open and Closed – Red, Main Spindle – Dark Blue, Counter Spindle – Green, Maximum Turning Length – Turquoise)

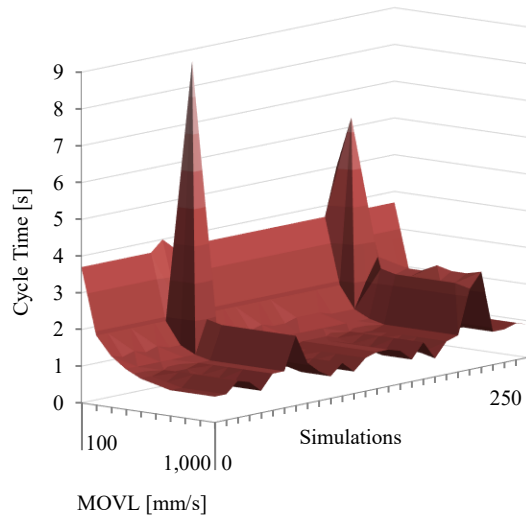


Appendix 11: Simulated Door and Spindle Positions for Collaborative (C) and Industrial (I) Robot and Stretched (S) and Top (T) Gripping

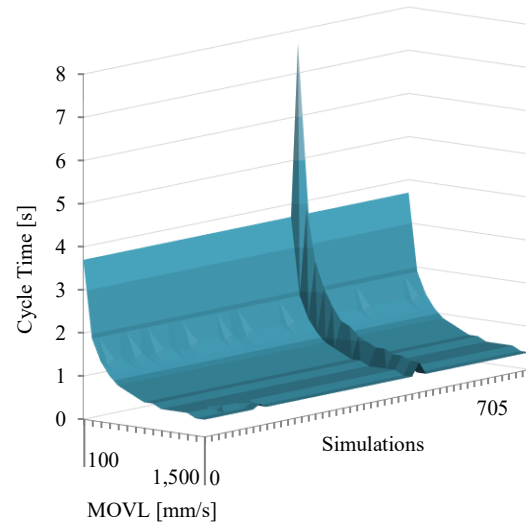
		Robot Position							
		AA01	AA02	A02	B02	C02	A03	B03	
Door Positions	b00	CT,CS	CT	CT, CS, IT, IS	CT, IT, IS	CT, IT, IS	CS, IT, IS	CS, IT, IS	
	c00	CT, CS		CT, CS, IT, IS	CT, CS, IT, IS	CT, IT, IS	IT, IS	CS, IT, IS	
	d00	CT, CS		CT, CS, IT, IS	CT, CS, IT, IS	CT, IT, IS	IS	CS, IT, IS	
	e00			CS, IT, IS	CT, CS, IT, IS	CT, IT, IS		IT, IS	
	f00			IT, IS	CT, CS, IT, IS	CT, IT, IS		IS	
	g00				IT, IS	IT, IS			
Spindle & Spindle Feed Positions	10	a10	CT, CS	CT	CT, CS, IT, IS	CT, IT, IS	CT, IT, IS	CS, IT, IS	CS, IT, IS
		b10	CT, CS	CT	CT, CS, IT, IS	CT, IT, IS	CT, IT, IS	CS, IT, IS	CS, IT, IS
		c10	CT, CS		CT, CS, IT, IS	CT, IT, IS	CT, IT, IS	IT, IS	CS, IT, IS
		d10	CT, CS		CT, CS, IT, IS	CT, IT, IS	CT, IT, IS	IS	CS, IT, IS
		e10			CS, IT, IS	CT, IT, IS	CT, IT, IS		IT, IS
		f10			IT, IS	CT, IT, IS	CT, IT, IS		IS
		g10				IT, IS	IT, IS		
	20	a20	CT, CS		CT, CS, IT, IS	CT, CS, IT, IS	IT, IS		
		b20	CT, CS		CT, CS, IT, IS	CT, CS, IT, IS	IT, IS		
		c20	CT, CS		CS, IT, IS	CT, CS, IT, IS	IT, IS		
		d20	CS		CS, IT, IS	CT, CS, IT, IS	IT, IS		
		e20			IT, IS	CS, IT, IS	IT, IS		
		f20				CS, IT, IS	IT, IS		
		g20				IT, IS	IT, IS		
	30	a30	CT, CS		CS, IT, IS	CS, IT, IS			
		b30	CT, CS		CS, IT, IS	CS, IT, IS			
		c30	CS		IT, IS	CS, IT, IS			
		d30			IS	IT, IS			
		e30				IT, IS			
		f30				IS			
		g30							
	40	a40	CS						
		b40	CS						
		c40							
		d40							
		e40							
		f40							
		g40							

Appendix 12: Door-Spindle Feed (DSF) Movement 1 Field in y-Direction for Collaborative (CR) and Industrial Robot (IR) – Simulation Results, Statistical Analysis, and Modeling

Behavior - DSF 1 Field - CR



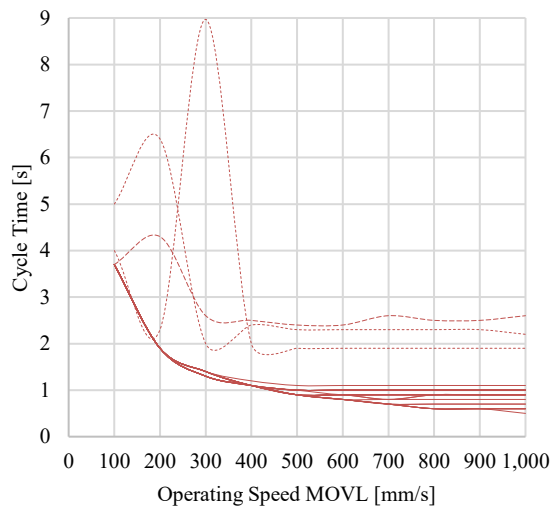
Behavior - DSF 1 Field - IR



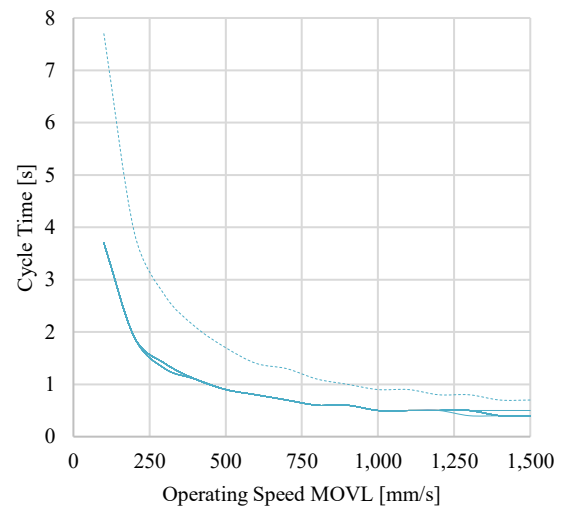
Outliers CR: b00-b10-A03-S, d00-d10-B03-S, e00-e10-A02-S

Outliers IR: e00-e10-B02-T

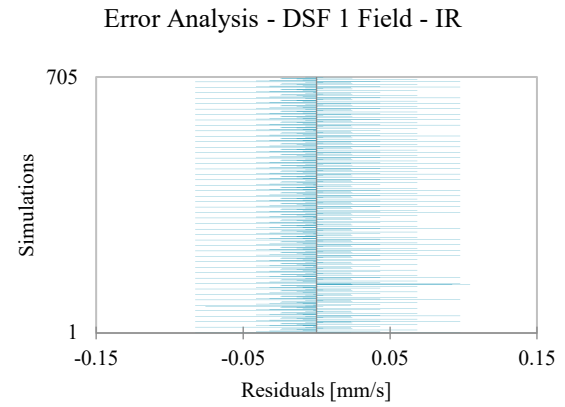
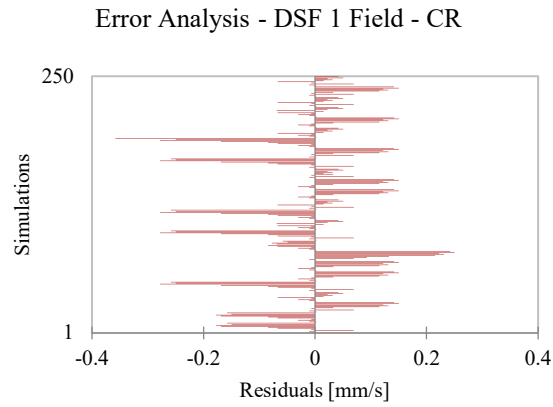
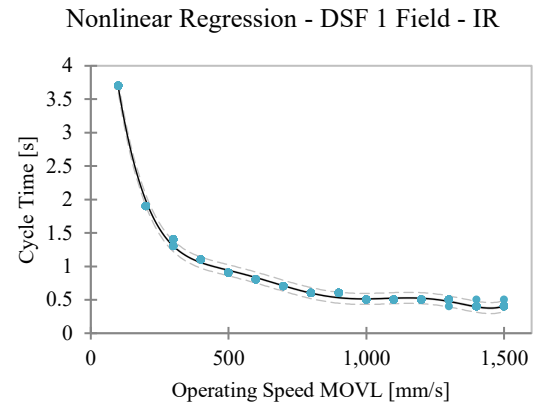
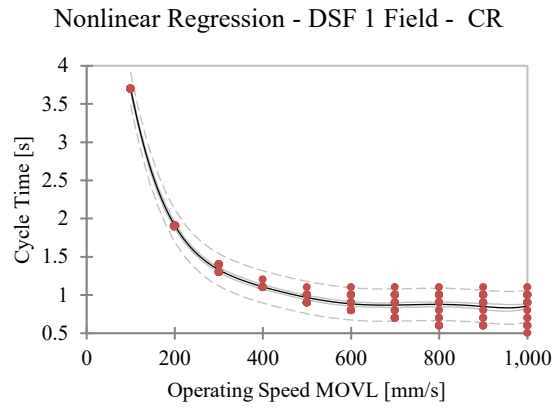
Outliers - DSF 1 Field - CR



Outliers - DSF 1 Field - IR



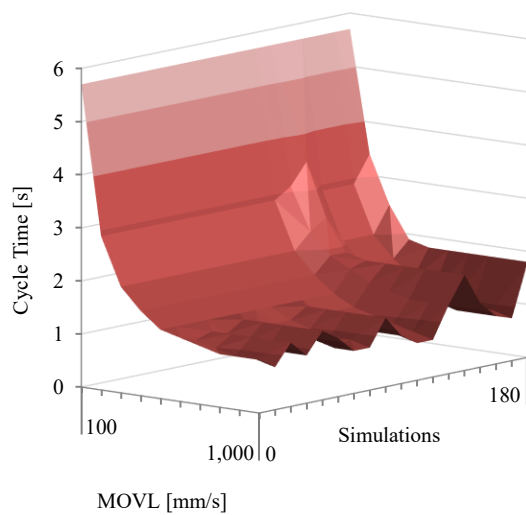
Appendix 12 (Continuation)



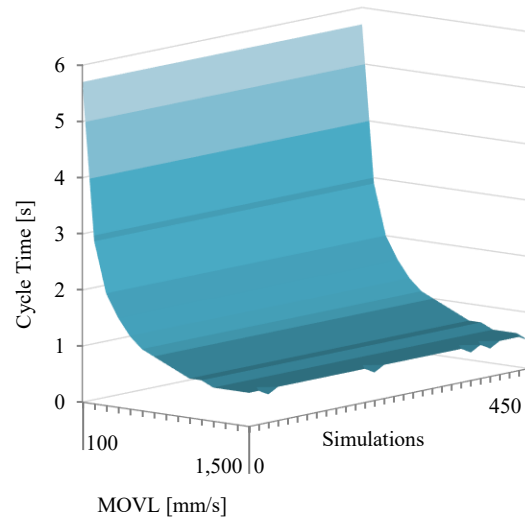
	n	a	b	c	d	e	f
$CT_{DSF,1y,CR}$	8.57481	$-7.41726 \cdot 10^{-2}$	$3.19283 \cdot 10^{-4}$	$-7.41317 \cdot 10^{-7}$	$9.50144 \cdot 10^{-10}$	$-6.30266 \cdot 10^{-13}$	$1.68612 \cdot 10^{-16}$
$CT_{DSF,1y,IR}$	7.34645	$-5.09959 \cdot 10^{-2}$	$1.69766 \cdot 10^{-4}$	$-2.93905 \cdot 10^{-7}$	$2.72008 \cdot 10^{-10}$	$-1.27406 \cdot 10^{-13}$	$2.37002 \cdot 10^{-17}$

Appendix 13: Door-Spindle Feed (DSF) Movement 2 Fields in y-Direction for Collaborative (CR) and Industrial Robot (IR) – Simulation Results, Statistical Analysis, and Modeling

Behavior - DSF 2 Fields - CR

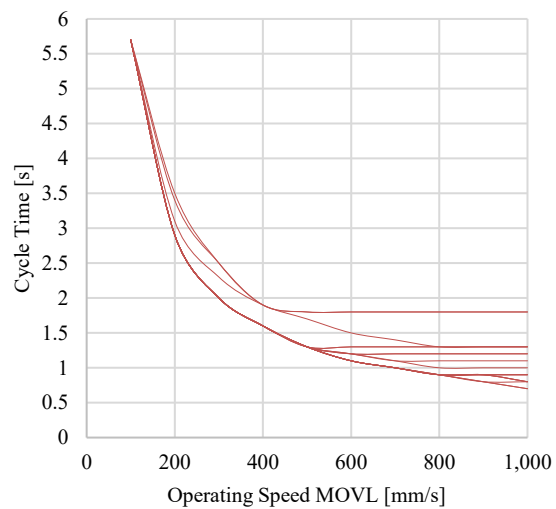


Behavior - DSF 2 Fields - IR

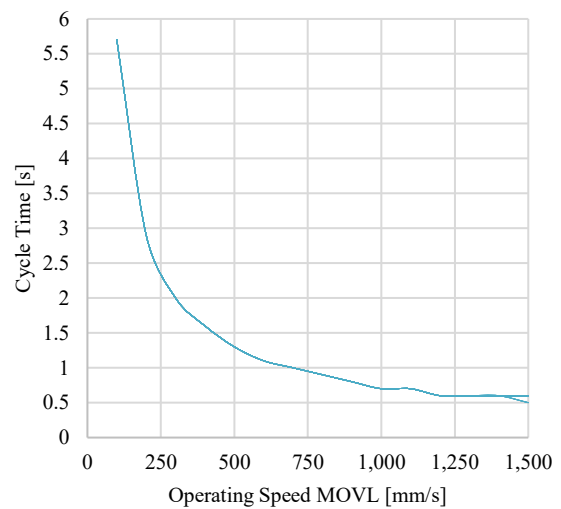


Outliers: none

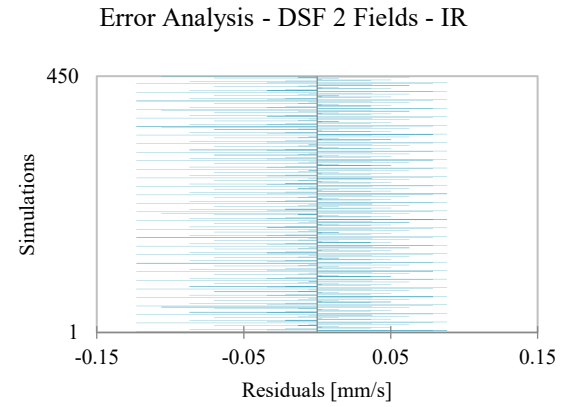
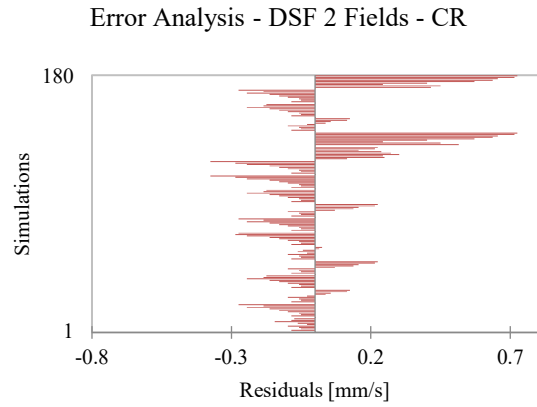
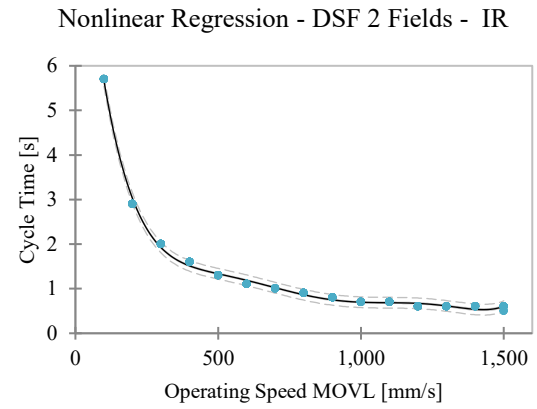
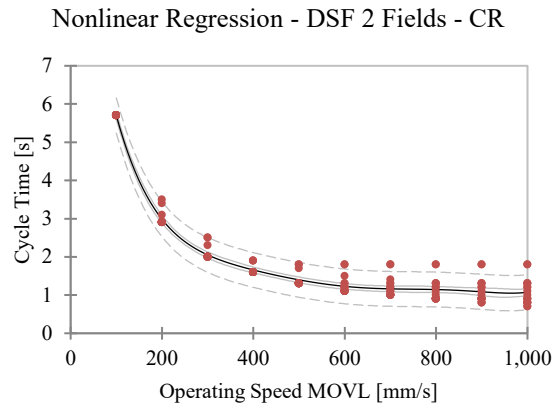
Outliers - DSF 2 Fields - CR



Outliers - DSF 2 Fields - IR



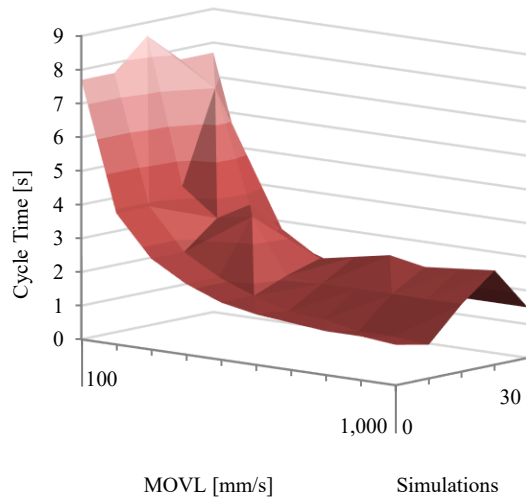
Appendix 13 (Continuation)



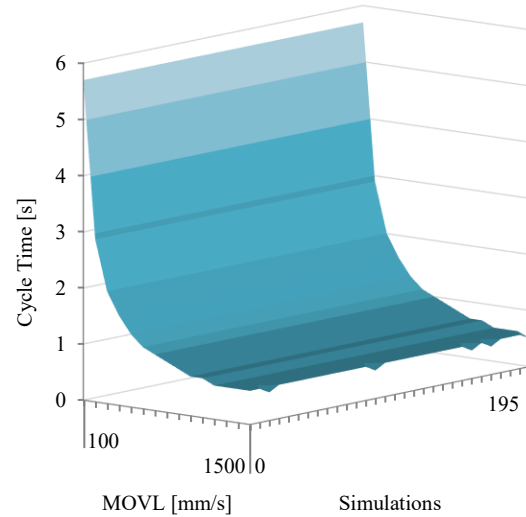
	n	a	b	c	d	e	f
$CT_{DSF,2y,CR}$	12.8989	-1.08737 $\times 10^{-1}$	4.60601 $\times 10^{-4}$	-1.05986 $\times 10^{-6}$	1.34826 $\times 10^{-9}$	-8.88205 $\times 10^{-13}$	2.36109 $\times 10^{-16}$
$CT_{DSF,2y,IR}$	11.2204	-7.64469 $\times 10^{-2}$	2.46576 $\times 10^{-4}$	-4.14682 $\times 10^{-7}$	3.74702 $\times 10^{-10}$	-1.72309 $\times 10^{-13}$	3.16358 $\times 10^{-17}$

Appendix 14: Door-Spindle Feed (DSF) Movement 3 Fields in y-Direction for Collaborative (CR) and Industrial Robot (IR) – Simulation Results, Statistical Analysis, and Modeling

Behavior - DSF 3 Fields - CR



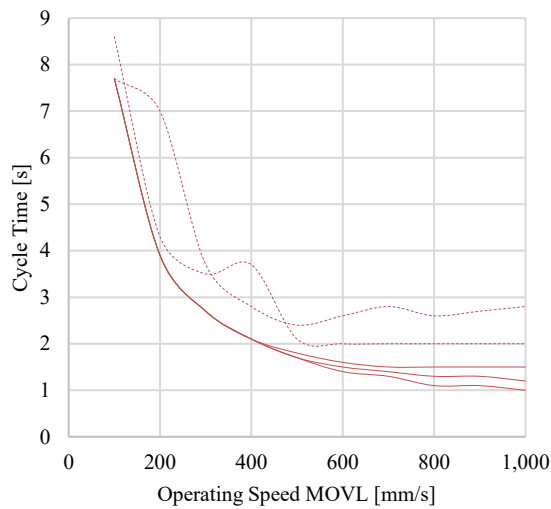
Behavior - DSF 3 Fields - IR



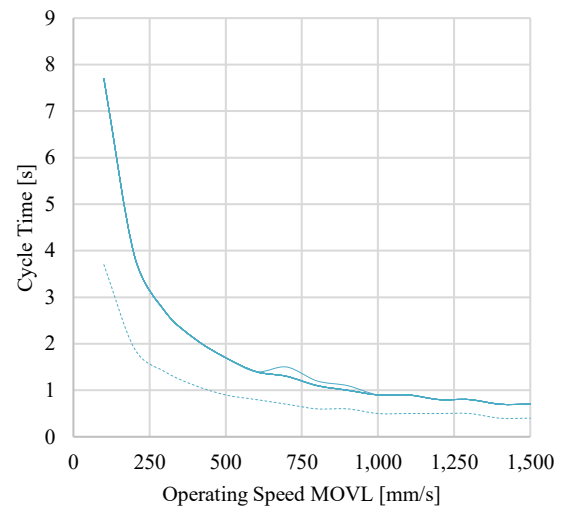
Outliers-CR: b00-b30-A02-S, c00-c30-AA01-S

Outliers-IR: d00-d30-B02-T

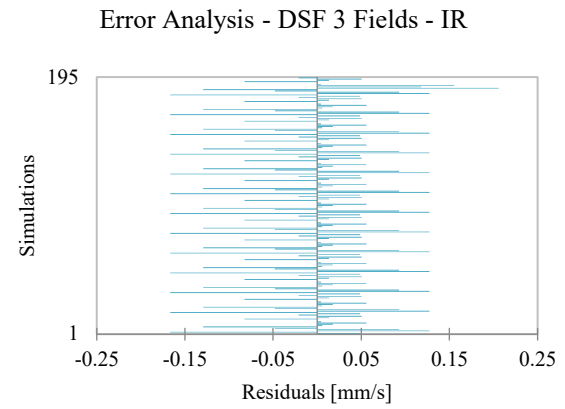
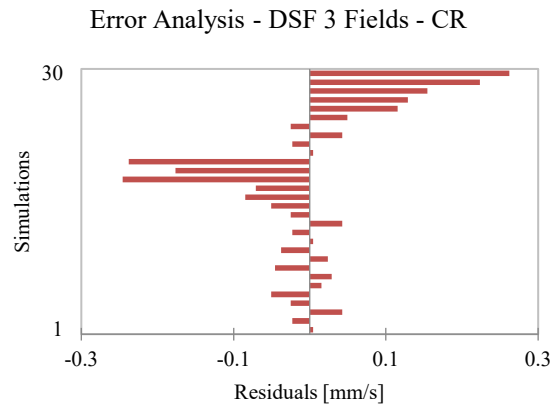
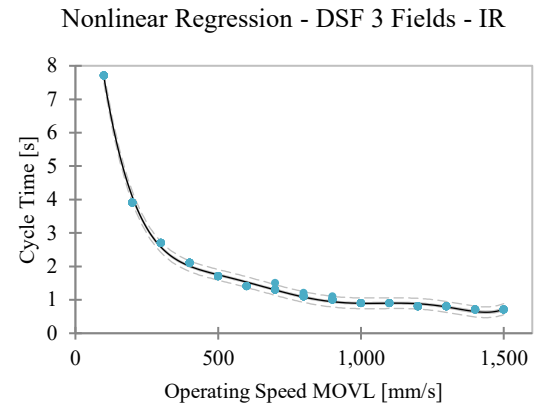
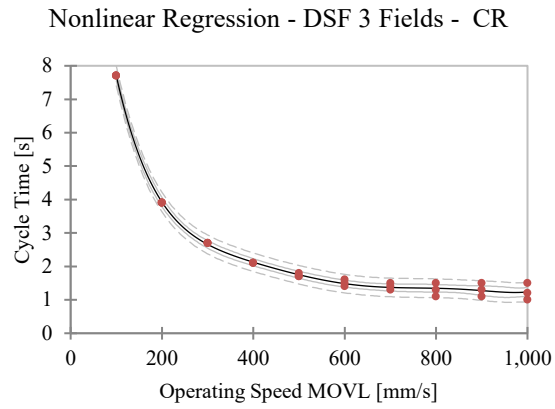
Outliers - DSF 3 Fields - CR



Outliers - DSF 3 Fields - IR



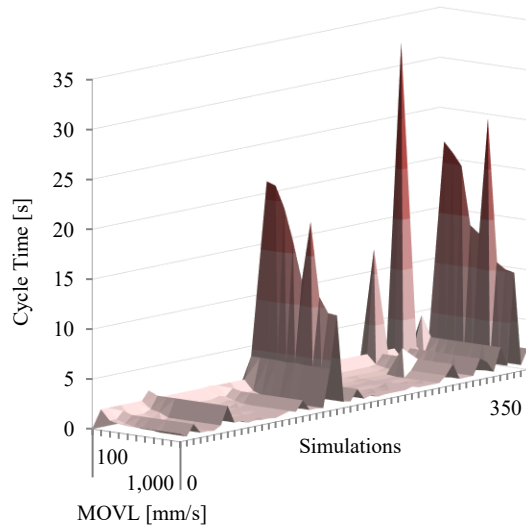
Appendix 14 (Continuation)



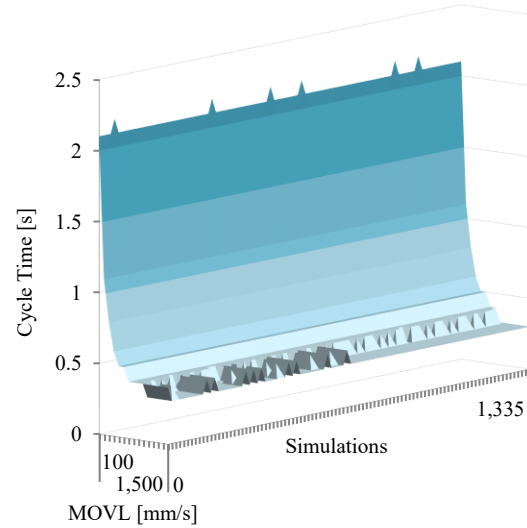
	n	a	b	c	d	e	f
$CT_{DSF,3y,CR}$	17.8578	$-1.53984 \cdot 10^{-1}$	$6.5697 \cdot 10^{-4}$	$-1.51264 \cdot 10^{-6}$	$1.91444 \cdot 10^{-9}$	$-1.2501 \cdot 10^{-12}$	$3.28703 \cdot 10^{-16}$
$CT_{DSF,3y,IR}$	15.2391	$-1.04627 \cdot 10^{-1}$	$3.40372 \cdot 10^{-4}$	$-5.79214 \cdot 10^{-7}$	$5.29914 \cdot 10^{-10}$	$-2.4648 \cdot 10^{-13}$	$4.5691 \cdot 10^{-17}$

Appendix 15: Spindle Feed-Spindle (SFS) Movement 1 Field in x-Direction for Collaborative (CR) and Industrial Robot (IR) – Simulation Results, Statistical Analysis, and Modeling

Behavior - SFS 1 Field - CR



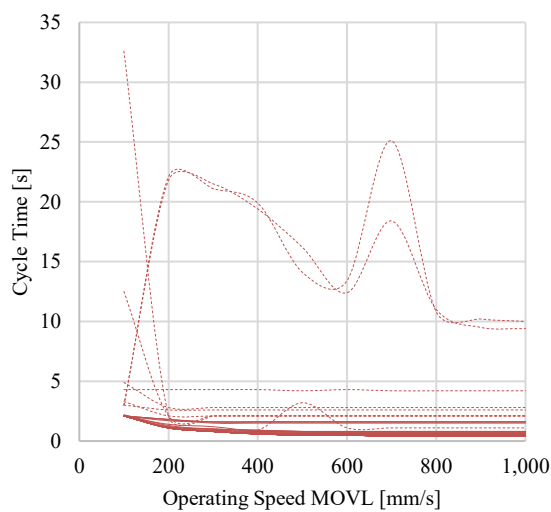
Behavior - SFS 1 Field - IR



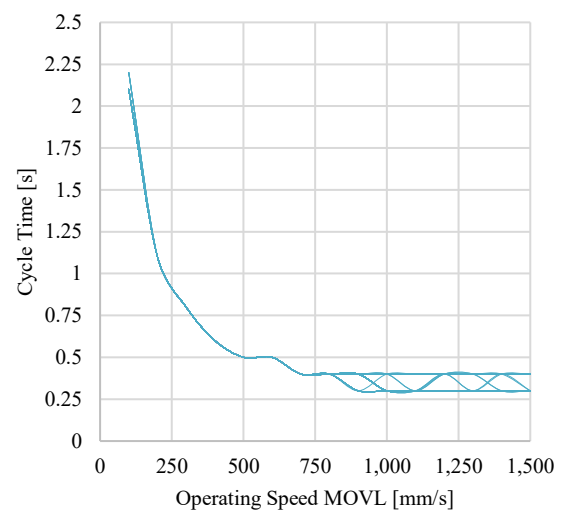
Outliers-CR: b10-a10-AA02-T/A03-S, d10-c10-A02-T/B03-S, e10-d10-AA01-T, f10-e10-B02-T, d20-c20-AA01-S/A02-S, f20-e20-B02-S, b30-a30-AA01-T/A02-S, c30-b30-AA01-S, b40-a40-AA01-S

Outliers-IR: none

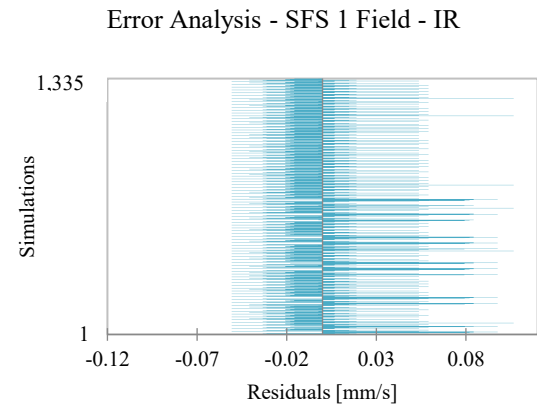
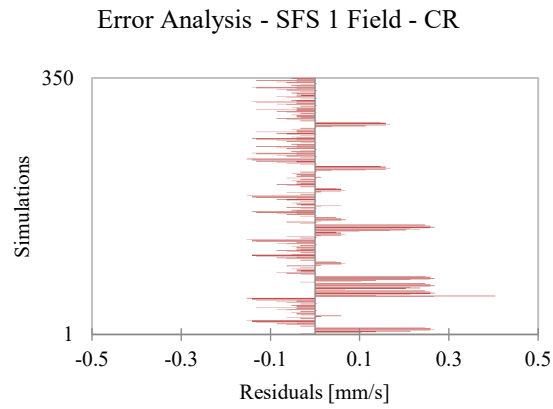
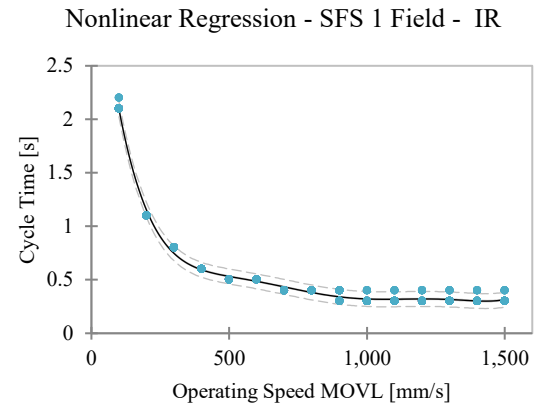
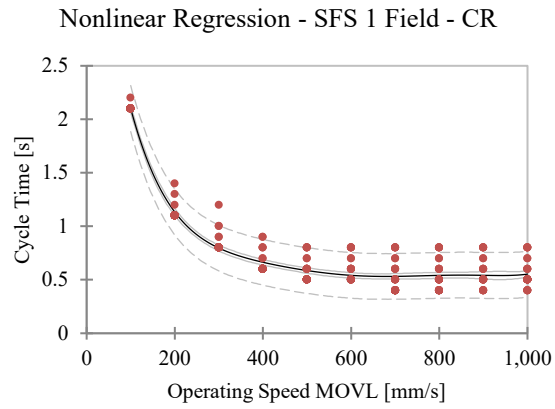
Outliers - SFS 1 Field - CR



Outliers - SFS 1 Field - IR



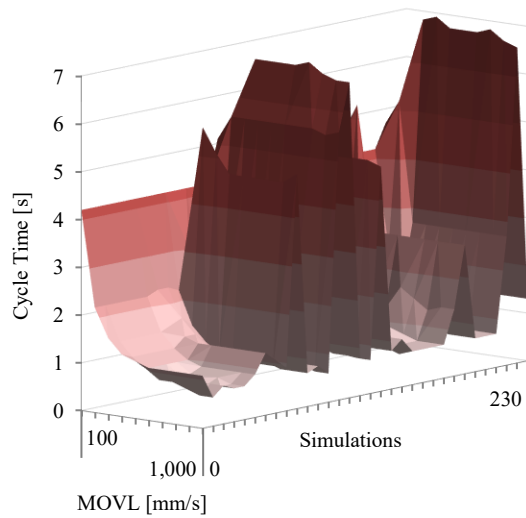
Appendix 15 (Continuation)



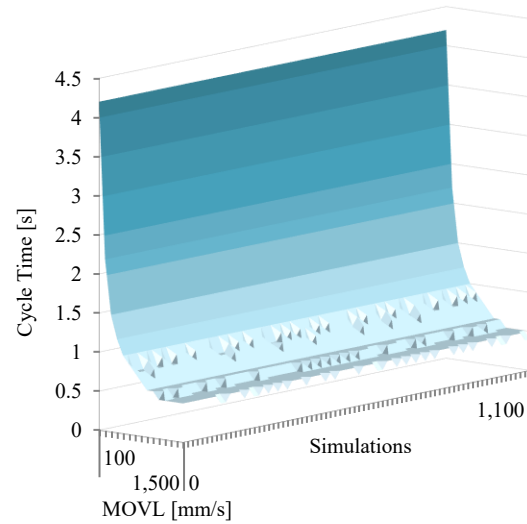
	n	a	b	c	d	e	f
$CT_{SFS,1x,CR}$	4.60667	$-3.75011 \cdot 10^{-2}$	$1.55142 \cdot 10^{-4}$	$-3.48718 \cdot 10^{-7}$	$4.3499 \cdot 10^{-10}$	$-2.8177 \cdot 10^{-13}$	$7.38094 \cdot 10^{-17}$
$CT_{SFS,1x,IR}$	4.03278	$-2.64422 \cdot 10^{-2}$	$8.28659 \cdot 10^{-5}$	$-1.35209 \cdot 10^{-7}$	$1.1859 \cdot 10^{-10}$	$-5.29775 \cdot 10^{-14}$	$9.46071 \cdot 10^{-18}$

Appendix 16: Spindle Feed-Spindle (SFS) Movement 2 Fields in x-Direction for Collaborative (CR) and Industrial Robot (IR) – Simulation Results, Statistical Analysis, and Modeling

Behavior - SFS 2 Fields - CR



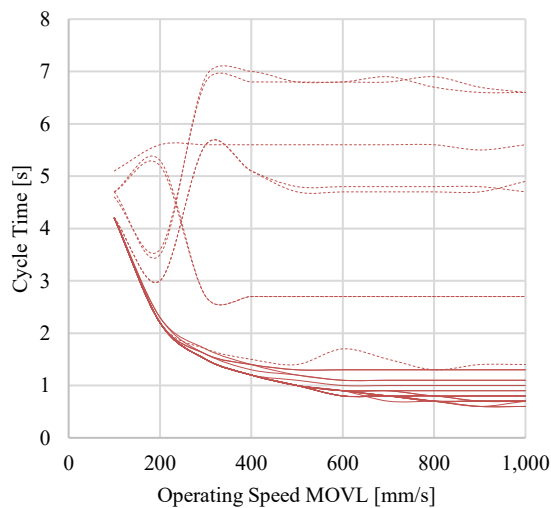
Behavior - SFS 2 Fields - IR



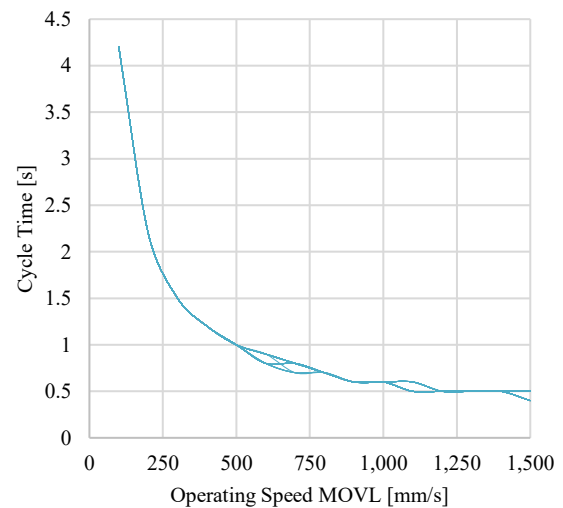
Outliers-CR: c10-a10-B03-S, d10-b10-A02-T, d10-b10-B03-S, e10-c10-AA01-T, f10-d10-B02-T, d20-b20-AA01-S/A02-S, f20-d20-B02-S, c30-a30-AA01-S

Outliers-IR: none

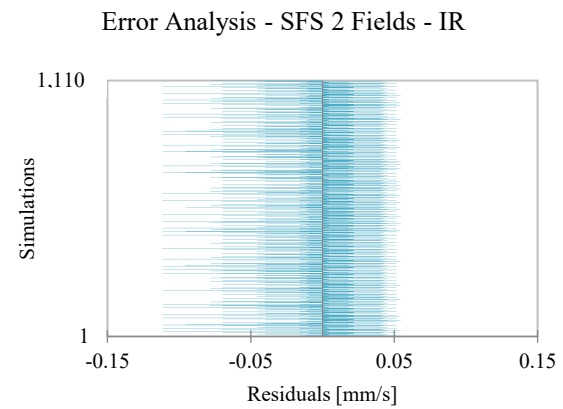
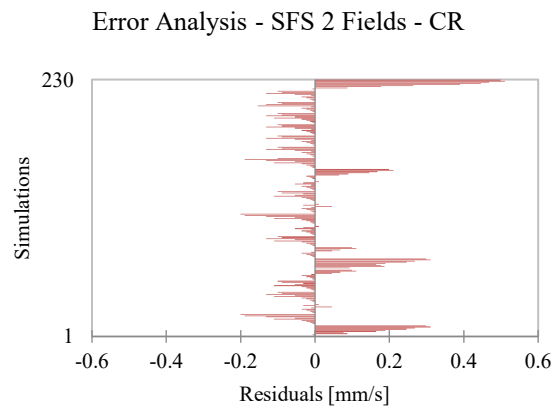
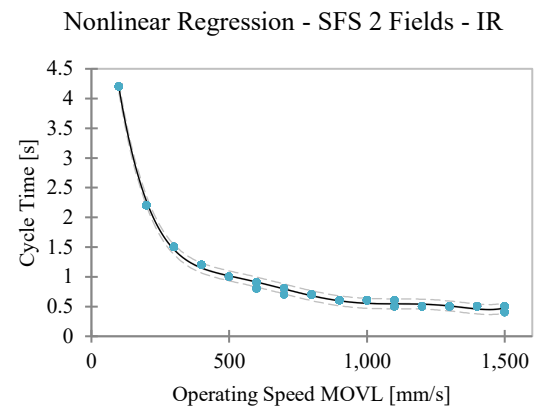
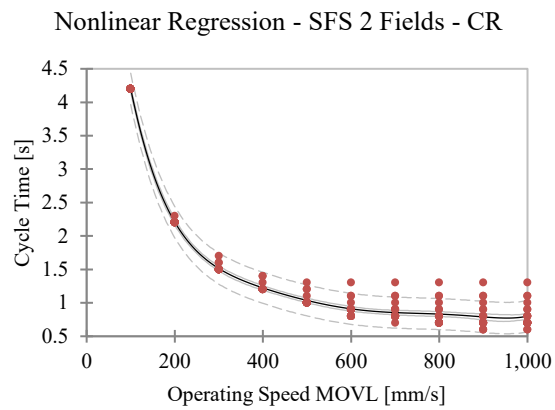
Outliers - SFS 2 Fields - CR



Outliers - SFS 2 Fields - IR



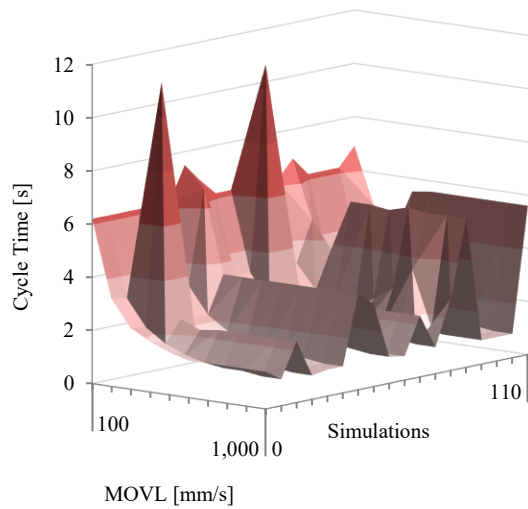
Appendix 16 (Continuation)



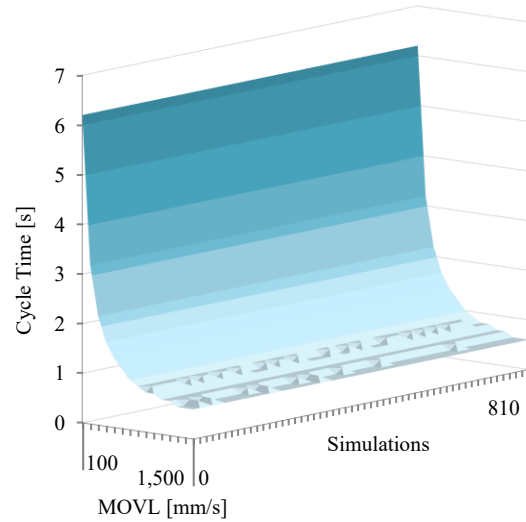
	n	a	b	c	d	e	f
$CT_{SFS,2x,CR}$	9.4258	$-7.8592 \cdot 10^{-2}$	$3.29564 \cdot 10^{-4}$	$-7.51761 \cdot 10^{-7}$	$9.50089 \cdot 10^{-10}$	$-6.23384 \cdot 10^{-13}$	$1.65459 \cdot 10^{-16}$
$CT_{SFS,2x,IR}$	8.13981	$-5.42054 \cdot 10^{-2}$	$1.71962 \cdot 10^{-4}$	$-2.8464 \cdot 10^{-7}$	$2.53265 \cdot 10^{-10}$	$-1.1472 \cdot 10^{-13}$	$2.07534 \cdot 10^{-17}$

Appendix 17: Spindle Feed-Spindle (SFS) Movement 3 Fields in x-Direction for Collaborative (CR) and Industrial Robot (IR) – Simulation Results, Statistical Analysis, and Modeling

Behavior - SFS 3 Fields - CR



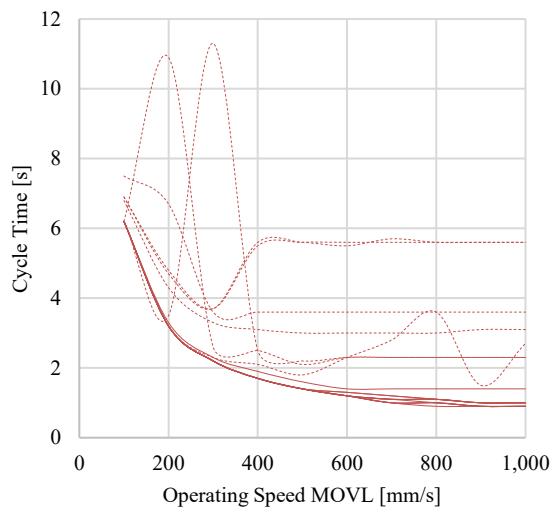
Behavior - SFS 3 Fields - IR



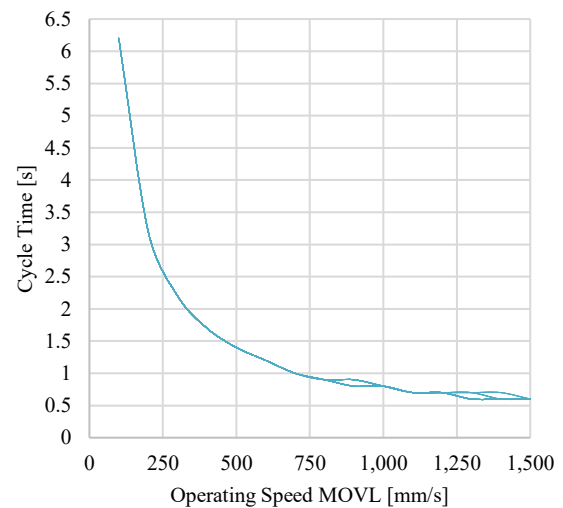
Outliers-CR: d10-a10-A02-T/B03-S, e10-b10-AA01-T, f10-c10-B02-T, d20-a20-A02-S, f20-c20-B02-S

Outliers-IR: none

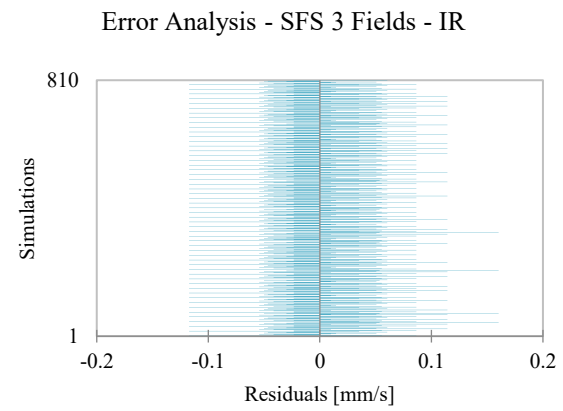
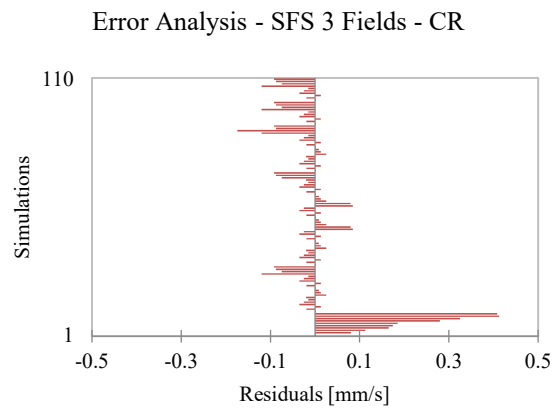
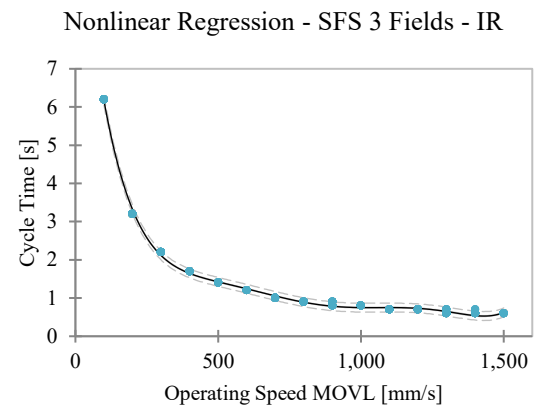
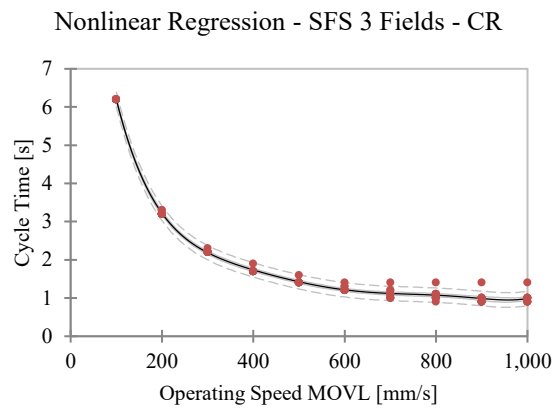
Outliers - SFS 3 Fields - CR



Outliers - SFS 3 Fields - IR



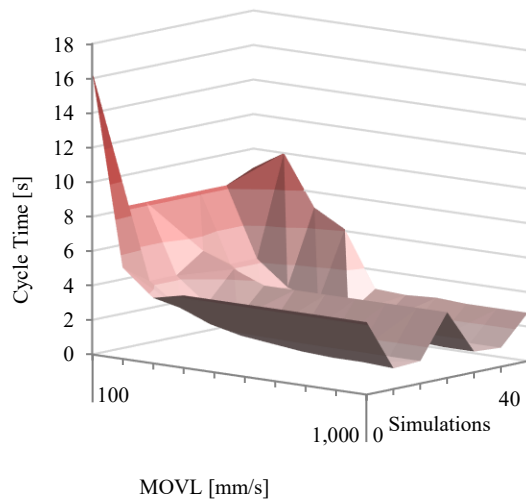
Appendix 17 (Continuation)



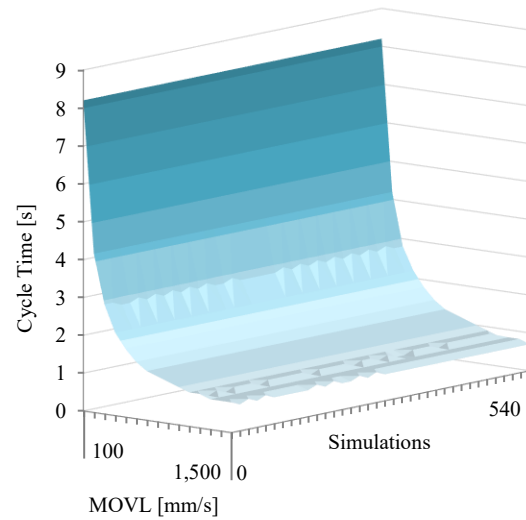
	n	a	b	c	d	e	f
$CT_{SFS,3x,CR}$	14.1439	$-1.20287 \cdot 10^{-1}$	$5.131 \cdot 10^{-4}$	$-1.19103 \cdot 10^{-6}$	$1.5279 \cdot 10^{-9}$	$-1.01493 \cdot 10^{-12}$	$2.72096 \cdot 10^{-16}$
$CT_{SFS,3x,IR}$	12.1555	$-8.24746 \cdot 10^{-2}$	$2.67173 \cdot 10^{-4}$	$-4.54721 \cdot 10^{-7}$	$4.17208 \cdot 10^{-10}$	$-1.94914 \cdot 10^{-13}$	$3.63226 \cdot 10^{-17}$

Appendix 18: Spindle Feed-Spindle (SFS) Movement 4 Fields in x-Direction for Collaborative (CR) and Industrial Robot (IR) – Simulation Results, Statistical Analysis, and Modeling

Behavior - SFS 4 Fields - CR



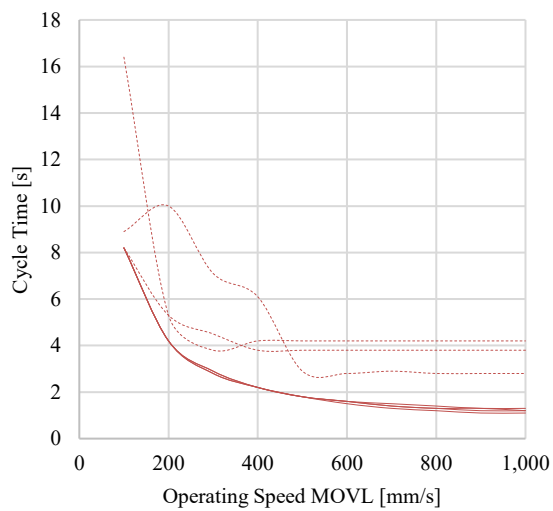
Behavior - SFS 4 Fields - IR



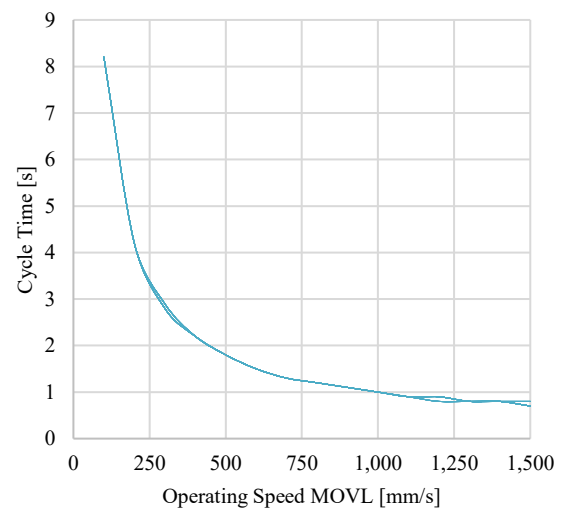
Outliers-CR: e10-a10-AA01-T, f10-b10-B02-T, f20-b20-B02-S

Outliers-IR: none

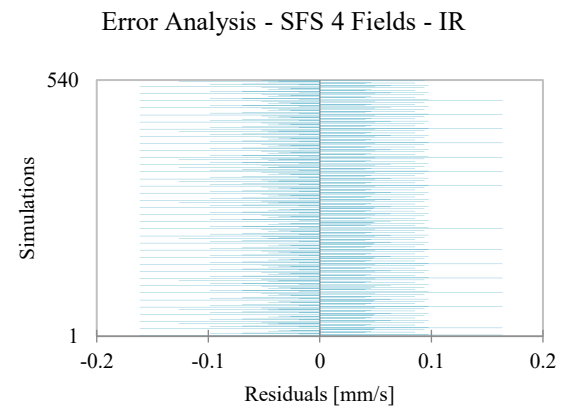
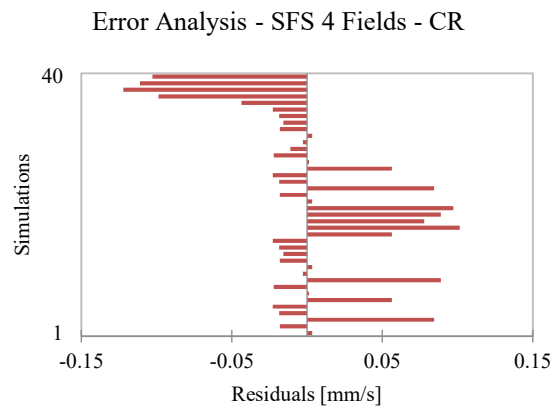
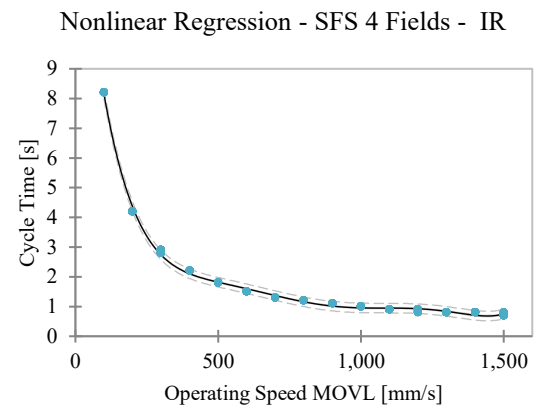
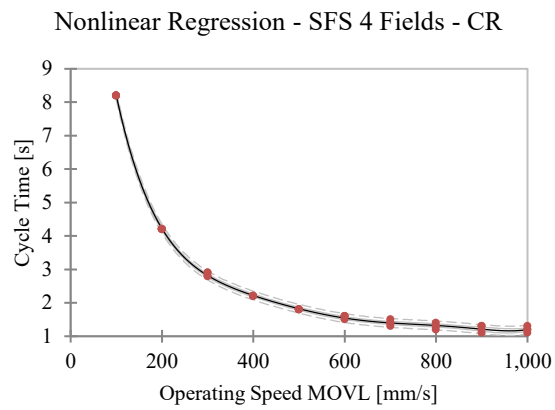
Outliers - SFS 4 Fields - CR



Outliers - SFS 4 Fields - IR



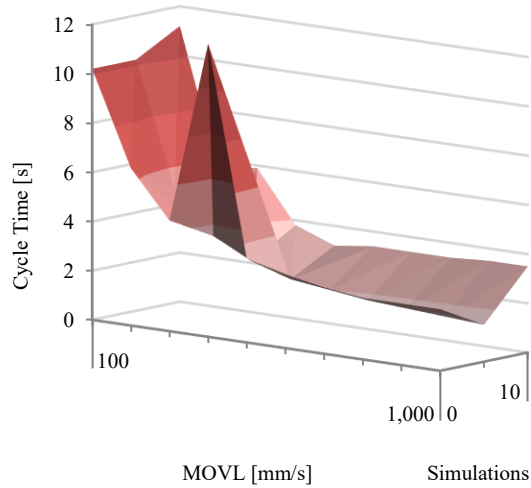
Appendix 18 (Continuation)



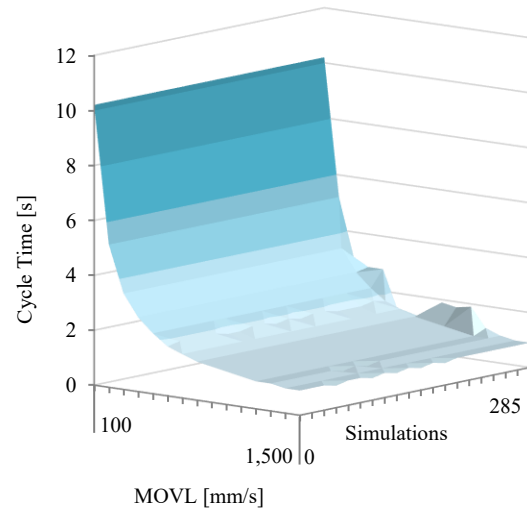
	n	a	b	c	d	e	f
$CT_{SFS,4x,CR}$	18.5675	$-1.55652 \cdot 10^{-1}$	$6.49659 \cdot 10^{-4}$	$-1.47627 \cdot 10^{-6}$	$1.8581 \cdot 10^{-9}$	$-1.21438 \cdot 10^{-12}$	$3.21181 \cdot 10^{-16}$
$CT_{SFS,4x,IR}$	16.0121	$-1.07647 \cdot 10^{-1}$	$3.42594 \cdot 10^{-4}$	$-5.72053 \cdot 10^{-7}$	$5.15273 \cdot 10^{-10}$	$-2.36626 \cdot 10^{-13}$	$4.3401 \cdot 10^{-17}$

Appendix 19: Spindle Feed-Spindle (SFS) Movement 5 Fields in x-Direction for Collaborative (CR) and Industrial Robot (IR) – Simulation Results, Statistical Analysis, and Modeling

Behavior - SFS 5 Fields - CR



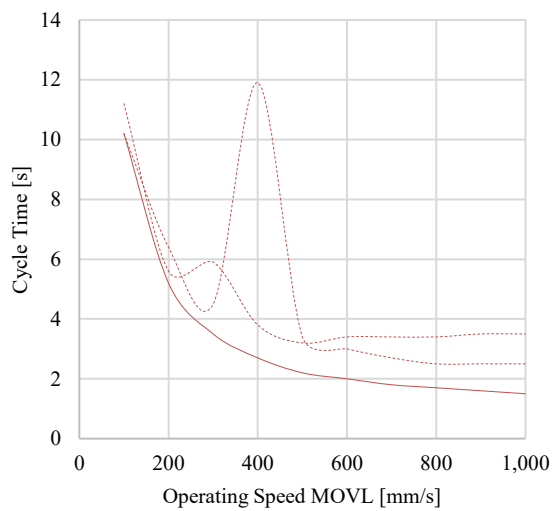
Behavior - SFS 5 Fields - IR



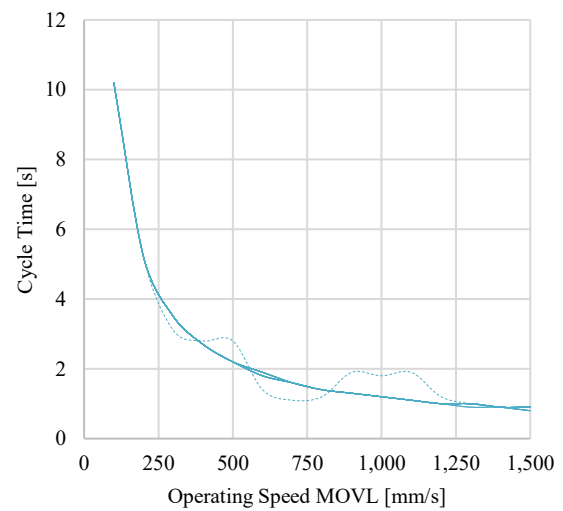
Outliers-CR: f10-a10-B02-T, f20-a20-B02-S

Outliers-IR: f30-a30-B02-S

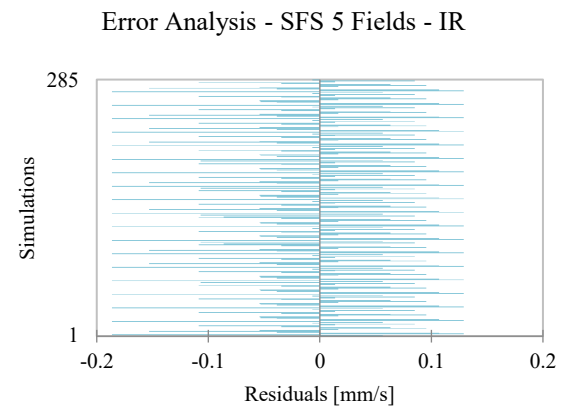
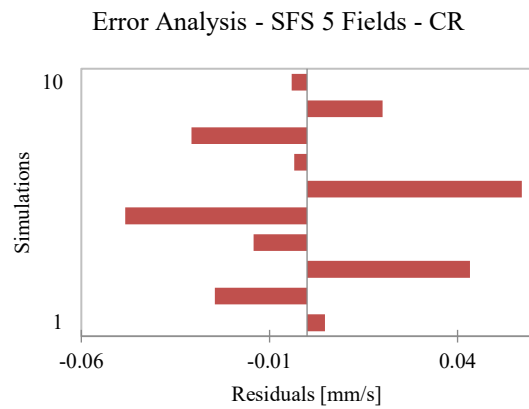
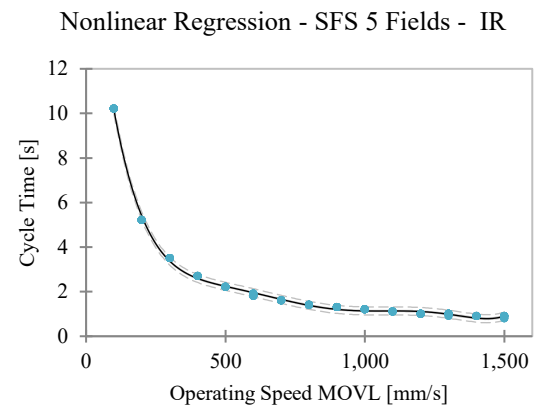
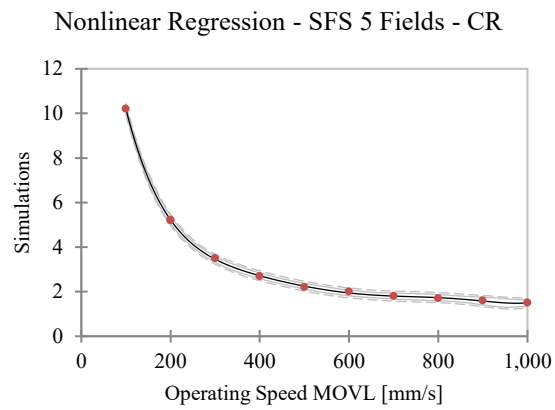
Outliers - SFS 5 Fields - CR



Outliers - SFS 5 Fields - IR



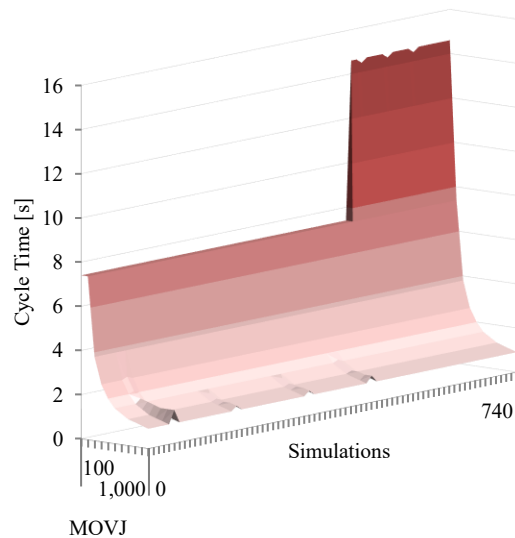
Appendix 19 (Continuation)



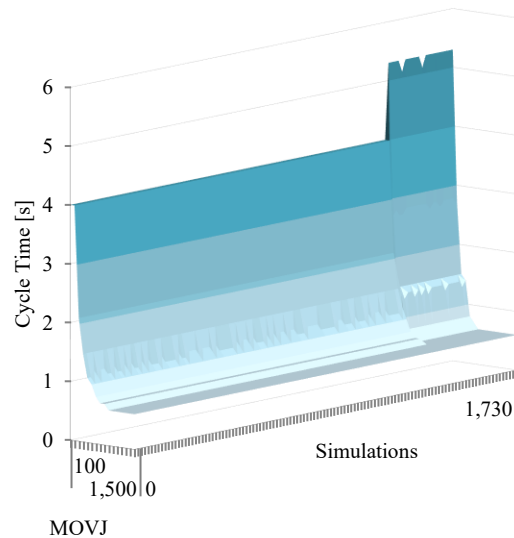
	n	a	b	c	d	e	f
$CT_{SFS,5x,CR}$	23.0567	$-1.92604 \cdot 10^{-1}$	$7.99846 \cdot 10^{-4}$	$-1.81317 \cdot 10^{-6}$	$2.28325 \cdot 10^{-9}$	$-1.49471 \cdot 10^{-12}$	$3.95833 \cdot 10^{-16}$
$CT_{SFS,5x,IR}$	20.1074	$-1.36902 \cdot 10^{-1}$	$4.40524 \cdot 10^{-4}$	$-7.43293 \cdot 10^{-7}$	$6.75818 \cdot 10^{-10}$	$-3.12945 \cdot 10^{-13}$	$5.78268 \cdot 10^{-17}$

Appendix 20: Turning (T) Movement for Collaborative (CR) and Industrial Robot (IR) – Simulation Results, Statistical Analysis and Modeling

Behavior - T - CR



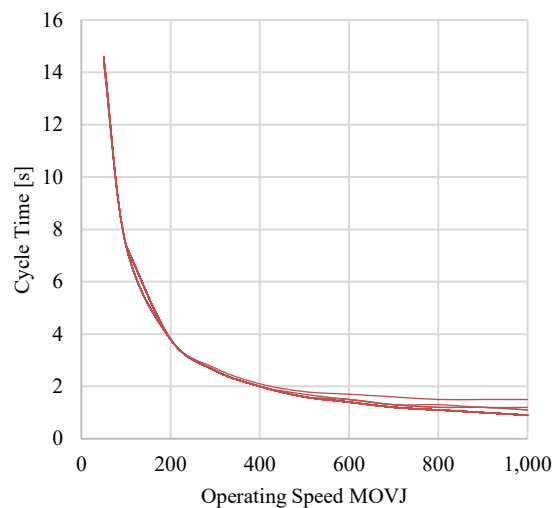
Behavior - T - IR



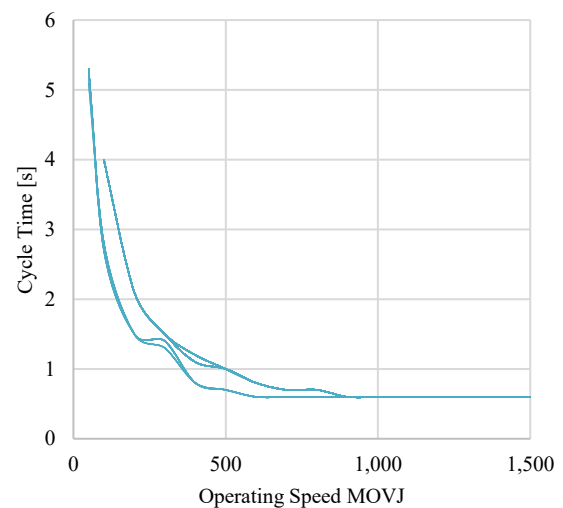
Outliers-CR: none

Outliers-IR: none

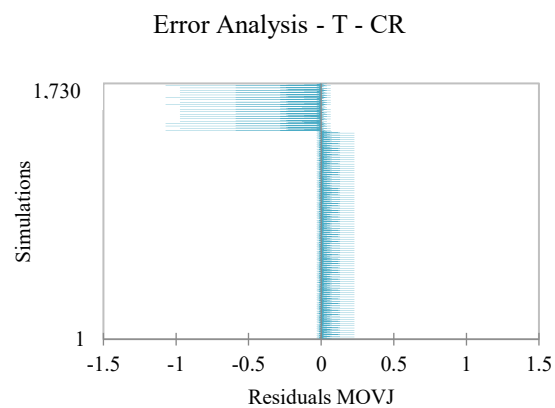
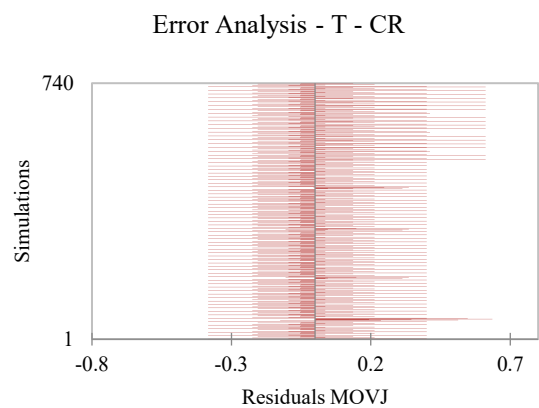
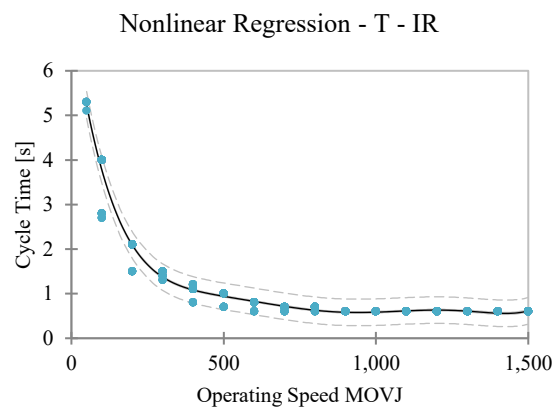
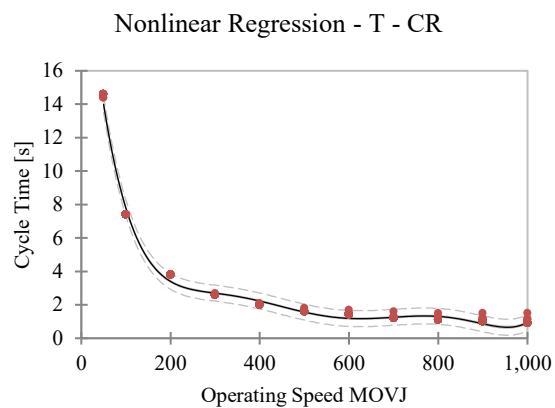
Outliers - T - CR



Outliers - T - IR



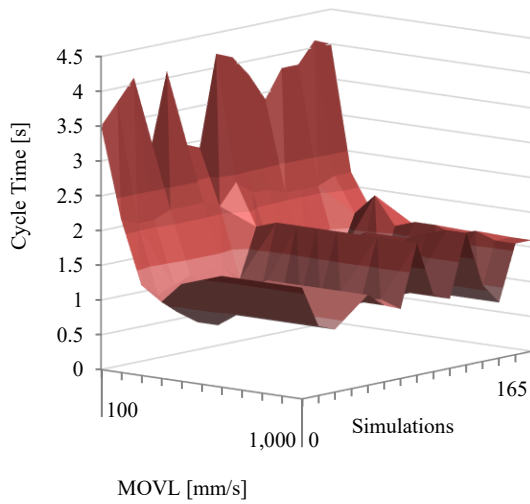
Appendix 20 (Continuation)



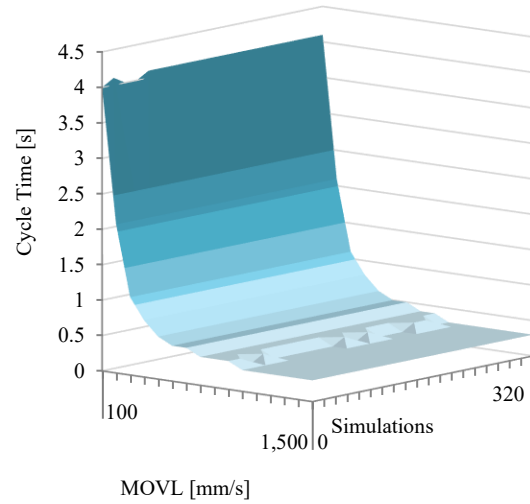
	n	a	b	c	d	e	f
$CT_{T,CR}$	25.3533	$-2.96044 \cdot 10^{-1}$	$1.57331 \cdot 10^{-3}$	$-4.26826 \cdot 10^{-6}$	$6.12727 \cdot 10^{-9}$	$-4.42444 \cdot 10^{-12}$	$1.26375 \cdot 10^{-15}$
$CT_{T,IR}$	7.29981	$-4.85522 \cdot 10^{-2}$	$1.57211 \cdot 10^{-4}$	$-2.68575 \cdot 10^{-7}$	$2.4758 \cdot 10^{-10}$	$-1.16022 \cdot 10^{-13}$	$2.16428 \cdot 10^{-17}$

Appendix 21: Material Feed-Material (MFM) Movement for Collaborative (CR) and Industrial Robot (IR) – Simulation Results, Statistical Analysis, and Modeling

Behavior - MFM - CR



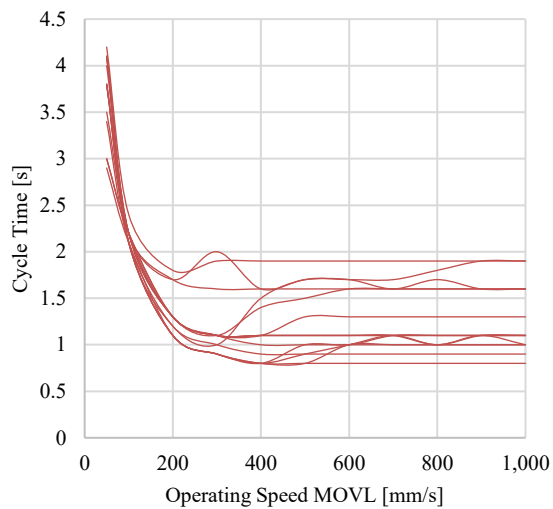
Behavior - MFM - IR



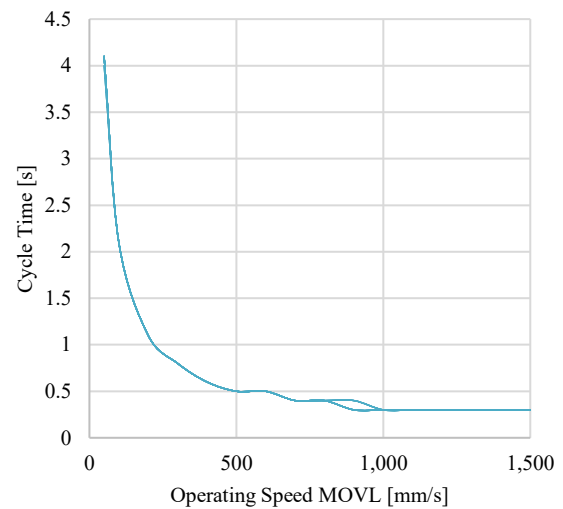
Outliers-CR: none

Outliers-IR: none

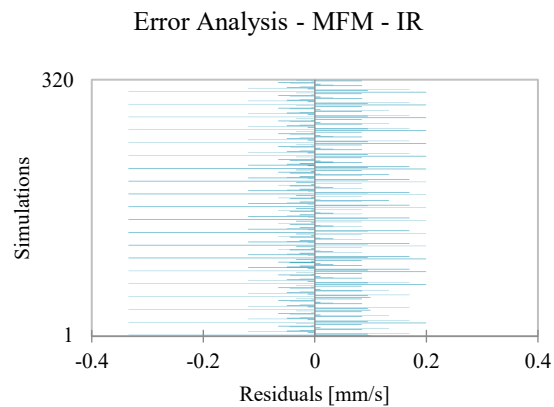
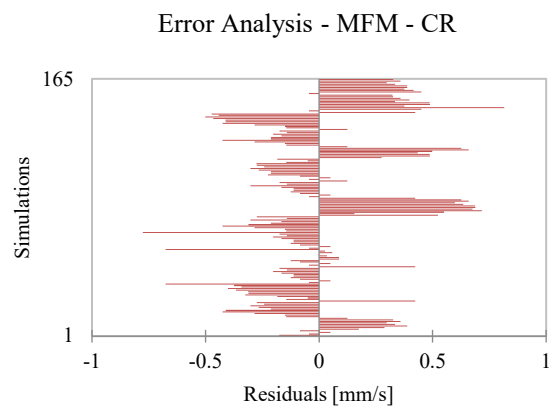
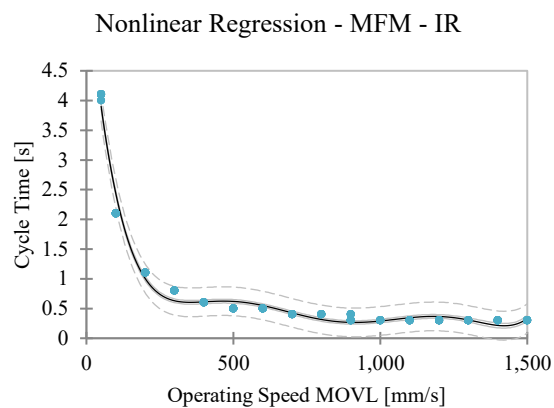
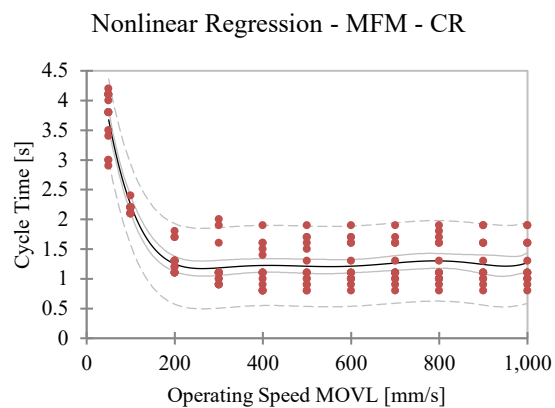
Outliers - MFM - CR



Outliers - MFM - IR

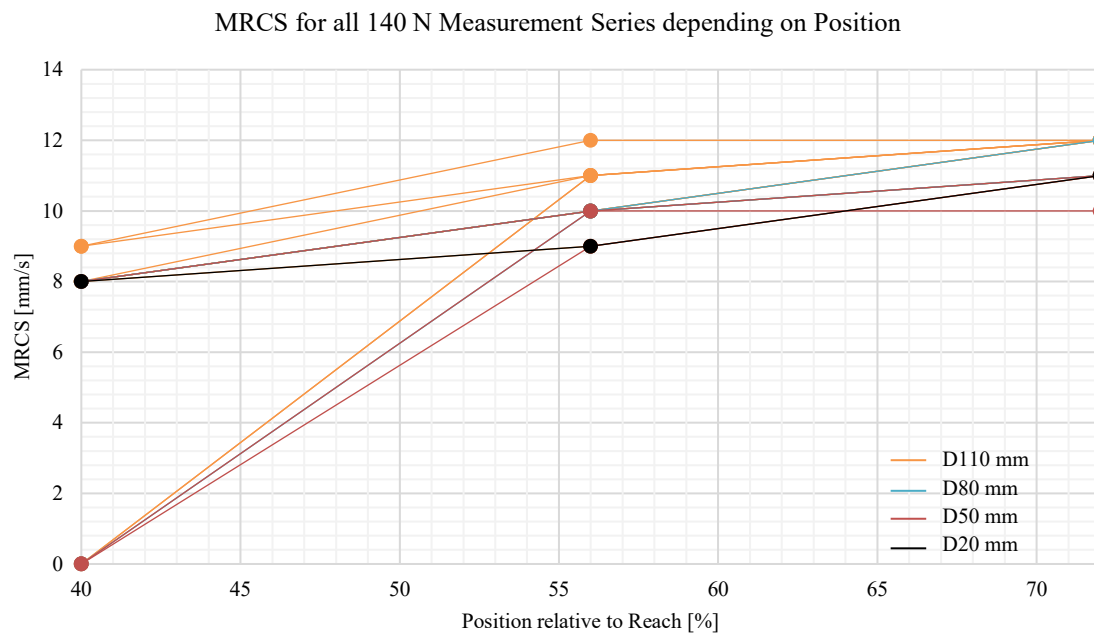


Appendix 21 (Continuation)

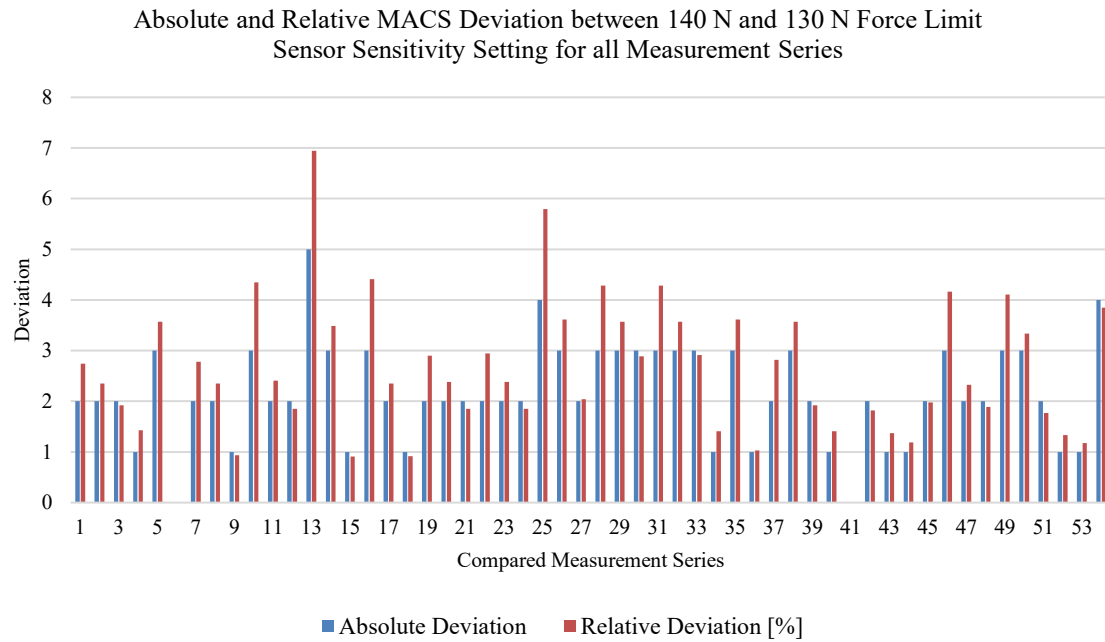


	n	a	b	c	d	e	f
$CT_{MFM,CR}$	6.26575	$-6.70302 \cdot 10^{-2}$	$3.46785 \cdot 10^{-4}$	$-9.02054 \cdot 10^{-7}$	$1.25076 \cdot 10^{-9}$	$-8.80227 \cdot 10^{-13}$	$2.4677 \cdot 10^{-16}$
$CT_{MFM,IR}$	6.13876	$-5.41614 \cdot 10^{-2}$	$2.06412 \cdot 10^{-4}$	$-3.88784 \cdot 10^{-7}$	$3.81031 \cdot 10^{-10}$	$-1.86133 \cdot 10^{-13}$	$3.57866 \cdot 10^{-17}$

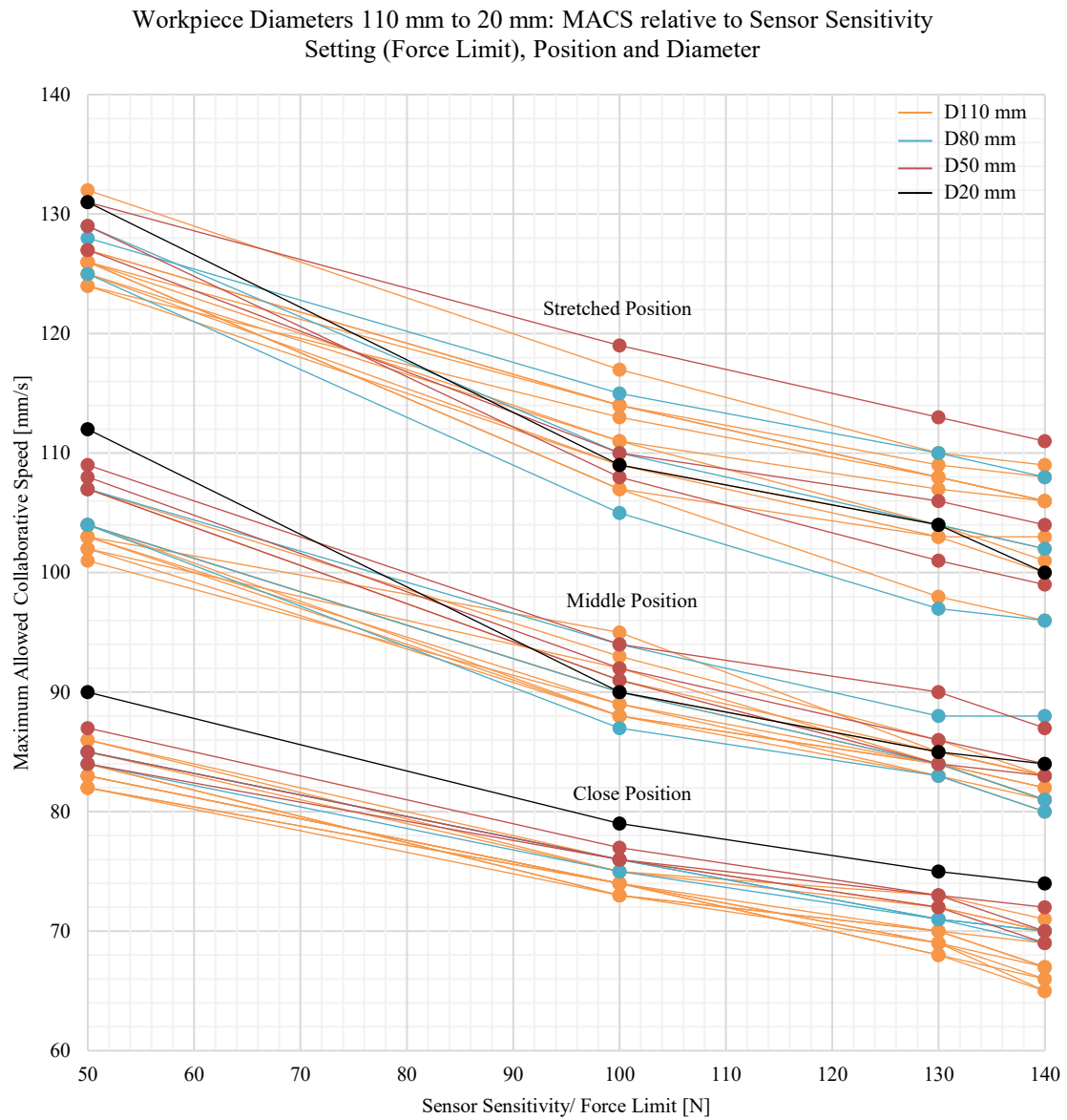
Appendix 22: Minimum Required Speed (MRCs) depending on Position for all Measurement Series



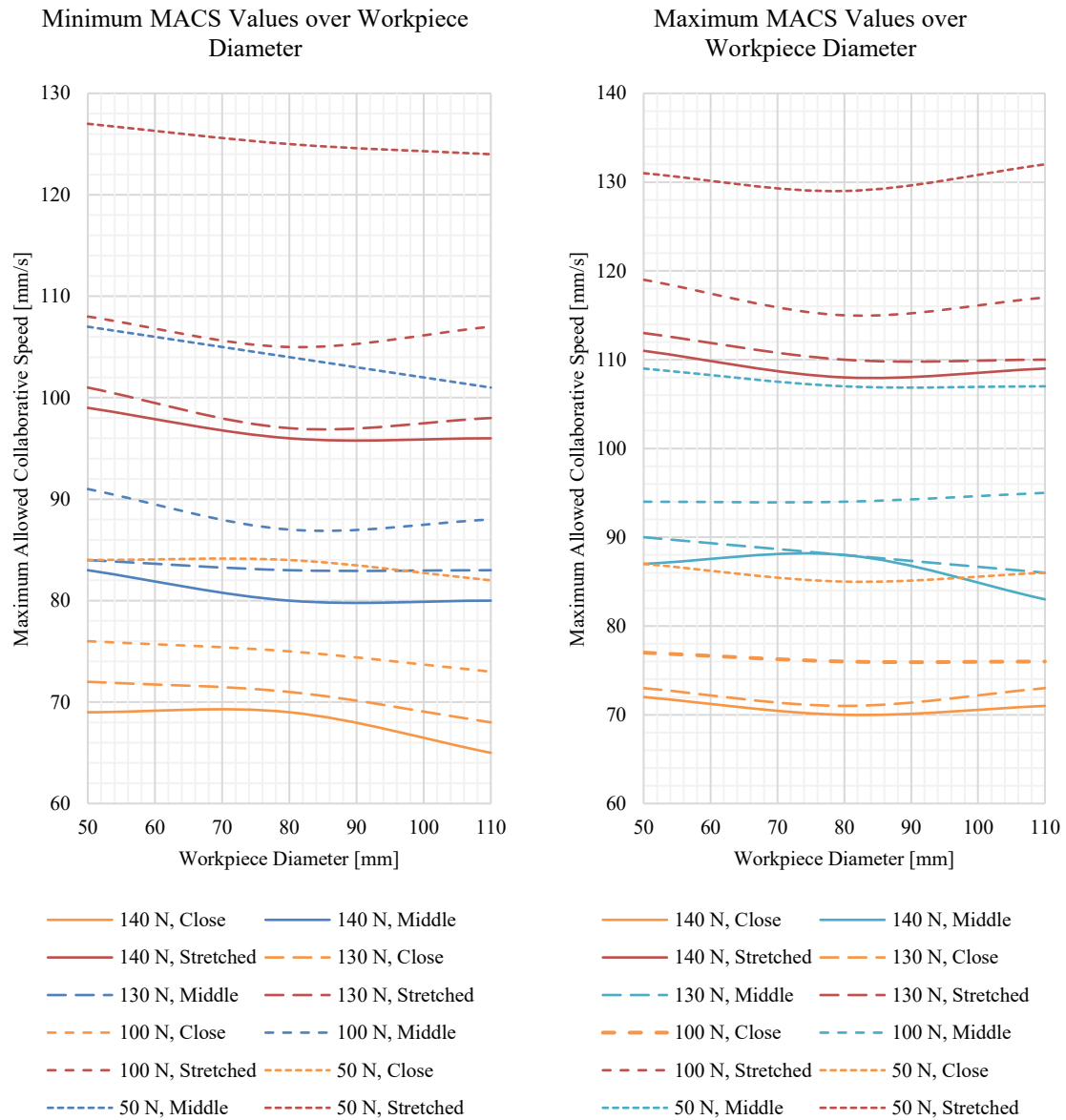
Appendix 23: Absolute and Relative Deviation of the Maximum Allowed Collaborative Speed (MACS) between 140 N and 130 N Sensor Sensitivity/ Force Limit Setting for all Measurement Series



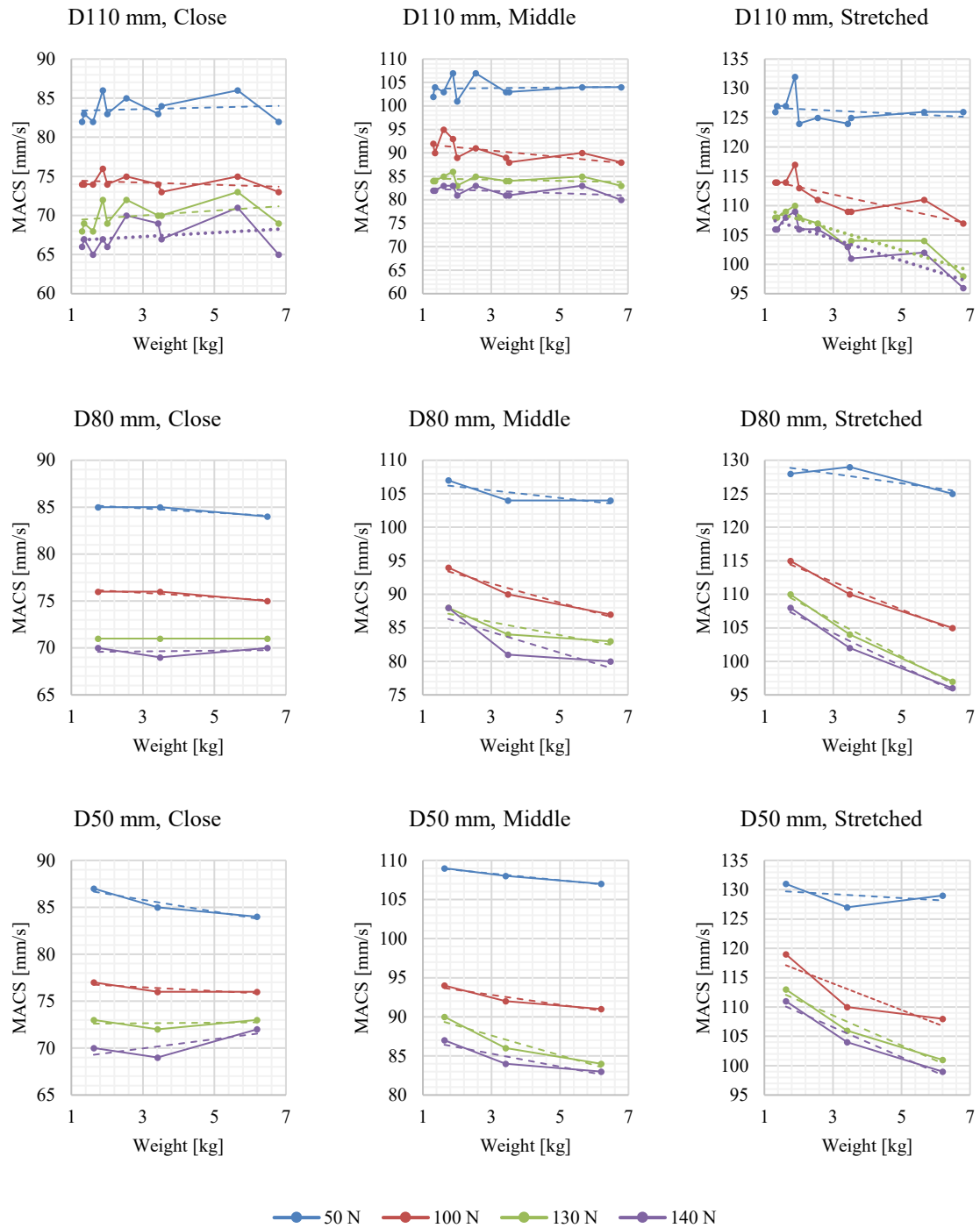
Appendix 24: Maximum Allowed Collaborative Speed (MACS) relative to Sensor Sensitivity/ Force Limit Setting and Position for Workpiece Diameters 110 mm to 20 mm



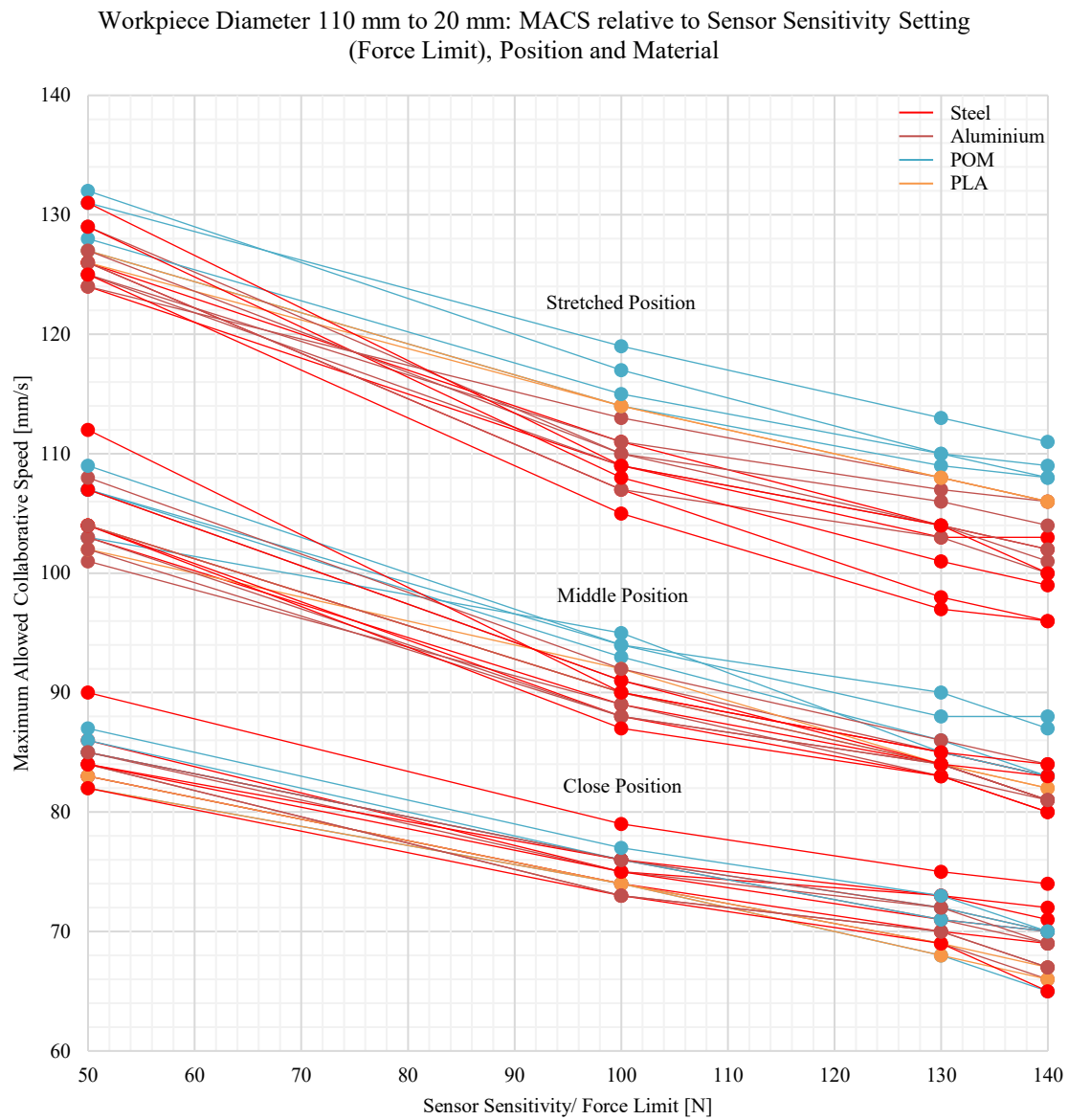
Appendix 25: Minimal and Maximal Values for the Maximum Allowed Collaborative Speed (MACS) over Diameter for all Measurement Series



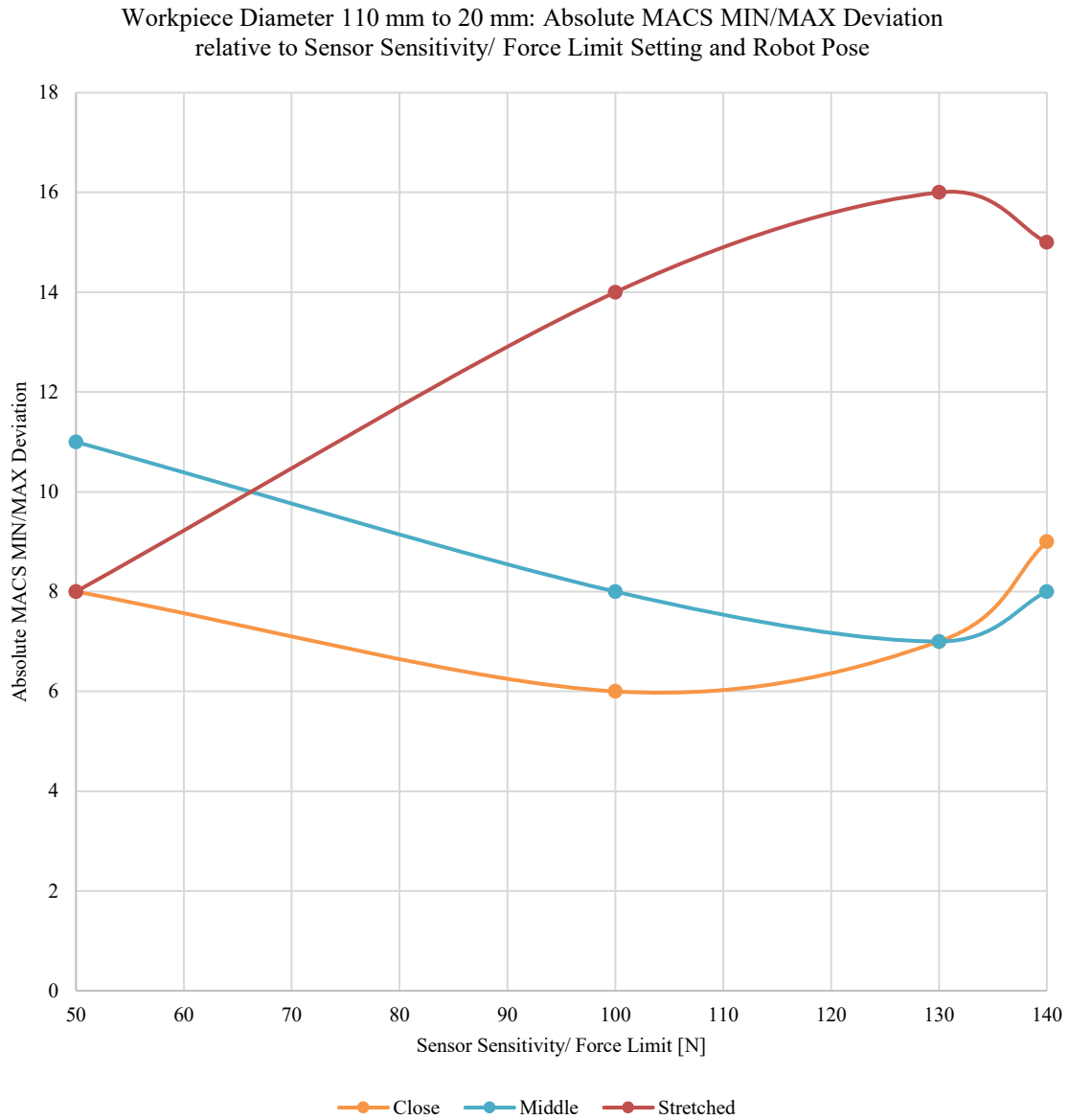
Appendix 26: Influence of the Attached Weight on the Maximum Allowed Collaborative Speed (MACS) depending on Position and Sensor Sensitivity/ Force Limit Setting



Appendix 27: Maximum Allowed Collaborative Speed (MACS) relative to Sensor Sensitivity/ Force Limit Setting, Position and Material for Workpiece Diameters 110 mm to 20 mm

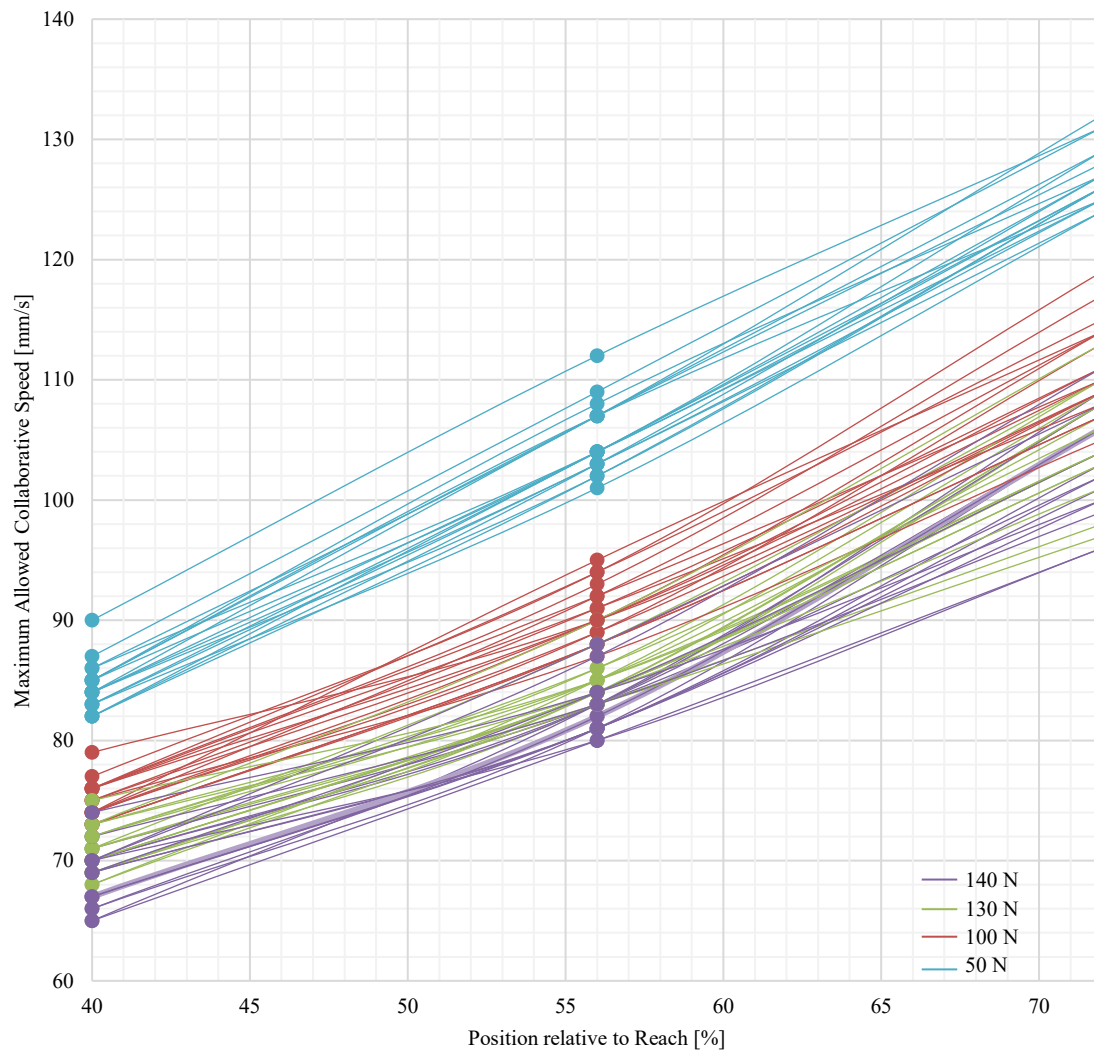


Appendix 28: Absolute MIN/MAX Deviation of the Maximum Allowed Collaborative Speed (MACS) relative to Sensor Sensitivity/ Force Limit Setting and Robot Pose for Workpiece Diameters 110 mm to 20 mm

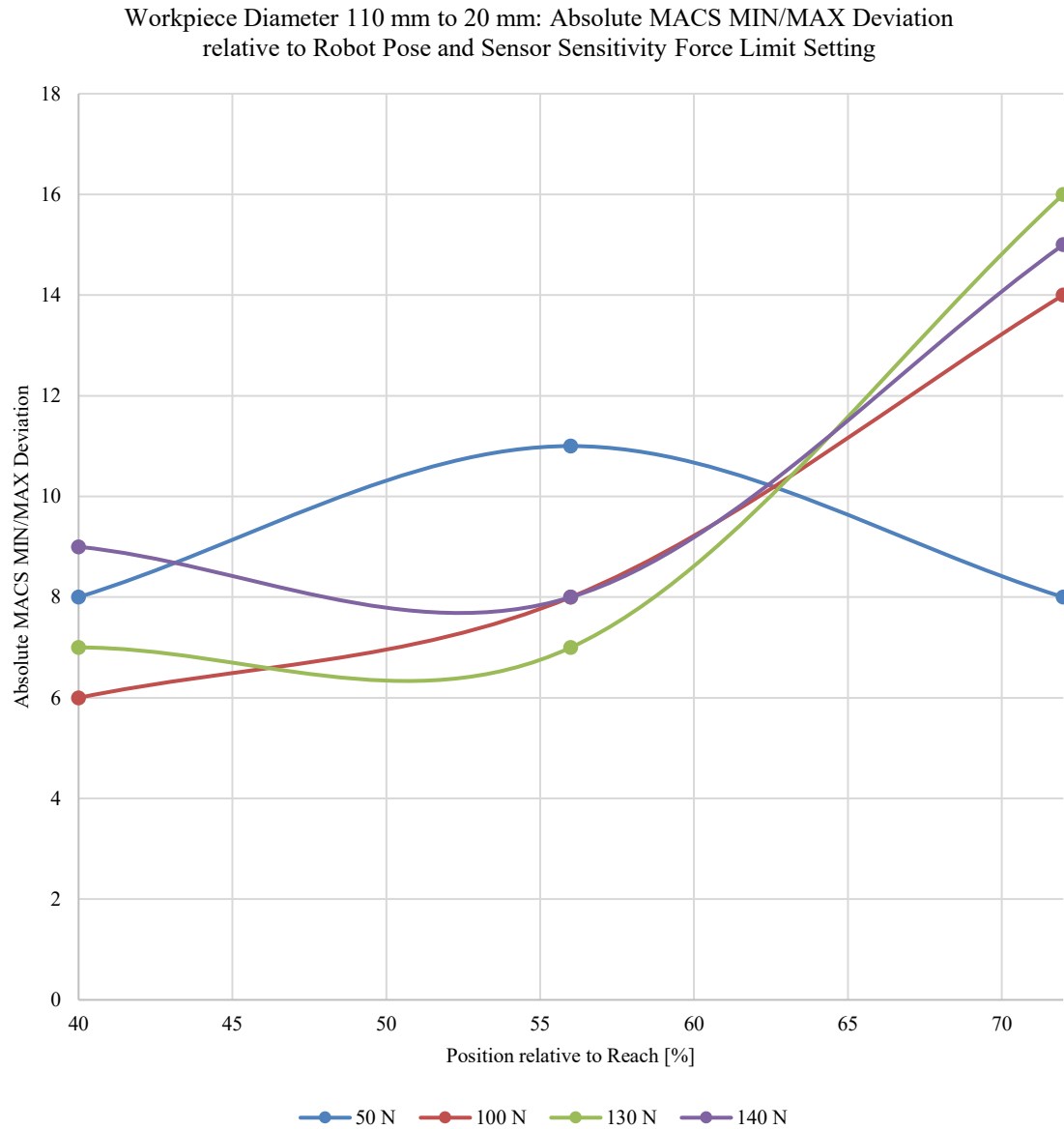


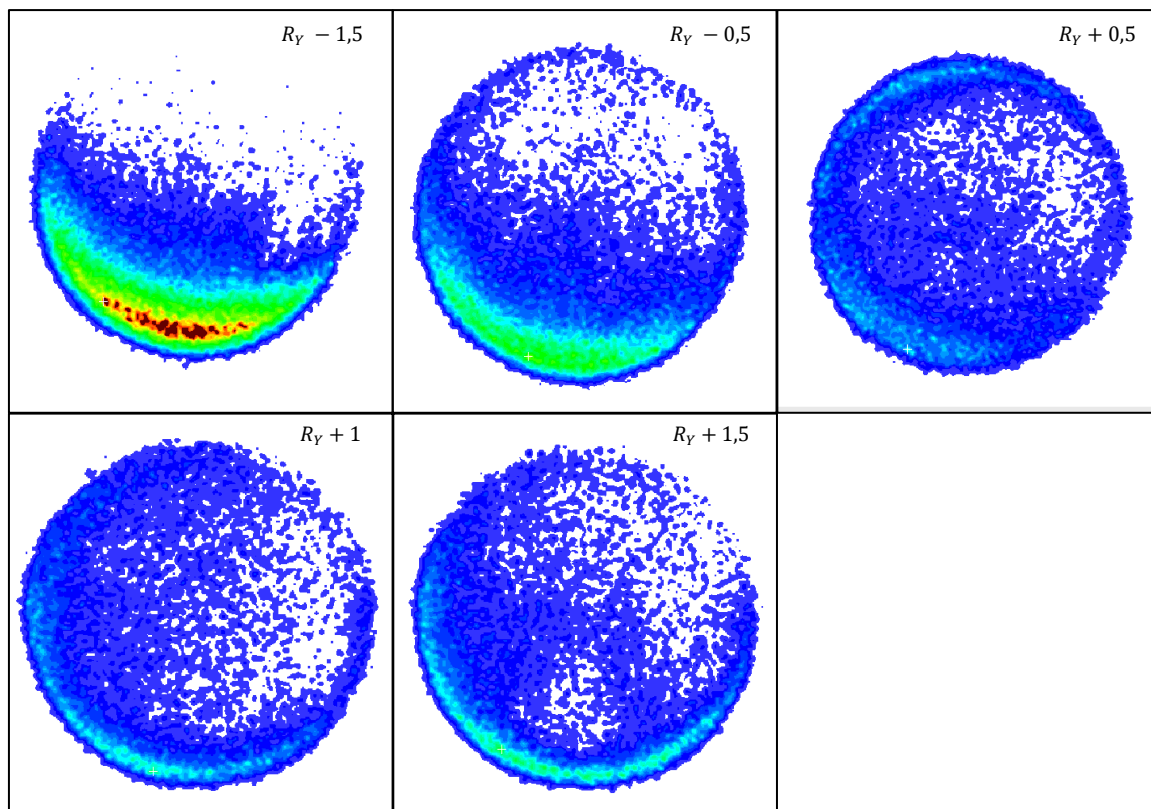
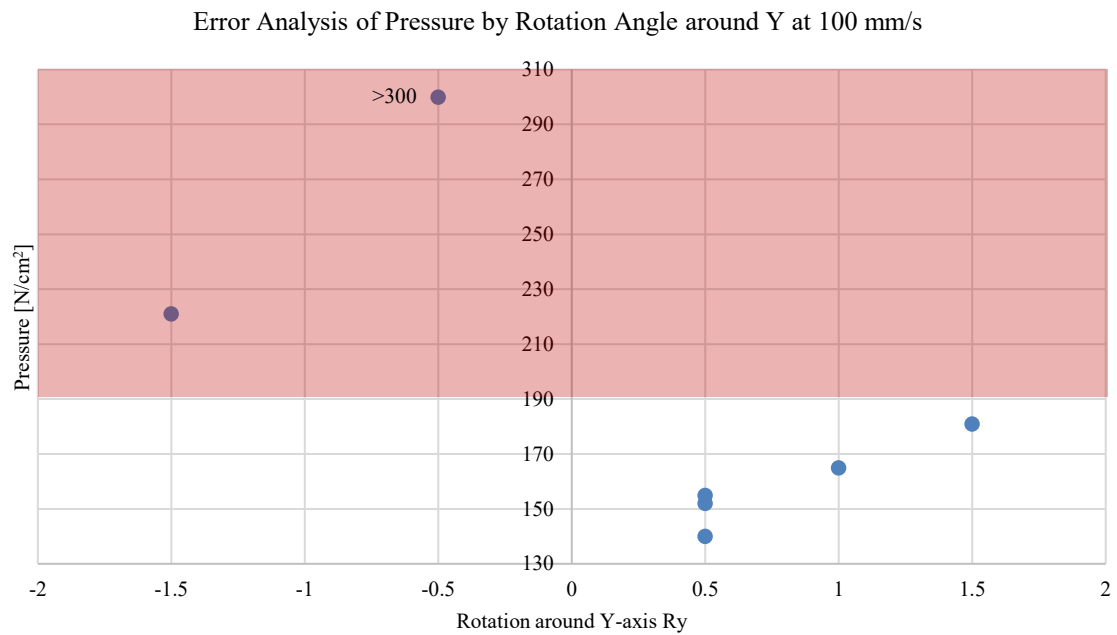
Appendix 29: Maximum Allowed Collaborative Speed (MACS) relative to Robot Pose and Sensor Sensitivity/ Force Limit Setting for Workpiece Diameters 110 mm to 20 mm

Workpiece Diameter 110 mm to 20 mm: MACS relative to Robot Pose and Sensor Sensitivity Setting (Force Limit)

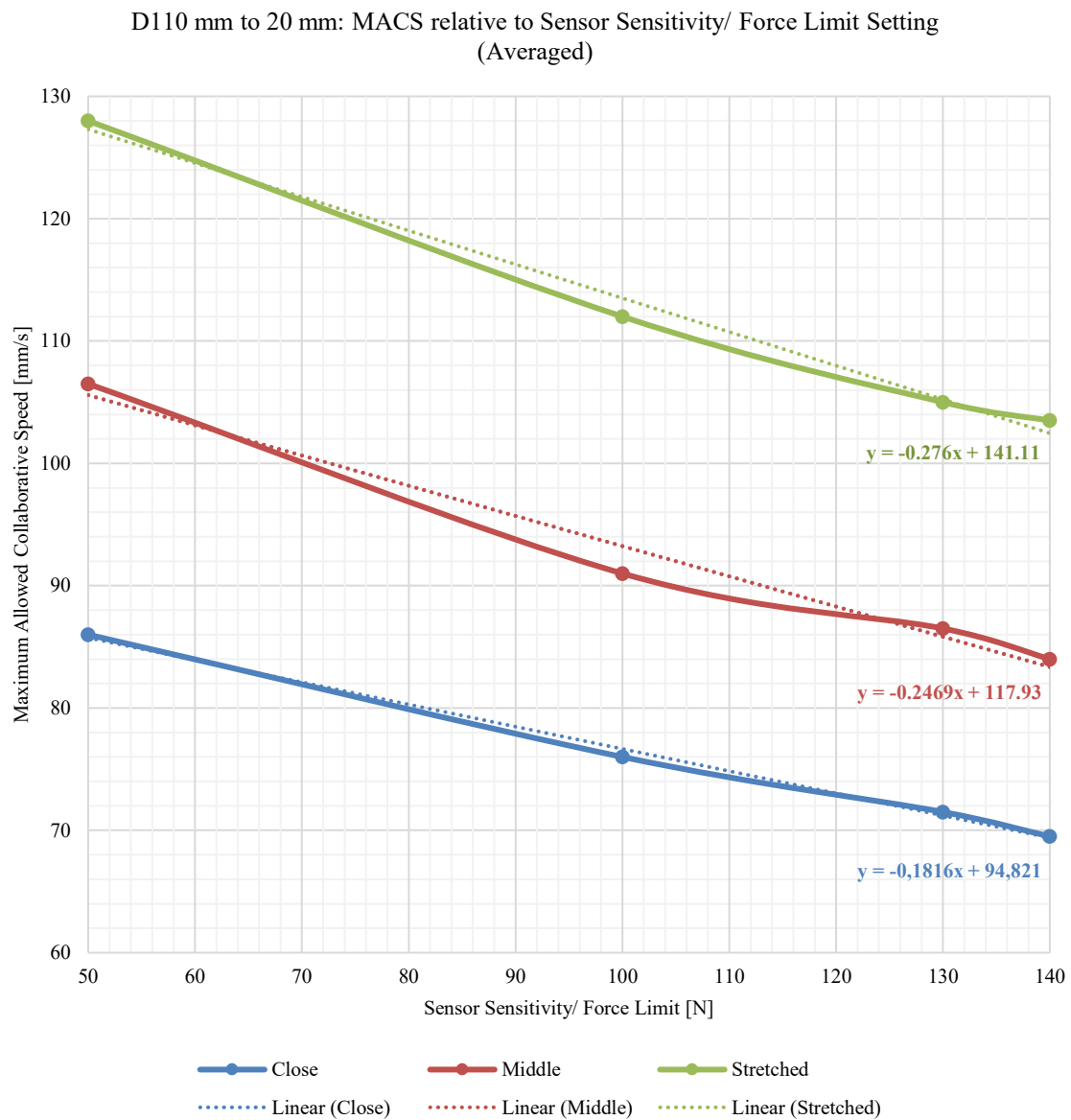


Appendix 30: Absolute MIN/MAX Deviation of the Maximum Allowed Collaborative Speed (MACS) relative to Robot Pose and Sensor Sensitivity/ Force Limit Setting for Workpiece Diameters 110 mm to 20 mm

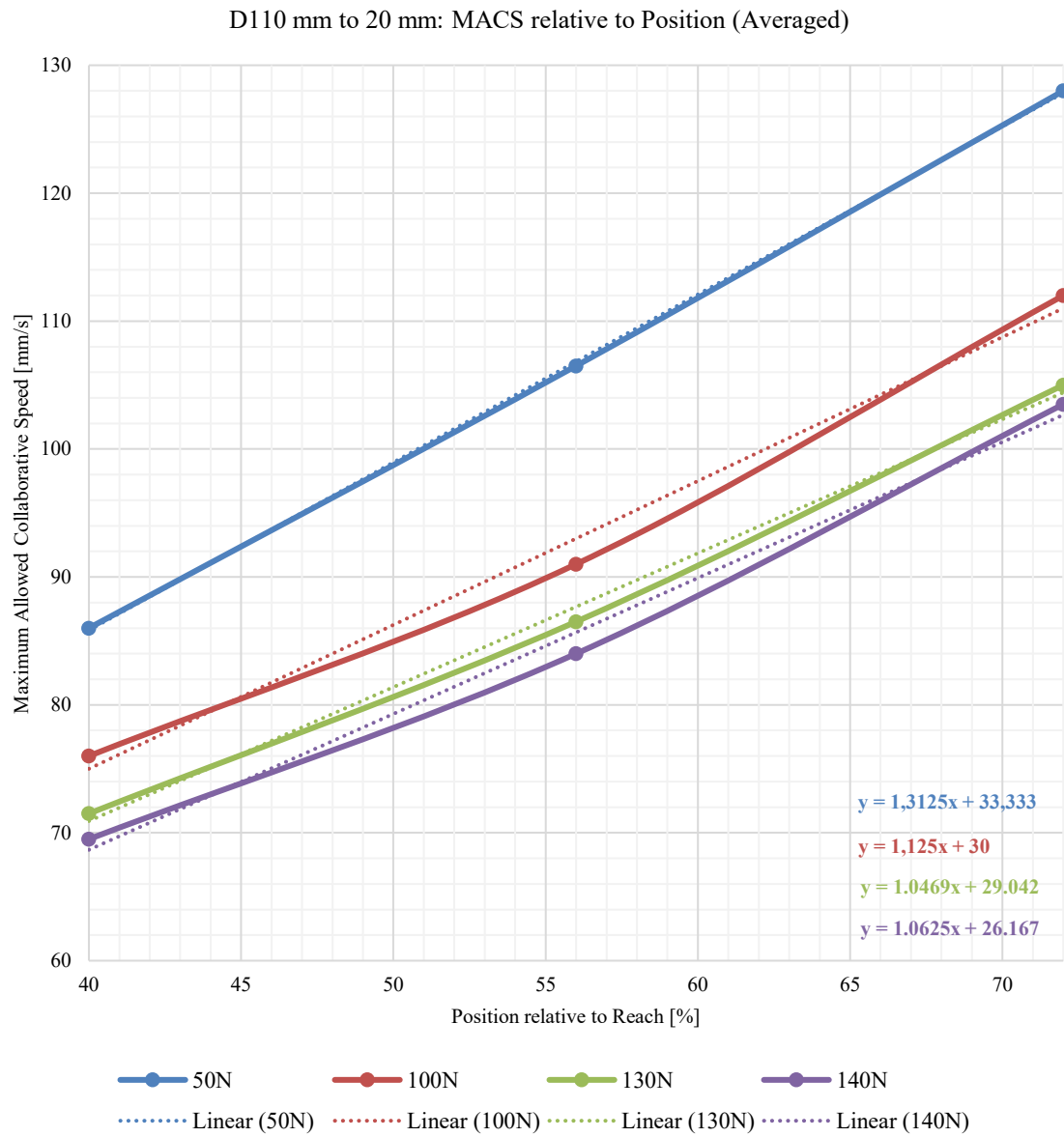


Appendix 31: Error Analysis of Pressure by Rotating around Y at 100 mm/s

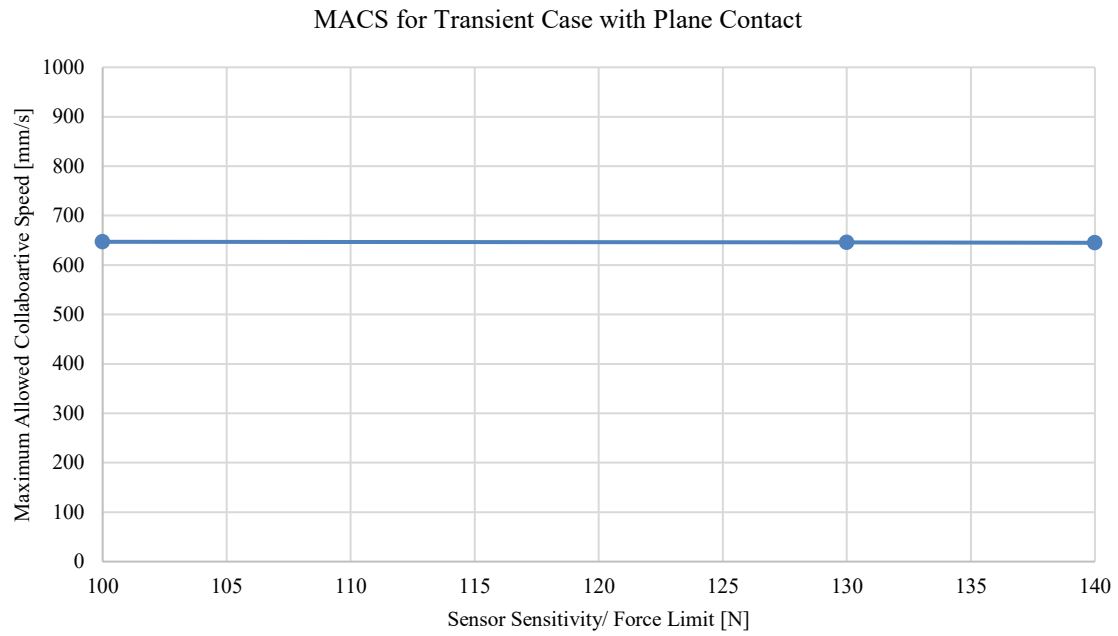
Appendix 32: Maximum Allowed Collaborative Speed (MACS) relative to Sensor Sensitivity/ Force Limit Setting for Workpiece Diameters 110 mm to 20 mm (averaged)



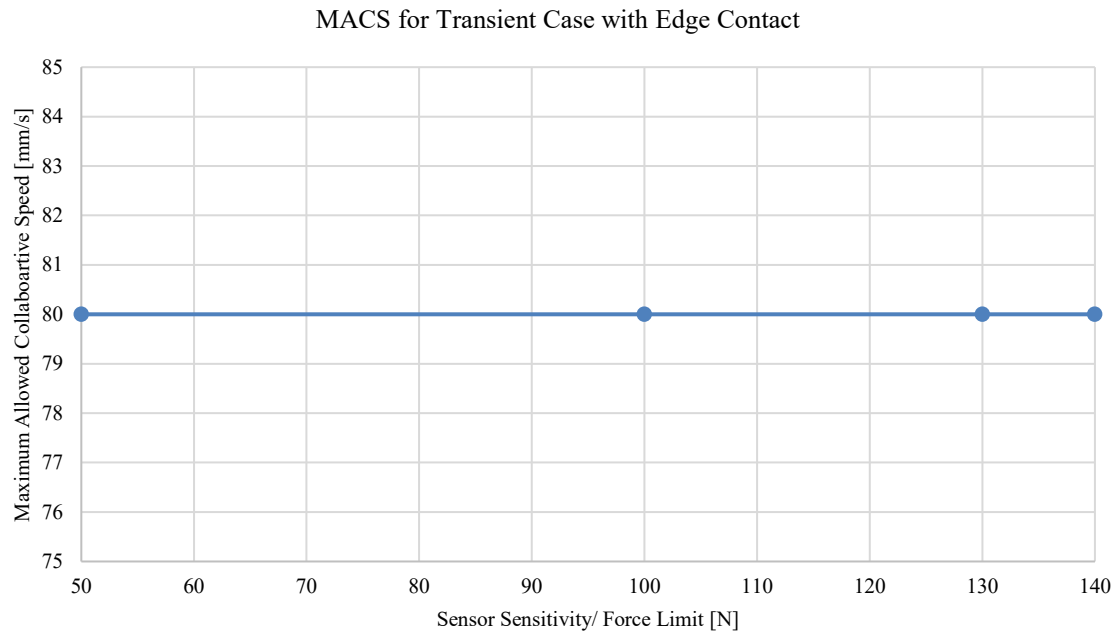
Appendix 33: Maximum Allowed Collaborative Speed (MACS) relative to Robot Pose for Workpiece Diameters 110 mm to 20 mm (averaged)



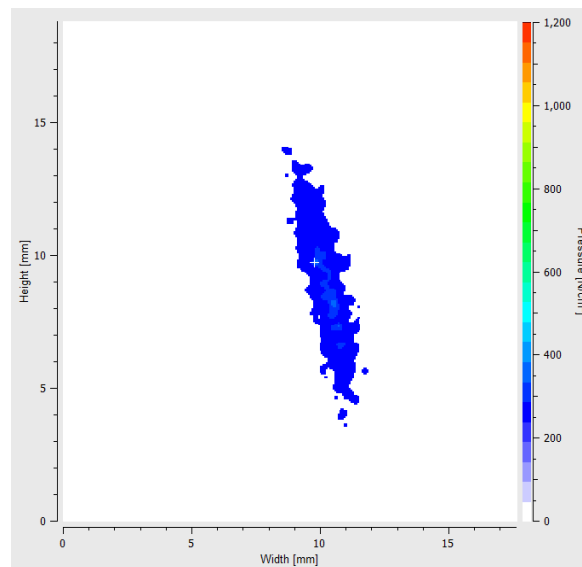
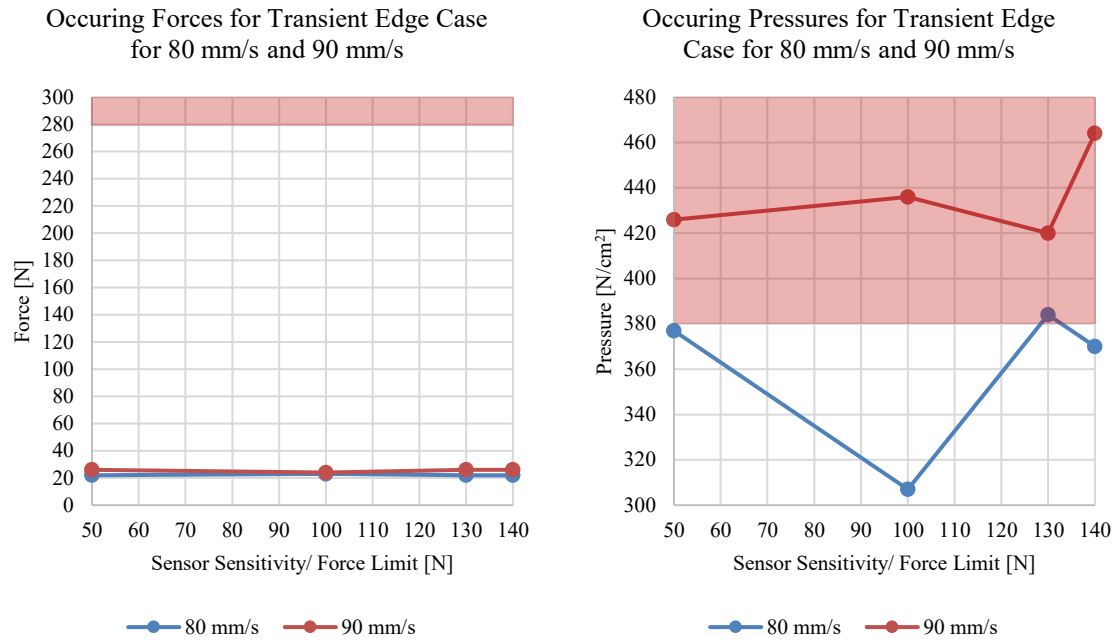
Appendix 34: Maximum Allowed Collaborative Speed (MACS) for Transient Case with Plane Contact of the 20mm Diameter Steel Basis Workpiece



Appendix 35: Maximum Allowed Collaborative Speed (MACS) for Transient Contact with the Edge of the 20 mm Diameter Steel Basis Workpiece



Appendix 36: Occurring Forces and Pressures for Transient Edge Contact with the 20mm Diameter Steel Basis Workpiece for 80 mm/s and 90 mm/s Operating Speed



Appendix 37: Coefficients for Approximation Equations to Calculate the Operating Speed-dependent Cycle Time for Motion Elements for Collaborative Robot

	n	a	b	c	d	e	f
$CT_{DSF,1Y,CR}$	8.57481	-0.0741726	0.000319283	-7.41317E-07	9.50144E-10	-6.30266E-13	1.68612E-16
$CT_{DSF,2Y,CR}$	12.8989	-0.108737	0.000460601	-1.05986E-06	1.34826E-09	-8.88205E-13	2.36109E-16
$CT_{DSF,3Y,CR}$	17.8578	-0.153984	0.00065697	-1.51264E-06	1.91444E-09	-1.2501E-12	3.28703E-16
$CT_{SFS,1x,CR}$	4.60667	-0.0375011	0.000155142	-3.48718E-07	4.3499E-10	-2.8177E-13	7.38094E-17
$CT_{SFS,2x,CR}$	9.4258	-0.078592	0.000329564	-7.51761E-07	9.50089E-10	-6.23384E-13	1.65459E-16
$CT_{SFS,3x,CR}$	14.1439	-0.120287	0.0005131	-1.19103E-06	1.5279E-09	-1.01493E-12	2.72096E-16
$CT_{SFS,4x,CR}$	18.5675	-0.155652	0.000649659	-1.47627E-06	1.8581E-09	-1.21438E-12	3.21181E-16
$CT_{SFS,5x,CR}$	23.0567	-0.192604	0.000799846	-1.81317E-06	2.28325E-09	-1.49471E-12	3.95833E-16
$CT_{T,CR}$	25.3533	-0.296044	0.00157331	-4.26826E-06	6.12727E-09	-4.42444E-12	1.26375E-15
$CT_{MFM,CR}$	6.26575	-0.0670302	0.000346785	-9.02054E-07	1.25076E-09	-8.80227E-13	2.4677E-16

Appendix 38: Coefficients for Approximation Equations to Calculate the Operating Speed-dependent Cycle Time for Motion Elements for Industrial Robot

	n	a	b	c	d	e	f
$CT_{DSF,1Y,IR}$	7.34645	-0.0509959	0.000169766	-2.93905E-07	2.72008E-10	-1.27406E-13	2.37002E-17
$CT_{DSF,2Y,IR}$	11.2204	-0.0764469	0.000246576	-4.14682E-07	3.74702E-10	-1.72309E-13	3.16358E-17
$CT_{DSF,3Y,IR}$	15.2391	-0.104627	0.000340372	-5.79214E-07	5.29914E-10	-2.4648E-13	4.5691E-17
$CT_{SFS,1x,IR}$	4.03278	-0.0264422	8.28659E-05	-1.35209E-07	1.1859E-10	-5.29775E-14	9.46071E-18
$CT_{SFS,2x,IR}$	8.13981	-0.0542054	0.000171962	-2.8464E-07	2.53265E-10	-1.1472E-13	2.07534E-17
$CT_{SFS,3x,IR}$	12.1555	-0.0824746	0.000267173	-4.54721E-07	4.17208E-10	-1.94914E-13	3.63226E-17
$CT_{SFS,4x,IR}$	16.0121	-0.107647	0.000342594	-5.72053E-07	5.15273E-10	-2.36626E-13	4.3401E-17
$CT_{SFS,5x,IR}$	20.1074	-0.136902	0.000440524	-7.43293E-07	6.75818E-10	-3.12945E-13	5.78268E-17
$CT_{T,CR}$	7.29981	-0.0485522	0.000157211	-2.68575E-07	2.4758E-10	-1.16022E-13	2.16428E-17
$CT_{MFM,CR}$	6.13876	-0.0541614	0.000206412	-3.88784E-07	3.81031E-10	-1.86133E-13	3.57866E-17

Appendix 39: Empirically Measured Maximum Allowed Collaborative Speeds (MACS) for Quasi-static Contact Cases

	50 N, Worst Case	50 N, Best Case	100 N, Worst Case	100 N, Best Case	130 N, Worst Case	130 N, Best Case	140 N, Worst Case	140 N, Best Case	Overall Worst Case	Overall Best Case
Quasi-static - Hand [mm/s]	82	132	73	119	68	113	65	111	65	132
Approximation Equation	MACS = 53.1107 + 1.15885p – 0.2283s – 0.4578m								-	
	140 N	130 N	100 N	50 N	Overall Worst Case	Overall Best Case	-			
Transient – Hand - Plane [mm/s]	645	646	647	-	645	647				
Transient – Hand – Edge [mm/s]	80	80	80	80	80	80				
	50 N, no protection	50 N, neoprene	50 N, foam	100 N, no protection	100 N, neoprene	100 N, foam	Average - no protection	Average - protection	Overall Worst Case	Overall Best Case
Transient – Shoulder – Elbow Big Cap [mm/s]	60	720	770	60	700	750	60	735	60	900
Transient – Shoulder – Elbow Small Cap [mm/s]	910	910	900	890	880	900	900	897.5		
Transient – Shoulder – Forearm [mm/s]	720	700	700	750	730	740	735	717.5		
Transient – Shoulder – Wrist Cap [mm/s]	680	700	710	670	700	700	675	702.5		

Curriculum Vitae

Personal Details

Name	Christopher Schneider
Date and Place of Birth	14.11.1992 in Chemnitz
Nationality	German
Marital Status	Single

Educational Background

Master Studies (M.Sc.) 10/2015 – 09/2018	Chemnitz University of Technology - Business Administration and Engineering Specializations: Automation Technology, Factory Planning, Accounting Master Thesis Title: “Technical Design and Profitable Evaluation of the Collaborative Robot Yaskawa HC10 through an Example in the Electrotechnical Industry”
Semester abroad 07/2016 – 12/2016	National University of Ireland, Galway - ERASMUS Research Project for International Students and Several Courses
Bachelor Studies (B.Sc.) 10/2011 – 10/2015	Chemnitz University of Technology - Business Administration and Engineering Specializations: Production Management, Logistics, Work Design Bachelor Thesis Title: “Prozess-FMEA kollaborierender Robotersysteme mittels Virtual Reality Technik”
Abitur 25.06.2011	Dr. Wilhelm-André-Gymnasium Chemnitz

Professional Background

Cobot Business Coordinator & Industrial PhD Candidate 10/2021 - today	Yaskawa Europe GmbH – Robotics Division, Department Product Management Team Leader for Collaborative Robotics EMEA
Product Manager & Industrial PhD Candidate 01/2020 - 09/2021	Yaskawa Europe GmbH – Robotics Division, Department Product Management Product Manager for Collaborative Robotics EMEA
Junior Product Manager & Industrial PhD Candidate 10/2018 – 12/2019	Yaskawa Europe GmbH – Robotics Division, Department Product Management Product Manager for Collaborative Robotics EMEA
Master’s Candidate & Working Student 10/2017 – 09/2018	Yaskawa Europe GmbH – Robotics Division, Department Product Management

Honorary Positions

Committee Member 10/2021 - today	International Organization for Standardization (ISO) Working Group Validation Methods for Collaborative Applications
Member of Organization 10/2020 - today	Deutsches Institut für Normung (DIN) Working Group Safety of Industrial Robotics